Investigation into the role of odontocete teeth in sound reception on the example of the common bottlenose dolphin, Tursiops truncatus.

Graf, Sabine

Award date:
2015

Awarding institution:
University of Bath

UNIVERSITY OF BATH

Investigation into the role of odontocete teeth in sound reception on the example of the common bottlenose dolphin, *Tursiops truncatus*.

Sabine Graf

Thesis submitted for the degree of Doctor of Philosophy

University of Bath

Department of Mechanical Engineering

September 2014

Abstract

Echolocation is the primary tool dolphins depend on for their survival underwater. Without this ability, the localization of food and navigation would be much harder for the animals. This active sonar is characterised by narrow transmission and reception directivity patterns, over a variety of ranges. In Cetaceans, only toothed whales and dolphins (odontocetes) are able to echolocate. The main concept for echolocation is to emit sound and listen to the returning echoes. Where sound enters the head first and how the signals are transmitted to the mandibular fats and inner ears is not fully understood. There are several theories on how sound reaches the fatty tissues in the lower jaw: through a thin region in the lower jaw called the pan bone, through the throat region and an opening in the rear mandibles and through the teeth, acting as an end-fire array and enhancing the directional hearing.

The hypothesis on sound reception via the teeth was investigated further in this thesis. The sound pressure was modelled at the teeth of a bottlenose dolphin (*Tursiops truncatus*) using acoustic characteristics of different components of the entire jaw. The angle of the jaw was changed from 0° to ±10° in 1 degree steps and from ±10° to ±90° in 5 degree steps. The pressure was measured at 3 front and back teeth and the difference between pressure values compared. The pressure was also measured at each of the 22 teeth on both sides of the jaw for two different angles, 0° and +5°. Multiple scattering and the influence from the relative positions and sizes of teeth as well as the effect of missing teeth was investigated. Results show that the propagation of sound varies with size and position of the teeth. The simulations display the relation between neighbouring teeth and the attenuation or amplification of the signals at other teeth. Teeth cannot be considered as individual point-like receivers. A pressure tendency can be seen at the back teeth for the first ±15°, which indicates that directional hearing occurs for the first degrees the dolphin moves its head. It also shows that hearing takes place primarily at the back of the jaw.

Acknowledgements

This research was funded by the University of Bath studentship programme.

A very special thank you goes to my supervisors Sally Clift, Philippe Blondel and William Megill. Thank you for your support and extreme patience throughout this work and for motivating me whenever I reached a barrier. All your help and guidance over the years was very much appreciated and I don't know what I would have done without you.

I would also like to thank my fabulous housemates over the last years who endured my ups and downs and always had an ear for me when I needed it. Jen, Pete, Giusi, Val and Paul, thank you so much for being there for me whenever I needed someone to talk to.

A big thank you goes to my friends who encouraged me throughout my PhD, especially Tina, Britta, Keri, Eva and Kerstin who gave me motivational speeches and told me I can do this. Tina, we can now finally go on our long due Australia/New Zealand trip. Thanks go to Steffi, Bettina and Laura for the amazing vacations in the UK and abroad. It was always a very welcome distraction with you guys and I am already looking forward to our next trips.

Finally, I would like to thank my parents for all their love and encouragement and for all the support. Thanks for believing in me and for your reassurance over the last years. Without you none of this would have been possible.

Table of Contents

List of Abbreviations

ABC	Absorbing Boundary Condition
ABR	Auditory Brainstem Response
CF	Correction Factor
CFL	Courant-Friedrichs-Lewy Condition
CNS	Central Nervous System
CT	Computer Tomography
DBS	Dolphin-Based Sonar
DI	Directivity Index
DSL	Deep Scattering Layer
EAM	External Auditory Meatus
EMG	Electromyography
FA	Fatty Acid
FDTD	Finite-Difference Time-Domain
FEM	Finite Element Modelling
FFT	Fast Fourier Transform
IID	Interaural Intensity Difference
ITD	Interaural Time Difference
LDV	Laser Doppler Vibrometry
MAA	Minimum Audible Angle
MLDB	Monkey Lips Dorsal Bursa
MMP	Marine Mammal Program
MNTB	Medial Nucleus Trapezoid Body
PET	Positron Emission Tomography
PML	Perfectly Matched Boundary Layer
PVC	Polyvinyl Chloride
SNR	Signal-to-Noise Ratio

SOFAR	Sound Fixing And Ranging
SPECT	Single Photon Emission Computer Tomography
SPL	Sound Pressure Level
TAG	Triacylglycerol
TLM	Transmission Line Modelling
TPC	Tympanoperiotic Complex
TS	Target Strength
TWIPS	Twin Inverted Pulse Sonar
VAS	Vibro-Acoustic Simulator
VCN	Ventral Cochlear Nucleus

Table of Figures

1 Introduction

Dolphins have always fascinated humans by their impressive intellectual capabilities. This is today emphasized by potential applications to bio-inspired sonars.

Echolocation is the primary tool dolphins depend on for their survival underwater. Without this ability, the localization of food and navigation underwater would be much harder for the animals. In cetaceans, only toothed whales and dolphins (odontocetes) are able to echolocate. Though baleen whales (mysticetes) use low-frequency sound for long distance communication, these animals do not echolocate actively to find their prey underwater. The main concept of echolocation is to emit sound and listen to the returning echoes. Studies on the echolocation of cetaceans were mostly performed on the Atlantic bottlenose dolphin (*Tursiops truncatus*) (e.g. Norris 1969, Au et al. 1978, Au and Penner 1981, Au et al. 1982, Au and Moore 1984), but also on other odontocetes, for example killer whales (*Orcinus orca*) (Hall and Johnson 1971), harbour porpoises (*Phocoena phocoena*) (Anderson 1970), beluga whales (*Delphinapterus leucas*) (White et al. 1978), striped dolphins (*Stenella coeruleoalba*) and several other toothed whales (Au 1993). Bottlenose dolphins (*Tursiops truncatus*) have been observed to turn their head back and forth horizontally when localizing a target (Schevill & Lawrence 1956, Kellogg 1960, Norris et al. 1961). This behaviour also led to the assumption that dolphins emit trains of sound for directional hearing.

Electrophysiological as well as behavioural experiments showed that dolphins produce sound within their nasal system and then emit the produced signals through a region in their head called the melon (Ridgway et al. 1980, Ridgway 1980, Ridgway and Carder 1989, Cranford 1992, 2000, Au 1993). According to electrophysiological experiments, harbour porpoises, striped dolphins and bottlenose dolphins have the widest auditory bandwidth with the best hearing frequency between 15 - 110 kHz and a maximum sensitivity of 42 dB re 1 µPa for *Tursiops truncatus*. This threshold was measured at 60 kHz with a 20-dB increase at 120 kHz, increasing afterwards. It was not specified whether these are peak-to-peak, peak or rms levels (Johnson 1967). Much less is known about the actual mechanisms of hearing, which is important for the mitigation or regulation of ambient noise in the ocean.

1.1 Dolphin echolocation and hearing

1.1.1 Measurements at sea

Dolphins produce several types of calls: narrow-band and pulsed tonal sounds (Dudzinski et al. 2009). Narrow-band tonal sounds, also called whistles, are used for intraspecific communication. Au et al. (1999) suggested that every dolphin possesses its own signature whistle, lasting between one and two seconds. Frequencies of the fundamental component of whistles usually lie below 20 kHz, but can occasionally be higher depending on the species (Herman and Tavolga 1980, Madsen et al. 2012) (Fig. 1.1).

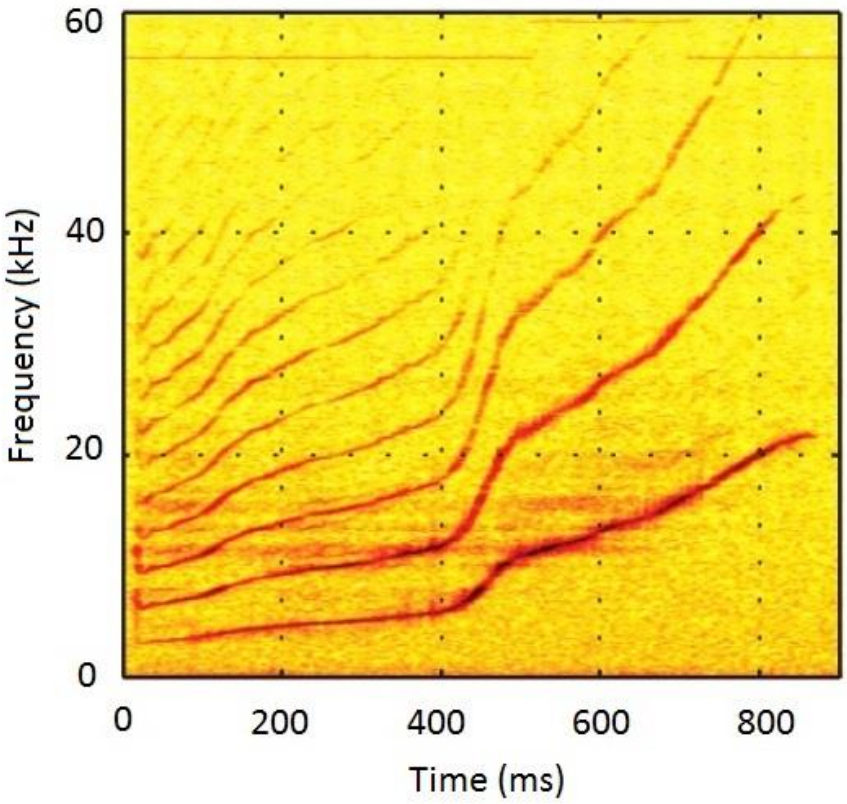

Fig. 1.1: Spectrogram of a bottlenose dolphin (*Tursiops truncatus*) whistle. Red = High amplitudes; yellow = low amplitudes (adapted from Madsen et al. 2011).

Burst pulsed sounds have been observed in connection with social behaviour as a form of communication between adjacent individuals, for example during aggressive behaviour or courtship (Overstrom 1983, Dawson 1991, Blomqvist and Amundin 2004, Lammers and Au 2006). Those broadband clicks are characterized by a high repetition rate or low interpulse

intervals with frequencies sometimes extending 100 kHz and interclick intervals between 0.5 and 10 ms (Fig.1.2).

Unlike whistles and burst pulses, clicks are not social signals, but are instead produced for sensing the environment, ranging and finding prey. Those echolocation clicks are also pulsed sounds and look similar to burst pulses, but differ in the number of clicks produced with time (Lammers et al. 2004) and in their amplitudes (Au et al. 1987).

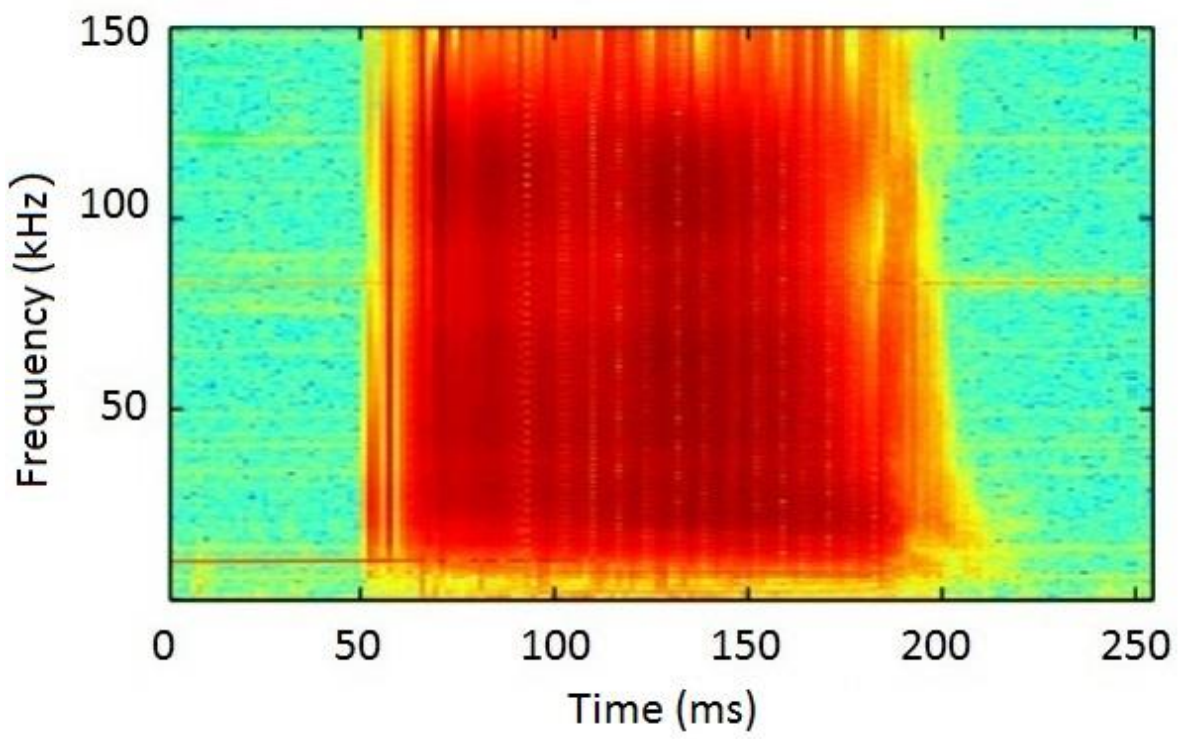

Fig. 1.2: Spectrogram of a bottlenose dolphin (*Tursiops truncatus*) burst pulse (adapted from Branstetter et al. 2012).

The frequency of echolocation clicks varies with dolphin species, typically extending beyond 120 kHz (Fig. 1.3). Ranging is done by measuring the time interval between the incoming and outgoing signals. Bottlenose dolphins (*Tursiops truncatus*) hear best around 50 kHz, but are also able to hear and produce signals at frequencies up to 150 kHz. The echolocation clicks of bottlenose dolphins are very short (<100 μsec). The animals generally wait until receiving the echo from an impinging signal, before emitting the next click (Au 1993). Those high frequency clicks are emitted from the animals' forehead, propagating in a directional beam along the long axis of the skull (Cranford et al. 1996).

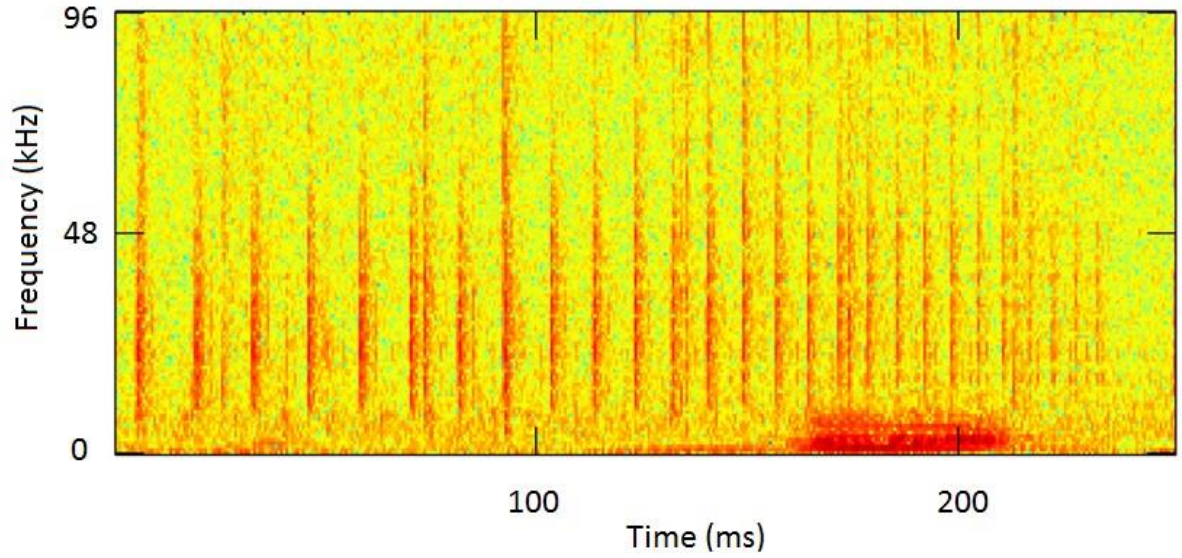

Fig. 1.3: Echolocation click train of a bottlenose dolphin (*Tursiops truncatus*). Red = high amplitudes; yellow = low amplitudes (Simard et al. 2011).

1.1.2 Sound Production

Contrary to initial assumptions of the larynx being the origin of sound production (Schevill and Lawrence 1956, Purves 1967, Purves and Pilleri 1986), multiple experiments on live dolphins have shown that sound is generated within the nasal region of the animals (Dierks et al. 1971, Blevins and Parkins 1973, Dormer 1979, Amundin and Andersen 1983, Fitzgerald 1999). Diercks et al. (1971) conducted experiments on *Tursiops truncatus*, *Orcinus orca* and *Inia geoffrensis*, attaching hydrophones to the animals' head and rostrum. By analysing arrival times, they found that echolocation clicks were produced in the vicinity of the nasal plugs (Fig. 1.4). Dormer (1979) observed the movements of the laryngeal and nasal region in experiments on *Tursiops truncatus*, *Tursiops gilli* and *Stenella longirostris* with high-speed X-ray motion picture cameras. He found that movements on the left nasal plug can be associated with the emission of whistles and movements on the right nasal plug, possibly with the production of clicks. Measurements of muscle activities and air pressure in the nasolaryngeal system during sound production of five bottlenose dolphins showed that the muscles fired just before and after the emission of sound (Ridgway et al. 1980). Muscles associated with the larynx showed on the other hand no reaction during sound production. The pressure was measured by inserting catheters into the nares, nasal sacs and trachea. Results showed an increase in pressure in the nares and premaxillary sacs just before sound production, but no pressure change in the trachea.

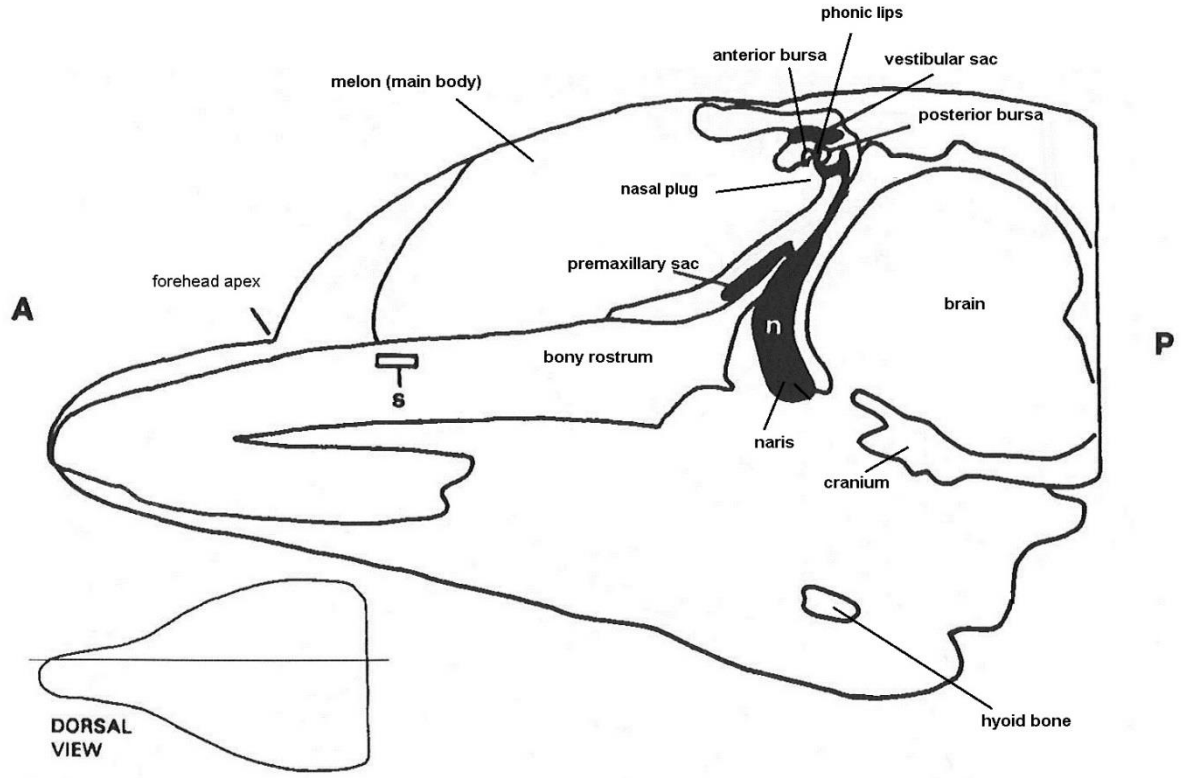

Fig. 1.4: Dorsal view of the head of a bottlenose dolphin (*Tursiops truncatus*). s, scale (1.5 cm). Anterior and posterior are indicated as A and P (adapted from Cranford et al. 1996).

Mackay and Liaw (1981) used an ultrasonic Doppler motion detector to measure tissue vibrations in *Tursiops truncatus* and *Delphinus delphis* during sound production. A Doppler probe was held against several places of the animals' head, including a position below the jaw in order to measure possible vibrations of the larynx. Results showed no vibrations near the laryngeal region, but vibrations of the nasal plugs as well as air sacs in synchrony with the production of echolocation clicks. Observations also showed that the nasal diverticula on the right side vibrated always with click production, whereas the left side vibrated only occasionally. Amundin and Andersen (1983) conducted experiments similar to those of Ridgway et al. (1980). The muscle activity and air pressure of the nasal region were measured during sound production in *Tursiops truncatus* and *Phocoena phocoena*. For the electromyography (EMG), platinum fine-wire electrodes were implanted into the muscles of the animals' nasal plugs. In both species, the pressure in the bony nares increased before click production, in both nares with equal amplitude and timing. EMG recordings demonstrated activity in the nasal plug muscle during sound production.

After noticing movement along the left posterior margin of the blowhole of an Arctic white whale (*Delphinapterus leucas*) during a target discrimination task, Ridgway and Carder (1988) trained the animal to let catheters being inserted into its blowhole to measure pressure activity during sound production. For the discrimination task, the animal was trained to wear suction cups over its eyes and stay at a bite-plate station behind an acoustically opaque screen until the screen was raised. It was then required to discriminate between the presence and absence of an aluminium pipe and whistle when the target was present. This was the first experiment in which a cetacean was required to actively produce a sound in order to report the presence of a target. The whale was then gradually trained to have three catheters of different sizes inserted into its blowhole and nasal cavities, either alone or in combination, and to then seal its blowhole around the catheter. The animal was required to perform the target discrimination task with the catheters in place. Results showed a pressure increase in the nasal cavities prior to sound emission and a change in pressure during the whistle, falling when the tone swept down and rising when the tone swept up. During trials with an open catheter of about 2 mm diameter and a pressure catheter inserted in the nasal cavity, the animal was able to produce sounds when a thumb was placed over the open catheter. If the thumb was lifted from the open catheter, it created an opening in the nasal cavity and the whale was not able to produce any sound. The intratracheal pressure remained unchanged during the experiments.

Experimental and morphological findings by Cranford et al. (1996, 1997) settled the controversy on the site of sound generation by odontocetes. They used a dual-camera high-speed system for their experiments. An endoscope with one of the high-speed cameras was inserted into the blowhole of two bottlenose dolphins and recorded movements of the monkey lips dorsal bursa (MLDB) complexes. The MLDB complex is located on either side and just above the membranous nasal septum, below the ventral floor of the vestibular air sac (Fig. 1.4). It consists of a pair of anterior and posterior dorsal bursae, in which the monkey-lips, today rather termed phonic lips, are embedded. Results showed that movements of the MLDB complex occurred simultaneously with the production of whistles and clicks. Acoustic pulses were generated by pressing air through the phonic lips, their opening and closing interrupting the air flow and thereby determining the repetition rate of the clicks.

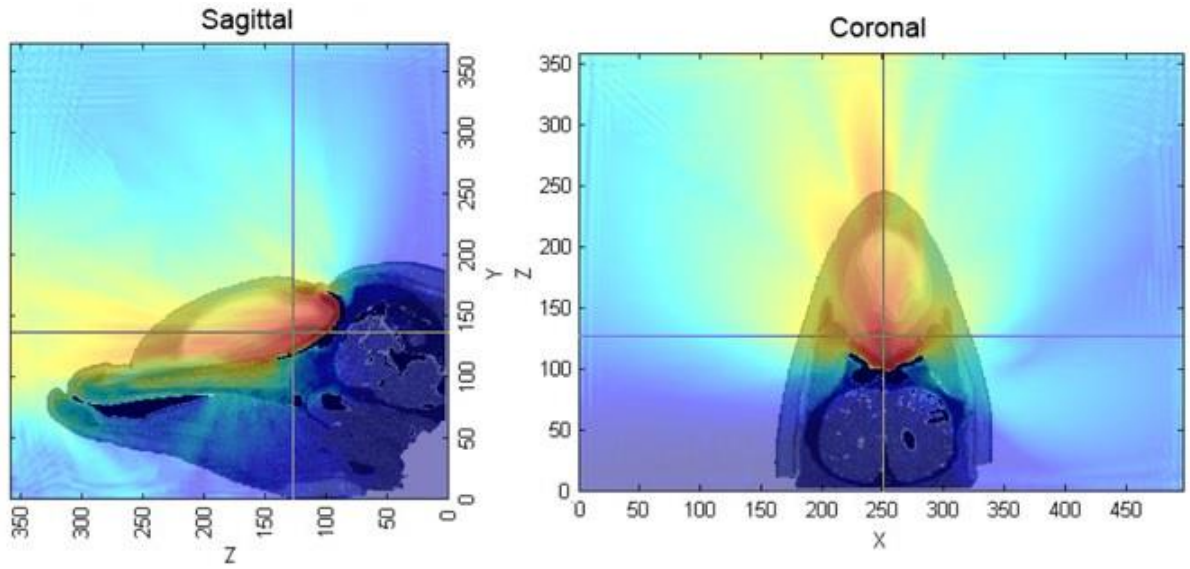

Fig. 1.5: Simulation of the sound generation and beam formation of a bottlenose dolphin; the images show the sagittal and coronal view of the dolphin's head (adapted from Cranford et al. 2014).

The highly directional beams with 3-dB beamwidths of about 10° in both vertical and horizontal planes are emitted from the melon, an oval shaped, fatty-tissue mass lying at the centre of the forehead of most odontocetes (Au et al. 1986). The melon acts like an acoustic lens, focusing the sound beam (Fig. 1.5). Its unique fat composition defines tissues that have been implicated in acoustic processing in the melon as well as in the lower jaw, which contains the same acoustic lipids (Varanasi et al. 1975). The path of sound emitted from the melon and received by the lower jaw can be seen in Fig. 1.9.

1.1.3 Sound Reception

The mechanisms of dolphin sonar have been used to design man-made sonar systems. Improving the resolution of existing sonar systems is still in development. Kuc (1996, 1997) developed an adaptive sonar system based on bats' and dolphins' echolocation. The sonar device was able to change its location and configuration according to the information it received from detected echoes. It consisted of a transmitter in the centre and two receivers on each side with the whole construction being mounted at the end of a robot arm. When receiving an echo, the receivers rotated to maximise echo amplitude and bandwidth. This enhanced the ability of the sonar system to differentiate objects.

Houser et al. (2003) developed a dolphin-based sonar (DBS) system especially designed for shallow (12 – 61 m water depth) and very shallow (3 – 12 m) water zones to detect underwater

mines (Fig. 1.6). Their sonar system took various variables into account, amongst others directivity index, sensitivity, echolocation frequency as well as the anatomy of a bottlenose dolphin. The DBS system consisted of a projector and receiver array, with the projector array having a 12 degree transmission beamwidth at 110 kHz and side lobes with a source level of approximately 17 dB re 1 µPa. It was not specified whether these are peak-to-peak, peak or rms levels (Houser et al. 2003). The projector produced pulse types based on a dolphin's emission clicks. Two directional hydrophones formed the receiver with a distance of about 12.5 cm between each other, which is the approximate distance between a bottlenose dolphin's ears. The hydrophones had a 20 degree beamwidth at 80 kHz. Results showed that the DBS was able to detect all of the targets in shallow as well as very shallow water.

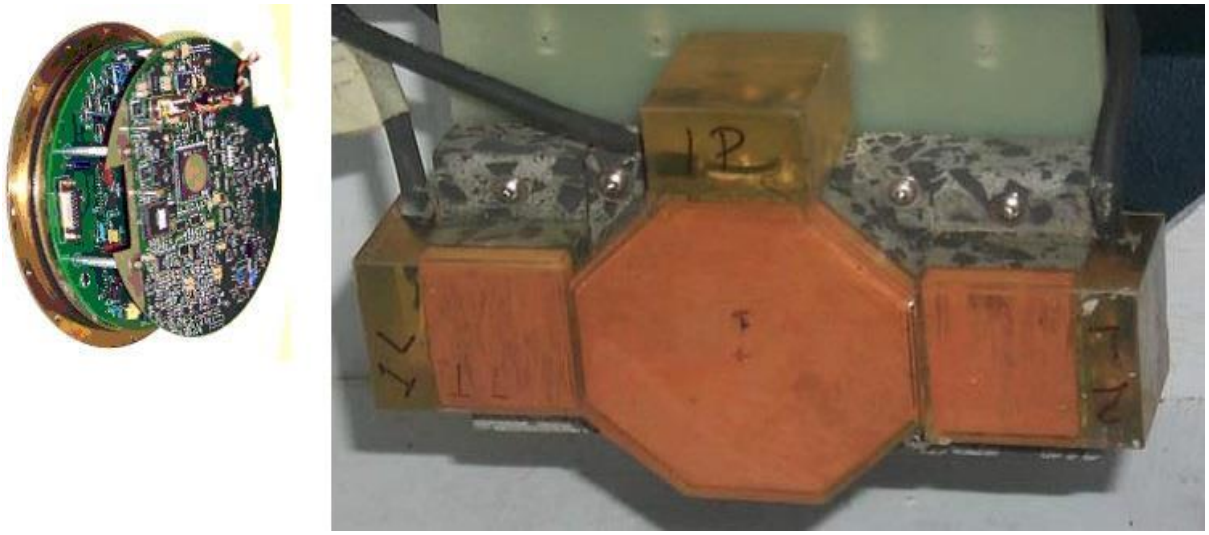

Fig. 1.6: Dolphin-Based Sonar (DBS) and biomimetic array (adapted from Houser et al. 2003).

Another underwater sonar device called TWIPS (Twin Inverted Pulse Sonar) has been developed recently at the University of Southampton (Leighton et al. 2010). This device is also particularly aimed for shallow waters. Breaking waves at the surface make it difficult for standard sonars to work due to the bubbles created. Dolphins are known to occasionally generate nets of bubbles when echolocating, forcing their prey to cluster together. For their sonar system to still work, the researchers at the University of Southampton suggested that the animals had to have a special way to process the receiving sound (Leighton et al. 2010). TWIPS emits twinned pairs of echolocation pulses with the first pulse being emitted shortly before the second pulse. The waveform of the 2nd pulse is the inverse of the 1st. The researchers processed

the resulting information using nonlinear mathematics and suggested that dolphins might also use nonlinear processing in order to differentiate between prey and bubbles.

Directional hearing is an important feature in the sound reception system of dolphins. The receiving beam patterns of bottlenose dolphins (*Tursiops truncatus*) were measured by various researchers (Zaytseva et al. 1975, Au and Moore 1984). Au and Moore (1984) measured the beamwidth in a vertical and horizontal plane at frequencies of 30, 60, and 120 kHz. In a vertical plane the beamwidth was 30.4°, 22.7°, and 17° respectively, whereas measurements in the horizontal plane showed a beamwidth of 59.1°, 32.0°, and 13.7° respectively (Fig. 1.7). This led to the conclusion that the capability of directional hearing was dependent on the frequency, with the beam becoming narrower as the frequency increased. Au and Moore (1984) also discovered an asymmetry in the beam above and below the dolphin's head, indicating a better auditory sensitivity for the angles below the dolphin's head. The authors suggested that sound was received through the lower jaw, causing a shadowing of the received sound by the upper part of the head.

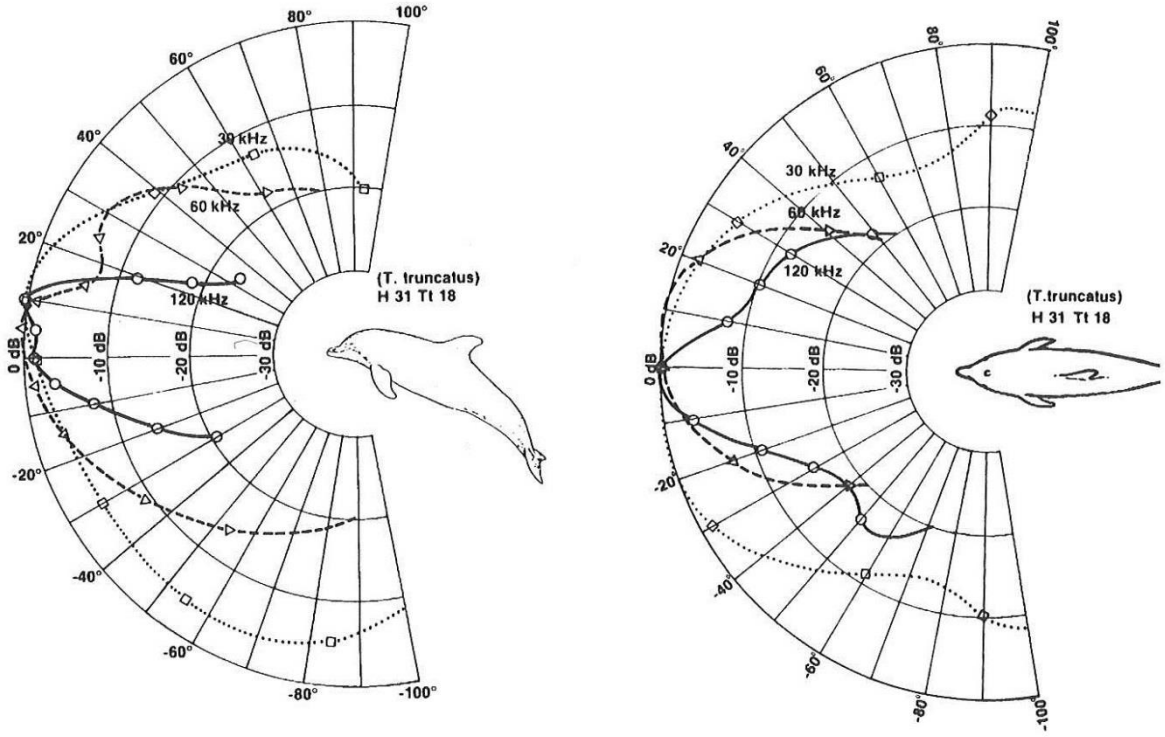

Fig.1.7: Smoothened receiving beam patterns of a bottlenose dolphin (*Tursiops truncatus*) in the vertical and horizontal plane for frequencies of 30, 60, and 120 kHz (adapted from Au and Moore 1984).

Measurements for the horizontal plane by Zaytseva et al. (1975) showed a beamwidth of 8.2° for a frequency of 80 kHz, being even narrower than the beamwidth measured by Au and Moore for a frequency of 60 kHz. Au and Moore (1984) suggested that one explanation for this noticeable discrepancy could be differences in the construction of the experiment. While Au and Moore used two noise transducers and a fixed stationing device, Zaytseva et al. (1975) used only one noise source with the dolphin being able to move its head and swimming towards the signal hydrophone. This gave the dolphin the possibility to move its head away from the noise and therefore minimize its effects on the animal's directional hearing.

The degree of directionality can be determined by the directivity index (DI). It is the ratio of the power received by an omni-directional receiver compared to the power by the directional receiver in the same isotropic noise field (Au 1993).

$$\mathrm{DI} = 10 \log D = 10 \log\left(\frac{P_O}{P_D}\right), \tag{1.1}$$

where D is the directivity of the hydrophone, P_O is the total acoustic power received by an omni-directional hydrophone and P_D is the total acoustic power received by a directional hydrophone. The larger DI, the more directional the hydrophone. The DI of a transducer was derived as

$$\mathrm{DI} = 10 \log \frac{4\pi}{\int_0^{2\pi} \int_{-\pi/2}^{\pi/2} \left[\frac{P(\theta,\varphi)}{P_O}\right]^2 \sin\theta \, d\theta \, d\varphi} \tag{1.2}$$

The hearing directivity index of a bottlenose dolphin (*Tursiops truncatus*) was estimated by Au (1993). It is measured as a function of both direction (θ) and azimuthal angle (φ) (Fig. 1.8). $P(\theta,\varphi)/P_O$ is the beam pattern of the directional transducer with P_O as total acoustic power received by an omni-directional hydrophone.

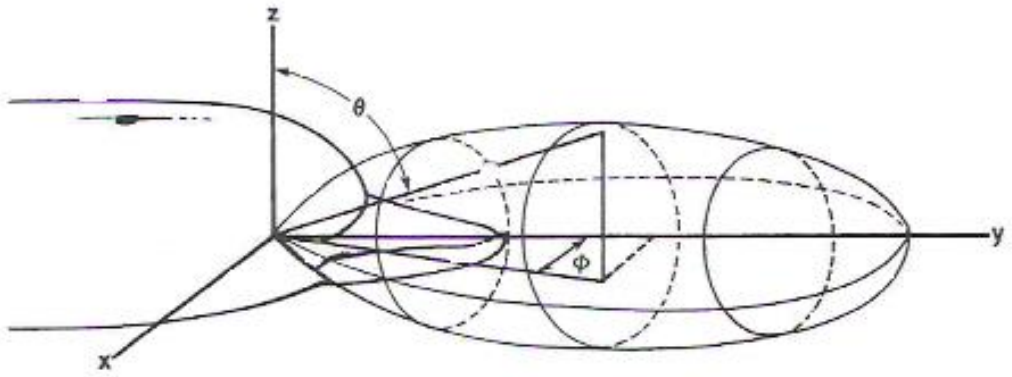

Fig. 1.8: Geometry of the measured DI for dolphins (Au and Hastings 2008).

Directivity indices of 9.4, 15.3, and 20.6 dB re 1 µPa were measured for frequencies of 30, 60, and 120 kHz respectively. After plotting, the indices showed a linear curve, leading to the equation

$$\text{DI (dB)} = 16.9 \log f - 14.5 \qquad (1.3)$$

f is the frequency measured in kHz (Au 1993). The DI for *Tursiops* can also be applied to other dolphins, using a correction factor (CF), which depends on the diameter d_D of the head of the dolphin species under consideration and the diameter d_T for the head of a *Tursiops*, measured at the location of the blowhole in the vertical plane:

$$\text{CF (dB)} = 20 \log (d_D / d_T) \qquad (1.4)$$

The DI for any different dolphin species can therefore be expressed as

$$\text{DI (dB)} = 16.9 \log f - 14.5 + \text{CF (dB)} \qquad (1.5)$$

Being able to determine the position of a sound source underwater is also important in order to determine the relative position of a target within the sonar beam. The acuity of sound localization is normally defined in the form of a minimum audible angle (MAA). The MAA for *Tursiops truncatus* was measured by Renaud and Popper (1978) in both the horizontal and the vertical plane. A dolphin was trained to station on a bite plate, with two transducers positioned at equal angles in front of it. After a signal was transmitted from one of the transducers, the dolphin had to swim to and touch the paddle on the side of the transmitting transducer. Depending on a correct or incorrect trial, the transducers were moved by 0.5° closer

or further away respectively. For a horizontal plane the MAA for *Tursiops* showed a value of 3.6° at 6 kHz, with a minimum of 2.1° at a frequency of 20 kHz, and increasing again to 3.8° at 100 kHz. The MAA in a vertical plane showed a smaller angle than the MAAs for the horizontal plane. A minimum audible angle of 2.3° was given at a frequency of 20 kHz and 3.5° at 100 kHz. This led to the conclusion that the animal could localize sound in the vertical plane almost as well as in the horizontal plane.

1.2 General overview of the competing hypotheses

Odontocetes use echolocation for navigation and prey detection. The existence of an echolocation system in toothed whales was first observed by McBride in 1947, noticing that dolphins could recognize and avoid nets with fine meshes in water with bad visibility. Research on bottlenose dolphins (*Tursiops truncatus*) conducted by Kellogg and Kohler (1952), Kellogg et al. (1953) and Kellogg (1958, 1959 and 1960) supported that observation and led also to the discovery that dolphins emit clicking sounds to navigate. Today dolphin sonar is known to be superior to man-made sonar systems, especially in shallow water. While the process of sound transmission in an echolocation system is relatively well understood, it is still not entirely clear how dolphins receive sound.

1.2.1 Sound reception through the lower jaw

One of the first hypotheses for a possible sound reception pathway in echolocating odontocetes was suggested by Norris (1964, 1968). He hypothesized that sound enters the thin wall of the lower jaw, propagates through the fatty tissue filling the hollow part of the mandible and is then transmitted to the tympanic bulla to which the lipid tissue is attached (Fig. 1.9). Norris called this region of the pan bone the “acoustic window”. The low sound absorption of the soft tissue and the ability to conduct sound efficiently as well as the absence of the medial bony wall in the lower jaw is the main reason for the jaw-hearing hypothesis. Other researchers supported Norris’ theory and conducted behavioural as well as electrophysiological experiments.

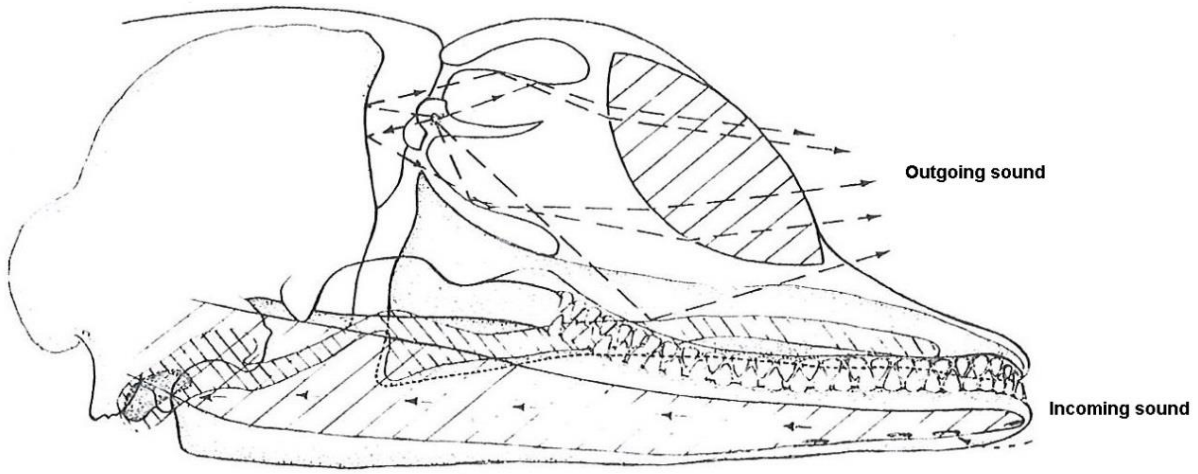

Fig. 1.9: Possible reception pathway for sound through the lower jaw of a dolphin (adapted from Norris 1964).

The experiments showed that, when acoustically shielding the lower jaw and teeth of a dolphin, the animal was not able to localize its target accurately (Brill et al. 1988). Hydrophones held against the region of the head closest to the acoustic window showed highest auditory evoked responses compared to the rest of the head (Bullock et al. 1968). Other methods to investigate the possible role of the lower jaw as a sound reception pathway included the cochlear potential method, measuring the potential along the jaw created by hair cells in the organ of Corti (McCormick et al. 1970, 1980). High sensitivity could be seen above the pan bone and at the tip of the lower jaw as well as near the melon. The lower jaw hypothesis will be elaborated in more detail in Chapter 2.

1.2.2 Teeth as receptors

The supposition that the teeth of the lower jaw play a role in the sound reception system of toothed whales was first mentioned by Goodson and Klinowska (1990). Odontocetes have evenly spaced conical teeth, lying in two straight rows along the lower jaw bone (Fig. 1.10). The animals have no teeth for grinding or chewing. Several authors hypothesized that this unique arrangement of the teeth occurred for a reason and that the teeth function as kind of a receiving array (Dobbins 2001, 2007; Potter and Taylor 2001; Nelson 2005).

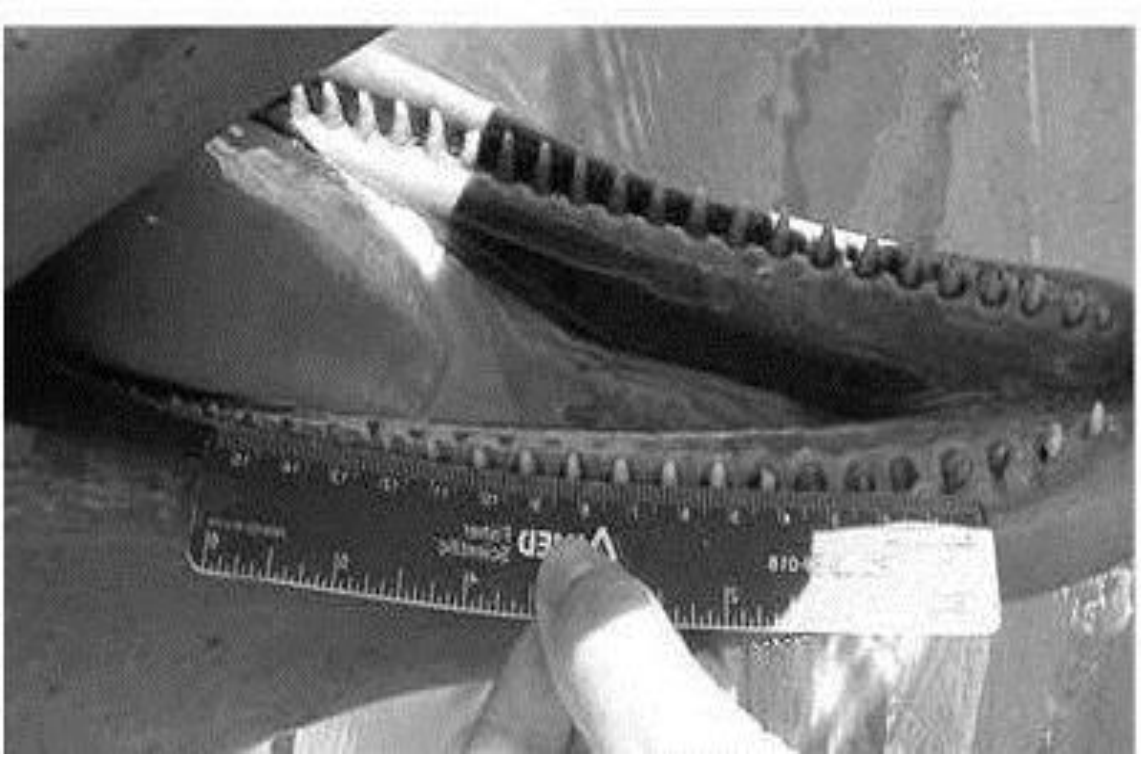

Fig. 1.10: Dental arrangement of a *Tursiops truncatus* (Potter and Taylor 2001).

Goodson and Klinowska (1990) considered the teeth as passive resonant transducers and suggested that signals arriving at the tooth nerves were delayed before being sent simultaneously to the Central Nervous System (CNS). Potter and Taylor (2001) investigated this hypothesis further and also the possible sound reception through the jaw bone. The authors discovered delay line mechanisms in the auditory cortex of a bottlenose dolphin and also found that sound conduction in bone is faster than in tooth nerves. For the jaw bone, they assumed a sound velocity in the range of 1900 – 3300 m/s. The sound velocity of the dental nerves was considered to be 100 m/s. They therefore suggested the jaw bone as part of the sound reception rather than the tooth nerves. Dobbins (2001, 2007) focussed on the concept of the teeth acting as resonant transducers and as a form of end-fire array rather than the tooth nerves. He hypothesized that signals entering the lower jaw bone are first coupled and then transmitted with delays to the inner ear for processing. Investigation into the teeth as resonant transducers were also performed by Dible et al. (2006, 2009) and Nelson (2005), for a bottlenose dolphin (*Tursiops truncatus*) and sperm whale (*Physeter macrocephalus*) respectively. Strong resonances are shown at both animals' echolocating frequencies. Dible et al. (2006, 2009) measured strong resonant modes between 115 – 135 kHz for *Tursiops*. Their findings indicated that the teeth act as periodic array of scattering elements, creating an angular dependent band-

gap. This would mean that the animal's teeth function as a passive beam-forming structure, improving the animal's directional hearing. According to Dible et al. (2009), the teeth provide binaural performance by filtering the passing frequencies depending on the angles of the impinging sound wave. The authors' hypothesis is elaborated in more detail in Chapter 2.

1.2.3 Gular pathway

The latest theory for sound reception in dolphins' teeth was suggested by Cranford et al. (2008a, 2008b, 2009, 2010), after the beginning of this thesis. Vibroacoustic simulations in a Cuvier's beaked whale's head (*Ziphius cavirostris*) developed by using finite element modelling (FEM) made it possible to look at sound transmission through the whale's head.

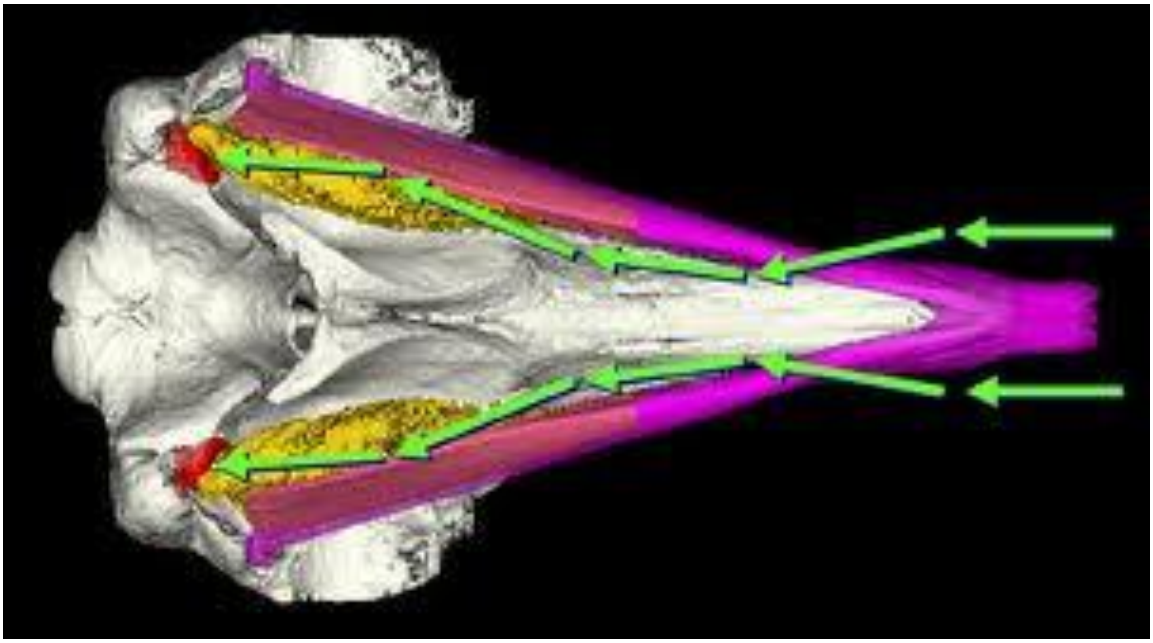

Fig. 1.11: Image of the underside of a Cuvier's beaked whale head, showing the acoustic pathway through the throat region in form of arrows. Bones are coloured in purple, fat body is coloured in yellow and the tympanoperiotic complex in red (Cranford et al. 2008a).

This Vibroacoustic Simulator was produced by combining the geometry of the animal's head obtained via X-ray CT scanner, the tissue properties and the FEM software. The X-ray CT scanner produced tomographic images using computer processed X-rays; the tissue properties like elasticity, density and sound velocity were measured by Soldevilla et al. (2005). The simulations showed a pathway through the gular region for sound coming from the front of the jaw (Fig. 1.11). Sound was entering the lower jaw underneath the tongue region and then

passing through the oral cavity, throat and the hollow part of the jaw containing the fatty tissue to the bony ear complex called tympanoperiotic complex (TPC). Sound was then transmitted from the TPC to the cochlea (inner ear). The absence of a medial bony wall in the back of the lower jaw was a necessary requirement for this sound pathway, which occurs in all odontocetes. This hypothesis will be described in detail in Chapter 2.

1.3 Evidence of echolocation abilities in Cetaceans

Research on the auditory system of dolphins has been conducted in various forms over the last decades, on live as well as on dead dolphins, and more recently using computer modelling. The following sections list the main hypotheses on how dolphins receive sound and the hereto conducted experimental studies.

1.3.1 Experiments on live odontocetes

The theory of a sonar system in dolphins first led to behavioural studies on wild and subsequently captured animals. First observations of dolphins in the wild led to the assumption that the animals must have the same capability as bats to find their prey and use acoustic waves for navigation, communication and foraging. Bottlenose dolphins were observed to navigate in the dark as well as in water with bad visibility and could also be seen to avoid very small mesh nets (McBride 1956, Norris and Prescott 1961). Porpoises were reported to be very sensitive and swim away at great speed when exposed to acoustic emissions of vessels (Fraser 1947, Kellogg and Kohler 1952). Those observations on dolphins in the wild led to the hypothesis of a sonar system in dolphins. This was investigated further by performing behavioural experiments on captured dolphins and eventually by training captured dolphins for behavioural as well as electrophysiological experiments.

Simple behavioural experiments were conducted by Kellogg and Kohler (1952) who exposed several bottlenose dolphins (*Tursiops truncatus*) as well as Atlantic spotted dolphins (*Stenella plagiodon*) to a wide range of frequencies, and observed the animals' behaviour. Sound was generated by an oscillator with frequencies ranging from 20 Hz to 200 kHz, with a transducer projecting the frequencies as bursts of 2 - 3 s into the water. They found that the animals were able to hear frequencies up to 50 kHz and suggested that the dolphins may also be able to produce high ultrasonic vibrations, leading to the first public presumption of dolphins orienting themselves by echolocation. The authors also mentioned an either aggressive or

evasive reaction of the animals to low-frequency sound. The dolphins either attacked the transducer or dove out of the water, presumably in order to avoid the low-frequency vibrations.

In a simple conditioned response experiment, the reaction of a fresh-caught bottlenose dolphin was observed to the exposure of tones between 150 Hz and 153 kHz at -20 dB re 1 µPa to 28 dB re 1 µPa sound levels. It was not specified whether these are peak-to-peak, peak or rms levels. The animal was held in a 20 x 55 m enclosure at the end of a tidal inlet. The water was murky and visibility after 30 cm non-existent. The animal was required to swim to a food source presented by a trainer, when hearing a transducer generated sound. The experiments showed high responses for frequencies up to 120 kHz and a decline in positive responses for frequencies above 120 kHz (Schevill and Lawrence 1953). In 1958 Kellogg also performed behavioural tests in a 17 m by 21 m tank with two trained bottlenose dolphins. The water in the tank was extremely turbid and therefore visibility-impairing. The experiment consisted amongst others in object avoidance and discrimination between two types of fish. For the former, galvanized sheet metal poles were suspended in the tank and the animals observed while swimming through these obstacles. The poles gave off a metallic sound when struck lightly, which was recorded by the hydrophone. Four collisions were recorded in a first 20 minute session, which, according to Kellogg, were made after the animal had passed the obstruction. No collisions were recorded in the second session. For the fish discrimination experiment, the animals were first fed with mullet (*Mugil cephalus*), which they soon refused, and eventually with their preferred fish, spot (*Leiostomus xanthurus*). The two fish were simultaneously submerged into the water behind a plywood screen, with the *Leiostomus xanthurus* looking out 15 cm below the screen and *Mugil cephalus* 30.5 cm. The dolphins were then required to swim and touch the *Leiostomus xanthurus*. The first session of 16 trials showed four errors in discriminating the two fish, the final 140 trials showed no errors. Underwater recordings of this experiment also showed that the dolphins were emitting sound signals with increasing intensity and continuity once the experiment had started and the fish were inserted into the water. A different experiment was then conducted, in which the dolphins had to differentiate between a spot fish behind a glass plate and a spot fish behind an aperture with metal frame, and were required to swim and touch the fish in the open window. This experiment required preliminary training, since the animals had to learn to put their mouth through the aperture of the metal frame. Results showed that the animals did not approach the fish behind the glass during the entire session. For the final experiment, a steel net with an open section

and a Plexiglas door of the same size was spanned across the pool and the animals were required to identify and swim through the open section. A collision could be detected by shaking of the net. Two collisions only were recorded out of 100 trials.

Norris et al. (1961) were the first to perform an experiment with a dolphin's sight completely eliminated. The animal was kept in a concrete tank of 11 m diameter and was trained to wear rubber cups over its eyes. For this, several time-consuming steps had to be taken. First, the dolphin had to learn to take cut fish and then take the fish from the trainers' hands. The animal was then required to let the trainers touch the tip of its rostrum, while being given a reward. A whistle was blown afterwards as a sign of reinforcement. The trainers then moved on to the next step, first covering the dolphin's eyes with their hand in order to accustom the animal to being blindfolded and finally placing latex suction cups over its eyes. After this was achieved, several experiments were conducted to observe the animal's ability to avoid obstacles and find food when visibility was non-existent. An 18-kHz transducer emitted two bursts, which was the signal for the dolphin to locate a target in the pool, swim to it and press it with the tip of its rostrum. After successfully performing this task, the animal was rewarded with a fish, which was placed in front of a hydrophone while the dolphin was still blindfolded. A scanning of the head was observed, beginning at about 4 m from the reward. These scanning movements increased noticeably when the animal was less than one metre from the reward. The dolphin was observed scanning the area by moving its head at the beginning of the experiment. An attempt at placing a rubber foam mask over the dolphin's melon and upper jaw resulted in the animal violently shaking off the mask.

Suction eye cups were also used in several other experimental discrimination studies on *Tursiops truncatus* (Turner and Norris 1966, Johnson 1966, Evans and Powell 1966), *Phocoena phocoena* (Busnel and Dziedzic 1966) and the Pacific pilot whale (*Globicephala melaena*) (Wood and Evans 1980). To test the directional hearing of a Rough-toothed dolphin (*Steno bredanensis*), Norris and Evans (1966) trained the animal to echolocate on a fish target in a 13.7 m diameter tank while swimming between two taut lines towards the fish. The dolphin's clicks were recorded by a hydrophone and frequency and sound pressure measured. The animal emitted sound with the highest frequencies coming from in front of its rostrum and lower frequency recorded on either side of its head. Scanning movements of the dolphin's head while approaching the fish were also observed.

Johnson (1966) performed a psychophysical experiment on a trained bottlenose dolphin to determine the auditory threshold of the animal. The dolphin which had already been in captivity for two years was held in a circular wooden tank 8.2 m in diameter. It was trained to perform a standard conditioning experiment and react to a light source in the tank. If the light was turned on, the dolphin had to push a lever. If a 2-s tone was emitted afterwards from a sound source, the dolphin was required to leave the stall and push another lever. The animal had only a certain amount of time to respond and, if successful, was rewarded with a fish. Results showed that the dolphin performed the tasks successfully and that the animal was able to hear a frequency range between 75 and 150 kHz. Hall and Johnson (1971) held a 5 m long killer whale (*Orcinus orca*) in a circular pool with 13 m diameter and tried to determine its auditory threshold by training it to respond to auditory stimulus. The animal was required to submerge its head in a listening stall. A light was switched on for 15 s and an auditory signal turned on afterwards. If the animal was able to hear the sound, it was required to take its head out of the stall and push a response manipulandum on the other side of the pool. The frequencies to which the whale responded correctly in the trials were between 500 Hz and 31 kHz. No responses were observed for frequencies above 32 kHz.

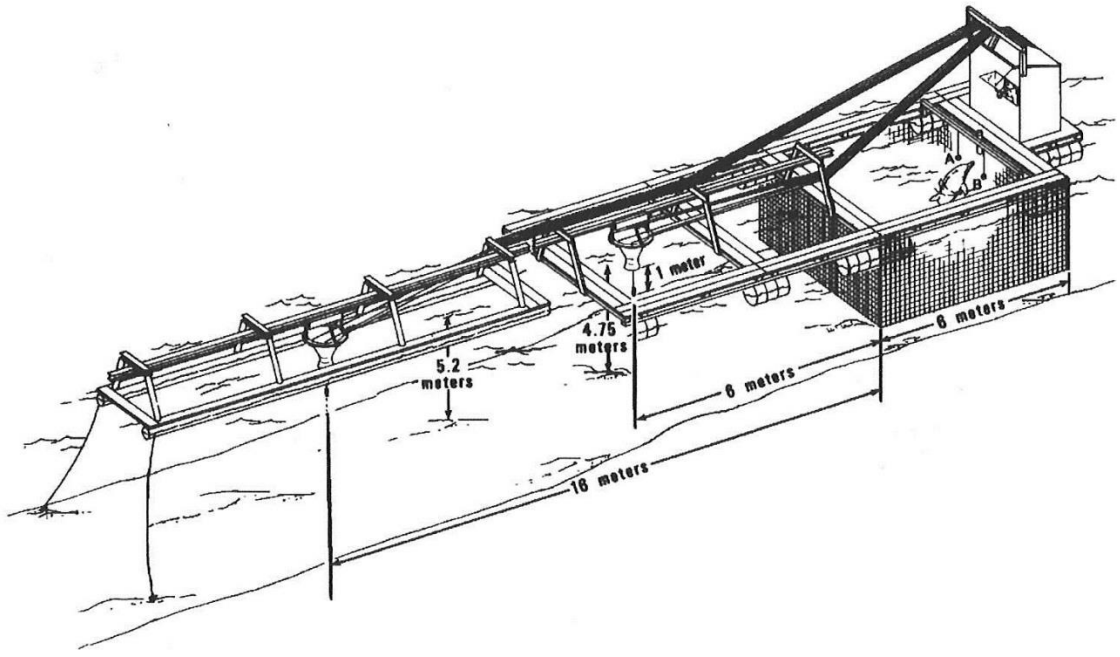

Fig 1.12: Experimental setting of a dolphin's floating pen (Hammer and Au 1990).

A three-dimensional discrimination experiment was performed on a beluga whale (*Delphinapterus leucas*) (Gurevich and Evans 1976). The animal was trained to wear a

blindfold and distinguish between two three-step pyramids, constructed of three PVC sheets with only the third and smallest step of the pyramid differing in size. The animal's mean correct response rate was 80.8 %.

Similar geometry discrimination studies were reported by other researchers (Evans and Powell 1967, Bel'kovich et al. 1969, Hammer and Au 1980, Au and Pawloski 1992). Hammer and Au (1980) investigated the ability of a bottlenose dolphin to discriminate between cylinders of different material as well as between cylinders with different diameters and internal structures. For this target-echo recognition task, the dolphin was held in a floating pen with low visibility. Two hollow aluminium cylinders with different diameters and two coral rock cylinders with the same diameter as the aluminium ones were lowered at different times from a funnel (Fig. 1.12). The animal was required to deflect one of two report balls designated to either the target indicating the presence of aluminium or the target indicating the presence of coral rock. The correct response rate during this target discrimination task exceeded 95 %. Au and Pawloski (1992) performed a similar experiment with a bottlenose dolphin and observed the animal's ability to discriminate between cylinders of different wall thicknesses. The dolphin was trained to swim to a hoop station at the beginning of each experiment and start echolocation when an acoustically impenetrable screen was lifted. The standard target was a cylinder with a wall thickness of 6.35 mm and a length of 12.7 cm. Cylinders with different wall thicknesses were placed next to the standard cylinder and the animal was required to determine the standard cylinder. It then had to strike the response paddle next to the standard cylinder. The difference between the wall thickness of the standard cylinder and the other cylinders was minimal. The dolphin's performance for a wall thickness difference of ± 0.8 mm was between 95 % and 96 %, decreasing to a 75 % correct response rate as the difference between wall thicknesses decreased to 0.23 mm and 0.27 mm respectively.

Penner and Murchison (1970) trained an Amazon river dolphin (*Inia geoffrensis*), which was held in a 7.3 m diameter circular aluminium-plastic tank and trained the animal to swim to an opaque, acoustically transparent screen after hearing a sound signal emitted at 30 kHz. If a target was present behind the screen, the dolphin was required to swim to a response manipulandum and activate it. If there was no target behind the screen, the animal had to swim to a different manipulandum. After initial training with an aluminium tube as target, a target-diameter discrimination task was performed and the animal had to distinguish between copper wires with different diameters. The animal showed a 97 % correct response rate out of 200

trials if a target with a diameter of 1.90 cm was present. For a target with a smaller diameter of 1.27 cm the dolphin demonstrated a 95 % correct response rate. A 50 % threshold of correct responses was found at a diameter of 1.12 mm. 50 % responses were regarded as chance success. Echolocation frequencies during the experiments showed frequencies between 25 and 200 kHz for *Inia geoffrensis*.

Thomas et al. (1988) performed a similar experiment with a false killer whale (*Pseudorca crassidens*). The animal was required to detect a target behind a visually opaque, acoustically transparent screen by using pulse trains. It had to rest on an aluminium crook until it received a signal to start the task and determine if a target was present or absent. When a target was present, the animal had to back out of the crook immediately. The detection performance was tested at distances of 1, 2, 4 and 6 m. Correct response rates between 90 % and 95 % were observed for distances from 1 to 4 m. The performance for 6 m was inconsistent. Scanning movements of the animal's head were observed during the experiment.

Moore and Pawloski (1990) performed a target detection experiment on a captured bottlenose dolphin in order to investigate the animal's capability to control amplitude and frequency of its emitted pulses. The study lasted three years. The animal was held in a floating pen and was required to bite a plate consisting of an acoustically transparent polystyrene material while resting its tail on a designated assembly (Fig. 1.13). This way, the dolphin's melon was positioned in a direct line to the hydrophone. The animal was then trained to emit either low- or high-frequency clicks with different amplitudes for 3 s depending on a certain audio-cue during target discrimination. Two underwater speakers determined the sound pressure level (SPL) of the animal's clicks. The dolphin was required to increase the SPL if the right speaker emitted a tone, and to decrease the level for tone emission of the left speaker. Bimodal frequency clicks were emitted when the animal produced signals with high amplitudes. Results showed a 90 % correct response for a task combining amplitude control and target discrimination. Tasks involving simply target discrimination showed correct responses of 98 %. Experiments in which the animal was required to solely control the amplitude of its clicks showed a 95 % correct performance. Frequency control tasks demonstrated an 80 % performance.

After observations of wild Dall's porpoises (*Phocoenoides dalli*) avoiding gillnets and swimming through small holes in the nets, Hatakeyama and Soeda (1990) postulated that the

animals have a high-resolution sonar capability. They subsequently captured a Dall's porpoise and tried to keep the animal in a pool for acoustic studies, resulting in the animal's decline in health and eventually its death. Five harbour porpoises (*Phocoena phocoena*), belonging to the same family as the Dall's porpoise, were then caught and their acoustical behaviour studied in a pool. A gillnet was placed in the pool with an opening at the end of the net. The harbour porpoises were observed to avoid the net and perform a U-turn before touching it. One porpoise got entangled on one occasion while turning around, injuring its caudal fin in the process.

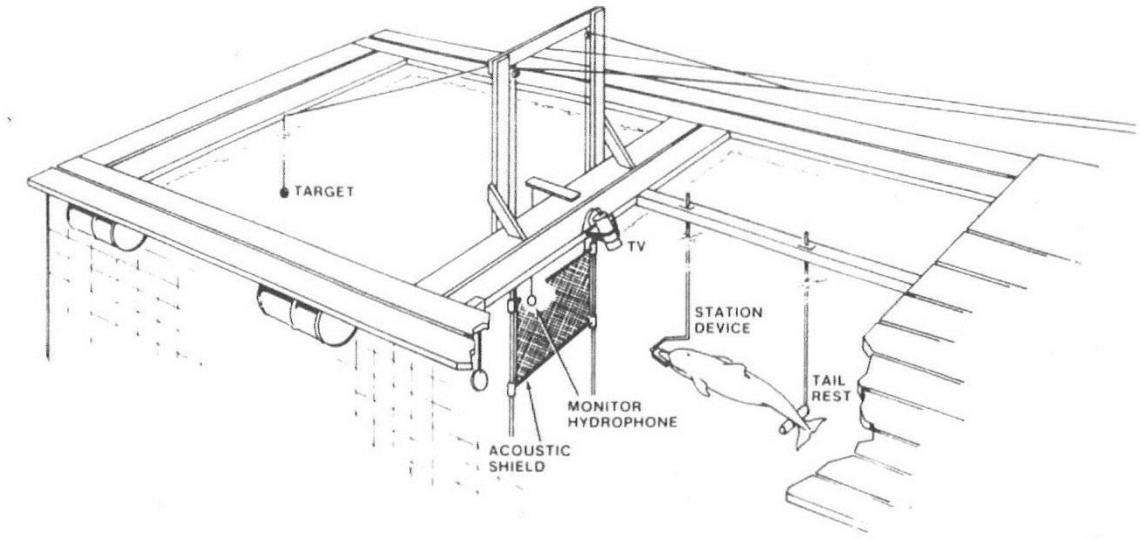

Fig. 1.13: Dolphin in a pen stationed at a bite-plate/tail rest-device. The target is behind an acoustic shield (Moore and Pawloski 1990).

After establishing that odontocetes possess a sonar system and emit sound pulses through their head, various researchers turned their focus to the possible mechanism of sound reception. The first experiments regarding the lower jaw hypothesis were conducted on captured animals. Several hearing sensitivity experiments have been performed by researchers with trained dolphins wearing jawphones over their pan bone.

Jawphones were used by Moore and Pawloski (1993) and Moore et al. (1995) to test the binaural capabilities of dolphins. A bottlenose dolphin, which had already been trained for a different experiment, was required to perform detection threshold experiments while having jawphones attached to its lower jaw in the area of the pan bone. The animal was first held in an open-bay floating pen in Hawaii and then moved to another floating pen in San Diego. For the task it was trained to swim to an underwater station and wait for a light signal indicating

the beginning of the experiment. The animal was then required to press a response ball, if a signal sound and background noise were present. If only background noise was present, it was required to remain stationary until the light was turned off. Results showed that the dolphins had a higher ability to discriminate interaural time and intensity differences at much higher frequencies compared to other mammals.

Brill et al. (1988) conducted also experiments with jawphones as well as behavioural experiments in order to examine the hypothesis of jaw hearing. A trained bottlenose dolphin was blindfolded and required to wear one of two neoprene rubber hoods over its lower jaw. One rubber hood was sound transparent, while the other attenuated incoming acoustic signals. The animal was then required to position its head in a hoop and one of two targets was lowered into the water for four seconds, three metres in front of the animal. This was done with either one of the hoods covering the animal's lower jaw. If the "go" target was lowered, the dolphin was required to immediately strike a nearby float. For the "no-go" target, the animal had to maintain stationary and wait for a signal by its trainer. The dolphin's performance decreased considerably when wearing the sound-attenuating rubber hood.

For the auditory threshold measurement, two bottlenose dolphins were required to wear jawphones placed at 41 positions on their head. The jawphones consisted of a transducer and a surrounding silicone rubber compound and could easily be dislodged at will by the animals (Fig. 1.14). For this go/no-go experiment, the animals were required to maintain stationary for a stimulus signal to be presented. The animals were trained to leave their station and touch a response paddle if a tone was emitted, and to stay at their station if no tone was presented. The auditory sensitivity was measured for tones with frequencies of 10, 30, 60, and 80 kHz. High-frequency sound was best detected by the animal along the lower jaw, while low-frequency sound was best detected near the opening of the ear canal. An asymmetric pattern of sensitivity across the dolphins' head was shown, indicating the presence of a head related transfer function (Brill et al. 2001).

Supin and Popov (1993) conducted neurophysiological experiments on an Amazon River dolphin (*Inia geoffrensis*), measuring the auditory brainstem response (ABR) in order to investigate the direction-dependent spectral sensitivity. The animal was held in a 5 x 5 m pool and released into its habitat after the experiments. Needle-shaped electrodes were inserted 3 to 5 mm into the dolphin's skin at the left and right side of the head near the auditory meatus and a reference electrode into the dorsal fin. The spectral sensitivity was measured for several

frequencies. Results indicated that the sensitivity and the response of left and right side depended on the sound frequency, with a greater spectral sensitivity for frequencies above 30 kHz.

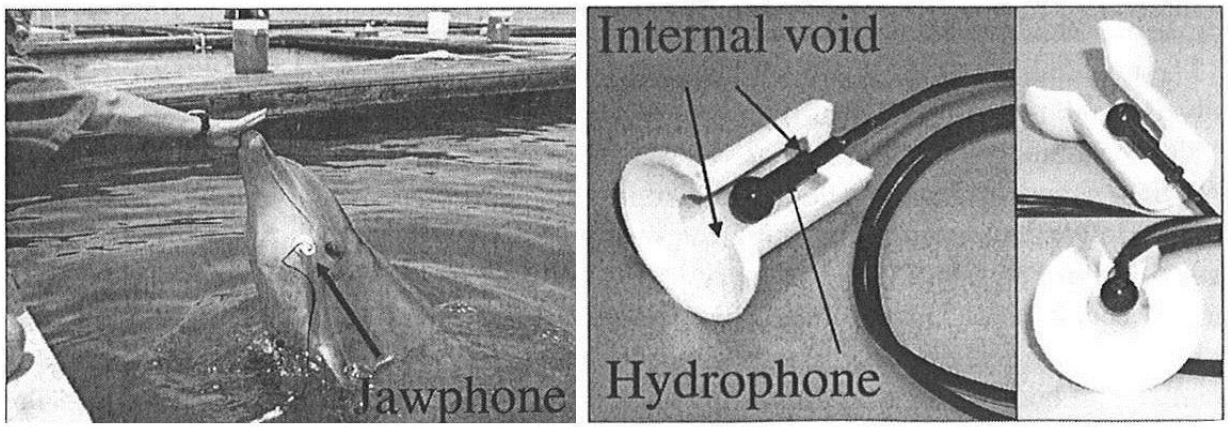

Fig. 1.14: Auditory threshold experiment conducted on a bottlenose dolphin. Jawphones were placed over the animal's pan bone to measure the sensitivity. The picture on the right shows a cutaway view of the jawphone (Brill et al. 2001).

Houser et al. (2004) performed CT scans on three living bottlenose dolphins in order to study the animals' anatomy. The animals were trained to slide out of the water onto a mat and remain still. They were then transported in a van to the scanning facilities, accompanied by several animal care assistants as well the animals' trainer and a veterinarian. The dolphins were tranquilised and structural and functional scans were performed in order to look at the animals' cranial morphology and the blood flow in the head tissue. The scans showed an extensive blood flow in the acoustic lipid of the melon and the posterior region of the lower jaw, indicating the thermoregulation of the lipid density.

Research on live dolphins shows that animals are occasionally moved from one research facility to another, sometimes even being transported by plane. This is a considerable stress factor for the animals. Captured animals also have to be looked after by veterinarians and have to be fed regularly. Their maintenance requires substantial manpower. Schevill and Lawrence (1953) avoided working with captured dolphins from the Oceanarium in Marine Studios, Florida, stating that the animals' prolonged captivity may have had a psycho-physical effect. They instead worked with a fresh-caught animal. This is also an indication of possible changes in the animals' usual behaviour during captivity. Studies on live animals, requiring for example click and whistle production or discrimination of underwater targets, have on the other hand

presented results that could not have been obtained by acoustic modelling or experimentation on dead animals.

These first behavioural and electrophysiological experiments carried out on live odontocetes showed that the animals were able to actively use sonar. After initial experiments established the way of the sound production in odontocetes, researchers began to focus on the animals' reception system and, after conducting various experiments, discovered that the lower jaw played a role in sound reception. One example was as already mentioned the performance of a blindfolded dolphin which decreased considerably, after a rubber hood was placed over the animal's lower jaw (Brill et al. 1988).

1.3.2 Experiments on postmortem dolphins

Aside from behavioural and electrophysiological studies on live odontocetes, experiments were also conducted on postmortem animals, examining their anatomy as well as studying the sound generation in odontocetes.

Evans and Prescott (1962) performed experiments on the head of two Pantropical spotted dolphins (*Stenella attenuata*) and one bottlenose dolphin (*Tursiops truncatus*) and investigated the sound production through the blowhole by forcing air through the animals' larynx. Results showed that sound was produced through the head, similar to sounds emitted by live dolphins. Similar experiments on the carcasses of dolphins were conducted by Fraser and Purves (1954) and Purves (1967), both suggesting that sound is produced in the larynx region and the nasal sacs of dolphins. Purves (1967) inserted a Galton's (or silent) whistle into the trachea of a freshly dead harbour porpoise (*Phocoena phocoena*), hourglass dolphin (*Lagenorhynchus cruciger*) and bottlenose dolphin (*Tursiops truncatus*) and analysed the sound propagation through the animals' head. He discovered that a certain air pressure led to the production of a high-pitched tone. Evans et al. (1964) tested the directional properties of sound on the carcass of a Spinner dolphin (*Stenella longirostris*) and the skull of a bottlenose dolphin in an anechoic lagoon as test site. The whole body of the postmortem Spinner dolphin was immersed into the water and strapped to a floating rig (Fig. 1.15).

The angular position of the rig was flexible and could be changed, with sound signals emitted by the hydrophones in the dead animal's body impinging on the hydrophones in the lagoon from different angles. The sound source was implanted near the naso-laryngeal system of the animal and measurements were made every 15° in the vertical and horizontal planes at

different frequencies. The same experiment was conducted on the skull of *Tursiops truncatus*. Sound produced above the skull near the nasal sacs was emitted in form of a beam out of the dolphin's head. Little sound was emitted for sound sources placed below the level of the rostrum (0°). Evans (1967) also discovered that the beamwidth became narrower with increasing frequency.

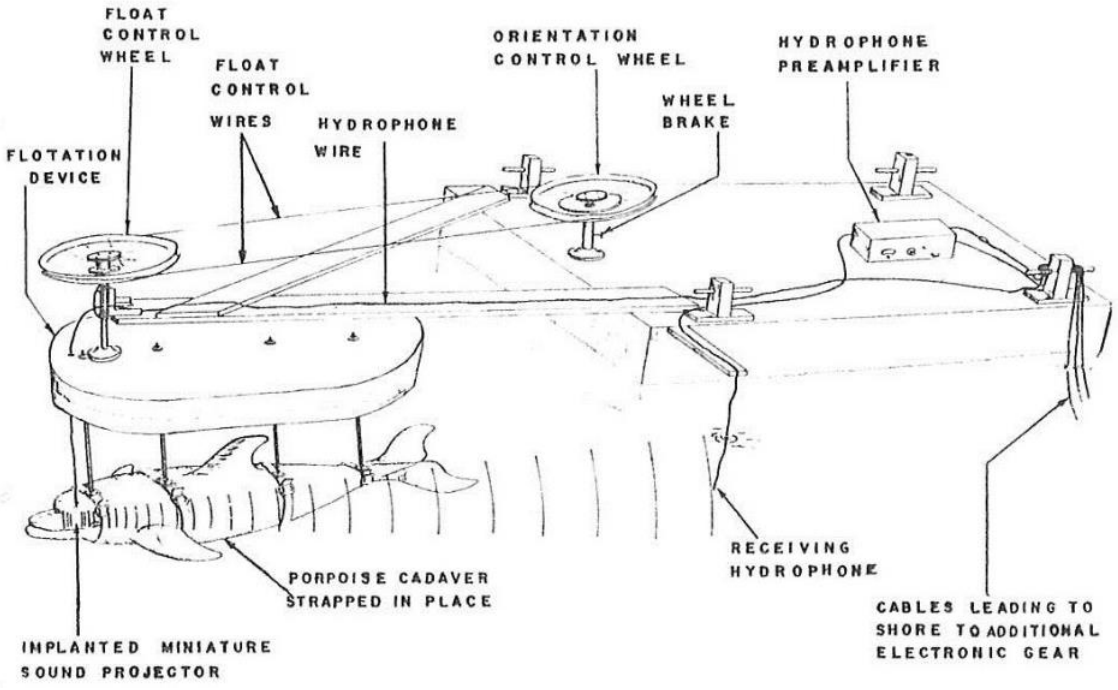

Fig. 1.15: Floating rig with dead dolphin. The hydrophone is mounted to a frame 3 m from the animal (Evans et al. 1964).

Varanasi and Malins (1971, 1972) and Varanasi et al. (1975, 1982) analysed the chemical composition of the fatty tissue in the melon and the hollow lower jaw of a bottlenose dolphin and discovered that a mixture of several lipid components resulted in a low sound velocity, with each lipid having a higher sound velocity on their own. They suggested that a low sound velocity in the melon generated a channelling effect to focus sound, sending it in a beam outward of the dolphin's head. The properties of this special fat have also been analysed by various other researchers (Blomberg 1974, Blomberg and Jensen 1976, Blomberg and Lindholm 1976).

Norris and Harvey (1974) investigated sound transmission in a bottlenose dolphin (*Tursiops truncatus*) by implanting small broadband hydrophones in various parts of a freshly dead animal's head. The head was immersed into a salt water-filled pool and short pulses were

emitted from a transducer. The sound velocity of the different tissue parts was then measured. For the transmission tests in blubber and muscle, a bottlenose dolphin was caught alive, killed and experiments begun right away on a boat in order to minimize postmortem changes in the tissue. Tissue slices were placed between two hydrophones, a sending apparatus and a receiving apparatus, and the transmission speed through the tissue samples measured. The intensity was highest on the side of the intact dolphin's head on which the transducer was emitting the signals. No signals were received in the mandibular lipid when the emitting transducer was placed in the horizontal plane of the rostrum. Sound velocity measurements of the melon showed a low velocity in the core of the melon and high velocities around it.

Zook and DiCaprio (1990) examined the auditory brainstem cells of two dolphin species, *Tursiops truncatus* and *Stenella coeruleoalba* and studied their unusual arrangement. They suggested that the cell arrangement of the ventral cochlear nucleus (VCN) and the medial nucleus of the trapezoid body (MNTB) are part of a system of delay lines. The cell rows of the VCN were found to run perpendicular to the reticulating fibres of the trapezoid body (MNTB). Different sizes of the fibres and conduction velocities could create delay lines. Cranford et al. (2008a) investigated sound reception via the throat region in odontocetes by using tissue data of postmortem animals as well as by computer modelling. They performed CT scans on two Cuvier's beaked whale (*Ziphius cavirostris*) specimens. To minimize the change in tissue quality, the heads were frozen and then scanned using X-ray CT. They were thawed and dissected afterwards and the sound velocity and elasticity of the tissue measured by Soldevilla et al. (2005).

Acoustic properties of a bottlenose dolphin's jaw bone and teeth were analysed using Laser Doppler Vibrometry (Dible et al. 2006, 2009). This non-invasive, non-contact method was used to determine the vibrational modes as well as the transverse and longitudinal sound velocity of dolphins' teeth. Piezoceramic bimorph[1] vibrational elements were attached to both sides of a freely-suspended tooth of a bottlenose dolphin in order to determine the tooth resonance in air. A 400-µs pulse was then transmitted from one element and received on the second, outgoing and incoming signals recorded and the propagation delay determined. This procedure was

[1] Bimorph devices are electromechanical transducers consisting of two active piezoelectric crystal layers aligned to each other with one expanding and the other contracting when exposed to an electric field

repeated with uni-morph elements in place of the bimorph ones. Measurements showed a strong resonance for frequencies between 115 and 135 kHz.

A possible problem with studies on postmortem animals was mentioned by MacKay (1966), who suggested that tissue properties of dead animals change due to gas bubbles generated by bacteria during decomposition, possibly affecting sound transmission in the animals. This was also investigated by McKenna et al. (2007), who analysed postmortem changes in the tissue properties of dead bottlenose dolphin heads to test the accuracy of experiments with dead dolphins and the possible distortion of the resulting data. The authors compared CT scans of one live, one freshly dead and two frozen and thawed bottlenose dolphins' heads and examined the effect of decomposition on the physical properties of the tissue, especially density and sound velocity. The data for the CT scans of the live dolphin were provided by Houser et al. (2004). The heads of the two frozen dolphins were separated from the body and put in a freezer 4-6 hours and 6-8 hours after death respectively. They had to be thawed in a water bath for 36 hours until they were ready to be scanned. The recently dead specimen was scanned 4 hours after death. Sound velocity measurements were only conducted on this animal's head. The head was cut in half, one half was frozen and the other used for the measurements. Sound velocity of the tissue was then measured using an ultrasonic digital flaw detector and longitudinal acoustic transducers. The measurements were conducted at different times after death for comparison. Results showed no significant differences in the morphological structure, tissue density or tissue sound velocity of the live, recently dead and thawed dolphins, suggesting that data obtained from tissue of postmortem dolphins are still accurate enough.

As mentioned in Section 1.1, the hypothesis of a laryngeal sound production mechanism originated from experiments on dead odontocetes and consideration of the animals' anatomy (Lilly and Miller 1961, Purves 1967, Purves and Pilleri 1986, Blevins and Parkins 1973, Schenkkan 1973). Since it is proven today that sound is produced in the nasal region and not the larynx and this proof was the result of experiments on live animals, it leads to the indication that work on dead dolphins may not be as accurate as experiments with live animals.

However, studies on live as well as on postmortem odontocetes both led to the conclusion of an active sonar system of the animals. The most recent experiments on dead odontocetes focused primarily on the throat region and the animals' teeth as sound receptor (e.g. Cranford et al. 2008a, Dible et al. 2009).

1.3.3 Acoustic modelling

The first studies on sonar systems in dolphins were conducted experimentally on trained dolphins. For this purpose dolphins had to be captured, which is an extensive undertaking. The capturing process is also stressful for the animals with the procedure occasionally resulting in physical injuries or even death (Hatakeyama and Soeda 1990). Captured dolphins are then held in pools or tanks of comparatively small sizes. Dolphins are very social animals and live in large groups called pods. Most dolphins also migrate seasonally with the length of the destinations varying. It is not possible to implement either of those conditions for the animals in a pool or tank. Today, investigations are mainly done by means of already existing data obtained from dolphin carcasses and the creation of true-to-life simulations with computer modelling. Experiments with dolphins in captivity provide on the other hand more definite results than computer models. Investigations of dolphins wearing suction cups over their eyes showed that the animals clearly do not need their eyes for navigating, finding their prey or discriminating for example between favourite and non favourite food. This could not have been observed by computer models or the analysis of a dead dolphin. Deceased odontocetes and the analysis of their anatomy are on the other hand necessary to acquire accurate data for subsequent acoustic modelling.

Research on the dolphin's tooth array concept has been conducted almost solely by computer modelling. Dobbins (2001, 2007) used a cast of a bottlenose dolphin's lower jaw and plotted the teeth in a line. He suggested that odontocete teeth act as point receivers and also as pressure transducers with the tooth nerves delaying the propagation of signals and sending them simultaneously to the central nervous system. He modelled the beam patterns for this line array by picking the front tooth on the line as 1, considering the array to lie along the x-axis in Cartesian coordinates (Fig.16).

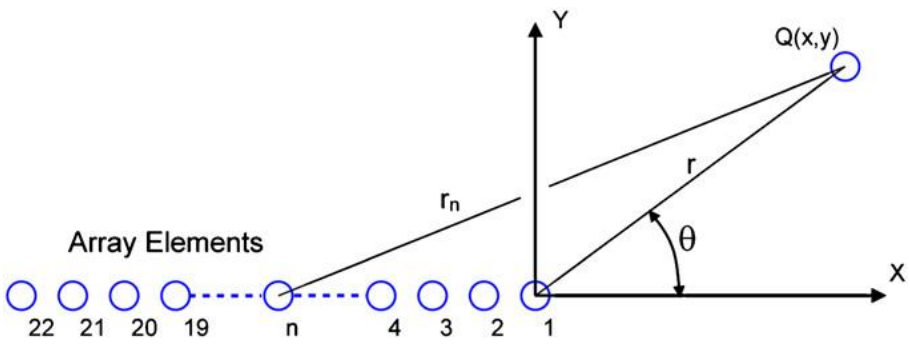

Fig.16: Tooth array geometry, beginning with the front tooth, numbered as 1 (Dobbins 2007).

Dobbins then derived the equation for the beamformer output by calculating r, which is the distance from the source Q(x,y) from tooth 1 as reference element at range r_n to the nth element at (x_n, y_n). The bearing θ is relative to the x-axis. $r_n = \sqrt{(x - x_n)^2 + (y - y_n)^2}$, with x = r cos θ and y= sin θ. The results gained from Dobbins' modelling indicate that dolphins' teeth may act as sonar receiver.

1.4 Aims and Objectives

The aim of this PhD is to further the understanding of the sound reception of a bottlenose dolphin (*Tursiops truncatus*) by investigating the role of the teeth in the animal's directional hearing. Previous research indicates that the lower jaw plays an important role in dolphin hearing. Although there was no exact analysis, researchers believed that odontocetes pick up sound waves through the fatty tissues of the lower jaw. The assumption of the teeth being a receptor appeared for the first time in 1990 (Goodson and Klinowska); however, there was no specific research on this hypothesis until recently. The aim of this PhD is to follow up the hypothesis of Goodson and Klinowska (1990), Dobbins (2001, 2007) and Dible et al. (2009) and develop different methods by means of which the role of the teeth in sound reception could possibly be resolved.

The objectives of this thesis are:

- Measuring the diameter of the teeth as well as the spacing between teeth on the basis of a bottlenose dolphin's lower jaw cast with teeth. Two different tooth diameters will be chosen, at the tip and above the gum line.
- Creating a 2-D tooth array model in Matlab with the teeth as solid circles, projected onto a constant sound velocity background with 1490 m/s for sea water. A plane wave will be created to propagate through the tooth model, calculating the pressure around the teeth
- Pressure distribution at each tooth will be measured and compared. This will be performed for two different frequencies of the plane wave as well as different angles of the tooth array.
- Pressure distribution at the teeth will be measured for a tooth array model with several teeth missing.

Questions that will be investigated are:

1. Is there a difference in sound pressure for an incident sound wave with the frequency in which a bottlenose dolphin whistles and echolocates?
2. Does a change of the size of the area the sound wave impinges on have an effect on the sound pressure and to what extent? Tip and bottom of the teeth are in this case chosen as an example.
3. Is there a difference in sound pressure at the teeth after the sound wave impinges on different angles of the dolphin jaw?
4. Are there characteristic features in the sound pressure around the area of the gular pathway?

2 Acoustic Pathways in Cetaceans

2.1 Lower jaw

As outlined in Chapter 1, there are three main hypotheses on how odontocetes may receive sound: through the lower jaw, the teeth or the throat region. These hypotheses will be addressed in more detail in this chapter. The odontocete tympanic membrane, also called tympanic ligament due to its conical structure, is not connected to the external meatus (Wever et al. 1971a, 1971b, 1972; Ridgway et al. 1974). First implications of the larynx as pathway for receiving sound have been excluded after experiments on live dolphins showed no response in the laryngeal region during sound production (see Chapter 1). This led to the assumption that the ear itself is not the primary acoustic pathway to the inner and middle ear.

That the lower jaw plays a role in sound reception has been demonstrated in several behavioural and electrophysiological experiments (e.g. Norris 1964, 1968; Møhl et al. 1999; Houser et al. 1999, 2004; Aroyan 2001). Over the last decades it has been suggested that either the fatty tissue in the hollow lower jaw or the lower jaw bone itself is the primary pathway to the inner ear for acoustic signals.

Norris (1964, 1968) was the first to suggest that toothed whales receive sound through a region in the animals' lower jaw which he subsequently called the "acoustic window". He pointed out that the fatty tissue in the pan bone led directly to the tympanic bulla and suggested that sound penetrates the thin pan bone of the rear mandible, enters the mandibular fat body and is then transmitted to the middle ear. According to Norris (1980), the angle at which sound hits the dolphin's lower jaw is important for an optimum transmission into the fat body. He suggested that this angle of incidence is between 15° - 30°. Another explanation for the pan bone as sound-receiving feature is the consistence of the fatty tissue overlying the mandibular bone. This tissue is nearly completely devoid of muscle strands and directly overlies the thinnest part of the mandible (Norris 1980). Biochemical experiments showed that the lipid, which occurs also in the melon of odontocetes, is not homogenous and that it has a very low sound absorption (Varanasi and Malins 1971, 1972). Its unusual composition of wax esters and isovaleric acids (iso5:0) is uncharacteristic for mammalian fatty tissue. Iso5:0 consists of 5 carbon atoms and has a branched structure, which is unusual for fatty acids (FAs), typically unbranched and comprised of long straight chains with an even number of carbons (Stryer 1995). Houser et al. (1999, 2000, 2004) investigated these specialized lipids by performing

Computed Tomography (CT) scans as well as Single Photon Emission Computed Tomography (SPECT) and Positron Emission Tomography (PET) scans on live bottlenose dolphins. CT scans showed the animals' cranial morphology, while SPECT scans displayed the blood flow in the head tissues and PET was used to analyse the relative metabolic activity within the cranial tissues. Melon, brain and posterior region of the mandible displayed an extensive blood flow, the melon showing a four times greater blood flow than the brain. Houser et al. (2004) suggested that the blood flow in these tissues served as a form of thermoregulator for lipid density, impacting the sound velocity within the lipid and thereby the sound emission and reception pathways. The density of lipids decreases with increasing temperature, sound velocity in these lipids decreases therefore also with increasing temperature. The effect of the temperature of the melon lipid of a deceased dolphin on the sound speed was also shown by Fitzgerald (1999), who measured sound velocities of 1390 m/s and 1280 m/s for temperatures of 10°C and 40°C respectively. Sound velocity was thus inversely related to the temperature of the acoustic lipids. Since these findings imply that sound velocity entering the lipid of the lower jaw also decreases with increasing temperature, it implicates as well that the hearing accuracy of dolphins decreases with increasing temperature.

Aroyan (2001) created a 3-D model of sound propagation in a common dolphin's (*Delphinus delphis*) head, simulating sound emission and reception pathway for a frequency of 50 kHz with the sound beam coming from the forward direction of the head. The author used data from CT scans of the deceased dolphin's head, first examining sound propagation through the head without peribullar cavities, pterogyoid sinuses, soft tissues or acoustic fats, then without soft tissues and lipids and finally the entire head including the lower jaw fats. The results for sound propagation in the entire head including the lipids showed that receptivity patterns increased in the forward direction, which led to the indication that the fat bodies serve as a channel, focussing sound towards the tympanoperiotic complexes. Figure 2.1 illustrates the locations of the pterygoid and peribullar plexus, intramandibular fat body plexus and the anterior lobe.

Koopman et al. (2006) examined the topographic distribution of these unusual composed lipids in two Gervais' beaked whales (*Mesoplodon europaeus*), one Sowerby's beaked whale (*Mesoplodon bidens*), one Atlantic spotted dolphin (*Stenella attenuata*), one harbour porpoise (*Phocoena phocoena*) and one Pygmy sperm whale (*Kogia breviceps*). They found higher concentrations of wax esters and short branched-chain Fatty Acids (FA) in the centre of the

animals' inner mandibular fat body, connected directly to the ears. Sound travels slower through these short branched-chain FA, that are found in the form of triacylglycerols (TAG) and wax esters, than through longer straight-chain FA. This led to the authors' assumption that the topographical arrangement of the lipids function as a channel for incoming sound with sound bending towards the inner low-velocity fat centre, then propagating through the short branched-chain FA and finally to the middle and inner ears.

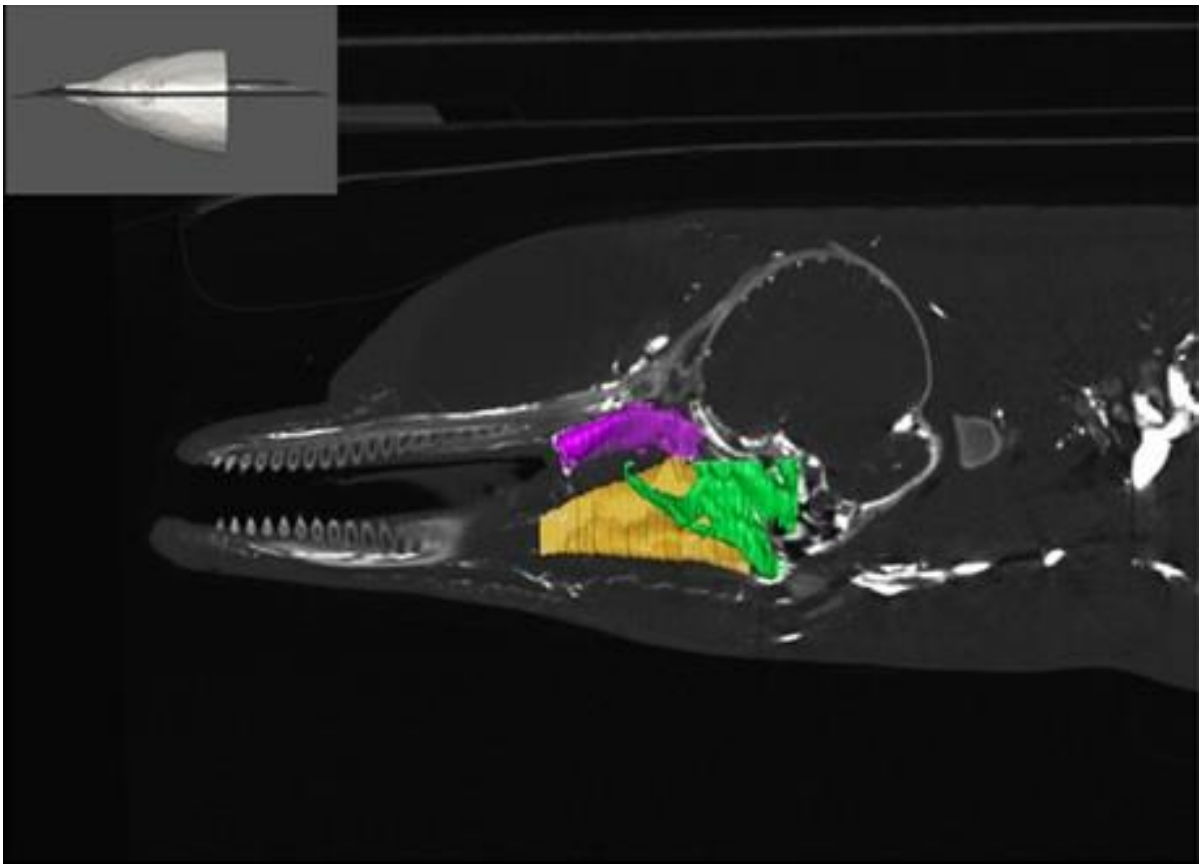

Fig. 2.1: Sagittal view of a bottlenose dolphin's head, showing the locations of the pterygoid and peribullar plexus (green), intramandibular fat body plexus (yellow) and anterior lobe (purple) (adapted from Costidis and Rommel 2012).

Zahorodny et al. (2009) analysed the acoustic lipid for different age classes (from foetus to adult) in 10 bottlenose dolphins and found that these unusual lipids and their spatial arrangement occur in all age classes, although in lower concentrations in younger dolphins. In contrast to other odontocete species, bottlenose dolphins showed a uniform spatial distribution of FA in the inner jaw fats. Analyses of cranial blubber superficial to the outer jaw fat showed atypical high concentrations of iso-acids in a small region, suggesting an acoustic function for this tissue part rather than the usual metabolic one. Zahorodny et al. (2009) believed this region

to be the entry point for sound. Blubber usually shows stratification and is comprised of high concentrations of polyunsaturated FA of dietary origin in the inner layers and endogenous FA in the outer layers (Koopman 2007), which was not the case for the cranial blubber. Costidis and Rommel (2012) analysed the vascular anatomy in a bottlenose dolphin's head and observed an extensive vascularization in the animal's melon and its intra- as well as extra-mandibular fat body. Mammalian fats are usually poorly vascularized; the authors suggested that the notable venous plexus of the fat bodies in odontocetes plays therefore a physiological and pathological role.

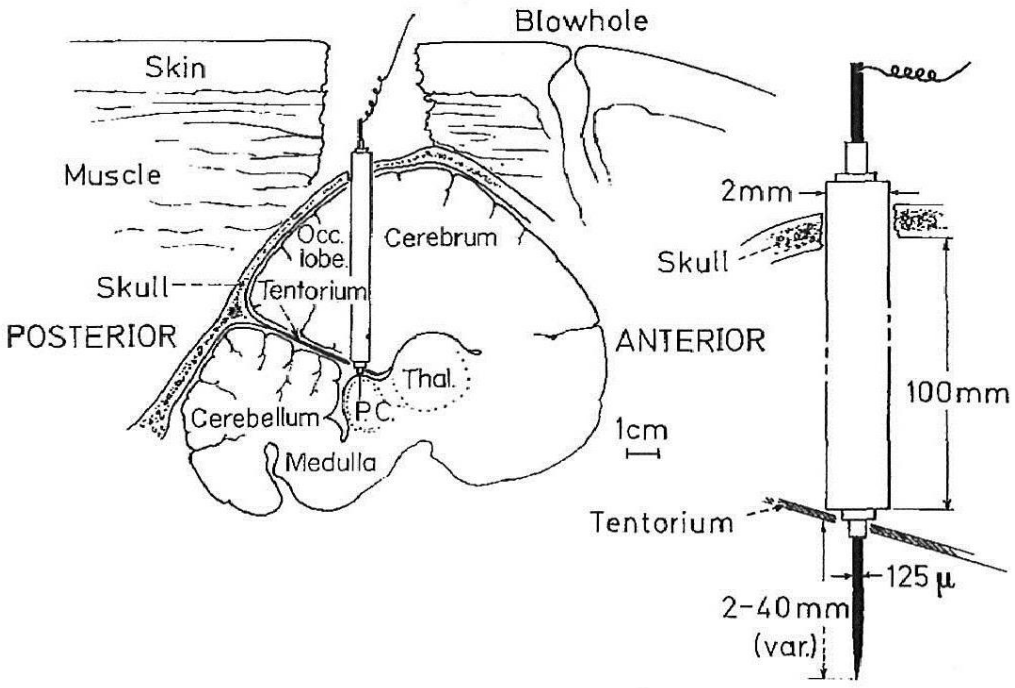

Fig. 2.2: Sagittal section through a dolphin head, showing the location of the electrode in the brain (Bullock et al. 1968).

Electrophysiological studies were conducted by Bullock et al. (1968) on twenty-nine dolphins, the Pantropical spotted dolphin (*Stenella attenuata*), the Rough-toothed dolphin (*Steno bredanensis*), the Pacific bottlenose dolphin (*Tursiops gilli*), and mainly on the striped dolphin (S*tenella coeruleoalba*). The animals were anesthetised and electrodes surgically implanted into parts of their brain: the inferior colliculi and auditory nuclei ventral to the colliculi (Fig. 2.2). Hydrophones were held against the dolphins' head and the generated potentials from the midbrain auditory structure measured. Auditory stimuli were first presented via sound produced in air and then by means of a transmitting hydrophone, which was held

against the surface of the animals' head. Largest potentials were measured when sound was emitted in the vicinity of the contralateral lower jaw. Only slightly smaller potentials were recorded for the ipsilateral lower jaw and ipsilateral melon. A decrease in the potential response was observed when a small cardboard or foam rubber sheet was held between the loudspeaker and the lower jaw or melon, functioning as an acoustic shield. High frequency emissions between 6 – 100 kHz showed no response at the external auditory meatus. Experiments with a hydrophone held against the surface of the head showed the same results as the airborne stimulus. The sensitivity was 10 dB higher than at any other point on the outside of the lower jaw when the hydrophone was placed under the animals' tongue. Sensitivity was highest for a frequency of 60 kHz and high for frequencies between 20 – 70 kHz. These results led to the authors' assumption that the best pathway for sound to the inner ear was via the lower jaw.

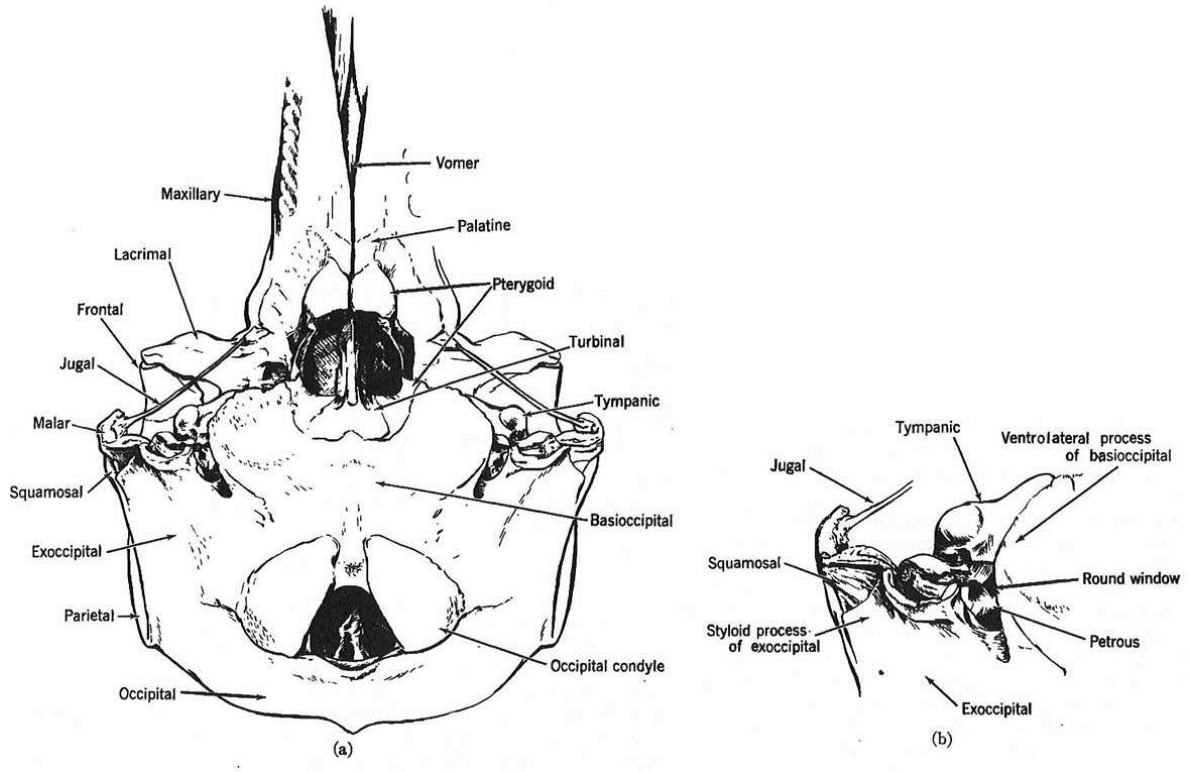

Fig. 2.3: (a): The skull of a bottlenose dolphin. (b): Enlarged view of the region of the petrotympanic complex with the round window (adapted from McCormick et al. 1970).

McCormick et al. (1970, 1980) investigated sound propagation in bottlenose dolphins (*Tursiops truncatus*) and Pacific white-sided dolphins (*Lagenorhynchus obliquidens*) by performing a similar electrophysiological experiment to Bullock et al.'s (1968). The animals were anesthetised and electrodes inserted into the inner ear and placed on the surface of the

round window membrane (Fig. 2.3). The electrodes consisted of a fine wire with a tip of 0.5 mm diameter. Airborne and underwater sound with frequencies between 5 and 100 kHz as well as mechanical vibrations was used as stimuli. Highest sensitivities were measured for sound arriving near the ear and at the side of the lower jaw, leading to the indication that sound is conducted through the lower jaw bone and then transmitted to the ear. The best sensitivity was reported for frequencies between 20 and 30 kHz.

The authors also concluded that the external auditory meatus (EAM) was vestigial and could therefore not be involved in sound reception. When holding a vibrator against one of the front teeth of the dolphin's mandible, McCormick et al. (1970) measured large electric potentials in the organ of Corti in the cochlea. Behavioural experiments on the lower jaw hearing were conducted by Brill et al. (1988). A bottlenose dolphin (*Tursiops truncatus*) was trained to perform an echolocation task while wearing suction cups and one of two rubber hoods, which covered the entire lower jaw (Fig. 2.4), excluding the EAM.

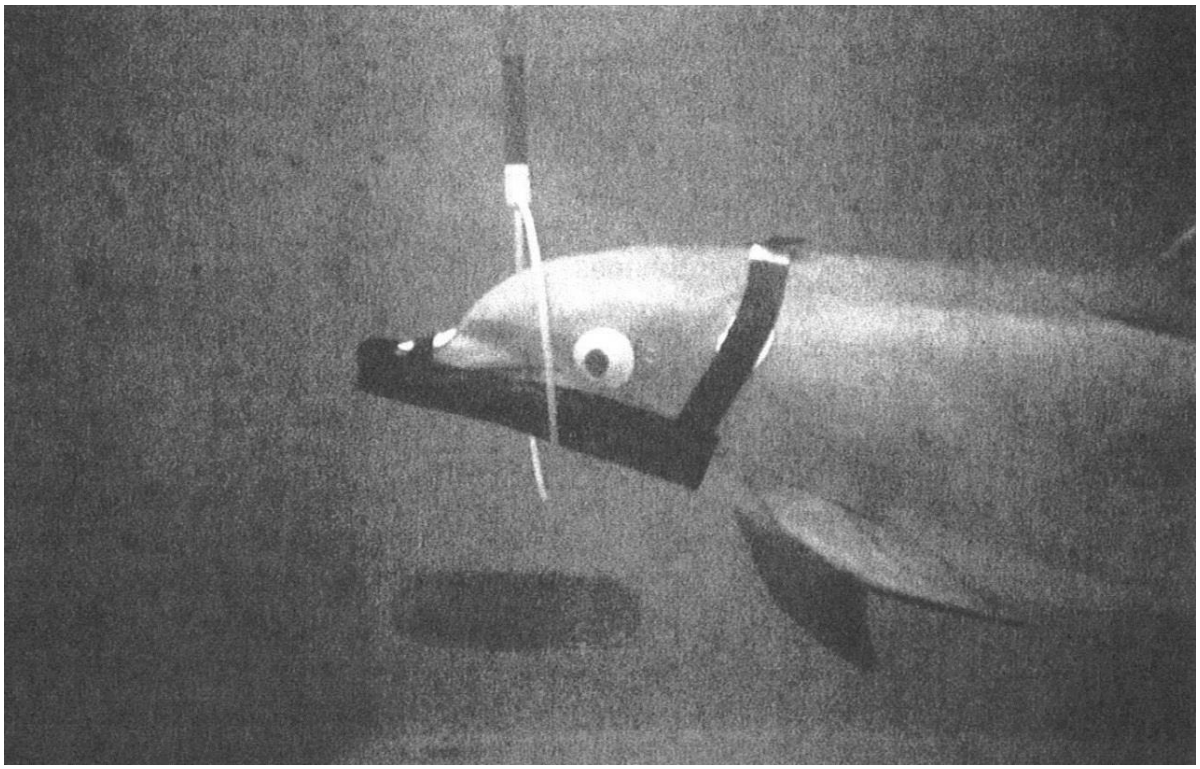

Fig. 2.4: Bottlenose dolphin with eyecups and rubber hood over the lower jaw (Brill et al. 1988).

One rubber hood let sound pass, while the other attenuated receiving signals. Acoustical stimuli presented to the lower jaw showed that the animal's performance was hindered when wearing the acoustically opaque hood. Since the EAM was not covered during these

experiments, the authors suggested that it did not play any role in the dolphin's performance at the target discrimination tasks. They concluded however that the involvement of the EAM in sound reception may be frequency-dependent and possibly play a part for frequencies below 30 kHz. Moore and Pawloski (1993) and Moore et al. (1995) were the first to use jawphones, transducers imbedded in suction cups, in order to measure the auditory sensitivity of a bottlenose dolphin. Contact hydrophones were attached to various places of the surface of the lower jaw and the animal trained to perform several detection tasks. A train of clicks was used as stimulus for Interaural Time Difference (ITD) and Interaural Intensity Difference (IID) thresholds and the dolphin's ability to detect these interaural differences was measured. The animal presented a superior binaural capability compared to other mammals previously tested. Contact hydrophones similar to jawphones were also used by Møhl et al. (1999). Piezoelectric transducers embedded in suction cups were attached to the surface of a bottlenose dolphin's lower jaw and the click of a dolphin was used as stimulus. Electroencephalograph electrodes recorded the Auditory Brain-stem Response (ABR) of the animal. The ABR electrodes were placed below the contralateral meatus and on the melon. The entire lower jaw showed a good sensitivity with maximum sensitivity recorded for sound sources at about 25 cm behind the tip of the jaw. A minimum delay was recorded at the rear of the lower jaw, below the ear (Fig. 2.5).

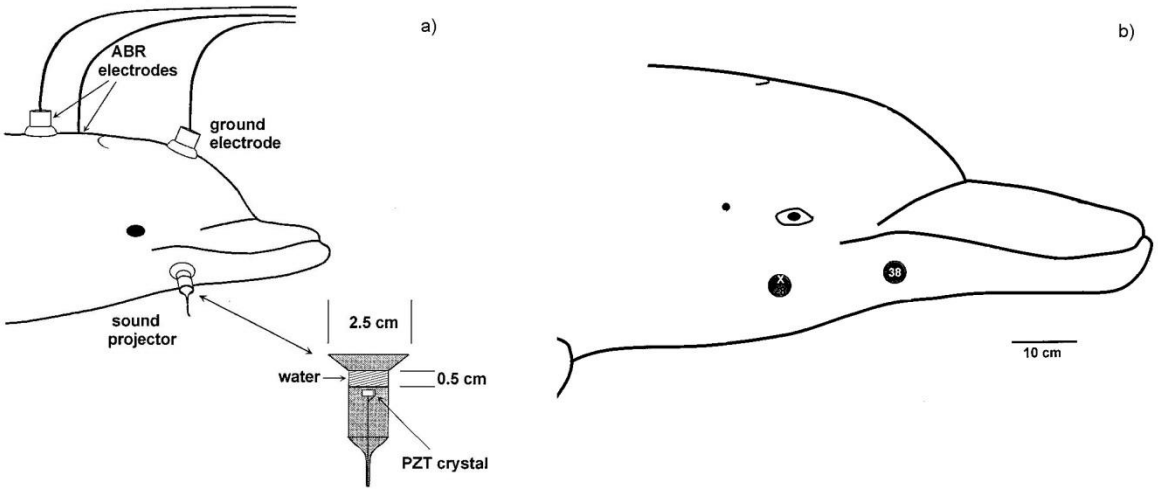

Fig. 2.5: a) Piezoelectric transducers are attached to the surface of a bottlenose dolphin's head; b) Points of stimulation; the point marked with an x is the position of minimum delay. The point marked 38 is the point of maximum sensitivity (Møhl et al. 1999).

Stimulations to the inside of the lower jaw showed sensitivities similar to those of the outside. These findings led to the indication of acoustic sensitivity to the inside of a dolphin's mouth.

Au and Moore (1984) investigated the receiving beam patterns in a bottlenose dolphin for different frequencies in both the horizontal and vertical plane. The wider the beam the more noise will be received with the returning echo; narrower beams lead therefore to better localization ability. For the experiments, the dolphin had to maintain stationary on a bite plate device. It was trained to turn its head to the side for measurements in the vertical plane. A sound transducer was positioned on an arc, 3.5 m in front of the animal at approximately the same level as the pan bone. A noise transducer was also attached to the arc, but moved accordingly in order to investigate the relation between the angle of incidence on the animal's head and its hearing threshold. Results showed 3-dB beamwidths of 59.1°, 32° and 13.7° for the horizontal plane and beamwidths of 30.4°, 22.7° and 17.0° for the vertical plane for frequencies at 30, 60 and 120 kHz respectively, indicating that the localization capability of the animal is dependent on the frequency.

As seen earlier in this section, experiments on the jaw hearing hypothesis were mainly conducted behaviourally and biochemically. However, a few researchers used numerical methods to investigate this hypothesis. Aroyan et al. (1992) constructed a simulated 2-D model to investigate dolphin sonar signal generation and emission. Using the same methodical approach, Aroyan created a 3-D model of a common dolphin's (*Delphinus delphis*) head and lower jaw tissues from the x-ray CT scan data and simulated the propagation of sound coming from in front of the animal's head (Aroyan 2001). The CT data were linearly interpolated and the sound propagation simulated numerically, integrating the acoustic wave equation. Finite-difference time-domain (FDTD) analysis, which is due to its simplicity a widely used simulation tool of electromagnetic problems, was used to propagate the solution of the linearized wave equation forward in time. The timestep of the FDTD is constrained by the Courant-Friedrichs-Lewy (CFL) stability condition, which puts a limit on the timestep, therefore making the simulation very time consuming. Another limiting factor of the FDTD is its pronounced numerical dispersion. An advantage of FDTD is its simple and robust numerical algorithm. Also, in case of a broadband pulse as source, FDTD requires only a single simulation in order to get the response of the system over a wide range of frequencies. However, unlike

finite element methods (FEM), finite difference methods are disadvantageous when it comes to more complex problems. To reduce the reflection from the grid edges, Aroyan (2001) used a third order Halpern and Trefethen absorbing boundary condition (ABC). ABC techniques are more general than for example perfectly matched boundary layers (PML) and not as numerically efficient. The suppression of reflection at the grid edges of PML is independent of the frequency of the incident wave, which is not the case for ABCs. A limitation of Aroyan's approach was also his simplified approximation of tissue properties. Tissues as well as jaw bones were modelled as inhomogeneous fluid. The author also ignored shear wave modes, which are damped in soft tissues, but may be necessary for the acoustic propagation through bone.

A numerical approach was also used by Houser et al. (1999, 2000). The authors created a biomimetic model of a bottlenose dolphin's ear by using evolutionary computation. The goal was to develop an optimal frequency-dependent Gaussian filter across the range of dolphin hearing in order to implement it as a signal pre-processor in biosonar models. The bandpass ear-filter model consisted of overlapping frequency-domain filters, constructed to calculate the auditory sensitivity threshold of the dolphin. A major strength of evolutionary computation is its simplicity and flexibility. It is a self-adaptive algorithm; robust and adapting easily to changing situations. Evolutionary computation is most suitable for problems where multiple solutions are required (Fogel 1997). A limitation of the algorithm is its efficiency loss when applied to simple problems. Houser et al. (2000) combined evolutionary programming with a Cauchy mutation operator, which was implemented to generate the variables controlling filter shape and distribution. This combination has the prospective for creating better solutions, but with less computational effort (Chellapilla 1998).

2.2 Teeth as receptors

Observations of odontocetes show that the arrangement of their teeth is highly regular. Bottlenose dolphins (*Tursiops truncatus*) for example have 20 to 28 small conical teeth on each side of their jaw, with each tooth about 1 cm in diameter at the base. The teeth are typically evenly spaced and lie in a straight line along the jaw bone. The space between teeth is about 11.4 mm. The jaw does not consist of flat teeth for grinding, as in other predators (Uhen 2002). The size of the nerve generally indicates the number of individual neurons it contains, or the diameter of those neurons. That dolphins' teeth may play a role in sound reception was first

suggested by Goodson and Klinowska (1990). They hypothesized that the tooth spacing and jaw geometry of odontocetes enhanced the target detection performance and that the tooth nerves acted as pressure sensors, transmitting sound signals to the central nervous system (CNS) with a delay. The authors also suggested that the teeth act as passive resonant receiver, combined as two equi-spaced line arrays with the tooth nerves introducing progressive propagation delays (Fig. 2.6).

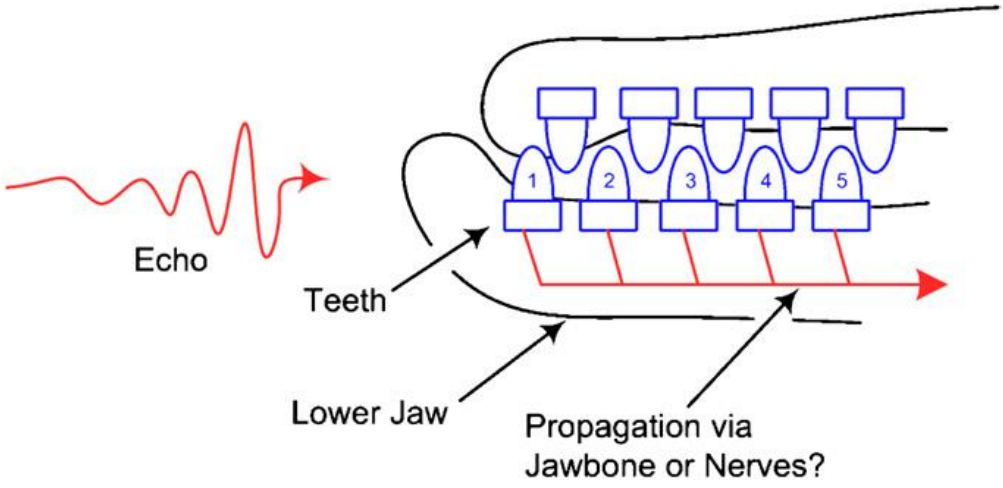

Fig. 2.6: Sound signals arriving at the front of a dolphin's jaw are received by the teeth of the lower jaw, then propagating simultaneously along the tooth nerves (Dobbins 2007, adapted from Goodson and Klinowska 1990).

In man-made sonar systems, multiple sensors arrayed together reinforce detection. Goodson and Klinowska (1990) suggested that the uniformly spaced teeth of odontocetes act as kind of end-fire array with peak sensitivities occurring in the same direction as the line of the teeth. This end-fire array is particularly advantageous for the short range detection of targets.

Conduction velocities measured for the tooth nerves of cats were slow compared to the sound velocity of water. The fastest intradental nerves of cats showed sound velocities between 30 and 45 m/s (Anderson et al. 1970). Smaller nerve fibres in human teeth and in their mandibular nerve were reported to have conduction velocities between 1 and 40 m/s. A sound velocity of 40 m/s was measured in a human's tooth pulp, conduction speeds between 80 and 100 m/s were measured in proprioceptive nerve fibres. (Matthews 1977). Myelinated nerves in humans had conduction speeds of 120 m/s. These comparatively slow propagations led to the indication of a delayed response in the tooth nerves. Once the tooth nerves exit the teeth, they propagate parallel to each other as part of the mandibular and then trigeminal nerve to the CNS,

which shows that the signal arrival times at the pons (a structure located at the brain stem) depend on the individual nerve length. Results showed an enhanced sensitivity at the front of the tooth array and a beamwidth between 25° and 30° at 120 kHz, with a 12° overlayed sector of the beam patterns (Fig. 2.7).

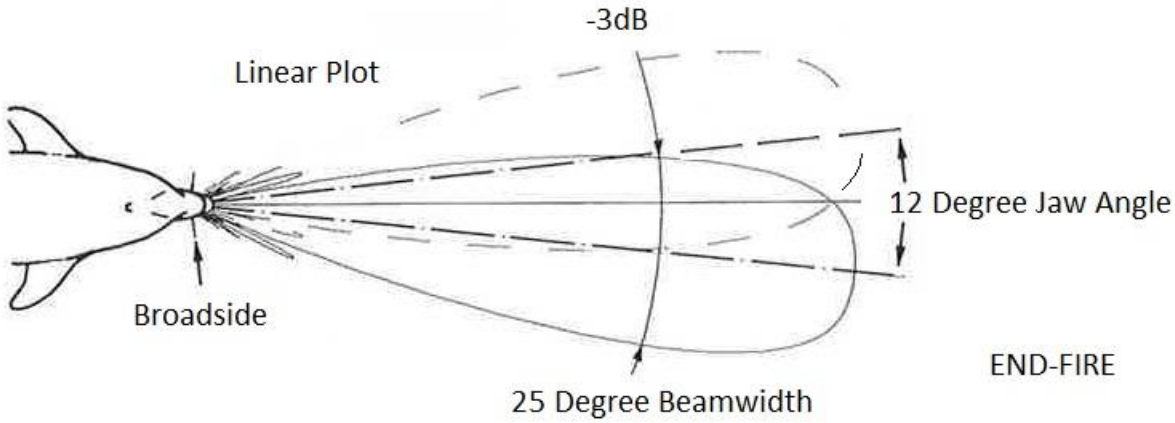

Fig. 2.7: Sensitivity beam patterns at 120 kHz, with overlayed beam for each side of the jaw (adapted from Goodson and Klinowska 1990).

Potter and Taylor (2001) investigated the possible role of the teeth in connection with either the tooth nerves or bone conduction in sound reception. Using tooth space measurements of a bottlenose dolphin, they created a single array model as a parabolic curve, taking all the teeth of both lower and upper jaw into account. The sensitivity was measured for frequencies between 100 and 170 kHz and a sound wave coming from 0° to 30° to one side of the array, with 0° being directly in front of the array. Results showed a high sensitivity at 160 kHz with a double-sided beamwidth of 4° at -3 dB. For the simulations on tooth nerves, the authors considered 100 m/s to be the most likely speed for dolphins' dental nerves. Results showed no distinguished peaks or stable coherent lobes, leading to the authors' suggestion that the tooth nerves play no particular part in sound reception.

Pointing out that the sound velocity in bone is faster than in nerves, they proposed instead that sound is transmitted via the jaw bone. A dolphin's tooth consists of a gomphosis, a fibrous mobile joint that binds the teeth to a bony socket. A small gap between the root of the tooth and its socket permits the root to be pressed into the socket during biting, thereby possibly transmitting a form of proprioception or movement via the trigeminal nerve. The function of the teeth was therefore not as a resonator. Potter and Taylor (2001) assumed the bone

conduction speed for dolphins to be between 1900 and 3300 m/s, basing these values on measured conduction speeds of human bones. Results showed a coherent sensitivity for a velocity of 1900 m/s for sound arriving between 25° and 35°.

Dobbins (2001, 2007) supported Goodson and Klinowska's (1990) theory of the teeth functioning as an end-fire array, but considered the transmission of signals via the tooth nerves as less possible. He suggested instead that the teeth act as passive resonators. Using the cast of a bottlenose dolphin's lower jaw, he created a model with the teeth plotted as Cartesian coordinates. Two lines were drawn between the teeth for each side of the lower jaw, excluding the front teeth in order to get straight lines, which created a 12° angle of the diverging jaw (Fig. 2.8). Dobbins considered the two rows of teeth to act as a line array, including an incremental delay for each tooth. Beam patterns for a 22-teeth array with 1-cm tooth spacing for frequencies of 50 and 120 kHz showed a beamwidth of 40° for 50 kHz and 26° for 120 kHz. The beamwidths for ranges of 3 m, 1 m, 0.3 m and 0.1 m demonstrated that the directivity still maintained in near field, although a wider beamwidth of 45° was measured for a close range of 0.1 m.

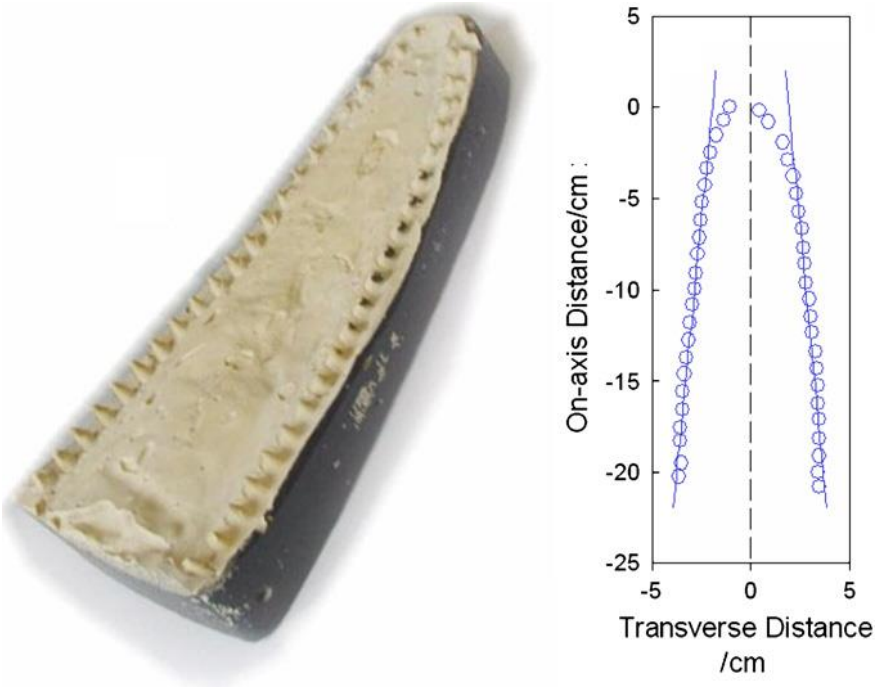

Fig. 2.8: Left: Cast of the lower jaw of *Tursiops truncatus*. Right: Teeth plotted as circles in a Cartesian coordinate system, with two lines drawn between the teeth of each side of the jaw, excluding the three front teeth on each side (Dobbins 2007).

Dobbins also suggested that the end-fire array model could be combined with monopulse localization. Monopulse is a "concept of precision direction finding of a pulsed source of radiation" (Rhodes 1959). This would provide a system operational at short range. Combining the rows of the teeth in a monopulse configuration gives an accurate angular resolution but with wide beams for rapid searching.

Nelson (2005) looked into the possible role of teeth in sperm whale (*Physeter macrocephalus*) echolocation. He modelled the dental geometry of the lower jaw of sperm whales and found an offset between the teeth on either side of the jaw, which is an important feature of an acoustic receiving dental array. Measurements at the sperm whale's teeth also showed resonances at the animal's echolocating frequency. The concept of the dolphin's jaw and teeth functioning as an array was also mentioned by Dible et al. (2006, 2009). First experiments on a bottlenose dolphin's teeth showed that the teeth were resonating, leading to the suggestion that they may play a role in sound reception (Dible et al. 2006). The speed of sound in a bottlenose dolphin's tooth was determined by means of Laser Doppler Vibrometry (LDV). A Laser Doppler Vibrometer is a non-contact velocity transducer, measuring the Doppler Shift frequency of a beam backscattered by the surface of a vibrating object, converting the Doppler signal into the velocity of the object. The LDV tests were performed on two mid-size teeth and the tooth resonances for a freely-suspended tooth were examined.

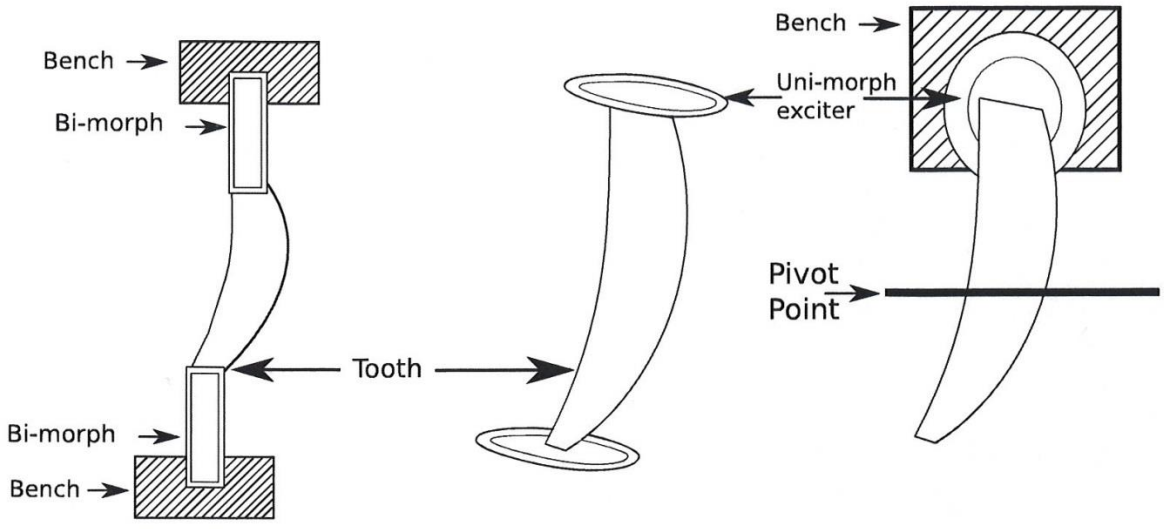

Fig. 2.9: Setup of two bi-morph vibrational elements attached to the ends of a dolphin's tooth (adapted from Dible 2008).

For the transverse mode, two piezoceramic bimorph vibrational elements were attached to the ends of the tooth and a pulse with a frequency of 100 kHz was transmitted from one of the elements and received by the other. This test was then conducted with two unimorph elements, consisting of one active and one inactive layer, in order to receive measurements for the longitudinal (compressional) mode (Fig. 2.9). The propagation delay was then measured with an oscilloscope and the sound velocity calculated. Velocities for the transverse and longitudinal propagation mode were 2200 m/s and 3380 m/s respectively. Strong resonant modes in the teeth were detected at 115-135 kHz, which is the frequency range bottlenose dolphins echolocate in.

The hypothesis of the teeth as sound reception pathway was tested mainly by acoustic modelling. While Goodson and Klinowska (1990) approached this hypothesis by using an idealized version of the tooth array, other researchers ran simulations using an actual model of a dolphin's jaw including teeth, which provided results closer to realistic conditions (Dobbins 2006, Dible et al. 2009). Goodson and Klinowska considered the teeth to act as either multiple sensor arrays or passive resonant elements and investigated the possibility of tooth nerves acting as pressure sensors. For the teeth acting as sensor array, they considered a continuous wave as ensonifying signal and the simultaneous contribution of all elements. This is not the case for a typical click signal and consequently proved to be a disadvantage of their 2-D model. The authors did not take tissue, gum or mandibular bone into account for their studies, focussing solely on the teeth and tooth nerves of odontocetes. Another limitation of their approach was that they made the assumption of a low sound velocity in odontocetes' intradental nerves by merely looking at sound velocity data of intradental nerves in cats instead of having the actual values. This was also the case for Potter and Taylor (2001), who estimated the values for dental nerve and bone speed of dolphins by comparing data of humans and cats, then taking the most likely speed. Another limitation of their 2-D model was the simulation of the teeth of a bottlenose dolphin as points on a parabolic curve. This was a very simplified modelling approach, not looking at actual tooth size or diameter. A disadvantage of the model was also that the authors considered an idealised beamforming system, a signal processing technique for directional signal reception, for their tooth array. The differential lengths of the nerves were therefore not taken into account, which added substantial delays to the summed signals. In order to estimate the pulse envelope, the authors used a Hilbert transform. An advantage of the Hilbert transform is that it does not require derivatives (Liu 2012).

Another simple analytical model is the one simulated by Dobbins (2001, 2007). He presented a 2-D model with a bottlenose dolphin's teeth as circles, all possessing the same diameter. As mentioned before for Potter and Taylor, this is a very simplified approach. Dobbins hypothesized that the 22 teeth on each side of the lower jaw act as passive endfire array, providing angular localization. A limitation of this approach is that the beam pattern of the endfire array varies with frequency; the linearity of the difference pattern is degraded with reducing frequency. In order to overcome this problem, the author used log-periodic arrays, which are directional narrow-beam antennas, operating over a wide range of frequencies. Advantages of log-periodic arrays are that they have reduced near-field variation and fewer sidelobes, making them less sensitive to signals coming from other angles than the main sound source. However, the gain of log-periodic arrays is relatively low in comparison to for example Yagi arrays, which have a higher gain, but only a narrow bandwidth. Another limitation of Dobbins's model is that he simulated a beam propagating from a sound source to the array elements, assuming spherical spreading and an undistorted noise-free signal. This ideal array did not take possible obstacles between source and receiver or coupling between array elements into account, which would distort the wavefront (Dobbins 2007).

Nelson (2005) investigated the tooth hearing hypothesis for sperm whales (*Physeter macrocephalus*). He hypothesized that the teeth act as an acoustic receiving array. The author first measured the sound velocity of the teeth using a dual trace analogue oscilloscope. He then measured tooth resonances by striking the teeth with a sound wave and measuring the frequency of their vibration. Dual trace analogue oscilloscopes are used to observe the change of electrical signals over time. An advantage of a dual beam oscilloscope is that it can capture two fast transient events. Disadvantageous is that, unlike multiple trace oscilloscopes which provide a continuous display of signals, the display of the two signals of dual beam oscilloscopes consists of small gaps.

The most diverse experimental approach regarding the tooth hearing hypothesis was conducted by Dible et al. (2006, 2009). The authors presented 2-D and 3-D models and performed various experiments calculating sound velocities of bone and teeth of a bottlenose dolphin, using Laser Doppler Vibrometry. A main part of Dible et al.'s (2009) research consisted of the work on the hypothesis of band gap hearing in the dolphin's lower jaw and teeth. Acoustic band gaps are energy ranges through which sound cannot propagate through. Transmission line modelling (TLM) and a 2-D slice from a CT scan of the dolphin were used

for numerical computer simulations and TLM mesh construction. TLM is a time-domain, differential numerical method, suited for solving field problems. It is based on the Huygens principle of wave propagation, which is that all points on a wave front act as secondary waves, thereby contributing to the overall wave phenomenon. A benefit of TLM is its accuracy and stability in the case of passive linear networks. Sensitivities with respect to time and time step are easily obtained, which makes this method applicable for automated networks. It also provides fast simulations and models complex geometrical problems effectively. The TLM mesh consists usually of cubic cells, representing individually termed nodes. One of the disadvantages of TLM is that it requires a lot of computer memory. The occurrence of dispersion with the numerical results is also disadvantageous (Morente et al. 1995). Although Dible et al.'s (2009) model is more realistic than the simulations of the previous authors, it still shows a simplified geometry, considering only the teeth of the bottlenose dolphin and not taking the gum tissues surrounding the teeth. However, this idealised version made it possible to compare periodic arrays. TLM was also used for the 3-D model, which presented a weaker formation of the band gap.

Regarding the above mentioned acoustic modelling, not every detail has been taken into account. Unlike Cranford et al. (2008), research on the tooth hypothesis consisted solely of the teeth. Neither jaw bone nor gum or surrounding tissue were considered in the models, thereby leaving out the interaction of propagating sound throughout the entire head of the odontocete. However, acoustic modelling can provide a greater amount and variation of data, which is not possible in real life. Electrophysiological as well as behavioural experiments on live odontocetes for example have to take movements of the animals' heads into account. It is not possible to keep a dolphin's head completely still nor is it possible to exactly measure an angle change of the head. Acoustic models are able to provide this accuracy.

2.3 Gular pathway

There are a few other suggestions on how sound may be received by odontocetes. Bullock et al. (1968) for example supposed that sound enters through a dolphin's mouth, in view of the fact that the tongue of odontocetes has been found to be very sensitive to sound. The most recent discovery is a possible acoustic pathway through the oral cavity and throat region of odontocetes (Cranford et al. 2008a). This so-called gular pathway is situated in the posterior mandible. Experiments were performed by means of CT scanners on two dead specimens of

Cuvier's beaked whale (*Ziphius cavirostris*), investigating simulated sound pathways into and out of the animals' head. A "Vibro-acoustic Simulator" (VAS) was created, combining tissue property measurements, Finite Element (FEM) software and the anatomic geometry of the whales' heads obtained by means of CT scanners (Krysl et al. 2006, 2007). The physical properties of the tissue like sound velocity, density and elasticity were measured by Soldevilla et al. (2005).

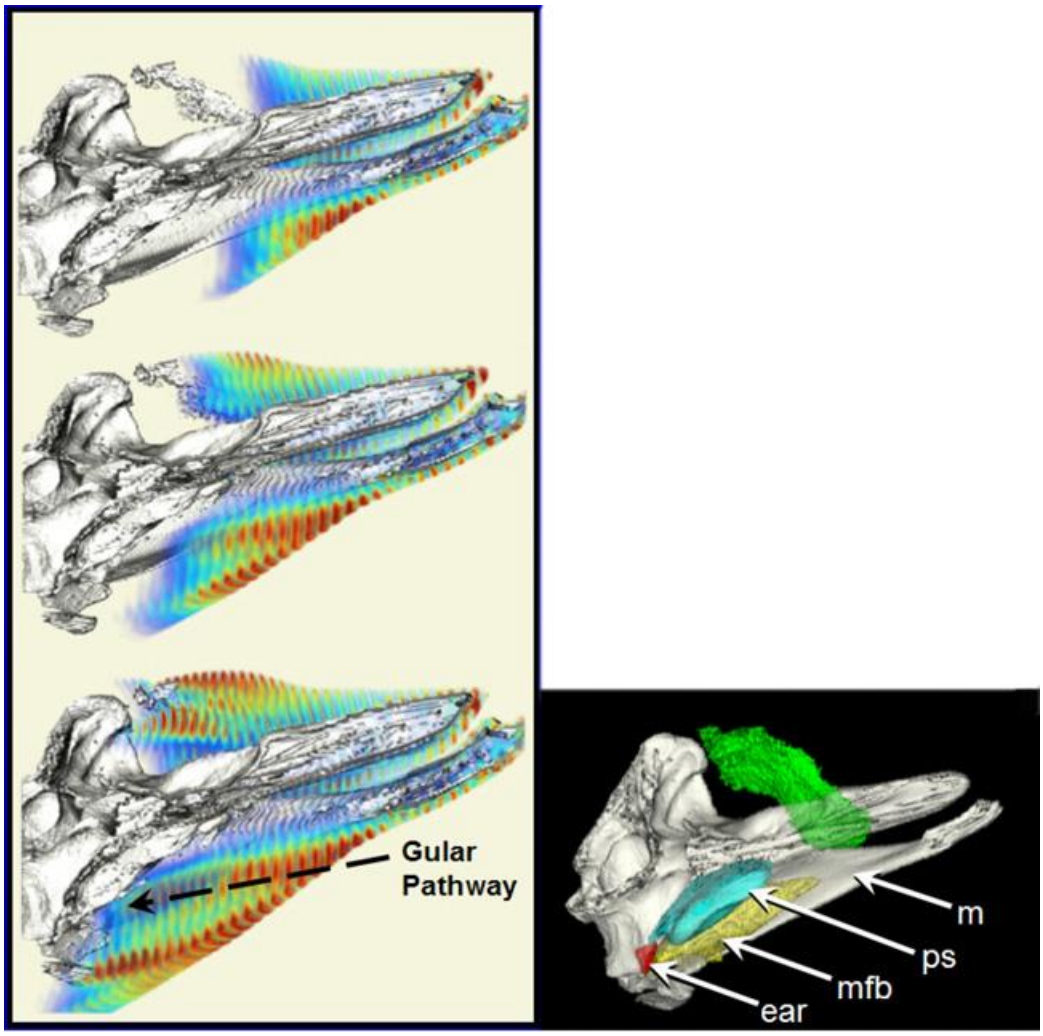

Fig. 2.10: Left side of a Cuvier's beaked whale's skull, as viewed from the right. Left: Gular region and oral cavity, building the gular pathway. The displacement amplitude is shown in three stages of the simulation for a wave coming from in front of the head (0°) at 40 kHz. Right: CT scan of the whale's head (ear = left tympanoperiotic complex; mfb = left mandibular fat body; ps = left pterygoid sinus; m = left mandible) (Cranford et al. 2008a).

A concept of lumping was applied for the simulations, showing the propagation of the acoustic disturbance in biological tissues. A sound source with a frequency of 40 kHz was

placed either inside the head or outside of it in simulated sea water. For the investigation of the sound reception pathway, a 40 kHz planar pressure wave was emitted from in front of the whale's head with an incidence angle of 0°.

Simulations showed that the sound wave refracted around, particularly below the mandibles, when striking the soft head tissue. The wave then entered the intramandibular fat bodies through an opening in the lower jaw and propagated via the fat body to the tympanoperiotic complex (TPC) (Fig. 2.10). This opening in the posterior part of the lower jaw is created by the absence of a medial bony wall. It is a requirement for making the gular pathway work. Sound sources hitting the whale's head from an angle of 18° and 45° in a horizontal plane showed a decrease in sensitivity as well as a delayed arrival time at the TPC. Sound arriving at -18° below the horizontal plane showed also a lower sensitivity. The highest sensitivity was measured for sound coming from directly in front of the head at an angle of 0°.

The advantage of the VAS is the combination of whale anatomy with FE modelling and tissue measurements. The strength of the simulator is also its flexibility and that properties can be changed systematically. Cranford et al.'s (2008) experiments provide a realistic 3-D image of a Cuvier's beaked whale's head, simulating the interaction between sound waves and anatomy. Taking only postmortem animals for their approach made the experiment easier and less time consuming, for example regarding possible animal training. However, living animals are on the other hand necessary for assessing the validity of simulated experiments. Also, using the severed head of a Cuvier's beaked whale made the blood drain from several vessels, leaving a series of circular gas-filled voids in the CT scan (Cranford et al. 2014). This may have changed the outcome of the results in comparison to possible results on living animals.

For the VAS, Cranford et al. used an image-based discrete model with an automatically generated voxel-based mesh. Voxel-based meshes provide enhanced accuracy in predicting structural behaviour and deformations. They are known to be used in the analysis of scientific data, and particularly in CT and MRI scans. The most important advantage of voxel-based meshes is probably that unlike many other methods, they convert for example CT scan datasets directly in 3-D meshes, thereby avoiding vectorial segmentation. Another advantage of the use of voxel meshes is that they are based on a simple algorithm, making it the fastest mesh generation program. A limitation of voxel-based meshes is their dependence on image resolution (Viceconti et al. 1998). For Cranford et al.'s VAS toolkit, a Lagrangian finite element formulation was implemented. Advantages of the Lagrangian model are that the nodes

move with the material points and boundary nodes remain on the boundary. However, mesh distortion can occur when the mesh deforms with the material.

2.4 Discussion

Findings by Cranford et al. (2008a, 2008b) showed that the sensitivity was highest when a sound source was arriving from the front of the jaw at an angle of 0° in the horizontal plane. Sound coming from an angle of 18° below the jaw showed a lower sensitivity and a delayed arrival time at the TPC. Since sound coming from beneath the mandible should have a direct access to the gular pathway, the sensitivity in this case should be higher than for sound coming from other angles. Findings of a delayed arrival time at the CNS are also contradictory to the fact that sound coming from beneath the lower jaw has direct access to the gular pathway and should therefore arrive at the CNS first.

Echolocation experiments performed by Au and Moore (1984) showed a maximum sensitivity for sound coming from 5° - 10° above the midline of the lower jaw, which contradicts Cranford et al.'s (2008a) result of a primary entry underneath the lower jaw as well. Although these observations indicate a logical discrepancy, sound reception through the gular region could on the other hand be advantageous for the echolocation. Sound via the gular pathway does not have to pass bone or teeth and can travel directly through skin to the intramandibular fat body where it is then being transmitted to the CNS. This would make sound transmission faster and the animals could emit and receive a larger number of clicks. The closer a dolphin gets to its target, the more clicks it emits. After emitting a click, the animal waits for the echo to return before emitting the next click. It would therefore be more useful for directional hearing to receive more clicks. Sound propagating through the lower jaw bone would on the other hand need more time to arrive at the CNS than sound entering the lipid directly.

Au and Moore (1984) also detected a rapid decrease in odontocetes' hearing sensitivity for increasing angles above the animals' head, whereas the hearing sensitivity below the vertical plane did not decrease as fast. This indicates that the upper jaw is unlikely to receive sound. Behavioural experiments with dolphins wearing acoustically opaque rubber hoods over their lower jaw showed that the animals' performance was attenuated (Brill et al. 1988). Although only intended to prove hearing via the lower jaw, these experiments included at the same time

teeth and gular region. This could imply that either the teeth of the lower jaw or the throat region, or possibly both, could also be part in sound reception.

Electrophysiological experiments conducted by McCormick et al. (1970, 1980) showed highest sensitivities for sound arriving near the ear and at the side of the lower jaw. Although these experiments were also only intended to investigate the lower jaw hypothesis, McCormick's findings can be seen as a support for the gular pathway as sound reception pathway. When holding a vibrator against a front tooth of a dolphin's lower jaw, McCormick et al. (1970) measured large potentials in the organ of Corti in the cochlea. These findings can on the other hand be seen as a connection between the teeth and sound reception.

Findings by Møhl et al. (1999) show a maximum sensitivity at the end of the lower jaw, which is the location of the gular pathway as well as the back teeth. The authors also mentioned observations of dolphins investigating targets with an open mouth. While neither the gular region nor the teeth were considered as pathway for sound reception, the findings can again be seen as a support for these hypotheses.

Many of the earlier experiments focused on the lower jaw and especially the mandibular lipids as sound reception pathway. Neither the teeth nor the gular region were considered for sound reception.

2.5 Conclusion

Echolocation is the process of acoustical ranging by emitting a sound signal and listening to the echo. This process is known to be used by odontocetes and while the process of sound emission is clear today, it is still not entirely proven how the animals receive sound.

The first hypothesis on the pathway of received sound was suggested in 1964 by Norris and was supported by several other authors (e.g. Varanasi and Malins, 1971, 1972; Møhl et al. 1999; Houser et al. 1999, 2004; Aroyan 2001; Zahorodny et al. 2009). Examining the skull of a bottlenose dolphin, he suggested that sound entered the animal's head through a thin region in the rear mandible, travelled through a fat body in the mandible and to the inner ear. Further examinations of the fatty tissue in the lower jaw showed that this lipid only occurred in the melon and the mandible and that it consisted of unusual wax esters and iso-acids which had not been found in other mammals. It was also suggested that, since the melon, consisting of

this special fat, was proven to play a role in the emission of sounds, the mandible, consisting of the same fat, had to play a role in echolocation as well.

That the special lipid in the mandible of odontocetes plays a role in sound transmission is now acknowledged by researchers. The sound pathway through the bone of the mandible is however still under debate. A different approach of sound entering the head of echolocating odontocetes was suggested by Goodson and Klinowska (1990). Pointing out the special arrangement of the animals' teeth, they hypothesized that the teeth act as passive resonant transducers with their nerves creating propagation delays so that all the signals arrive at the CNS at the same time. Several other authors examined this possibility further and proposed additionally to this hypothesis that the teeth act as a form of end-fire array, enhancing the directional hearing of odontocetes (Potter and Taylor 2001, Dobbins 2007, Dible et al. 2006). The most recent hypothesis investigated is a possible pathway through the gular region of toothed whales. According to this theory, sound is transmitted through an opening beneath the lower jaw, propagates through the fat bodies and to the TPC. The absence of a medial bony wall creates this opening, which is a requirement for the gular pathway to work (Cranford et al. 2008a, 2008b).

2.6 Acoustic Investigations

In order to examine the pathway for sound reception through the head, jaw or respectively the teeth of odontocetes, several processes like sound propagation and scattering of the incident sound waves have to be taken into account. Experiments conducted in order to check the three hypotheses showed that the localization ability of odontocetes depends on frequency and angle of incident sound waves. The following Chapter will describe these processes in more detail.

3 Acoustic Theory: Propagation and Scattering

3.1 Basics of underwater acoustics

The characteristics and physical properties of sound waves propagating underwater as well as their path when encountering objects and being scattered back, play an important part in the investigation of the hearing capability of echolocating odontocetes. This thesis looks into the role of dolphin teeth in sound reception and investigates the course of a plane sound wave impinging on the teeth from different angles. Parameters like sound velocity of sea water and teeth as well as density and other properties have to be taken into account, which will be elaborated in detail in this chapter.

Waves travel in two different ways: the transverse and the longitudinal one. Transverse waves oscillate perpendicular to the direction in which a wave propagates, whereas longitudinal waves travel along the direction of the wave propagation. Underwater sound propagates in form of longitudinal (compressional) waves, with the wave particles moving back and forth parallel to the wave propagation (e.g. Lurton 2002, 2010). These acoustic waves travel through a medium as pressure fluctuations and are measured in Pascal. A propagating sound wave carries an acoustic energy with it, also called intensity *I*. It equals the average amount of flow of energy transmitted through a unit area in the direction of the wave propagation. Intensity and sound pressure p_0 of a plane wave are related as follows:

$$I = \frac{p_0^2}{\rho c} \text{ in (Watts/m}^2\text{)} \qquad (3.1)$$

ρ is the density of the medium in which the wave travels, measured in kg/m^3; c is the sound velocity of the medium in m/s. The basic unit for sound intensity is Watts/m^2. However, the values for acoustic intensities can vary considerably and are therefore commonly expressed as a ratio to a reference intensity calculated for a pressure of 1 µPa and quantified on a logarithmic scale in decibels (dB). Decibel is a relative unit; the intensity is therefore defined as the ratio of the intensity of a sound wave to a reference intensity. The most often used measure in acoustics is the Sound Pressure Level (SPL), also measured in dB. Acoustic intensity is proportional to the square of a wave's pressure *p*; the SPL can therefore be expressed as

$$\text{SPL (dB)} = 20 \log_{10} \frac{p}{p_0} \qquad (3.2)$$

With p as the sound pressure and p_0 as reference pressure. The reference values of pressure and acoustic intensity are necessary to determine the absolute pressure or intensity of a sound wave. The reference pressure for sound underwater is p_0 = 1 µPa = 1 × 10^{-6} Pa = 0 dB, the reference sound intensity $I = 10^{-12}$ W/m^2. For a sinusoidal wave of frequency f, the solution of the wave equation with c as a constant velocity and a restricted propagation direction will be a plane wave (3.3). Plane waves are travelling at a constant frequency.

$$y(x,t) = y_0 \sin\left(f\,2\pi\left(t - \frac{x}{c}\right)\right) \tag{3.3}$$

y is the displacement of the point on the travelling sound wave and x the distance the point has travelled from the wave's source; t is the time elapsed, y_0 is the amplitude of the oscillations, c the sound velocity in m/s and f the frequency of the wave, measured in Hertz (Hz). The frequency is the number of vibrations for a given amount of time. The higher the frequency, the shorter is the wavelength. The wavelength λ is the distance from one point on a wave to the identical point on the next wave:

$$\lambda = \frac{c}{f} \tag{3.4}$$

The time a wave requires to travel from one point on the wave to the same point on the next wave is called period T.

$$T = \frac{1}{f} \tag{3.5}$$

The sound velocity is the speed at which an acoustic wave travels in a certain amount of time. It depends on the properties of the medium it travels in. In fluids (liquids and gases), only longitudinal waves occur. The sound velocity c of longitudinal waves depends on the bulk modulus K and the density ρ of the medium:

$$c = \sqrt{\frac{K}{\rho}} \tag{3.6}$$

The bulk modulus is the pressure divided by the strain and can be expressed as follows:

$$K = \frac{P}{(V_0 - V_n)\, V_0} \tag{3.7}$$

p is the applied pressure, V_0 the original volume of the material and V_n the new volume. The bulk modulus K can be applied in solids as well as fluids. It describes the elastic properties of a medium when it is under pressure on all surfaces. The sound velocity of shear (transverse) waves c_s, which occur in solids alongside longitudinal waves, depends on the shear modulus G and the density of the solid ρ.

$$c_s = \sqrt{\frac{G}{\rho}} \tag{3.8}$$

The shear modulus G is the ratio of shear stress to the shear strain and is usually expressed in GPa:

$$G = \frac{F/A}{\Delta x/l} \tag{3.9}$$

F/A is the shear stress, with F as shearing force and A as the area on which the force acts. $\Delta x/l$ is the shear strain or relative deformation, with Δx as the transverse displacement and l as the initial length.

Both elastic moduli occur in the generalised Hooke's law, which describes the stiffness of a material. Hooke's law is applicable for solids, liquids and gases. Sound travels faster through a medium with higher elasticity and lower density (Kinsler et al. 2000).

Other factors such as for example temperature, salinity and pressure determine also the velocity of sound in the ocean (Zuckerwar 1997). The sound velocity increases with increasing temperature, the temperature of sea water in turn decreases with increasing depth. Beyond a limit depth, the average temperature remains stable, decreasing very slowly with depth and not varying much from one place to another. The velocity in sea water lies between 1450 m/s and 1550 m/s. The hydrostatic pressure increases with increasing depth, sound velocity increases therefore as well. The approximate change of the sound velocity in sea water for a change of temperature is 1°C ~ 4 m/s, for salinity a change of 1‰ ~ 1.4 m/s and for depth 0.017 m/s per

meter down (Lurton 2010). The equation for the velocity of sound, using the values for temperature (T) in °C, salinity (S) in ‰ and depth (*z*) in m, is the following:

$$c = 1449.2 + 4.6T - 0.055T^2 + 0.00029T^3 + (1.34 - 0.01T)(S - 35) + 0.016z \quad (3.10)$$

The hydrostatic pressure in sea water is given by the Leroy formula:

$$p = [1.0052405\,(1 + 5.28 \times 10^{-3} \sin^2 \phi)\, z + 2.36 \times 10^{-6} z^2 + 10.196] \times 10^4 \quad (3.11)$$

Where p is the pressure in Pascal (Pa) and ϕ is the latitude (in º). The wave equation describes the propagation of a variety of waves. The displacement ξ at the phase velocity $v = \omega/k = \lambda f$ can be described by the wave function:

$$\xi = \xi_0 \sin\{2\pi f t - (2\pi / \lambda) z\} = \xi_0 \sin\{\omega t - k z\} \quad (3.12)$$

ξ_0 is the amplitude, *f* the frequency, $\omega = 2 f \pi$ the angular velocity, λ the wavelength, and *k* the wave number. The former wave function is a solution for the general wave equation:

$$\frac{\partial^2 \xi}{\partial t^2} = v^2 \frac{\partial^2 \xi}{\partial z^2} \quad (3.13)$$

The wave can be concentrated and directed by wave guides and by acoustic lenses. The melon of odontocetes for example functions as an acoustic lens, focussing sound waves into a beam and emitting it forward, in front of the animals' head. The acoustic impedance Z describes the conditions for sound propagation through a medium. It is the product of density ρ and sound velocity *c*, and is frequency dependent (3.11). For a plane wave, the specific acoustic impedance is resistive. The impedance in water is 1.5 MPas/m, which is about 3400 times higher than the impedance in air (Lurton 2010).

$$Z = \rho c \quad (3.14)$$

The main focus of this thesis will be on the sound reception of the Atlantic bottlenose dolphin (*Tursiops truncatus*). In contrast to the relatively limited hearing ability of humans with a range from 20 Hz to 20 kHz, the average hearing ability of cetaceans is 100 kHz. Bottlenose dolphins are known to hear even higher frequencies up to 150 kHz, harbour porpoises (*Phocoena phocoena*) frequencies up to 180 kHz. Higher frequencies are usually only produced for echolocation, whereas lower frequencies at about 40 kHz are used for communication. Dolphins produce sound in form of clicks or whistles in order to navigate, communicate or to find their prey (Norris 1969). The emission of clicks increases, the closer the animal gets to its target. Each click lasts about 50 to 128 µs. In general, in a free field, low frequency sound waves are less absorbed and will therefore travel further than high frequency sound waves due to absorption effects. High frequency sound is absorbed more easily. It therefore does not travel as far and is usually only effective for close ranges up to 200 m (Au 1993). As sound waves travel through a medium, they lose energy due to the generation of heat of the vibrating molecules in the medium. Sound waves with lower frequencies travel further than high frequencies due to lower attenuation. Scattering, sound absorption and reflection of sound waves with lower frequencies are held at a minimum. Sound absorption due to chemical effects is described in more detail in Section 3.2.

An important part in target discrimination of dolphins is the signal-to-noise ratio (SNR), measured in decibels. SNR measures how much a signal is corrupted by noise made by ships, breaking waves, air bubbles and other sources. It is the main parameter affecting the performance of target discrimination by a receiver or, in this case, an echolocating dolphin. A different kind of noise is reverberated sound, produced by scatterers such as for example fish and the sea surface and bottom. These reverberated signals corrupt the discrimination of the desired signal as well (Au and Martin 1989).

3.2 Sound Propagation

Sound waves propagating in the ocean lose energy due to absorption and spreading (Medwin and Clay 1998, Brekhovskikh and Lysanov 2003). Attenuation in the form of absorption is caused by factors such as viscosity, thermal conductivity and chemical reactions. The sound energy of a propagating wave is converted into heat and causes therefore an energy loss to the environment. Viscous absorption is significant at frequencies above 100 kHz. Moving particles generate heat through viscous drag. Sound absorption through chemical effects occurs

primarily due to Magnesium sulphate (MgSO4) and boric acid, which can be found in sea water. Both salts convert acoustic energy into heat energy (Ainslie and McColm 1998). The transformation is a function of frequency. While the impact on sound absorption by boric acids is at low frequencies up to a few kHz, the effect of MgSO4 on sound absorption is at frequencies up to 100 kHz. The attenuation of low-frequency sounds in water is very small due to lower effects by the salt (Fisher and Simmons 1977). The sound absorption α (in dB/km) by specific chemicals is:

$$\alpha = 0.106 \frac{f_1 f^2}{f^2 + f_1^2} e^{(pH-8)/0.56} + 0.52 \left(1 + \frac{T}{43}\right) \left(\frac{S}{35}\right) \frac{f_2 f^2}{f^2 + f_2^2} e^{(-z/6)} + 0.00049 f^2 e^{-(T/27 + z/17)} \quad (3.15)$$

with frequency f in kHz, depth z in km and the salinity S in ‰. Relaxation frequencies for boron (f_1) and magnesium sulphate (f_2) are given in kHz (Francois and Garrison 1982).

$$f_1 = 0.78(S/35)^{1/2} e^{T/26} \quad (3.16)$$

$$f_2 = 42 e^{T/17} \quad (3.17)$$

An increase in salinity decreases the sound absorption at low frequencies and increases sound absorption at higher frequencies. The Baltic Sea with its low salinity has for example a low absorption above 1 kHz. An increase in temperature causes a decrease in sound absorption at all frequencies except frequencies near the value of relaxation frequencies f_1 and f_2, where absorption is increased. This is shown by the example of the Red Sea, where absorption is high at the relaxation frequencies, and in the Arctic, where sound absorption is high at all frequencies due to low temperatures. Increasing depth and therefore increasing pressure decreases the sound absorption at high frequencies, but has no effect on lower frequencies (Ainslie and McColm 1998). These examples show that frequency causes the most significant variation in the absorption coefficient. The higher the frequency, the greater the energy loss.

Another reason for the attenuation of propagating sound waves in the ocean is geometrical spreading. Sound waves propagate from a source radially, thereby spreading their acoustic

energy in all directions over a large surface and reducing the intensity of the wave. The pressure of this spherical wave decreases proportional to $1/R$ in range, with R being the radial distance from the sound source. Intensity decreases in $1/R^2$. The transmission loss TL for spherical spreading, with I_1 as intensity 1 m from the sound source, I_2 as the intensity at the range R and R_{1m} = 1 m for the reference unit distance, is expressed in dB (Lurton 2010).

$$\mathrm{TL} = 10 \log \frac{I_1}{I_2} = 20 \log \left(\frac{R}{R_{1m}}\right) \tag{3.18}$$

Large fluctuations of sound velocity occur in the upper ocean due to seasonal changes in temperature and salinity. Below 1000 m, sound velocity increases mainly with increasing hydrostatic pressure. At a certain depth in the ocean, the sound velocity is very low and a horizontal channel called SOFAR (Sound Fixing And Ranging) or Deep Sound Channel occurs. The depth at which the lowest velocity occurs is called SOFAR axis. This horizontal layer is at equatorial and temperate latitudes in the ocean at which sound travels as kind of natural waveguide for thousands of kilometres without energy loss due to the lack of interaction with the surface or sea bed. This absence of interaction with the interfaces is an effect of total internal reflection of the sound waves in the channel (Brekhovskikh 2003). The energy loss through geometrical spreading is therefore minimal and the only factor decreasing the sound eventually is the absorption in sea water. The depth of this deep sound channel is usually at 1000 m, in tropical zones at around 2000 m and the depth of the SOFAR axis varies therefore with latitude. The SOFAR axis in the Arctic occurs for example near or at the ice-covered surface (Au and Hastings 2008). Baleen whales are thought to use the SOFAR channel for communication over long distances (Brekhovskikh and Lysanov 2003, Lurton 2002).

3.3 Sound Scattering

A different form of energy loss occurs when acoustic waves strike an object underwater and are scattered back. Sound can be scattered by marine life as well as by reflection from the surface and sea bed. The backscattered energy is known as reverberation (Kuperman and Roux 2007).

The angle of the reflected and refracted wave depends on the medium a sound wave reflects from. The reflection and transmission angle of a wave in water hitting another fluid medium differs from the angles of a wave in water hitting a solid medium. Sound waves incident on an

object are transmitted in a different direction, proportional to the change in sound velocity. This refraction follows Snell's Law (Fig. 3.1):

$$\frac{\sin\ \theta_1}{\sin\ \theta_2} = \frac{c_1}{c_2} \tag{3.19}$$

where θ_1 is the incidence angle and θ_2 the angle of refraction. Velocity c_1 is the speed of the transmitted sound, c_2 the sound speed of the refracted wave. This equation refers to an interface separating two fluid homogeneous media. The angle of the reflected wave is equal to the angle of the incident wave, relative to the normal of the interface. This is called specular or regular reflection.

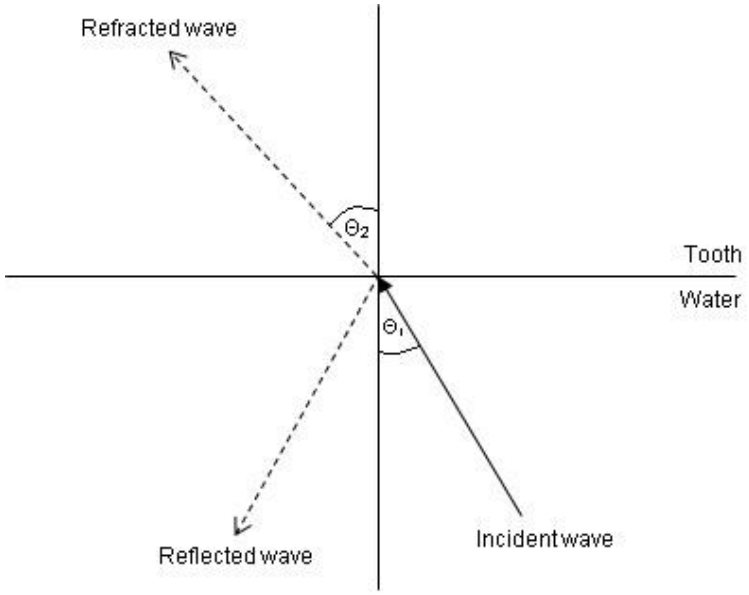

Fig. 3.1: Reflection and refraction of an incident wave on a solid interface.

The reflection coefficient *V* and the transmission coefficient *W* describe the amplitude of the reflected and transmitted wave. The equation for an incidence angle θ_1 is:

$$V(\theta_1) = \frac{\rho_2 c_2 \cos\ \theta_1 - \rho_1 c_1 \cos\ \theta_2}{\rho_2 c_2 \cos\ \theta_1 + \rho_1 c_1 \cos\ \theta_2} \tag{3.20}$$

$$W(\theta_1) = 1 + V(\theta_1) = \frac{2\rho_2 c_2 \cos\ \theta_1}{\rho_2 c_2 \cos\ \theta_1 + \rho_1 c_1 \cos\ \theta_2} \tag{3.21}$$

ρ_1 indicates the density of the medium in which the incident wave propagates, ρ_2 the density of the medium with the reflected wave. c_1 is the sound velocity of the incident wave, c_2 the sound velocity of the reflected wave. The phenomenon of total reflection occurs when the incident wave strikes a medium at an angle larger than a particular critical angle (Lurton 2010). This critical angle θ_c exists when $c_2 > c_1$. The incident wave cannot travel through the medium it strikes when $\theta_1 \geq \theta_c$:

$$\theta_c = \arcsin(c_1 / c_2) \tag{3.22}$$

In case of a wave impinging on a solid medium, a shear wave may occur along with the compressional longitudinal waves. Shear waves travel at about half the speed of compressional waves. The reflecting medium is then defined by the shear velocity c_s, the density ρ_2 as well as the Lamé coefficients λ and μ:

$$c_s = \sqrt{\frac{\lambda + 2\mu}{\rho_2}} \tag{3.23}$$

$$c_s = \sqrt{\frac{\mu}{\rho_2}} \tag{3.24}$$

For a solid reflecting medium, Snell's Law is expressed as:

$$\frac{\sin \theta_1}{\sin \theta_s} = \frac{c_1}{c_s} \tag{3.25}$$

The reflection coefficient is in this case expressed as:

$$V = \frac{B - 1}{B + 1} \tag{3.26}$$

with $B = \frac{\rho_2}{\rho_1} \frac{1}{k_s^4} \frac{k_{z1}}{k_{z2}} \left[\left(k_{zs}^2 - k_x^2 \right)^2 + 4 k_x^2 k_{zs} k_{z2} \right]$; i = 1, 2 or s for incident wave, reflected wave and shear wave respectively.

ρ_1 is the density of the medium in which the incident wave propagates, ρ_2 the density of the medium of the reflected wave. k_s describes the wavenumber of the shear wave. $k_{zi} = \sqrt{k_i^2 - k_x^2}$ with $k_i = 2\pi f / c_i$ and $k_x = k_1 \sin \theta_1$. c_i indicates the sound velocity with i = 1, 2 or s for the incident wave, reflected wave or shear wave respectively; θ_1 describes the incident angle.

Other wave modes such as Rayleigh, Lamb or Love waves can also occur in solids. Rayleigh waves travel over the surface of a solid medium combining longitudinal and transverse motion and creating an elliptical motion. The velocity of these surface waves is frequency-dependent. Lamb waves are a type of waves that travels in solid plates. These plate waves propagate parallel to the surface throughout the thickness of a solid medium. They are only able to travel through solids that are a few wavelengths thick. The propagation of Lamb waves depends on the solid's density, elastic material properties and the frequency of the wave. Love waves are surface waves that travel parallel to a plane layer and perpendicular to the wave direction. They are also frequency-dependent.

3.4 Target Strength

Sound waves impinging on a target are partly scattered back to the transmitter. The target strength TS is the ratio between the intensity I_{bs} scattered back from a target toward the transmitter to the incident intensity I_i. Both intensities are referenced to a distance of 1 m from the target and are expressed in dB.

$$\text{TS} = 10 \log \left(\frac{I_{bs}}{I_i} \right) \tag{3.27}$$

The target strength depends on the structure of the target as well as on characteristics like angle or frequency of the incident signal. How sound is scattered back depends on the dimension of the insonified target, usually differentiated into either a point or extended target. Point targets are, compared to the acoustic wavelength, very small targets. Their backscatter strength is independent from the distance to the sound source or characteristics like beamwidth or duration of the signal (Lurton 2010). The scattering function for an ideal rigid sphere is:

$$G(\theta_i, \theta_s) = \frac{1}{4\pi} \tag{3.28}$$

The backscattering strength is:

$$\sigma_{bs} = \sigma_s = \frac{\pi a^2}{4\pi} = \frac{a^2}{4} \tag{3.29}$$

The backscattering strength of a rigid sphere smaller than the wavelength of the incident wave is known as Rayleigh scattering with $k = 2\pi/\lambda$ as acoustic wavenumber and a as radius of the sphere:

$$\sigma_{bs} = \frac{25}{36} k^4 a^6 \tag{3.30}$$

The Rayleigh regime occurs for $ka < 1$ with the backscattering strength increasing rapidly with frequency. For $ka > 10$, scattering is independent of the frequency. An interferential regime appears for $1 < ka > 10$ with waves propagating at intermediate frequencies. Sound waves at low frequencies ($ka < 1$) are scattering the strongest back from the target, whereas scattering for high frequency ($ka > 1$) sound waves is strongest in the forward direction. Point targets other than a rigid sphere are for example fluid spheres, gas bubbles or fish, in particular the swim bladder of fish. This gas-filled organ is used for buoyancy and shows a strong impedance contrast with water. The target strength of fish is the energy reflected by the impinging sound impulse and depends mainly on the cross section area of the swim bladder and the tilt angle of the fish (Foote 1980). The average target strength at high frequencies with L as the fish length and f_k as the frequency in kHz is:

$$TS_{spec} = 19.1 \log L + 0.9 \log f_k - 24.9 \quad (3.31)$$

A more detailed equation by Simmonds and MacLennan (2005) shows a dependence of the target strength on the different species of fish:

$$TS_{fish} = 20 \log L - TS_{spec} \quad (3.32)$$

Where TS_{spec} is the target strength at a given frequency. The target strength constant for cod is relatively high with a TS_{spec} of -28.9 dB at a frequency of 30 kHz, Saithe has a TS_{spec} of -25.8 dB. Mackerels have a low TS_{spec} from -39.3 dB to -42.8 dB due to the lack of a swim bladder. The target strength increases at frequencies close to 1 kHz, which is the resonance frequency of the swim bladder. It can reach values from -25 dB to -20 dB (Lurton 2010).

Extended targets such as sea surface, sea bed, fish schools and Deep Scattering Layer (DSL) depend unlike point targets on their sonar characteristics. The dimension of extended targets is too large to insonify them completely with a single beam. The target strength depends in this case on the insonified space. The back scattering cross section is determined by the size of the target portion insonified by the sonar as well as the corresponding backscattering strength:

$$\sigma_{bs} = A_{s,v} \ \sigma_{bs}^{sy} \quad (3.33)$$

Where $A_{s,v}$ is the effective extent of the scattering surface or volume, and σ_{bs}^{sy} is the unit surface or volume backscattering cross section (Lurton 2002, 2010).

3.5 Discussion

This thesis investigates the distribution of a sound wave incident on the teeth of a dolphin. The rigid sphere can be seen as a single dolphin tooth with an average value of 0.001 m for the tooth radius. The plane wave used for the simulation has a velocity of 1490 m/s and a frequency of 100 kHz. While the dolphin jaw is in this case an extended target, the individual tooth is a point target, insonified by a single beam.

Since the target strength of fish depends on the species and on the size of their swim bladder, it can possibly be said that the scattered sound intensity of backscattered sound waves varies

also with the change of size of dolphins' teeth. Since point targets are independent of sonar characteristics, a change in frequency has no effect on the target strength.

3.6 Conclusion

Scattering plays an important part in the sound reception of marine mammals. Dolphins emit signals underwater which are reflected from potential targets. The backscattered sound is then received by the animal and transmitted to the inner ear, where it is being processed. The backscattered sound reveals the location of the desired target to a very narrow angle. This thesis investigates the role of dolphin teeth in sound reception. To understand this process, it is necessary to take a closer look at the propagation and scattering of sound waves bouncing off targets which the animals insonify. The angle of the incident wave is important, since it determines the precision of the directivity.

4 Acoustic Modelling

4.1 Time-domain modelling

The teeth of odontocetes are thought to play a role in sound reception by for example enhancing the directional hearing. The regular spacing of the teeth and that all odontocetes are homodonts led several researchers to the belief that odontocetes' teeth function as kind of an array (Goodson and Klinowska 1990, Potter and Taylor 2001, Dobbins 2007). This hypothesis has been investigated further by simulating the course of a plane pressure wave hitting the teeth of a bottlenose dolphin (*Tursiops truncatus*) from different angles.

4.1.1 Model development and verification

The 2-D modelling of sound propagation in the dolphin's jaw was implemented in Matlab, using a time-domain solution of the acoustic wave equation created by Anderson (2000). A modified version of the model was used for the simulations.

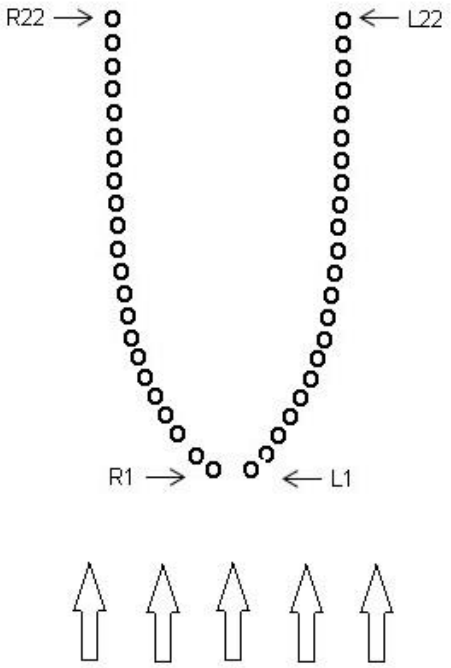

Fig. 4.1: Model of the teeth of *Tursiops truncatus*, with a plane wave propagating towards the front of the teeth. The teeth are displayed as circles; the arrows show the direction of the propagating sound wave.

The model shows the teeth of a bottlenose dolphin as circles with a plane wave propagating towards and eventually hitting the front of the teeth (Fig. 4.1). The pressure around the teeth was measured accordingly. Measurements of the space between the teeth as well as the diameter and length of the teeth were taken by means of a bottlenose dolphin's lower jaw cast (provided by P. Dobbins) (Fig. 4.2). This was done by using a calliper. The average measurement for the 44 teeth was for the tip of the teeth 2.1 mm, for the bottom of the teeth 4.6 mm. The bottom of the teeth referred in this case to the tooth base above the gum line.

All teeth of the lower jaw were taken into account for the model. Anderson's program (2000) was based on a pseudo-spectral derivative, time-domain integration algorithm formerly described by Wojcik et al. (1997). The program uses a staggered 4^{th} order Adams-Bashforth method, a linear multistep method storing and using information from previous steps, to integrate forward in time, including attenuation modeled with two relaxation mechanisms. The first step of the Matlab simulation was to create a sound wave propagating through a fluid medium. The calculation of pressure and velocity was staggered, with velocity at integer time steps and pressure at half-integer time steps. A perfectly matched boundary layer (PML) was then defined for absorbing 2-D acoustic waves and damping reflections from the grid boundary. The PML was originally formulated by Berenger (1994) and extended to an acoustic version for 2-D and 3-D waves by Yuan et al. (1997).

There are several reasons why Anderson's (2000) solver was chosen for the 2-D simulations in this thesis, the main one being that the author's program fulfilled all the requirements needed for the dolphin tooth model. Anderson's program simulated a plane wave propagating through a fluid medium, passing through a circular inclusion with a different sound velocity and calculating the pressure distribution for each node on the grid. This was precisely what was needed for the dolphin tooth model. An important advantage of Anderson's solver was its highly special accuracy and its ability to model propagation through a heterogeneous medium. The program solves the nonlinear wave equation for each node in the 2-D spatial domain. Another advantage was that sound could be generated from arbitrary geometries.

Pseudo-spectral time-domain methods are highly accurate and efficient. They use discrete Fourier transforms to evaluate spatial derivatives of functions. Pseudo-spectral algorithms solve large-scale problems for acoustic waves. An essential benefit of the pseudo-spectral/Adams-Bashforth method is that it gives the highest accuracy at long ranges and

requires fewer unknowns than for example FDTD methods. Pressure and particle velocity fields are all located in the grid centre. A staggered grid is therefore not able to alter the material properties. A limitation of the method is its spatial periodicity and relatively slow stable timestep (Liu 1998). Anderson's solver used a PML absorbing boundary, which suppresses reflections from the grid edges. An advantage of PML boundaries is that the reflection suppression is independent of the frequency of the incident wave; this is not the case for other ABCs. The combination of the pseudo-spectral method and PML boundary condition was developed to simulate acoustic wave propagation in a multidimensional and absorptive medium. PML does not cause numerical difficulties and the computational costs are minimal (Wojcik et al. 1997). As with the work of most of the other researchers who investigated the possibility of dolphin teeth as sound reception pathway, the 2-D simulations in this thesis showed a simplified version of the teeth, presenting them as circles. However, the diameter of each individual tooth was taken by using realistic data from a bottlenose dolphin's cast.

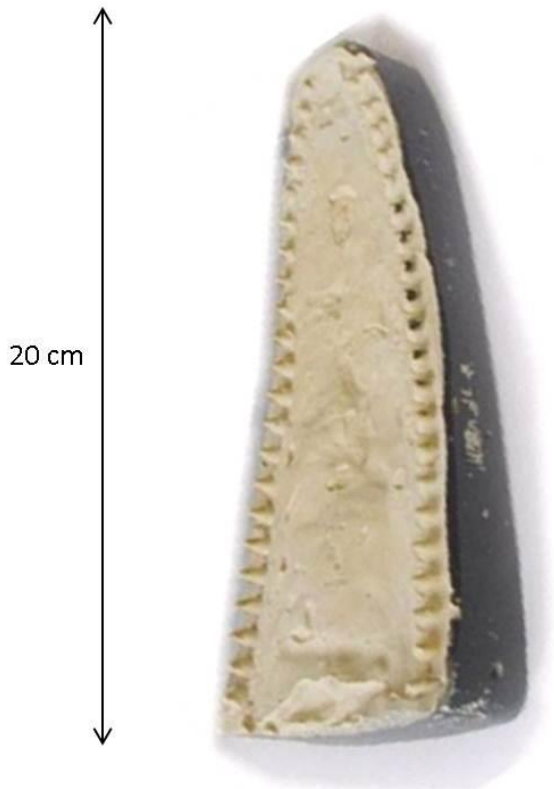

Fig. 4.2: Cast of the lower jaw of *Tursiops truncatus* (adapted from Dobbins 2007).

Parameters for dolphin teeth and surrounding medium were then defined and a transverse value of 2200 m/s was taken for the sound velocity in the dolphin's tooth. The density was

2035.4 kg/m^3 (Dible et al. 2009). The created tooth array was then projected onto a constant sound speed background with 1490 m/s for sound velocity in sea water and 1000 kg/m^3 for density in sea water. Values of 100 kHz and 20 kHz were chosen for the fundamental frequency f_c of the plane wave in order to look at pressure differences between echolocation and whistle frequencies of a bottlenose dolphin. The reference pressure of sea water p_0 = 1 µPa was taken and a value of 0.6 for the relative bandwidth.

Four different runs of the simulation were conducted to verify the program. The first simulation tested the pressure outcome when running a plane wave without any interference. Fig. 4.3a shows on the left the acoustic pressure across the simulation domain with the plane wave travelling from the bottom of the image. The sketch on the right was drawn for additional clarification. The arrows display the direction of the travelling wave, the white area displays water. The image shows the pressure distribution after the wave has travelled through the entire field in the time domain. The results show no clear change in pressure when observing the colour-coded image overall. There is however a minimal but constant attenuation of the pressure with time on closer examination (Fig. 4.3b). The pressure at the boundaries is equal to the pressure at the rest of the axial dimension, indicating that there is no wave reflection at the borders of the simulation.

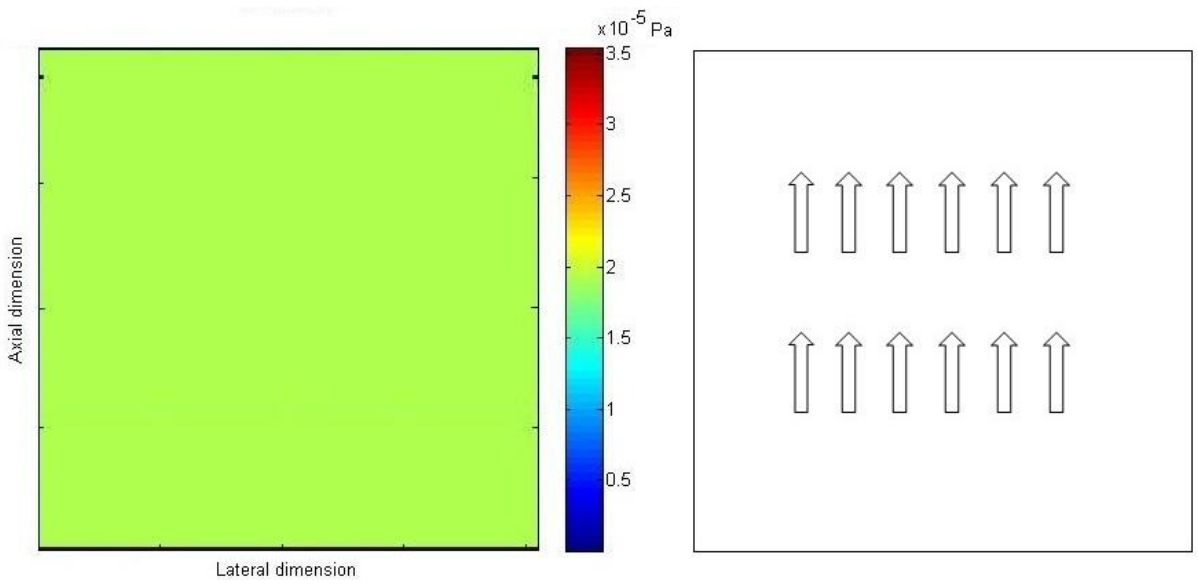

Fig. 4.3a: The pressure dispersion with a plane wave travelling in water without interference is shown on the left. On the right, a sketch of the wave direction is shown. The arrows display the direction of the plane wave.

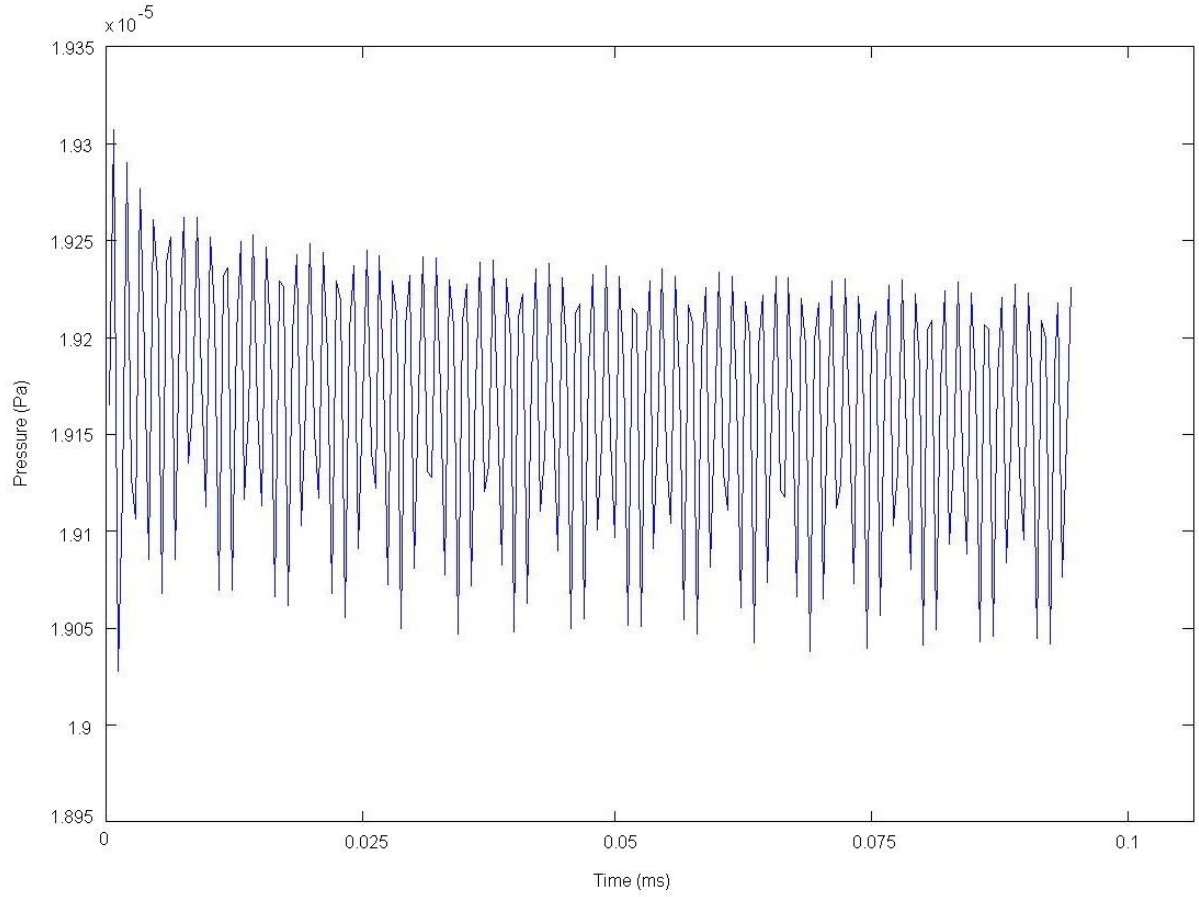

Fig. 4.3b: Pressure amplitude of a plane wave running through simulation without interference.

The second simulation looks at the pressure outcome for a wave incident on a plane interface (Fig. 4.4a). The acoustic simulation plot presented shows the summation of intensities in the time domain, after a pulsed plane pressure wave has run through the entire field. The pressure dispersion for a plane wave can be seen, travelling from the bottom and hitting a smooth solid interface from the front. For the solid medium, the parameters for a bottlenose dolphin's tooth were taken. The figure on the right shows the direction of the travelling wave, indicated by the arrows, with the grey area displaying the solid medium and the white area displaying water. The results show an increased pressure in water and an attenuated pressure in the solid medium.

There is no pressure change in the fluid medium overall and no change of pressure throughout the solid medium, indicating that the angle of the reflected and refracted wave is 0° and that there is, as expected, no wave scattering. Fig. 4.4b shows the change in pressure at the moment the wave impinges on the solid medium.

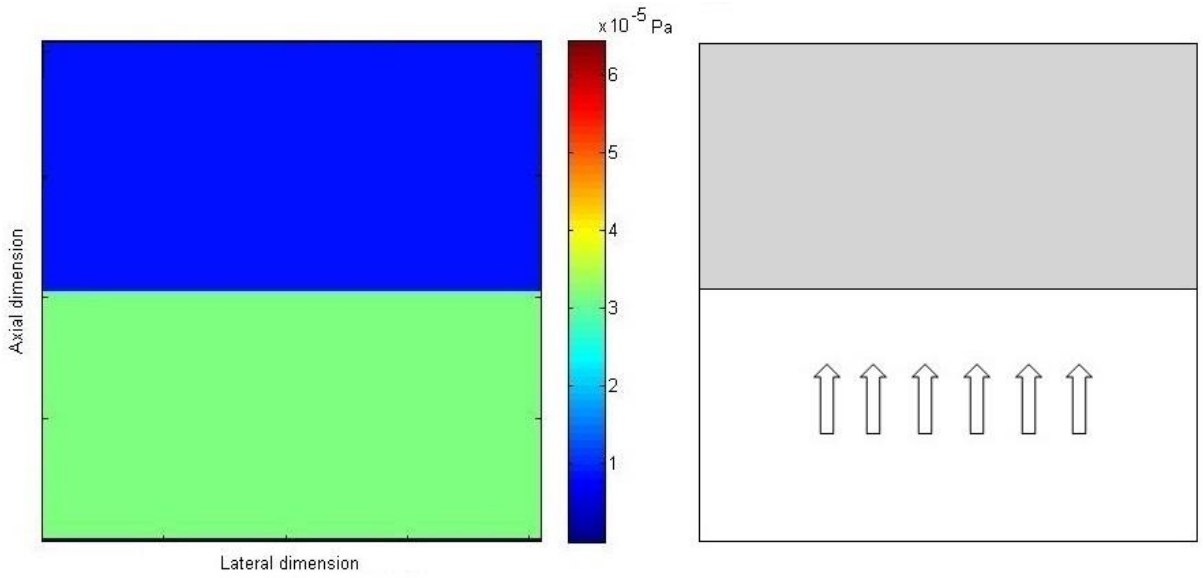

Fig. 4.4a: Pressure dispersion is shown for a plane wave in water with a plane interface on the left. The colour bar shows the pressure. The figure on the right shows the direction of the plane wave in the form of arrows. The grey area indicates the solid medium.

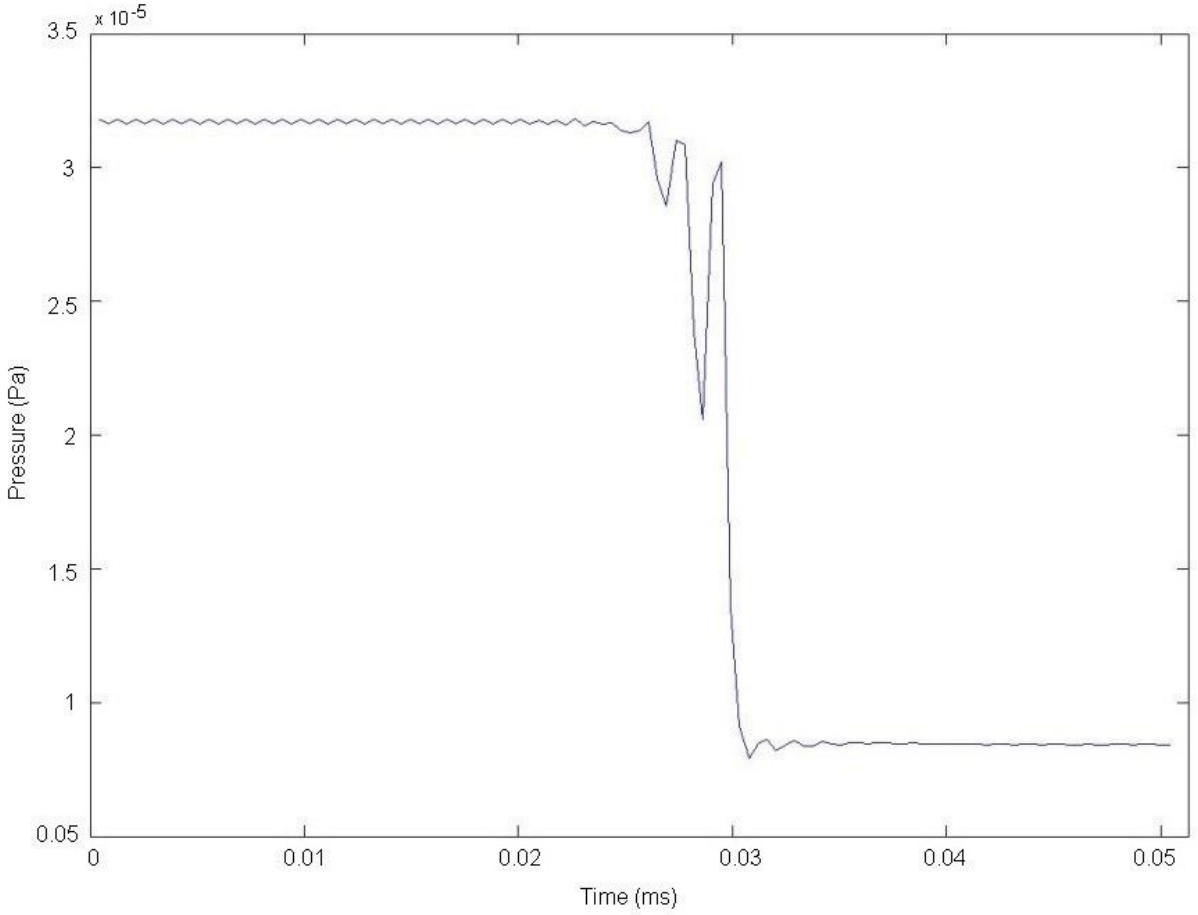

Fig. 4.4b: Pressure change of a plane wave incident on a plane interface.

In Fig. 4.5, the pressure distribution is shown for a plane wave travelling from the bottom, hitting a solid plane interface at an angle of 30°. The acoustic simulation plot shows the summation of intensities in the time domain after the pulsed plane wave has run through the entire field.

The variables for a bottlenose dolphin's tooth were taken for the solid medium and sea water for the fluid medium. As seen in the figures above, the sketch on the right shows the direction of the plane wave in the form of arrows, with the grey area displaying the solid medium and the white area displaying the fluid. The dotted lines display the reflection wave and refraction wave respectively, θ_2 is the angle of refraction. There is an increase in pressure at the area, where the plane wave hits the solid medium. The pressure of the reflected wave decreases with time. The pressure in the solid medium is attenuated compared to the pressure in the fluid. The pressure of the refracted wave decreases with time. The angle of reflection and refraction respectively was determined manually and compared with Snell's Law. Both manual calculation as well as the calculation through Snell's Law showed 30° for the reflection angle θ_1 and 48° for the refraction angle θ_2. According to Snell's Law, the angle of incidence is equal to the angle of reflection. This can also be seen in Fig. 4.6, with an angle of 30° for the incident wave as well as for the reflected wave. The angle of refraction θ_2 is arcsin $\theta_2 = (\sin \theta_1/c_1)c_2 = 48°$.

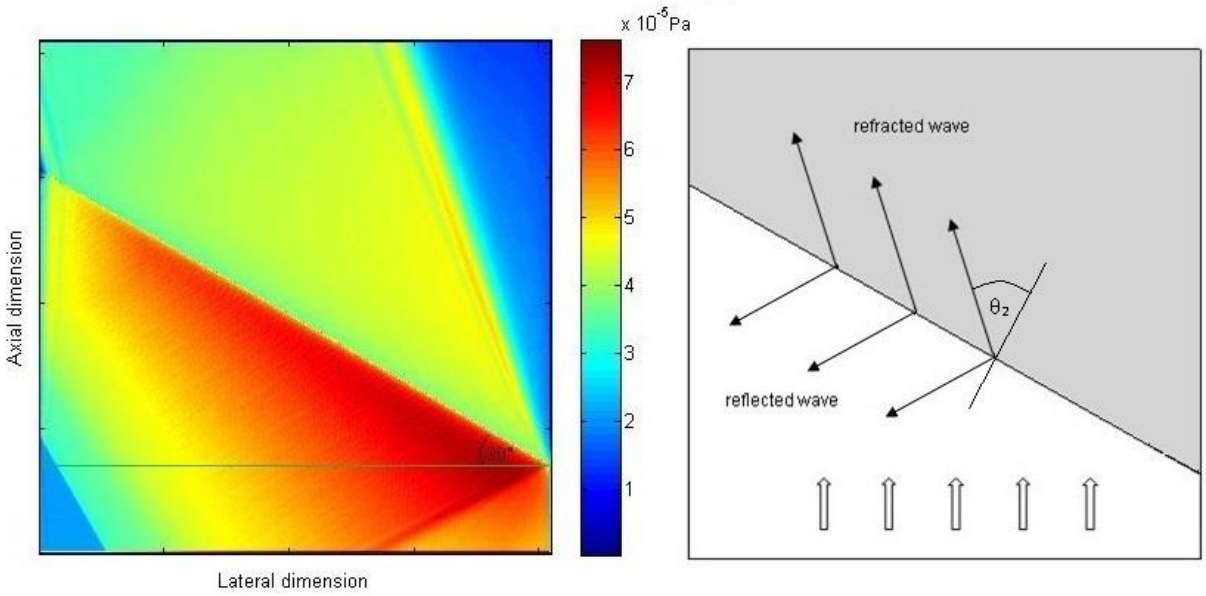

Fig. 4.5: On the left, the pressure dispersion is shown for a plane wave in water hitting an interface at a 30° angle. The colour bar shows the pressure. The figure on the right shows the direction of the plane wave in the form of arrows (hollow). The grey area indicates the solid medium. The black arrows indicate the reflection and refraction wave respectively, with θ_2 as the refraction angle.

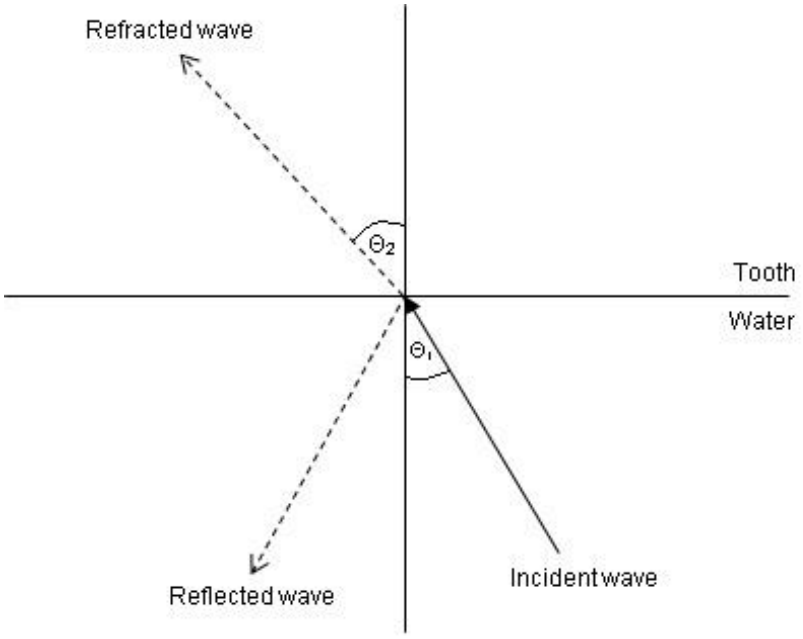

Fig. 4.6: Overview of different angles according to Snell's Law.

The fourth simulation shows the pressure distribution of a plane wave after hitting a solid circle (Fig. 4.7). The acoustic simulation plot shows again the summation of intensities in the time domain after the pulsed plane wave has run through the entire field. Pressure dispersion around and in the circle are as expected. Total reflection can be seen at the area where the wave hits the solid circle at an angle of 0°. The pressure behind the circle is very low and a noticeable high pressure distribution can be seen inside the circle due to reflection of the sound wave from its concave structure.

A catacaustic curve with a discontinuous two-part curve is shown inside the circle, which is formed by sound wave reflection from the curved surface of the circle. Catacaustic is the envelope of rays emanating from a radiant point. A focal point (F) is located along the principal axis, midway between vertex and the centre of the circle (C). It is the point at which the sound waves incident at the circle and travelling to the principal axis will meet after reflection (Glaeser 1999). That the focal point is as expected at half the radius of the circle is another verification that the acoustic model is correct. Another expected outcome is also the particularly low pressure behind the circle. This region of reduced sound levels displays the shadow zone and occurs due to the inability of the sound waves to bend around the circle.

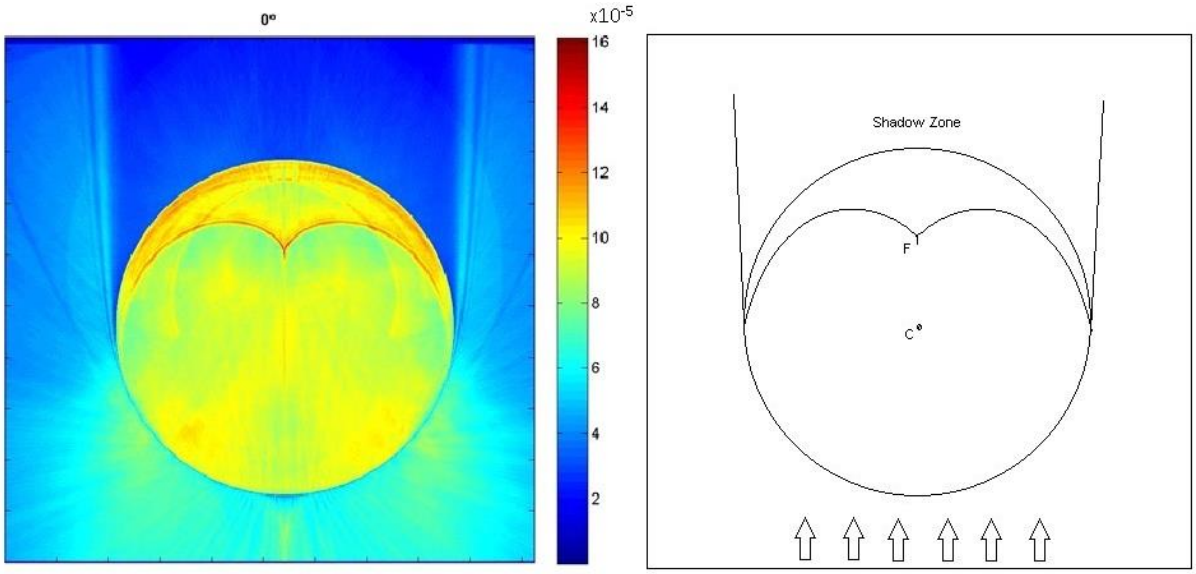

Fig. 4.7: Pressure dispersion of plane wave in water hitting a solid circular cross section. The colour bar shows the pressure in Pascal. The figure on the right shows the direction of the plane wave in the form of arrows and the point of the centre of the circle (C) as well as the focal point (F). The area of the shadow zone behind the circle is between the two displayed lines which are drawn along the circle.

4.1.2 Model validation

For the model validation, two benchmarks were used from Robertson and Rudy (1998) and Dible (2008). The outcome of their results was then compared with the results obtained by the model used in this thesis. Both authors investigated acoustic band gaps in two-dimensional periodic arrays, with Dible (2008) looking into the possibility of dolphins' teeth acting as acoustic stop band. Although this was not investigated in this thesis, their measurements were used as a comparison to validate the model.

A six-layer array was modelled on a square mesh with a diameter of 23.4 mm for the circles and a separation of 37 mm between the centres of adjacent circles. A measure point was set at a distance of 407 mm from the last circle (Fig. 4.8). A plane pressure pulse in the time domain was used as excitation and the normalized sound pressure was determined for various frequencies. The data were then plotted alongside Robertson and Rudy's (1998) and Dible's (2008) results and compared with each other.

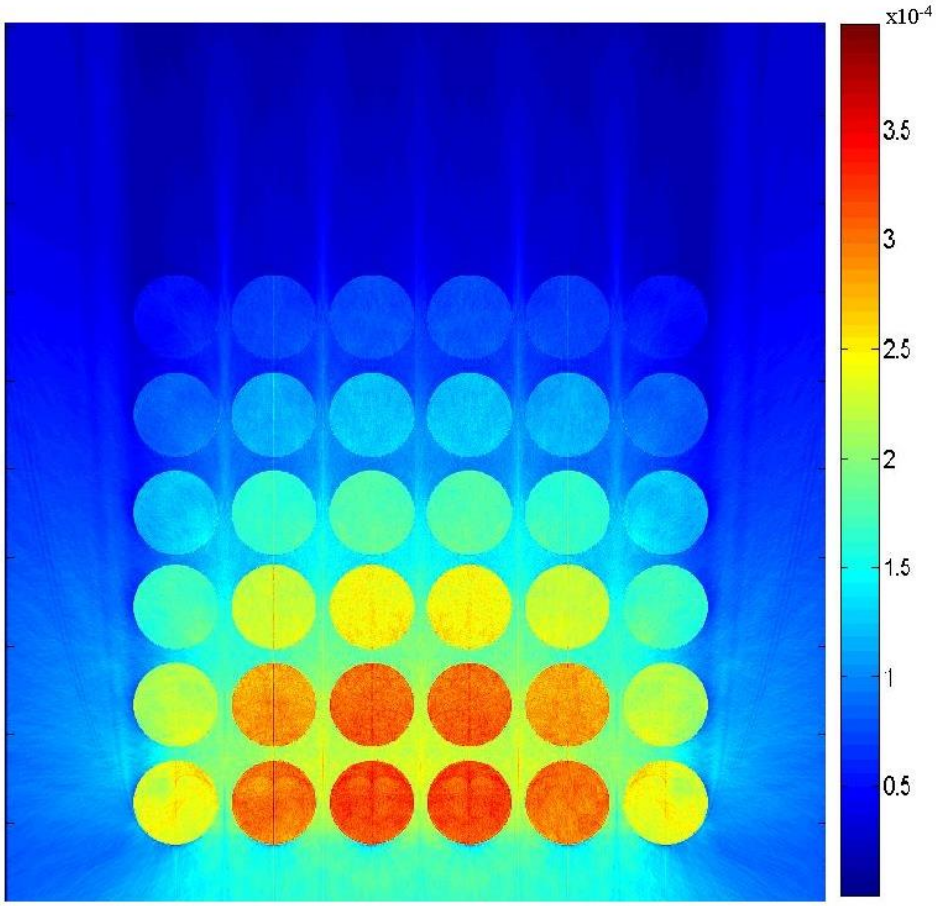

Fig. 4.8: Colour-coded simulation of sound propagating through six-layer element periodic array. The plane wave pulse is coming from the bottom of the graph.

The pressure was taken for five different frequencies, which was considerably less than it was the case for the two benchmarks from Robertson and Rudy (1998) and Dible (2008). However, the main focus laid on the two stop bands at a frequency of 5000 Hz and 9000 Hz and on the area of highest amplitudes at around 2500 Hz and 7000 Hz (Fig. 4.9).

The findings obtained by the Matlab model used in this thesis agree with both authors' measurements. As shown in Fig. 4.9, acoustic band gaps occur at a frequency of 5000 Hz and 9000 Hz. This can also be seen in the simulations of this thesis. These results confirm the validity of the Matlab model.

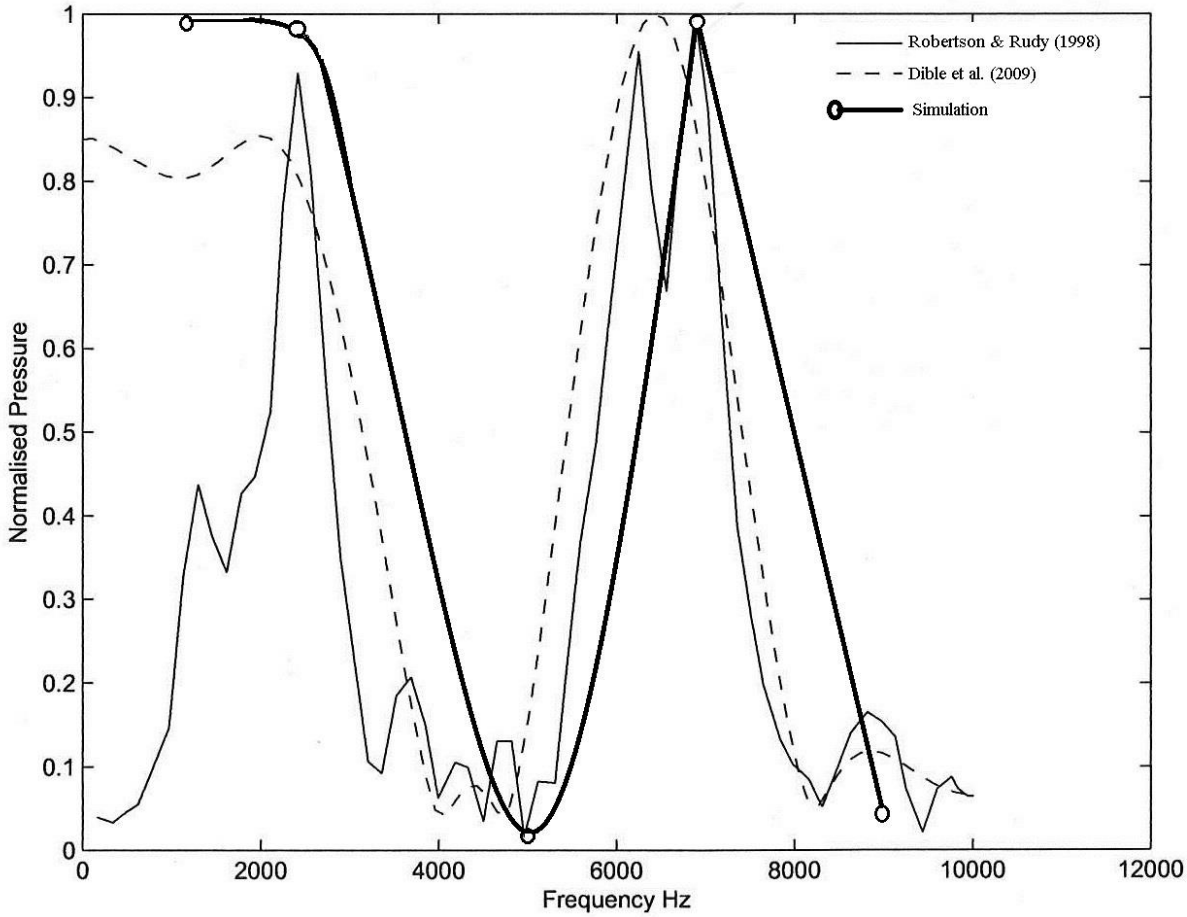

Fig. 4.9: Comparison between two benchmarks from findings by Robertson and Rudy (1998) and Dible (2008) and the simulated results. The thick solid line shows the findings of the model used in this thesis. Normalised pressure is plotted against various frequencies (adapted from Dible 2008).

4.1.3 Grid sensitivity analysis

The simulation is based on a 5000 x 5000 spatial grid, which was chosen after comparison with other grid sizes. The shape of the circles (teeth) changes for grid sizes below 5000. The circle shape at grid sizes 512, 1500, 2500 and 3500 was noticeably squared. Grid sizes were therefore enhanced in order to obtain a more realistic and circular shape. As seen in Fig. 4.10, there is only a minimal difference in shape between 4500 and 5000.

Fig. 4.11 shows the pressure distribution at the tip of teeth on the left jaw side at 100 kHz for six different grid sizes. The pressure is significantly lower for grid sizes below 5000 and noticeably fluctuating. Pressure distribution at a grid size of 5000 is comparably smoother. Since a higher grid size of 6000 showed no significant change in pressure distribution or shape

of the circle, but would result in more computational cost and time, 5000 x 5000 was found to be the optimal grid size for the model.

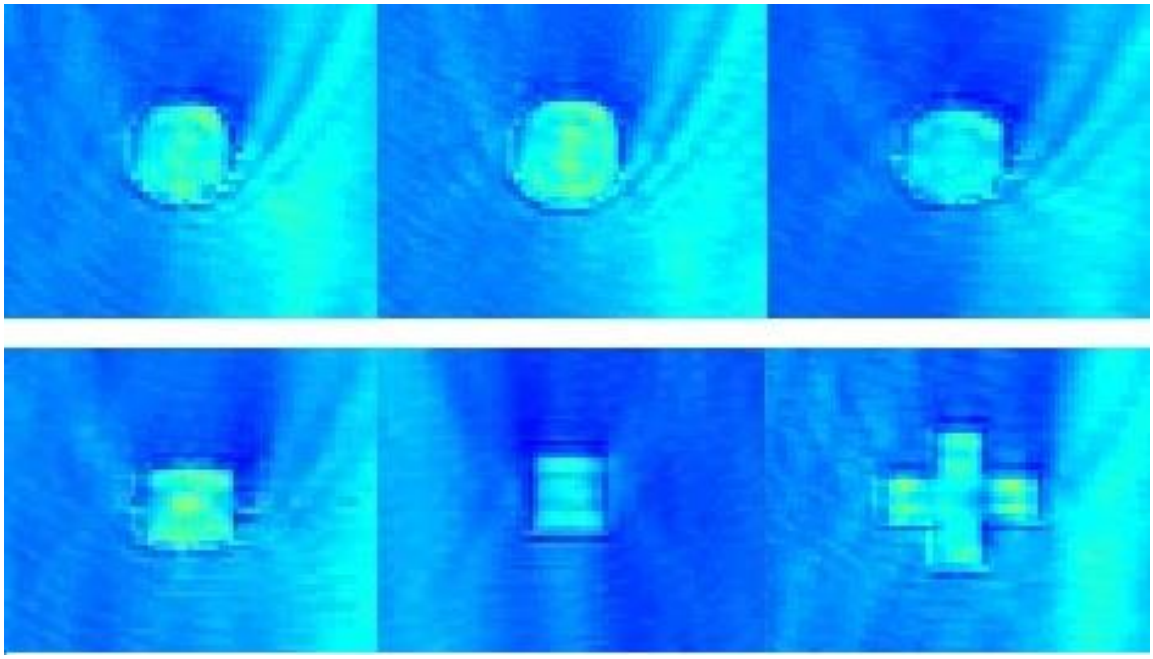

Fig. 4.10: Shape change of the circles for different grid sizes. Figure shows the circles from top left to top right and bottom left to bottom right for grid sizes of 5000, 4500, 3500, 2500, 1500 and 512.

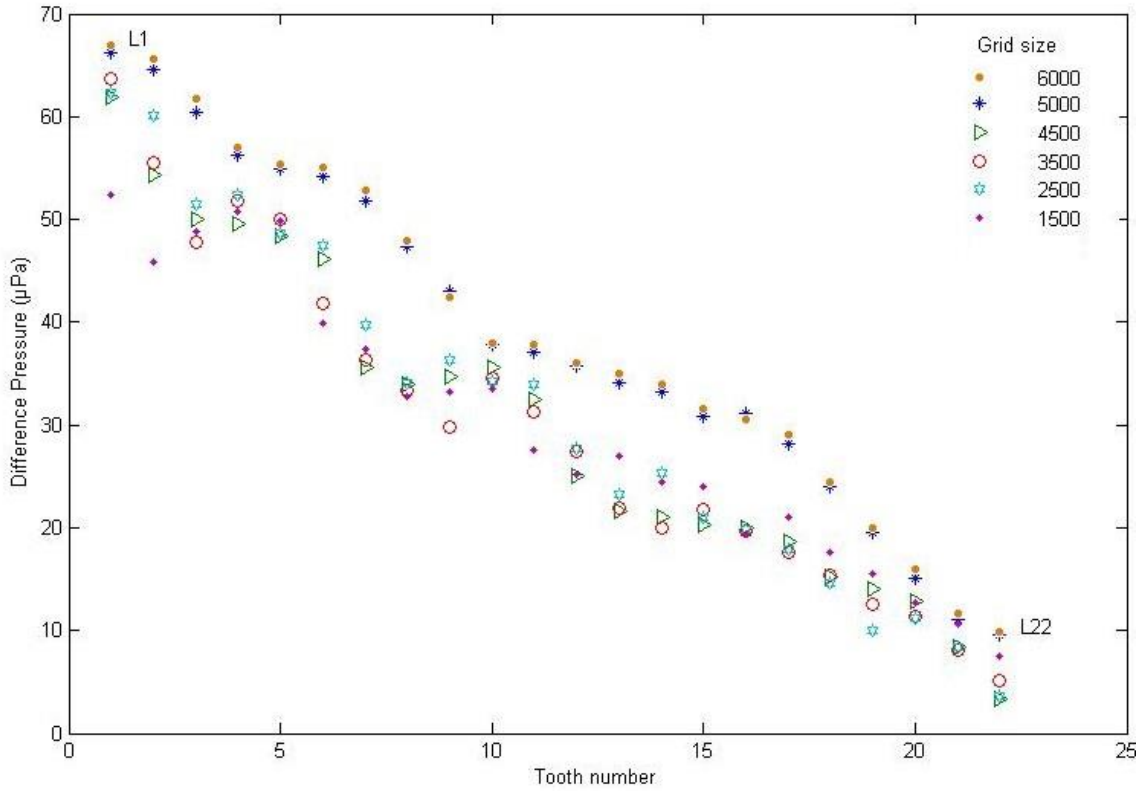

Fig. 4.11: Difference pressure at the teeth on the left side of the jaw for 100 kHz for different grid sizes.

4.1.4 Tooth geometry and justification for parameters

The tip and the base diameters of the teeth were used to create two different input datasets. The arrangement of the tip of the teeth with sea water filling the spaces between the teeth can be seen in Fig. 4.12. The 2-D model has been run looking at different angles of a narrow-band plane wave propagating in the plane of the jaw. The relation between the pressure distribution of a plane wave incident on the teeth of a bottlenose dolphin was investigated, which consequentially determined the level of sensitivity at the animal's jaw, and the change of parameters such as frequency, tooth diameter and missing teeth.

The greatest hearing sensitivity for a bottlenose dolphin was measured at a frequency range of 100 - 135 kHz, the maximum frequency at 150 kHz (Rossing 2007, Au 2010). Whistling frequencies typically lie below 50 kHz (Au and Hastings 2008). The pressure distribution for a frequency of 100 kHz and 20 kHz was measured to investigate the difference between echolocation and communication frequency. Pressure distributions at the tip and bottom of the teeth were measured in order to investigate the pressure change with changing tooth diameter. Several teeth were then removed to analyse the dependency of the pressure distribution when teeth were missing. Opposite teeth 17 on both sides of the jaw situated further in the back were chosen to see if missing teeth have an impact on the pressure dispersal, while symmetry in the jaw was still existing.

Multiple teeth were then removed on both sides of the jaw and the pressure change again examined. These teeth were picked at random. Angles from -90° to +90° were chosen with 1 degree intervals from -10° to +10° and 5 degree intervals from -10° to -90° and +10° to +90° respectively showing changes of the amplitude at each single tooth. The change from 1 to a 5 degree interval at +10° and -10° was chosen due to measurements by various authors of the hearing sensitivity in bottlenose dolphins. Highest sensitivities were measured for sound coming from in front of the dolphin as well as from an angle slightly further to the right and to the left of the jaw (e.g. Potter and Taylor 2001, Dobbins 2007, Au and Hastings 2008, Cranford et al. 2008a). Au (1993) measured a reception beamwidth of 13.7° at a frequency of 120 kHz for bottlenose dolphins.

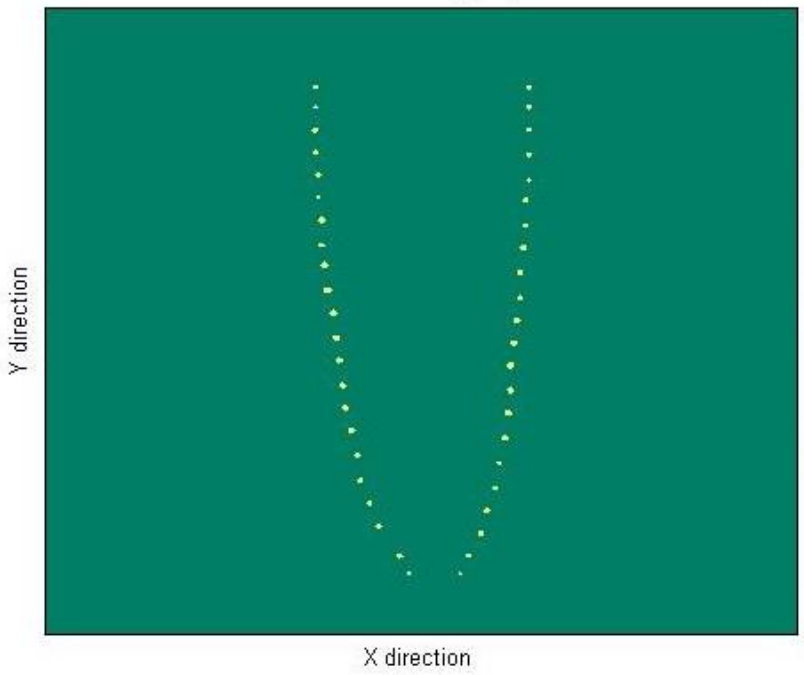

Fig. 4.12: Tip of a bottlenose dolphin's teeth as circles, input into an acoustic propagation model.

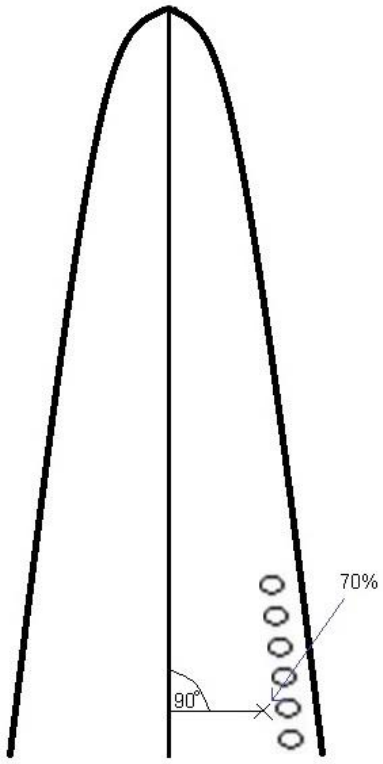

Fig. 4.13: Sketch of dolphin jaw showing the pressure point at 70% between tooth and middle line.

Pressure values were taken at a point 70 % between tooth and middle line of the jaw (Fig. 4.13) in order to be able to compare pressure distributions for different angles at a specific position in the jaw.

These values were chosen as they showed the pressure near the tooth, but not directly at the tooth. A pressure of 18.99 µPa was measured for a sound wave running through water without obstacles to determine the difference pressure. The pressure distribution at the teeth was investigated for different jaw angles in order to examine the relation between the angle of incoming sound and the directional hearing capability of the animal. Fig. 4.14 shows an example of an echolocating dolphin emitting sound with the jaw at an angle of 0° and 30° respectively; the returning sound wave with scattering at the teeth can be seen below. The colour-coded image shows the pressure distribution at the teeth, varying with changing angle. Scattering at the teeth and the impact of neighbouring teeth on the sound distribution was investigated and analysed.

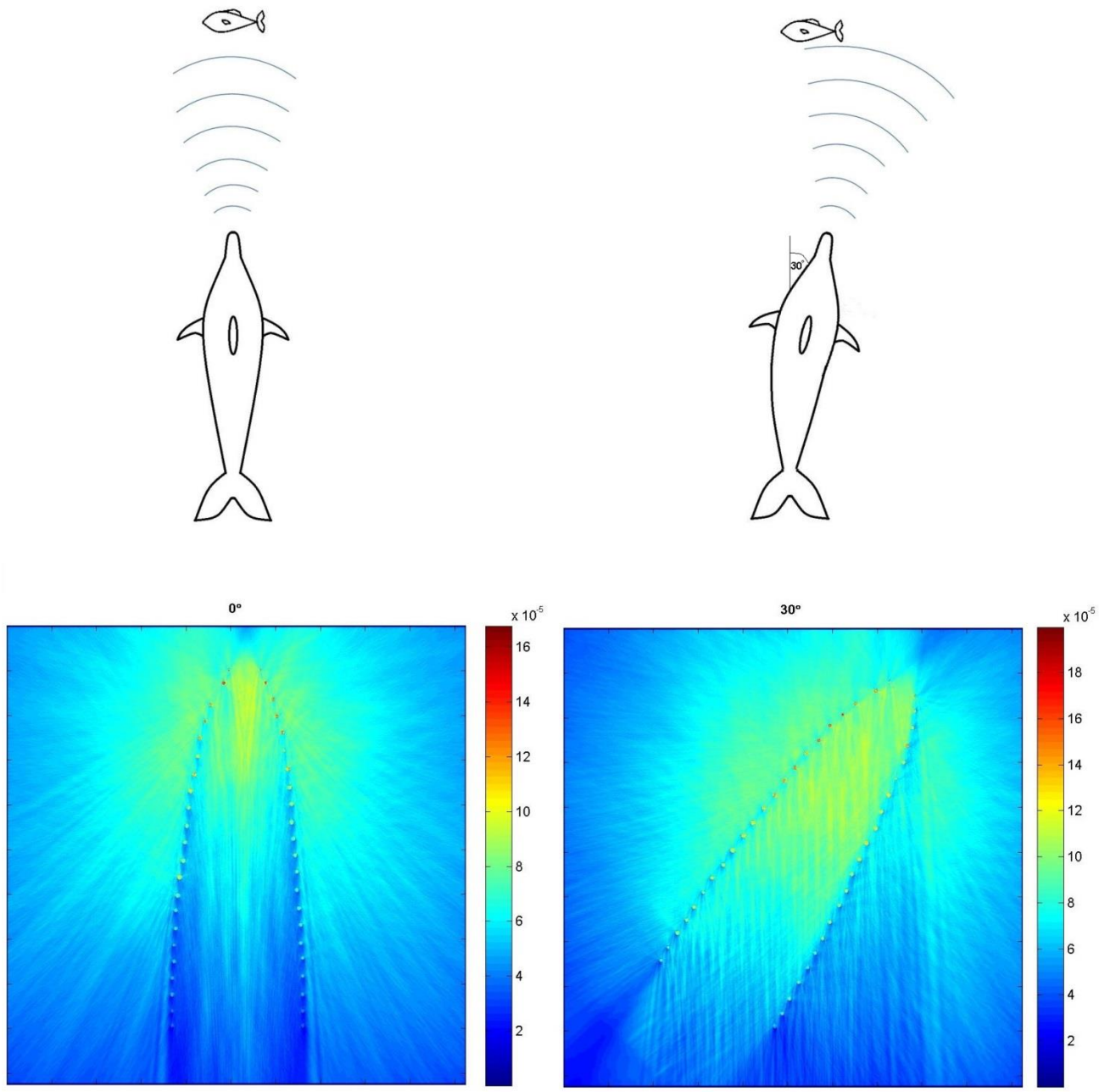

Fig. 4.14: Above: Target detection by an echolocating bottlenose dolphin with emitted sound wave at different angles. Top left: Echolocating dolphin pointing head directly towards the target at an angle of 0°. Top right: Echolocating dolphin with head turned at a 30° angle. Below: Returning sound wave propagating toward the front of the dolphin's jaw, hitting the tip of the teeth at an angle of 30˚ and 0˚.

5 Results

5.1 Normal incident plane wave

An example of the distribution of the acoustic pressure is shown in two time steps during a simulation of a plane wave coming from in front of the jaw (Fig. 5.1). There are areas where the sound pressure is reduced, increasing in size as the wave propagates toward the back teeth, areas of enhanced sound and multiple scattering on the neighbouring teeth. Teeth further away tend to be masked by teeth in the line of sight from the transmitter.

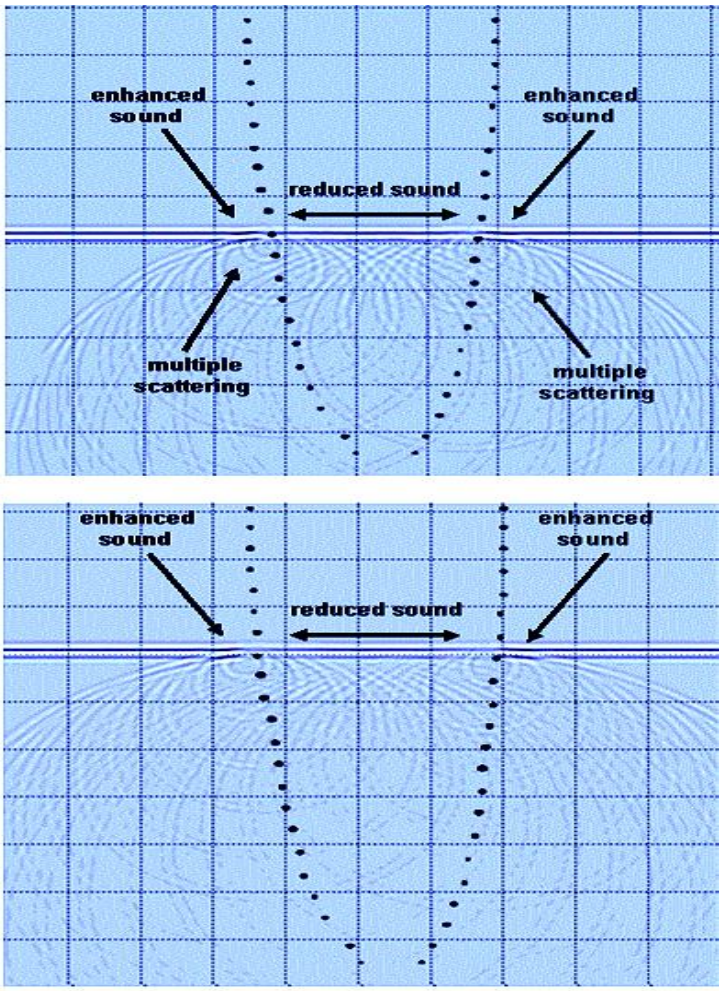

Fig. 5.1: Two time steps for a plane wave coming from the front of the jaw.

Figure 5.2 shows the pressure at the front teeth on the right side of the jaw with scattering for a wave coming from an angle of 0°. The first peak in the acoustic signal corresponds to the direct arrival of the wave on the tooth considered. Secondary peaks from neighbouring teeth

mix with the direct arrivals of the incoming sound on individual teeth and result in a high level of multiple scattering. In some configurations, individual clicks might become indistinguishable. Signals backscattering on teeth further back in the jaw create signals later in time on teeth already insonified.

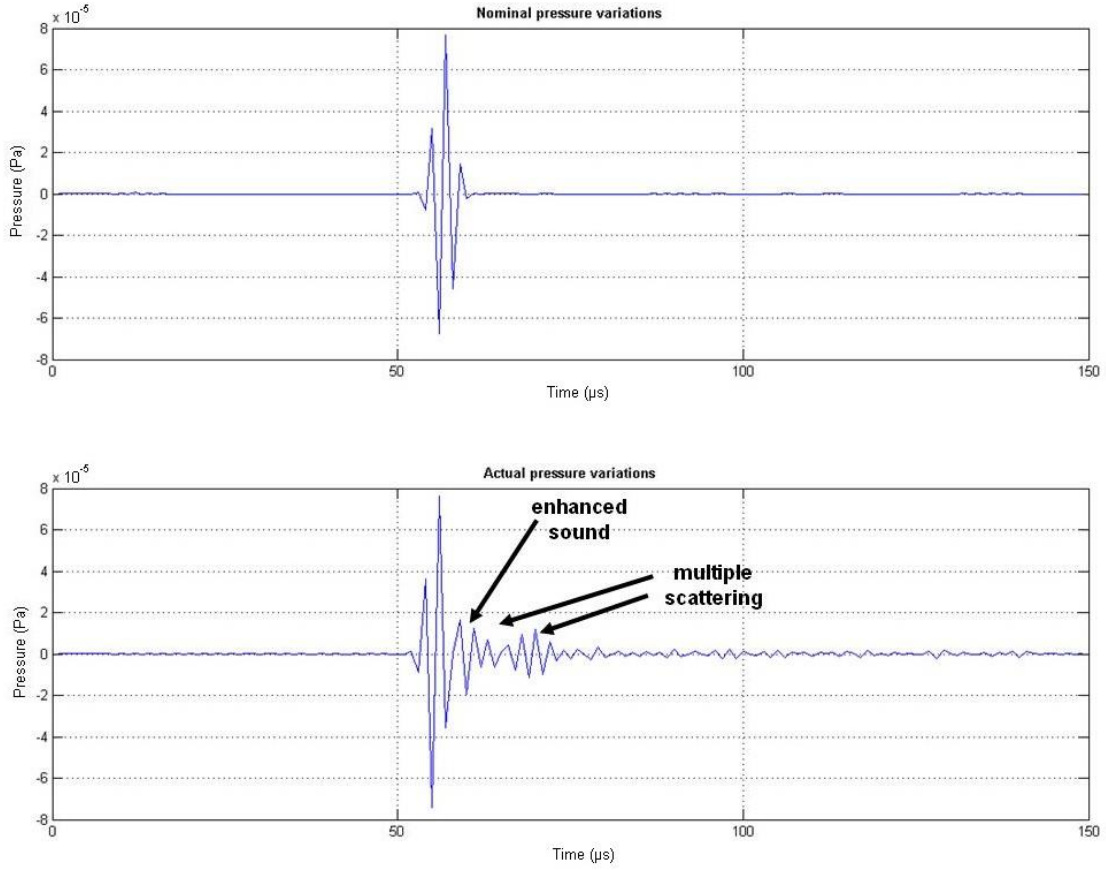

Fig. 5.2: Signal expected at a tooth modelled as a point receiver (top); the figure below shows the signal actually received at the tooth, if modelling tooth size and position.

The prediction indicates that the pressure at the teeth is highest nearest the incident wave; the amplitude of the sound behind the teeth is much lower. There are clear indications of multiple scattering, which shows the importance of neighbouring teeth in attenuating or amplifying the signal received at other teeth. This directional hearing can be amplified or attenuated depending on the tooth configurations. The propagation of sound will evidently vary with tooth size and position. Signals hitting various teeth (L2-L5) on the left side of the lower jaw at an angle of 0° show a peak signal directly after hitting the first tooth (Fig. 5.3). Sound is enhanced directly after reception of the signal and eventually attenuates with time. Multiple scattering occurs in particular when the plane wave is coming from the front of the jaw.

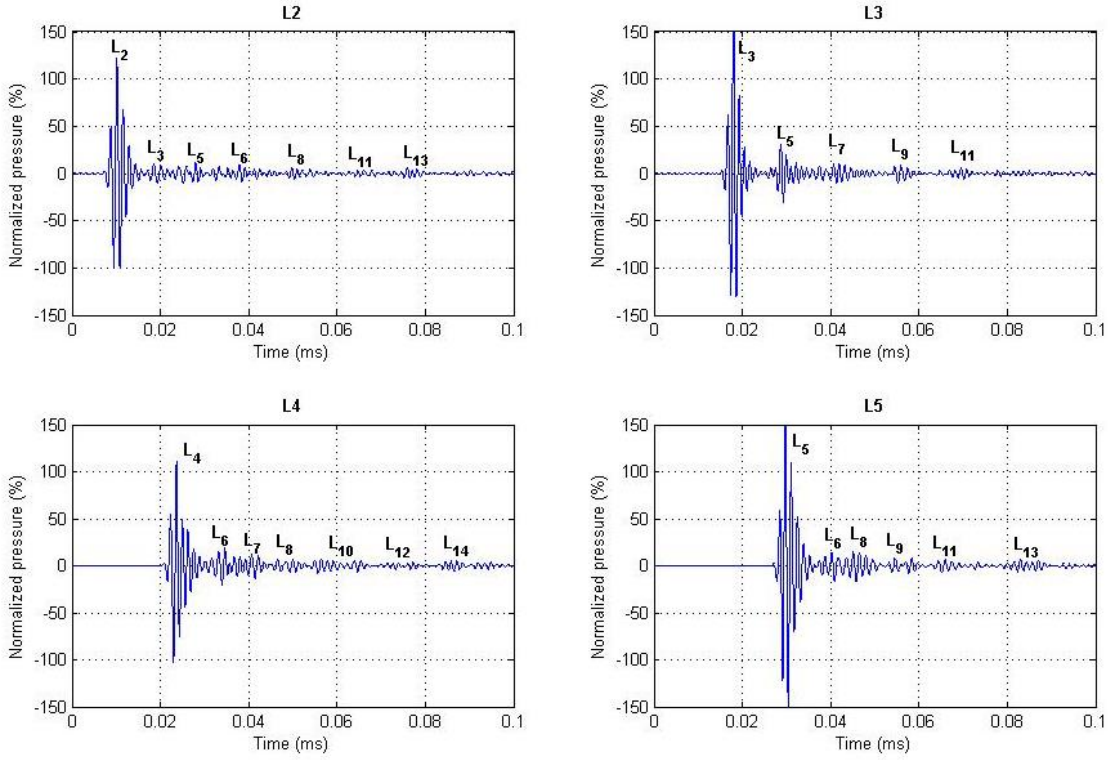

Fig. 5.3: Signals received on the left (L) side of a dolphin's lower jaw at teeth 2, 3, 4 and 5 (L2-L5) at an angle of 0°.

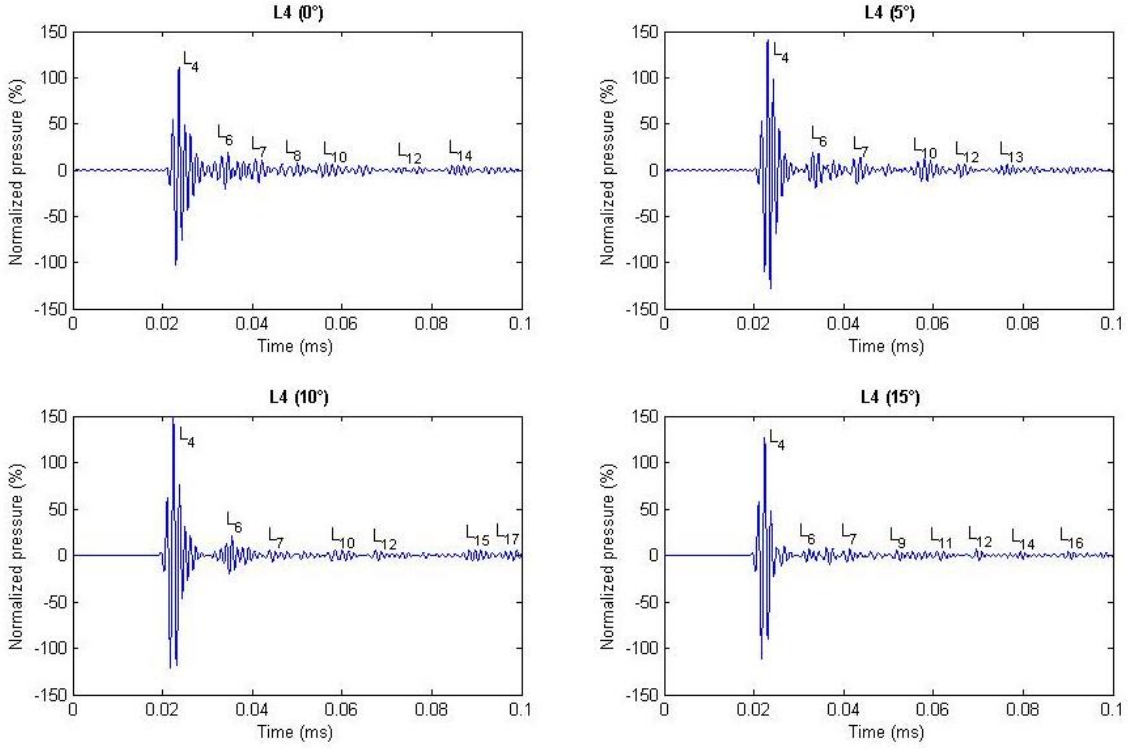

Fig. 5.4: Signals received on tooth number 4 on the left (L) side of a dolphin's lower jaw at angles from 0°-15° in 5 degree intervals.

The propagation of sound evidently varies with the position of the teeth. The simulations show that teeth cannot be considered as individual, point-like receivers. Multiple scattering is important, at all angles of rotation of the jaw. It is possible to identify individual teeth reflections on the acoustic signals measured at each single tooth. Sound is enhanced immediately after reception of the original signal, attenuating with time. Figure 5.4 shows the normalized pressure measured at tooth 4 on the left side of the jaw (L4) for angles 0°-15° in 5 degree steps. Multiple scattering is highest at an angle of 0° and decreases from 0° to 15°. Subsequent peaks in the signal have amplitudes of 10% or less, and are identified from their time of arrival to be reflections on nearby teeth. Reflections from some of the immediately neighbouring teeth cannot be identified, either because they are subsumed into the signal scattered by the previous tooth or because they are masked. This varies with the jaw geometry and with the angle of the incoming wave.

5.2 Effects of changing jaw angle for different frequencies

Sound pressure was measured for a plane wave propagating through the jaw at a jaw angle of -90° to +90° in 5 degree intervals. The pressure was measured after the sound wave had travelled through the entire jaw.

5.2.1 Pressure for a 20 kHz sound wave at tip of teeth

The pressure distribution of a plane wave with a frequency of 20 kHz at the tip of the teeth is shown in Fig. 5.5. The sound propagation was modelled for jaw angles 0° to 25° in 5 degree steps to show the dispersion of the pressure at the entire jaw. The simulation shows that the incoming sound does not penetrate much within the two lines of teeth. There is constructive interference at the front of the inner jaw between teeth leading to amplified pressure. This is possibly caused by an increased back and forth scattering of the sound waves between the teeth in the front of the jaw due to the narrowness of the two lines of teeth. The lowest sound pressure was measured at the rear teeth. The modelled sound fields show variation with different incident energy arrival angles of the two lines of teeth. This could indicate that a dolphin's sensory mechanism has the potential to receive information about the arrival angle of a signal, thereby providing sound localization. Looking at the inside of the jaw between the two lines of teeth, the pressure decreases at the back on the right side when a sound wave arrives from the right side of the head due to shadowing of the teeth on the right. The pressure increases on the

left side. The pressure distribution on the outside of the two lines of teeth at the back teeth is reversed, with an increasing pressure on the right side and a decreasing pressure on the left side (Fig. 5.5).

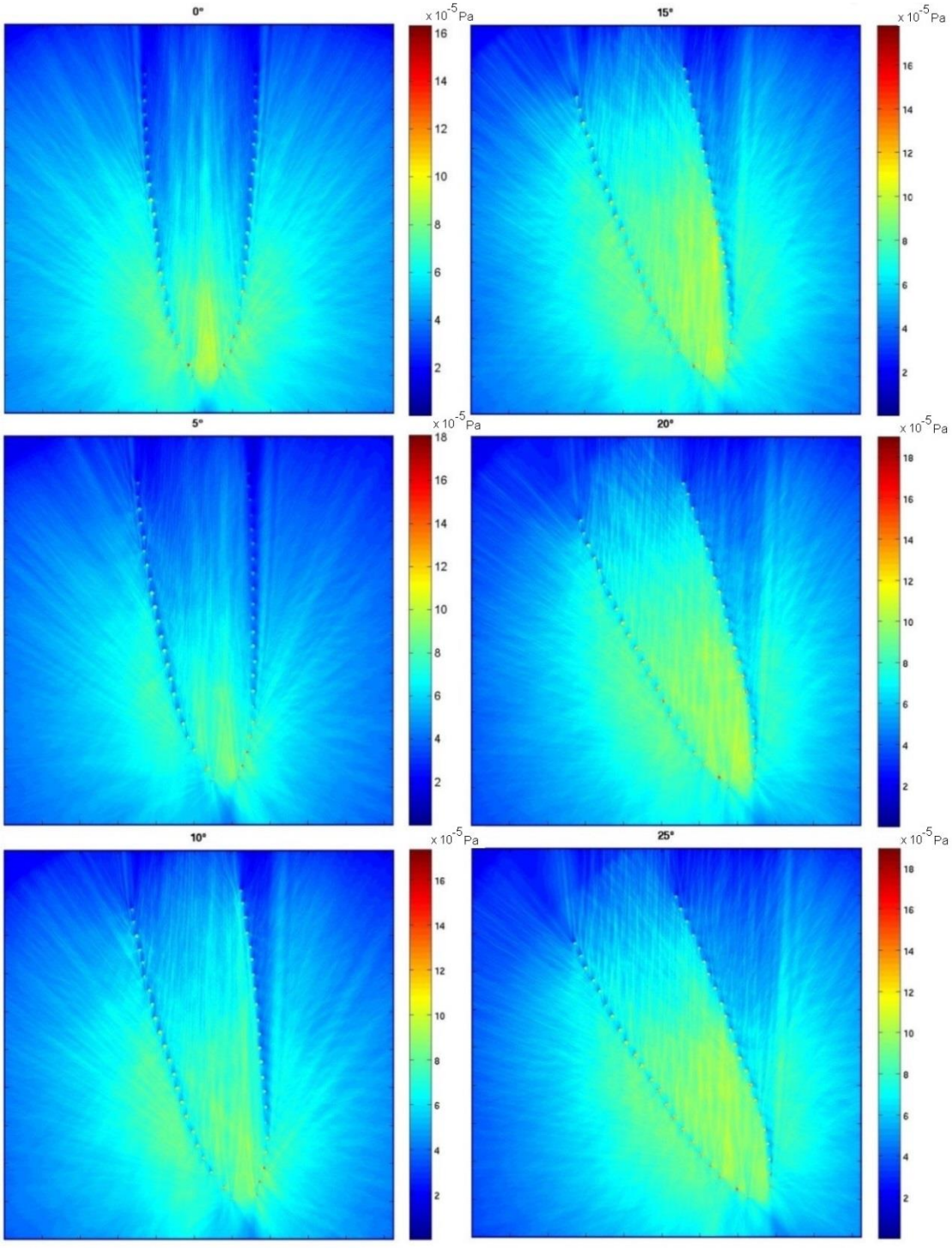

Fig. 5.5: Colour-coded simulation of sound propagation at the tip of the teeth of *Tursiops truncatus* for jaw angles 0° to 25° in 5 degree steps for a frequency of 20 kHz. Plane wave is coming from the bottom of each graph.

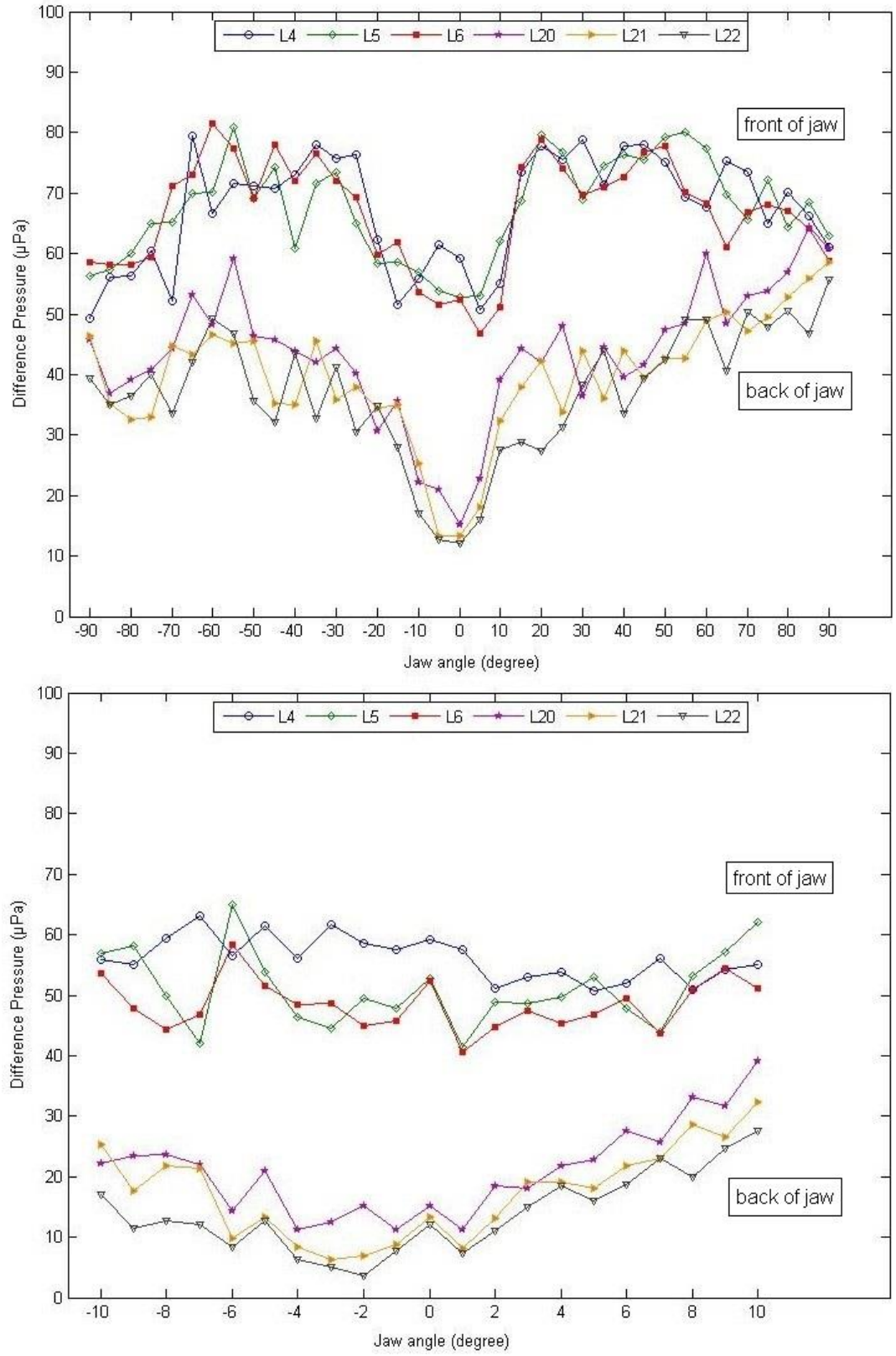

Fig. 5.6: Difference pressure at front and back teeth at the left side of the jaw for a frequency of 20 kHz and angles -90° to +90° in 5 degree steps (above) and -10° to +10° in 1 degree steps (below) for the tip of the teeth.

The difference pressure was measured for a 20 kHz plane wave propagating through the tip of the teeth at a jaw angle of -90° to +90° in 5 degree steps and for angles -10° to +10° in 1 degree steps (Fig. 5.6). The modelled pressure was measured at tooth 4, 5 and 6 (L4-L6) in the front of the jaw and tooth 20, 21 and 22 (L20-L22) in the back of the jaw for the left side of the jaw. The background pressure was subtracted. The pressure at the front teeth shows no tendency for the left side of the jaw for changing angles, particularly between angles +10° to +10°. The lowest pressure for L4 was measured at an angle of 2° with 51.06 µPa and at an angle of -90° with 49.20 µPa for negative degrees. The pressure increases from 0° with fluctuations until it reaches the highest pressure at 30° with 78.81 µPa and at -65° with 79.35 µPa. For L5, a lowest pressure was measured at an angle of 1° with a pressure of 41.35 µPa and at an angle of -7° with 42.01 µPa. The pressure then increases with fluctuations until it reaches the highest pressure at 55° with 79.97 µPa and at -55° with 80.89 µPa. The lowest pressure for L6 was measured at an angle of 1° with 40.56 µPa and at -8° with a pressure of 44.24 µPa. The pressure then increases gradually until it reaches its peak at 50° with 77.70 µPa and at -60° with 81.60 µPa and then decreases again.

The pressure at the back teeth shows a more regular behaviour with change of the jaw angle. A gradual increase on the left side of the jaw for tooth L20, L21 and L22 can be seen from the lowest pressure to an angle of 15° and -15° respectively, with pressure values fluctuating after that. The lowest pressure for L20 was measured at an angle of 1° with a pressure of 11.35 µPa and at an angle of -1° with 11.16 µPa. The pressure then increases with a few fluctuations for negative degrees until it reaches the first peak at 15° with a pressure of 44.39 µPa and at -15° with 35.54 µPa. It then fluctuates until it reaches the highest pressure at 85° with 64.27 µPa and at -55° with 59.10 µPa. The pressure at tooth L21 increases gradually from the lowest point at 1° with a pressure of 8.10 µPa to a pressure of 42.33 µPa at an angle of 20° and from the lowest pressure at -3° with 6.34 µPa to a first peak pressure at -15° with 35.10 µPa. The pressure then increases with fluctuations until it reaches the highest pressure at 90° with 58.48 µPa and at -60° with 46.67 µPa. The lowest pressure for L22 was measured at an angle of 1° with a pressure of 7.30 µPa and at -2° with 3.70 µPa. The pressure then increases until it reaches a peak at 15° with 28.87 µPa and at -20° with 34.74 µPa. A pressure increase with strong fluctuations can then be seen until the peak pressure of 55.70 µPa is reached at an angle of 90° and the highest pressure of 49.20 µPa at an angle of -60°.

The pressure values on the front teeth on the right jaw side show also no noticeable trend for any angles (Fig. 5.7). The lowest pressure for R4 was measured at an angle of 9° with 47.32 µPa and at an angle of -7° with 45.47 µPa. The pressure then increases to the highest point at an angle of 35° with 81.80 µPa. For negative degrees, a first peak is reached at -25° with a pressure of 76.91 µPa. The pressure then fluctuates until it reaches the highest point at -55° with 79.08 µPa. For R5, a lowest pressure was measured at an angle of 4° with a pressure of 52.20 µPa and at an angle of -2° with 46.98 µPa. The pressure then increases with fluctuations until it reaches its peak at an angle of 60° with 80.76 µPa and at -60° with 79.75 µPa. It decreases again after this. The lowest pressure for R6 was measured at an angle of 1° with 40.34 µPa and at -9° with 41.77 µPa. The pressure then increases until it reaches a peak at 45° with a pressure of 83.90 µPa and at -30° with 79.20 µPa.

The pressure at the back teeth shows a more regular behaviour with change of the jaw angle. A gradual increase on the left side of the jaw for tooth R20, R21 and R22 can be seen from the lowest pressure to an angle of 20° and -20° respectively, with pressure values fluctuating after that. The lowest pressure for R20 was measured at an angle of 1° with 10.78 µPa and at an angle of -1° with 10.20 µPa. The pressure then increases gradually until it reaches the first peak at 20° with a pressure of 44.64 µPa and at -20° with 44.48 µPa. It then fluctuates until it reaches the highest pressure at 80° with 56.88 µPa and at -80° with 59.97 µPa. The pressure at tooth R21 shows a gradual increase from the lowest point at 4° with 6.30 µPa and at -1° with a pressure of 10.16 µPa to a peak at 20° with 35.71 µPa and at -10° with 34.71 µPa. Pressure then fluctuates until it reaches the highest point at 80° with 52.73 µPa and at -65° with 56.44 µPa. The lowest pressure for R22 was measured at 0° with a pressure of 10.18 µPa and at -2° with 4.92 µPa. The pressure then increases until it reaches a first peak at 20° with 41.22 µPa and at -15° with 37.96 µPa. A pressure increase with strong fluctuations can then be seen until the highest pressure is reached at an angle of 75° with 55.34 µPa and at -90° with 55.2 µPa.

In summary, the results show strong pressure fluctuations and no apparent trend at the front teeth inside the jaw for all angles and on both jaw sides. The pressure at the back teeth inside the jaw displays a trend between ±15°. The lowest pressure at the rear teeth on the left was measured at around -2° with the pressure increasing afterwards (Fig. 5.6), the lowest pressure at the rear teeth on the right was measured at around 2° (Fig.5.7). This isolation between the right and left rear teeth indicates sound localization.

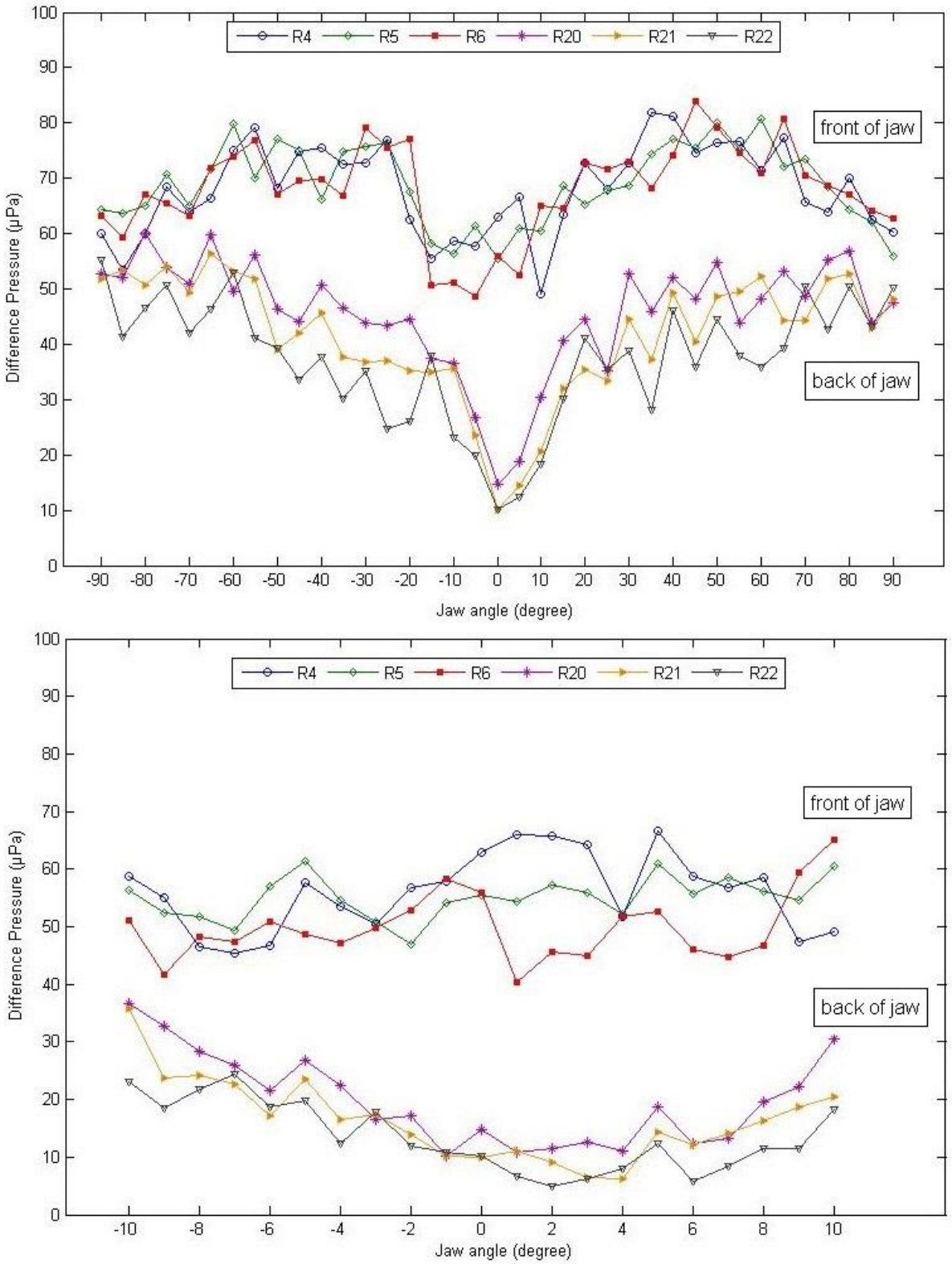

Fig. 5.7: Difference pressure at front and back teeth at the right side of the jaw for a frequency of 20 kHz and angles -90° to +90° in 5 degree steps (above) and -10° to +10° in 1 degree steps (below) for the tip of the teeth.

5.2.2 Pressure for a 100 kHz sound wave at tip of teeth

The overall pressure distribution of a plane wave with a frequency of 100 kHz is displayed in Fig. 5.8. The sound propagation was modelled for jaw angles 0° to 25° in 5 degree steps. As seen for a frequency of 20 kHz, the pressure at an angle of 0° is highest at the front teeth and lowest pressure values at the back teeth. The distribution of high pressure increases at the jaw with a 5° change of the jaw angle. High pressure can be seen for the first half of the jaw for angles 15° - 25°. The pressure for a sound wave coming from in front of the jaw at an angle of 0° in the horizontal is almost evenly distributed on both sides of the jaw in the back. The slight difference is due to the uneven spacing of the teeth in the front of the jaw. At the inside of the jaw, the pressure decreases at the back on the right side when a sound wave arrives from the right due to shadowing of the teeth. The pressure increases on the left side. The pressure distribution on the outside of the jaw at the back teeth is reversed, with an increasing pressure on the right side and a decreasing pressure on the left jaw side.

Figure 5.9 shows the difference pressure at the teeth on the left side of the jaw for angles -90° to +90° in 5 degree steps and for angles -10° to +10° in 1 degree steps. A closer look at angles ±10° was chosen, since studies of toothed whales showed that the animals echolocate in the beamwidth range of ± 10° (e.g. Au 1993). The pressure at the front teeth shows a fairly erratic behaviour with several fluctuations. For L5, a low pressure was measured for 0° and -10°, then gradually increasing until it reaches a peak at 20° and -30° respectively. The lowest pressure for L4 can be measured at an angle of 3° with 50.36 µPa for positive degrees and at an angle of -90° with 49.60 µPa for negative degrees, for L5 at an angle of 1° with a pressure of 42.78 µPa and at an angle of -7° with 42.48 µPa. The lowest pressure for L6 was measured at an angle of 1° with 41.96 µPa and at -4° with a pressure of 41.36 µPa. The peak pressure for L4 was measured at 45° with a pressure of 87.80 µPa and at -65° with 79.95 µPa. The highest pressure for L5 was at an angle of 20° with a pressure of 83.30 µPa and at an angle of -55° with a pressure of 81.40 µPa. A peak pressure of 84.20 µPa and 81.90 µPa was measured at an angle of 20° and -60° respectively for L6.

Contrary to the pressure distribution at the front of the jaw, the pressure at the back teeth shows a more regular behaviour with change of the jaw angle. A gradual increase on the left side of the jaw for tooth L20, L21 and L22 can be seen from the lowest pressure to an angle of 15° and -15° respectively, with pressure values fluctuating after this. The lowest pressure for

L20 was measured at an angle of 1° with 11.97 µPa and at -6° with 11.75 µPa. The pressure increases to 47.69 µPa for an angle of 15°, then fluctuates until it reaches a peak pressure of 77.68 µPa at 90°. For the negative angles, the pressure increases from the lowest point to a pressure of 35.54 µPa at -15°. It then fluctuates until it reaches a peak pressure of 59.36 µPa at -55° and decreases after this. The pressure at tooth L21 increases gradually from the lowest point at 0° with a pressure of 11.10 µPa to a pressure of 44.68 µPa at 30°. The pressure then increases with a few fluctuations until it reaches its peak of 70.84 µPa at 90°. For negative degrees, the pressure increases gradually from the lowest point at -3° with 8.17 µPa until it reaches an angle of -15° with 35.10 µPa. The pressure then fluctuates until it reaches its peak at -60° with 47.00 µPa, decreases afterwards and increases again towards the end until -90°. The lowest pressure for tooth L22 was measured at 0° with 9.52 µPa and at -2° with 3.79 µPa. The pressure increases gradually until it reaches a peak at 15° with 34.93 µPa. It then increases with fluctuations until it reaches the highest pressure at 90° with 75.66 µPa. For negative degrees, the pressure increases gradually until it reaches a peak at -20° with 34.74 µPa. The pressure then fluctuates until it reaches the highest point at 60° with 49.99 µPa and decreases after this.

Taking a closer look at ±10°, the pressure at the front teeth shows no trend and fluctuates strongly, whereas the pressure at the back of the jaw increases gradually with a few fluctuations for negative degrees. There is a pressure change for each degree the jaw angle changes. Figure 5.10 shows the pressure at the right side of the jaw for angles -90° to +90° in 5 degree intervals and -10° to +10° in 1 degree intervals at the tip of the teeth for tooth 4 (R4), 5 (R5) and 6 (R6) in the front of the jaw and tooth 20 (R20), 21 (R21) and 22 (R22) in the back of the jaw. The pressure at the front teeth shows again very strong fluctuations. There is no tendency for angles -10° to 10° for tooth R4, R5 and R6. The lowest pressure for R4 was measured at an angle of 9° with 40.02 µPa and at -7° with 45.84 µPa. The pressure then increases with fluctuations until it reaches its peak at 40° with 80.63 µPa. For the negative degrees, a first peak is reached at an angle of -25° with a pressure of 75.53 µPa. The pressure then fluctuates and eventually reaches the highest pressure for the negative degrees at 55° with 79.41 µPa. The lowest pressure for R5 was measured at an angle of 4° with 53.36 µPa and at -7° with 51.63 µPa. The pressure then increases until it reaches its peak at 50° with 82.60 µPa. For the negative angles, the pressure increases until it reaches a first peak at -25° with 76.35 µPa. It then fluctuates until it reaches the highest pressure at an angle of -60° with 79.94 µPa. The pressure at R6 increases

with fluctuations from the lowest point at an angle of 1° with a pressure of 41.52 µPa and at -9° with 41.97 µPa to the peak pressure at an angle of 35° with 85.50 µPa and at -30° with 79.20 µPa. The pressure then decreases with strong fluctuations.

The pressure at the front teeth shows erratic behaviour, whereas the pressure at the back teeth shows a trend with changing angle. A gradual increase for R20, R21 and R22 can be seen from the lowest pressure to an angle of ±15°, with pressure values fluctuating after this point. The lowest pressure for R20 was measured at an angle of 2° with 12.14 µPa and at 0° with 12.82 µPa. The pressure then increases gradually until it reaches a peak at an angle of 15° with a pressure of 57.39 µPa and at -10° with 39.11 µPa. It then increases with fluctuations until the highest pressure is reached at an angle of 90° with a pressure of 62.73 µPa and at -80° with 60.45 µPa. The pressure at tooth R21 increases gradually from the lowest point at 3° with 7.19 µPa and at 0° with 8.06 µPa for the negative degrees to a peak at an angle of 15° with 45.17 µPa and at -15° with 35.00 µPa. The pressure then increases with strong fluctuations until it reaches the highest pressure at an angle of 90° with 64.82 µPa and at -65° with 57.54 µPa. The lowest pressure for tooth R22 was measured at 2° with a pressure of 7.27 µPa and at 0° with a pressure of 8.38 µPa. The pressure increases gradually it reaches a peak pressure of 41.06 µPa at an angle of 20° and 37.96 µPa at an angle of -15°. The pressure then fluctuates strongly until it reaches the highest pressure at an angle of 90° with 65.51 µPa and at -90° with 56.08 µPa.

In summary, the results show strong pressure fluctuations at the front teeth inside the jaw between the two lines of teeth for all angles and on both sides. The pressure at the back teeth inside the jaw displays a trend between ±15°. The lowest pressure at the rear teeth on the left was measured at around -2° with the pressure increasing afterwards (Fig. 5.9), while the lowest pressure on the right teeth in the back was measured at around 3° (Fig.5.10). This isolation between the right and left rear teeth has the potential to provide sound localization.

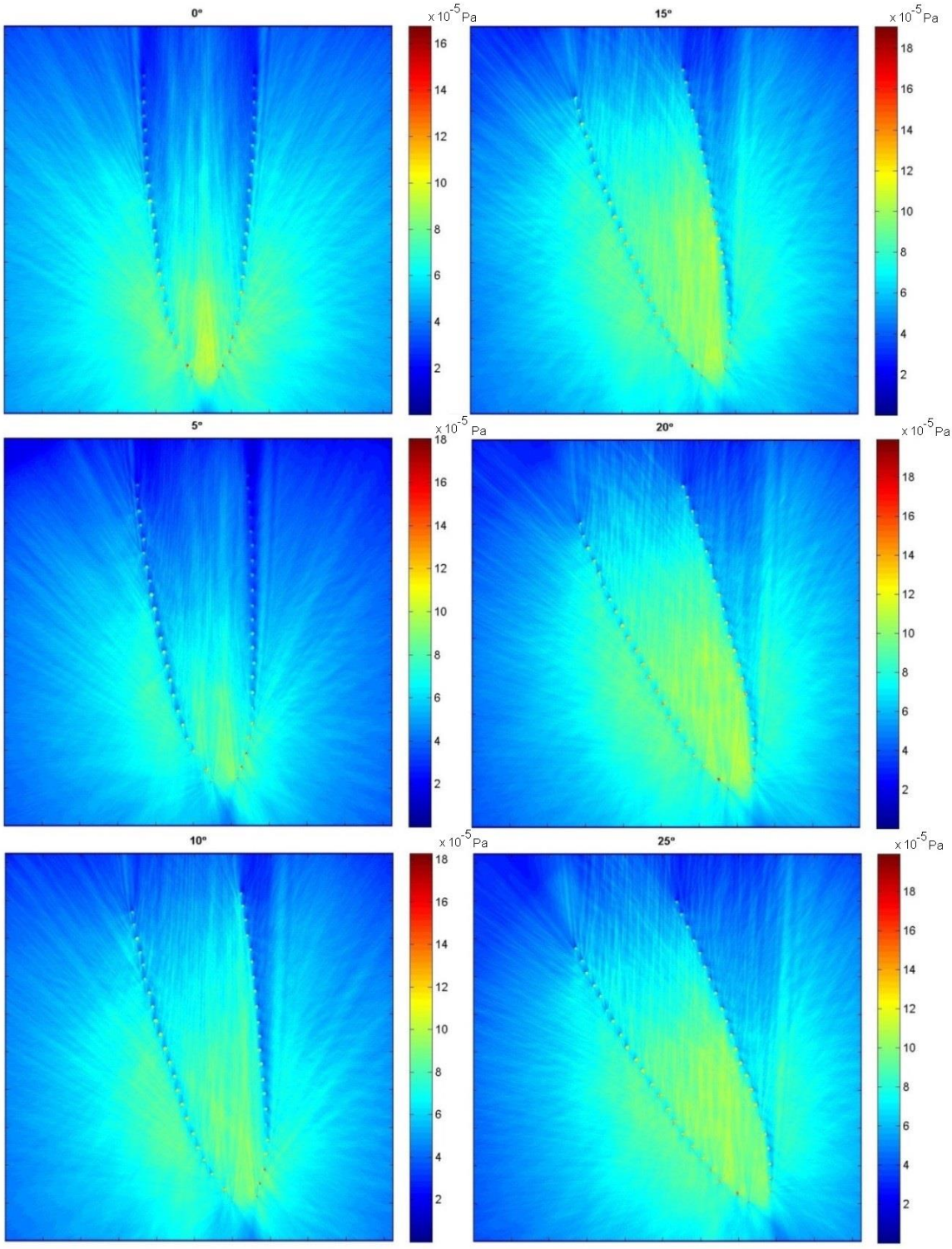

Fig. 5.8: Colour-coded simulation of sound propagation at the tip of the teeth of *Tursiops truncatus* for jaw angles 0° - 25° in 5 degree intervals for a frequency of 100 kHz. Plane wave is coming from the bottom of each graph.

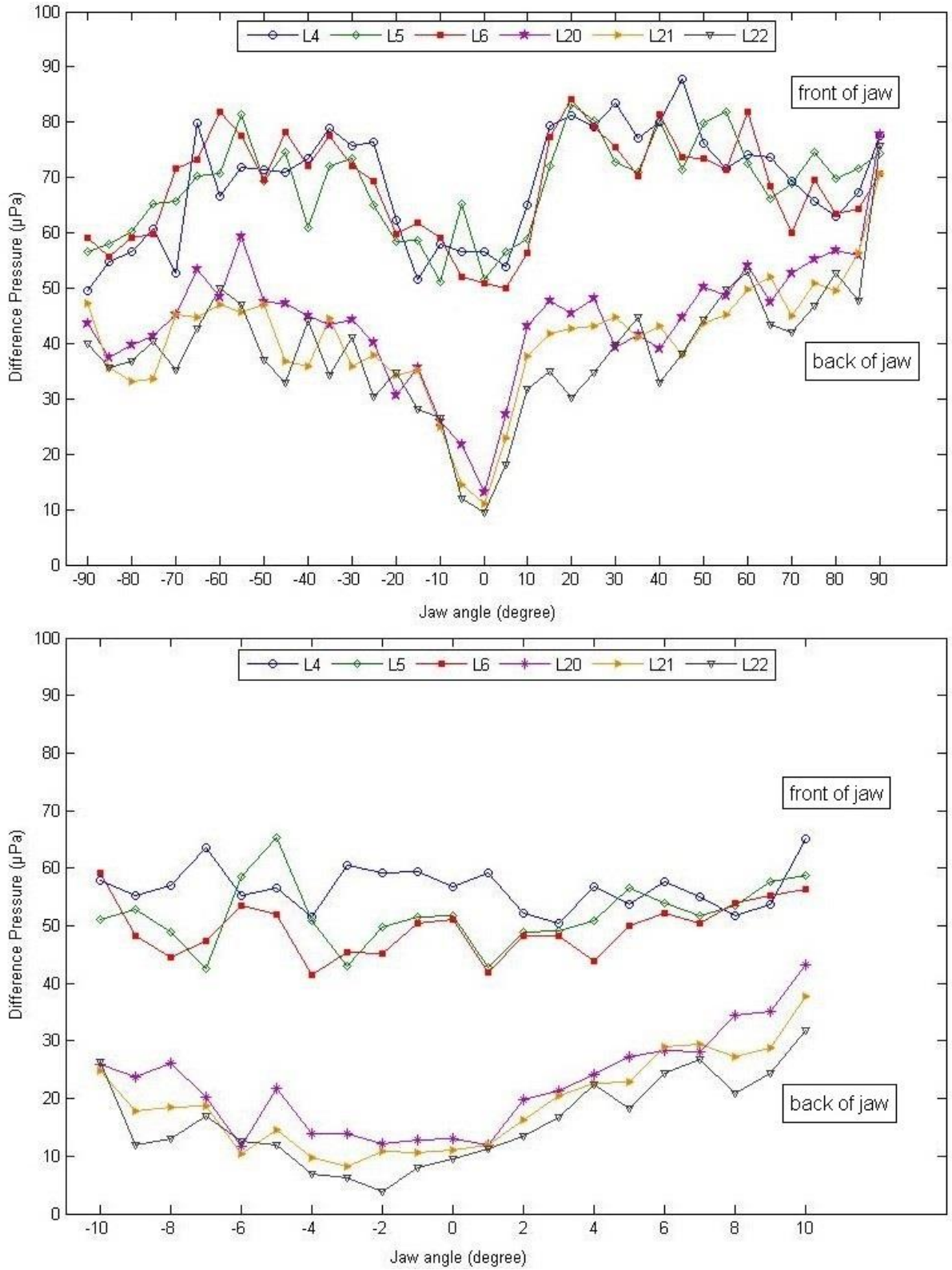

Fig. 5.9: Difference pressure at front and back teeth at the left side of the jaw for a frequency of 100 kHz and angles -90° to +90° in 5 degree steps (above) and -10° to +10° in 1 degree steps (below) for the tip of the teeth.

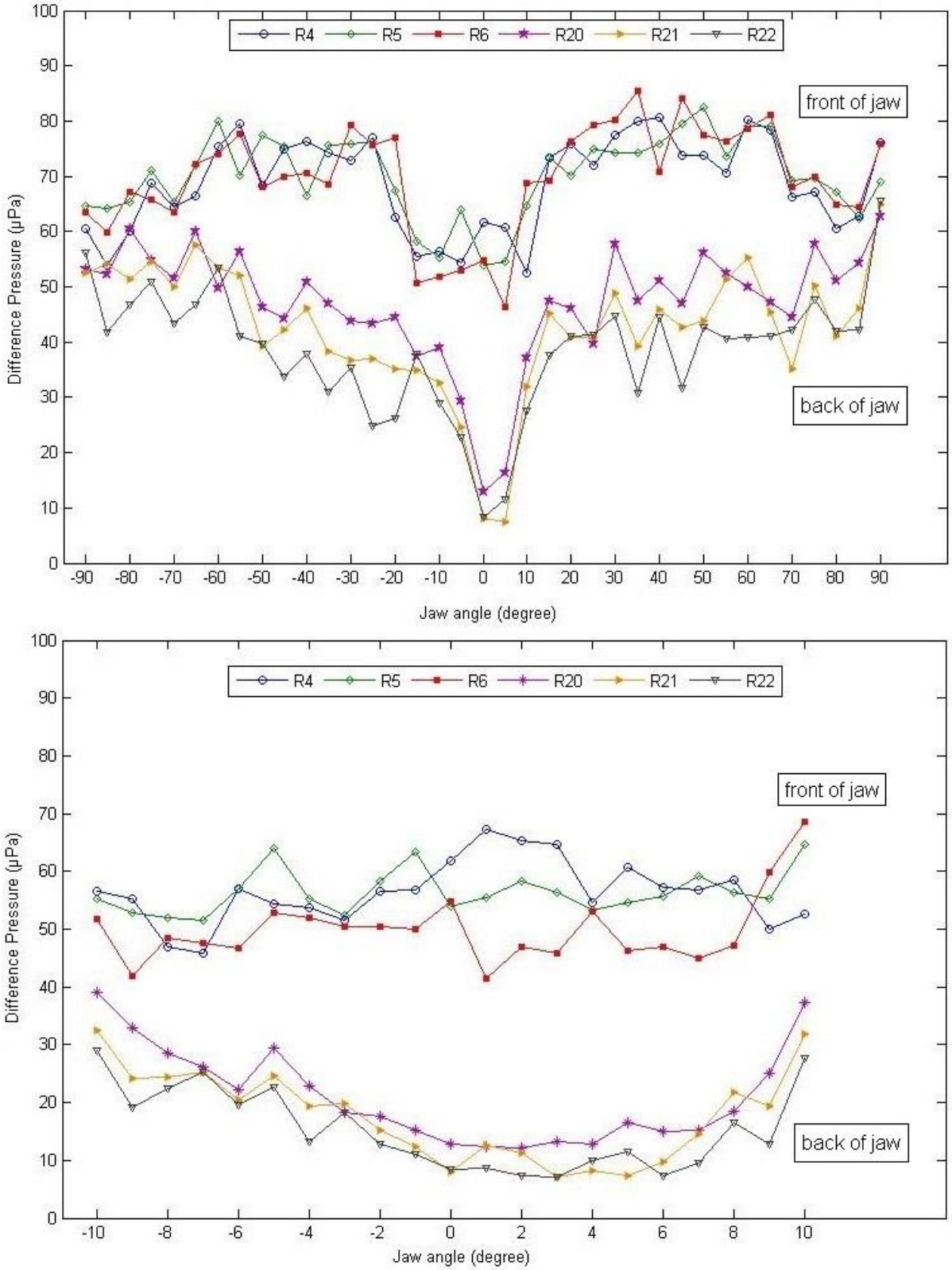

Fig. 5.10: Difference pressure at front and back teeth at the right side of the jaw for a frequency of 100 kHz and angles -90° to +90° in 5 degree steps (above) and for angles -10° to +10° in 1 degree steps (below) for the tip of the teeth.

5.3 Effects of change in tooth diameter on pressure distribution

The pressure distribution of a plane wave with a frequency of 100 kHz at the bottom of the teeth was measured for angles 0° to 25° in 5 degree intervals (Fig. 5.11). Highest pressure values for an angle of 0° are at the front teeth and decrease towards the rear of the jaw. The distribution of high pressure inside the jaw increases with the change of the jaw angle. The pressure measured for the bottom of the teeth and therfore larger diameter is higher than the pressure at the tip of the teeth. The pressure distribution for a sound wave coming from in front of the jaw at an angle of 0° in the horizontal is evenly distributed on both sides of the jaw in the back. At the inside of the jaw, the pressure decreases at the back on the right side when a sound wave arrives from the right due to shadowing of the teeth. The pressure increases on the left side. The pressure distribution on the outside of the jaw at the back teeth is reversed, with an increasing pressure on the right side and a decreasing pressure on the left jaw side.

Figure 5.12 shows the pressure for the bottom of the teeth at the left side of the jaw for angles -45° to +45° in 5 degree intervals and -10° to +10° in 1 degree intervals for tooth 4, 5 and 6 in the front of the jaw and tooth 20, 21 and 22 in the back of the jaw. The pressure at tooth L4 increases from the lowest point at an angle of 6° with a pressure of 54.55 µPa and at an angle of -6° with a pressure of 56.95 µPa for negative angles to a peak pressure of 115.60 µPa at an angle of 30° and 122.90 µPa at -35° respectively. The lowest pressure for L5 was measured at an angle of 2° with 49.70 µPa and at -3° with a pressure of 49.63 µPa. The pressure then increases until it reaches its peak at 25° with 124.50 µPa and at -35° with 119.10 µPa. For L6, a lowest pressure of 46.71 µPa and 43.20 µPa was measured at 1° and -7° respectively. The pressure then increases until it reaches its peak at an angle of 30° with a pressure of 117.40 µPa and at -40° with a pressure of 111.40 µPa. The pressure at the front teeth fluctuates from angles -10° to 10° and does not change noticeably. The pressure at the back teeth (L20-L22) shows a more regular behaviour for angles -10° to 10°. The lowest pressure for L20 was measured at 0° with 12.78 µPa for positive degrees and at -2° with 6.15 µPa for negative degrees. The pressure then increases gradually until it reaches a peak at an angle of 10° with 46.82 µPa and at -15° with a pressure of 41.70 µPa. It then fluctuates until it reaches the highest pressure at an angle of 45° with 65.11 µPa and at -30° with 74.23 µPa. The pressure at tooth L21 increases from the lowest point 0° with 8.14 µPa and at -4° with 3.62 µPa to a peak at 10° with 34.87 µPa and at -15° with 34.68 µPa. The pressure then increases with a few fluctuations

until it reaches the peak pressure at 45° with 62.79 µPa and at -40° with 52.07 µPa. The lowest pressure for tooth L22 was measured at 1° with a pressure of 7.91 µPa and at -3° with 0.62 µPa. The pressure then increases gradually until it reaches a peak at 15° with a pressure of 30.10 µPa and at -15° with 26.19 µPa. It then increases with fluctuations until it reaches the highest pressure at 35° with a pressure of 51.83 µPa and at -45° with 52.28 µPa.

Figure 5.13 shows the pressure at the right side of the jaw for angles -45° to +45° in 5 degree intervals and -10° to +10° in 1 degree intervals at the tip of the teeth for tooth 4, 5 and 6 in the front of the jaw and tooth 20, 21 and 22 in the back of the jaw. The pressure fluctuates strongly for angles between -10° and 10°. The lowest pressure for R4 was measured at 7° with 55.05 µPa and at -1° with 53.18 µPa. The pressure then increases to a peak pressure at an angle of 35° with 118.90 µPa and at -40° with 115.60 µPa. The lowest pressure at R5 is at 4° with 47.31 µPa and at -1° with 50.17 µPa. The pressure then fluctuates until it reaches the highest point at an angle of 45° with 129.80 µPa and at -35° with 116.50 µPa. For R6, the lowest pressure was measured at an angle of 4° with 41.57 µPa and at -2° with 39.53 µPa. The pressure then increases with strong fluctuations until it reaches the peak pressure at 40° with 116.10 µPa and at -40° with 120.00 µPa. A trend in pressure can be seen at the back teeth. The lowest pressure for R20 was measured at 6° with a pressure of 8.25 µPa and at -1° with 10.95 µPa. The pressure then increases gradually until it reaches a peak pressure of 58.65 µPa at an angle of 30°. It then fluctuates until it reaches the highest pressure at 45° with 62.97 µPa. For negative degrees, the pressure increases gradually until it reaches an angle of -15° with 46.97 µPa. It then fluctuates until it reaches its peak at -30° with 60.54 µPa. The lowest pressure for R21 was measured at 6° with 2.17 µPa and at -2° with 7.80 µPa. The pressure then increases until its peak at 35° with 57.05 µPa. A first peak pressure for negative angles was measured at -15° with 39.25 µPa. The pressure then fluctuates until it reaches the highest pressure at an angle of -30° with 58.67 µPa. The pressure at tooth R22 increases from the lowest point at 6° with 0.01 µPa and at -1° with 5.26 µPa to a peak pressure of 33.69 µPa at 25° and a pressure of 28.04 µPa at -10° respectively. The pressure then increases on both sides until it reaches the highest pressure at 45° with 39.52 µPa and at -40° with 45.79 µPa.

In summary, the results show as already seen for smaller tooth diameters strong pressure fluctuations at the front teeth inside the jaw between the two lines of teeth for all angles and on both jaw sides. The pressure at the back teeth inside the jaw displays a trend between around

±15°. As seen for the tip of the teeth, measurements for a larger tooth diameter show a lowest pressure at the rear teeth on the left at an angle of -2° with the pressure increasing afterwards (Fig. 5.12), while the lowest pressure on the right teeth in the back was measured at 6° (Fig. 5.13). These measurements between the right and left rear teeth show an increased isolation compared to the tip of the teeth. This isolation has, as already mentioned before for a smaller tooth diameter, the potential to provide enhanced sound localization.

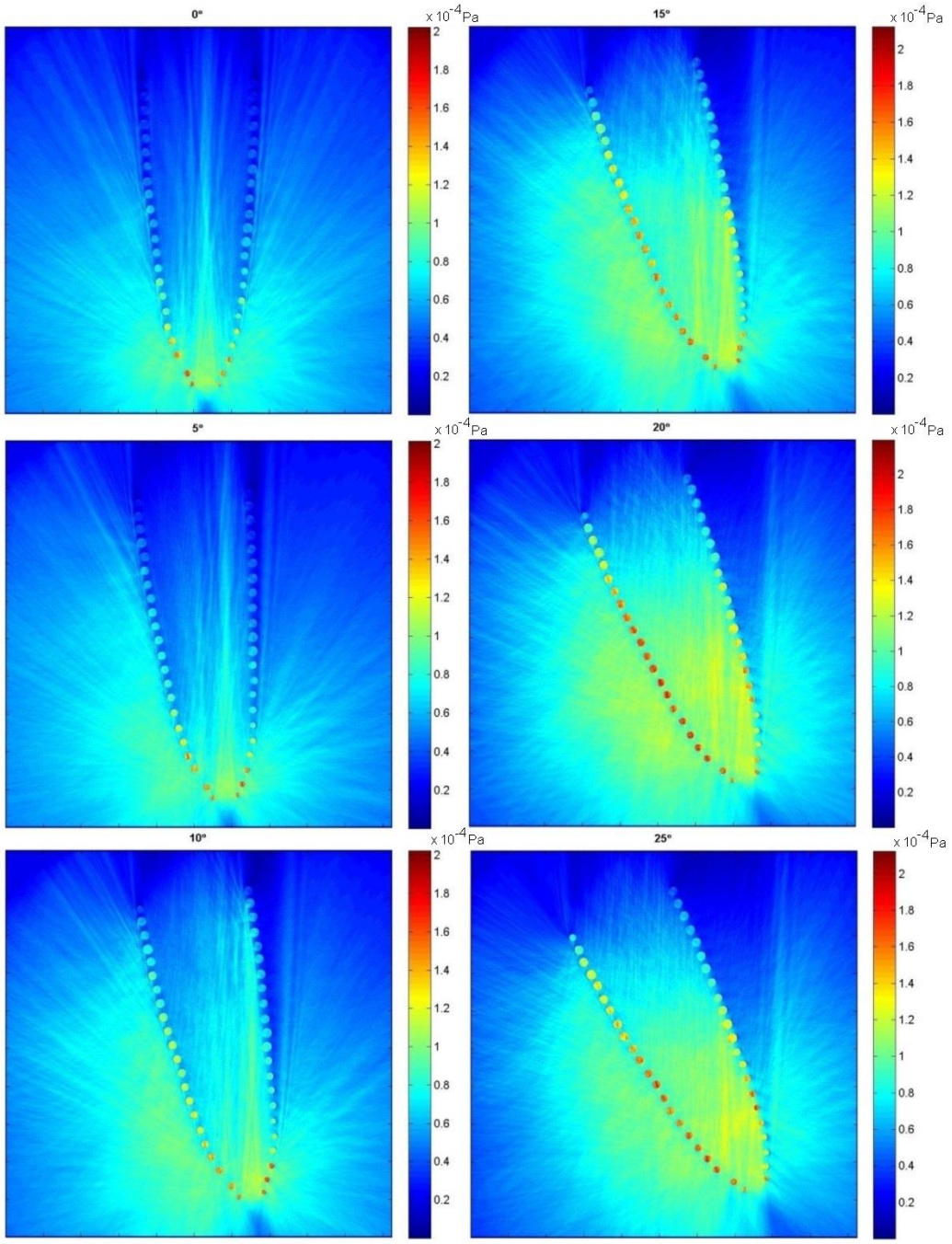

Fig: 5.11: Colour-coded simulation of sound propagation at the bottom of the teeth, for jaw angles 0° - 25° in 5° intervals at 100 kHz. Plane wave is coming from the bottom of each graph.

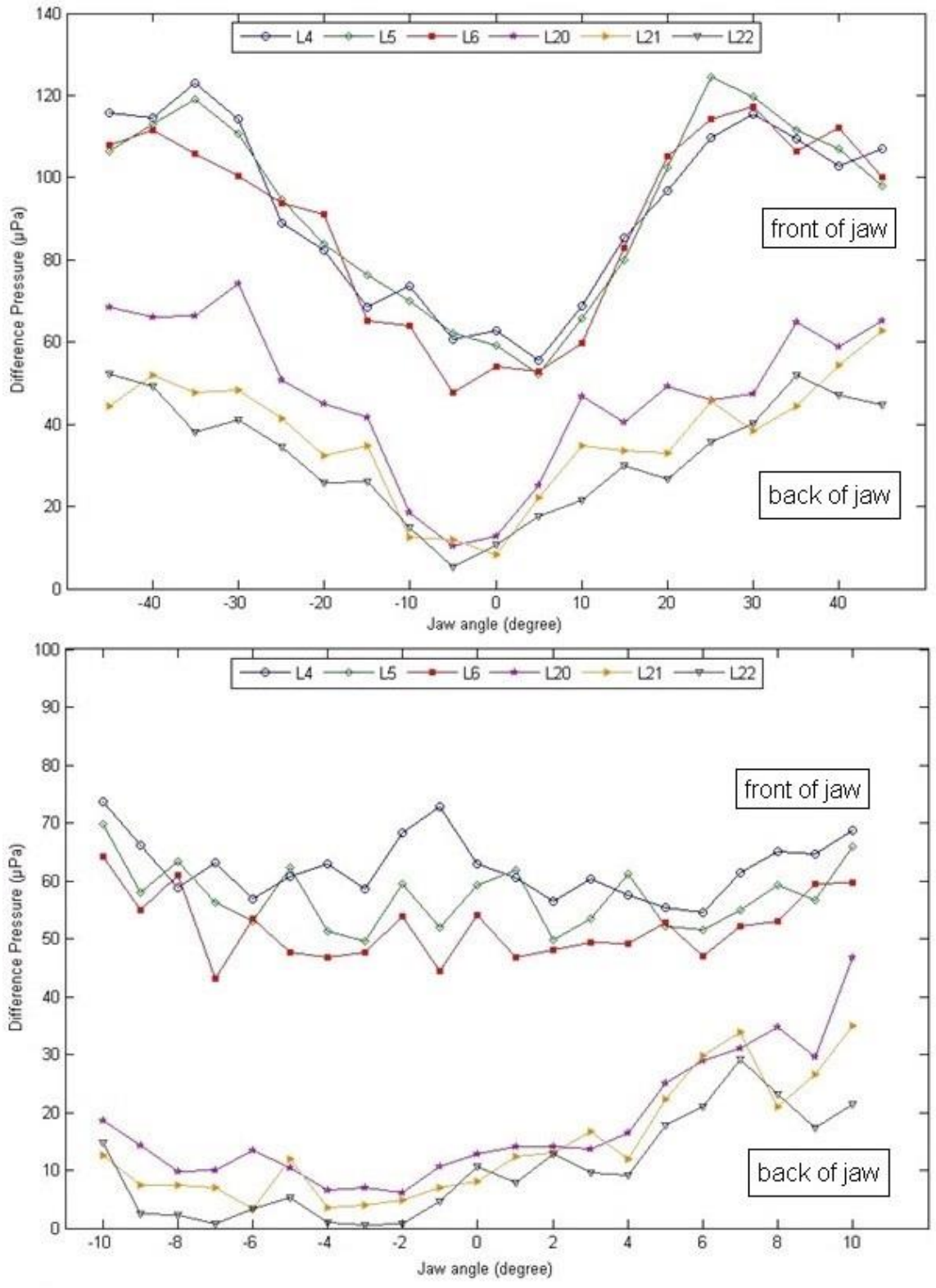

Fig. 5.12: Difference pressure at front and back teeth at the left side of the jaw for a frequency of 100 kHz and for angles -45° to 45° in 5 degree intervals (above) and for angles -10° to +10° in 1 degree intervals (below) for the bottom of the teeth.

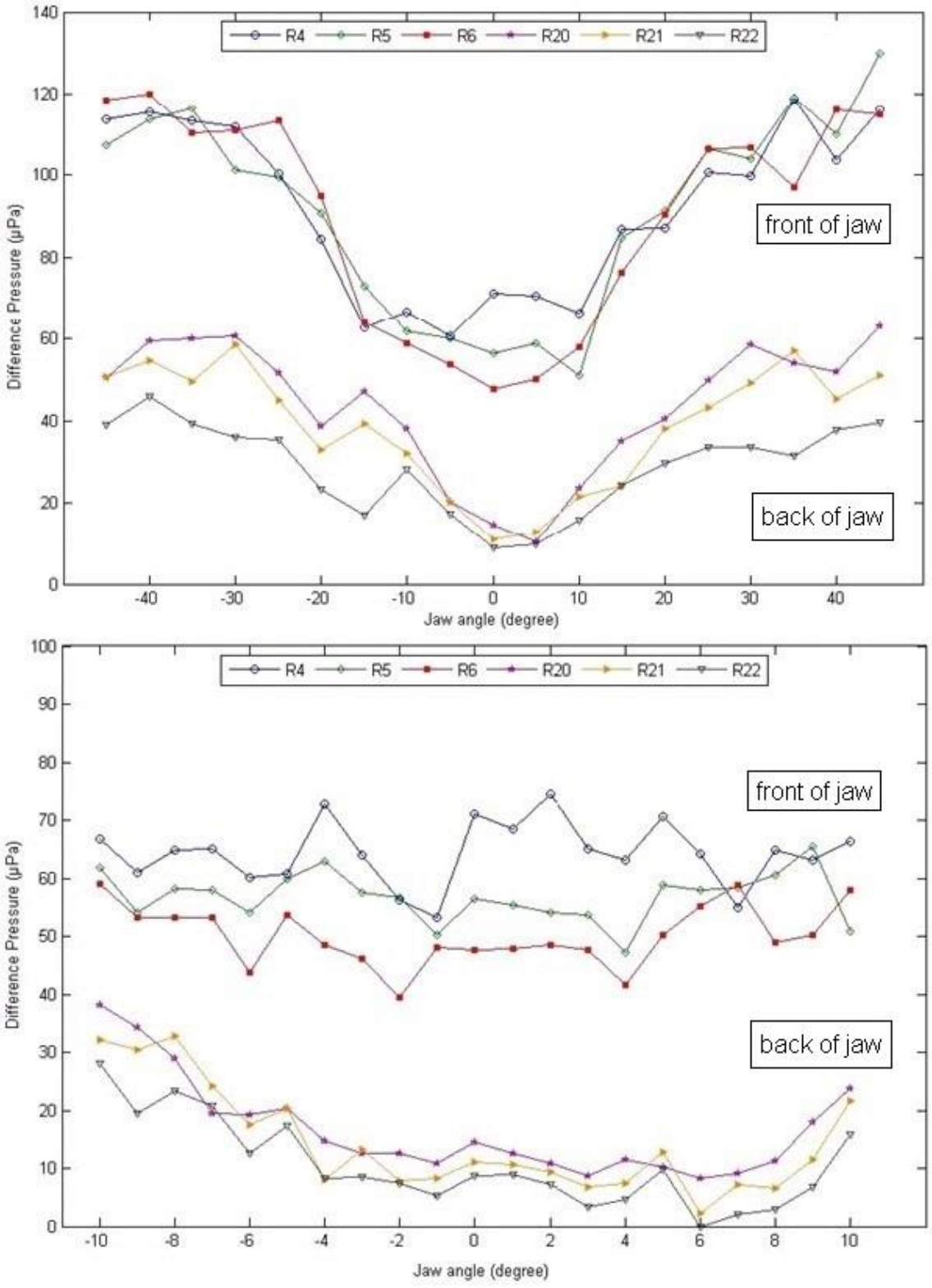

Fig. 5.13: Difference pressure at front and back teeth at the right side of the jaw for a frequency of 100 kHz and for angles -45° to +45° in 5 degree intervals (above) and for angles -10° to +10° in 1 degree intervals (below) for the bottom of the teeth.

5.4 Effects of missing teeth on sound pressure distribution

5.4.1 Opposite teeth missing

The pressure distribution of a plane wave with a frequency of 100 kHz is displayed in Fig. 5.14 for the tip of the teeth for angles 0° to 25° in 5 degree intervals. Teeth 17 on both sides of the jaw are missing, counting from the front. The highest pressure for an angle of 0° can again be seen at the front teeth and decreases towards the rear of the jaw. There is no significant effect of the missing teeth on the pressure distribution in comparison to all teeth present. The distribution of high pressure inside the jaw increases with the change of the jaw angle. The pressure distribution for a sound wave coming from in front of the jaw at an angle of 0° in the horizontal is evenly distributed on both sides of the jaw in the back. At the inside of the jaw, the pressure decreases at the back on the right side when a sound wave arrives from the right due to shadowing of the teeth. The pressure increases on the left side. The pressure distribution on the outside of the jaw at the back teeth is reversed, with an increasing pressure on the right side and a decreasing pressure on the left jaw side.

Figure 5.15 shows the pressure at the left side of the jaw for angles -45° to +45° in 5 degree intervals and -10° to +10° in 1 degree intervals at the tip of the teeth for tooth 4, 5 and 6 in the front of the jaw and tooth 20, 21 and 22 in the back of the jaw. Teeth L17 and R17 are missing. As seen in the previous figures, there is a trend in pressure for the back of the teeth. The pressure at the front teeth shows strong fluctuations and no tendency, particularly for the first ten degrees for both angles.

Pressure values fluctuate between -10° and 10° with a lowest pressure at an angle of 6° with 49.77 µPa and at -4° with 50.97 µPa for tooth L4. The pressure eventually increases until it reaches its peak at an angle of 30° with a pressure of 78.12 µPa and at -35° µPa with 74.10 µPa. The pressure at tooth L5 shows also strong fluctuations. The lowest pressure was measured at 1° with 41.37 µPa and at -7° with 47.01 µPa. The pressure then increases with fewer fluctuations until it reaches its peak at an angle of 20° with a pressure of 76.80 µPa and at -30° with 65.63 µPa. The pressure for tooth L6 shows similar tendencies. There are fluctuations between -10° and 10° with the lowest pressure of 40.56 µPa at 1° and 41.71 µPa at an angle of -2°. The pressure then increases with fluctuations until it reaches the peak pressure at an angle of 20° with 77.43 µPa and at -45° with 71.07 µPa.

The pressure at the back teeth on the left side of the jaw shows higher pressure values for positive degrees and comparatively lower values for negative degrees for angles -10° to 10°. There is a pressure decrease at tooth L20 from an angle of 0° to the lowest pressure at 1° with 11.34 µPa for positive degrees. The pressure then increases gradually until it reaches its peak pressure at 15° with 42.65 µPa. It then decreases with fluctuations. For negative degrees, there is a slight increase from 0°. The pressure then decreases until it reaches its lowest point at -3° with a pressure of 9.26 µPa and increases gradually after that until a peak pressure is reached at -15° with 29.51 µPa. The pressure then fluctuates until it reaches the highest pressure at -45° with 39.50 µPa. The pressure at tooth L21 decreases slightly from 0° until it reaches its lowest point at 1° with 10.02 µPa and at -3° with 7.74 µPa. It then increases with a few fluctuations until it reaches a first peak at 20° with a pressure of 32.37 µPa and at -15° with 29.51 µPa. The pressure then increases further with fluctuations until it reaches the highest pressure at 30° with 41.13 µPa and at -35° with 38.63 µPa. The pressure at L22 decreases from 0° to a lowest pressure at 1° with 5.18 µPa and at -3° with 4.23 µPa. It then increases with a few fluctuations until it reaches a first peak at 15° with 27.03 µPa and at -20° with 29.96 µPa. The pressure then increases further with fluctuations until it reaches the peak pressure at 35° with 39.08 µPa and at -40° with 37.07 µPa.

Figure 5.16 shows the pressure at the right side of the jaw for angles -45° to +45° in 5 degree intervals and -10° to +10° in 1 degree intervals at the tip of the teeth for tooth 4, 5 and 6 in the front of the jaw and tooth 20, 21 and 22 in the back of the jaw with opposite teeth L17 and R17 missing. There is no trend for the pressure at the front teeth, but a tendency for the pressure at the back of the jaw, particularly for the first 10 degrees for both positive and negative angles. The lowest pressure at tooth R4 was measured at an angle of 9° with a pressure of 47.08 µPa and at -7° with 45.48 µPa. For positive angles, the pressure first increases from 0° and then decreases until it reaches its lowest point. For a jaw angle change in the other direction, the pressure decreases continuously from 0° until it reaches the lowest pressure. The pressure then increases with strong fluctuations until it reaches its peak at 35° with 78.55 µPa and at -25° with 68.84 µPa. The pressure at tooth R5 first increases with fluctuations from an angle of 0° and then decreases until it reaches the lowest pressure at 5° with 50.29 µPa and at -10° with 43.74 µPa. It then increases again until it reaches a peak pressure at an angle of 40° with 80.98 µPa and at -25° with 65.82 µPa. A decrease in pressure can be seen after this. The lowest pressure at tooth R6 was measured at an angle of 1° with 40.34 µPa and at -10° with 41.50

µPa. The pressure then increases with fluctuations until it reaches its peak at an angle of 45° with 82.20 µPa and at -30° with 69.26 µPa.

Unlike the pressure at the front teeth, there is a trend with change of angle for the pressure at the back teeth, particularly for angles -10° to 10°. For tooth R20, the pressure changes only slightly from an angle of 0° to the lowest point of pressure. The lowest pressure was measured at an angle of 4° with 8.82 µPa and at -1° with 7.71 µPa. A gradual increase in pressure can then be seen until a first peak pressure is reached at an angle of 15° with 42.50 µPa and at -10° with 34.19 µPa. The pressure then fluctuates until the highest pressure is reached at 30° with 46.43 µPa and at -30° with 45.24 µPa. The pressure at tooth R21 decreases from 0° until it reaches its lowest point at 4° with a pressure of 4.89 µPa and at -1° with a pressure of 10.72 µPa. The pressure then increases gradually until it reaches a first peak at 20° with 34.76 µPa and at -10° with 32.34 µPa. There are strong fluctuations after this point until the highest pressure is reached at an angle of 40° with 42.60 µPa and at -40° with 40.06 µPa. The pressure at tooth R22 decreases from 0° until it reaches its lowest point at an angle of 2° with a pressure of 5.24 µPa and at -1° with 9.60 µPa. The pressure then increases with a few fluctuations until it reaches a first peak at 20° with 33.68 µPa and at -15° with 28.80 µPa. Strong fluctuations can be seen from the first peak to the highest pressure at 40° with 40.86 µPa and at -40° with 32.51 µPa.

In summary, the results show again strong pressure fluctuations at the front teeth inside the jaw for all angles and on both sides of the two lines of teeth. As already seen for different tooth diameters, the pressure at the back teeth inside the jaw displays a trend between ±15°. The lowest pressure at the rear teeth on the left was measured at -3° (Fig. 5.15), while the lowest pressure at the rear teeth on the right was measured at around 2° (Fig. 5.16). These measurements show that, even though several teeth are missing, there is still an isolation between the right and left teeth in the back of the jaw, which could have the potential to provide sound localization.

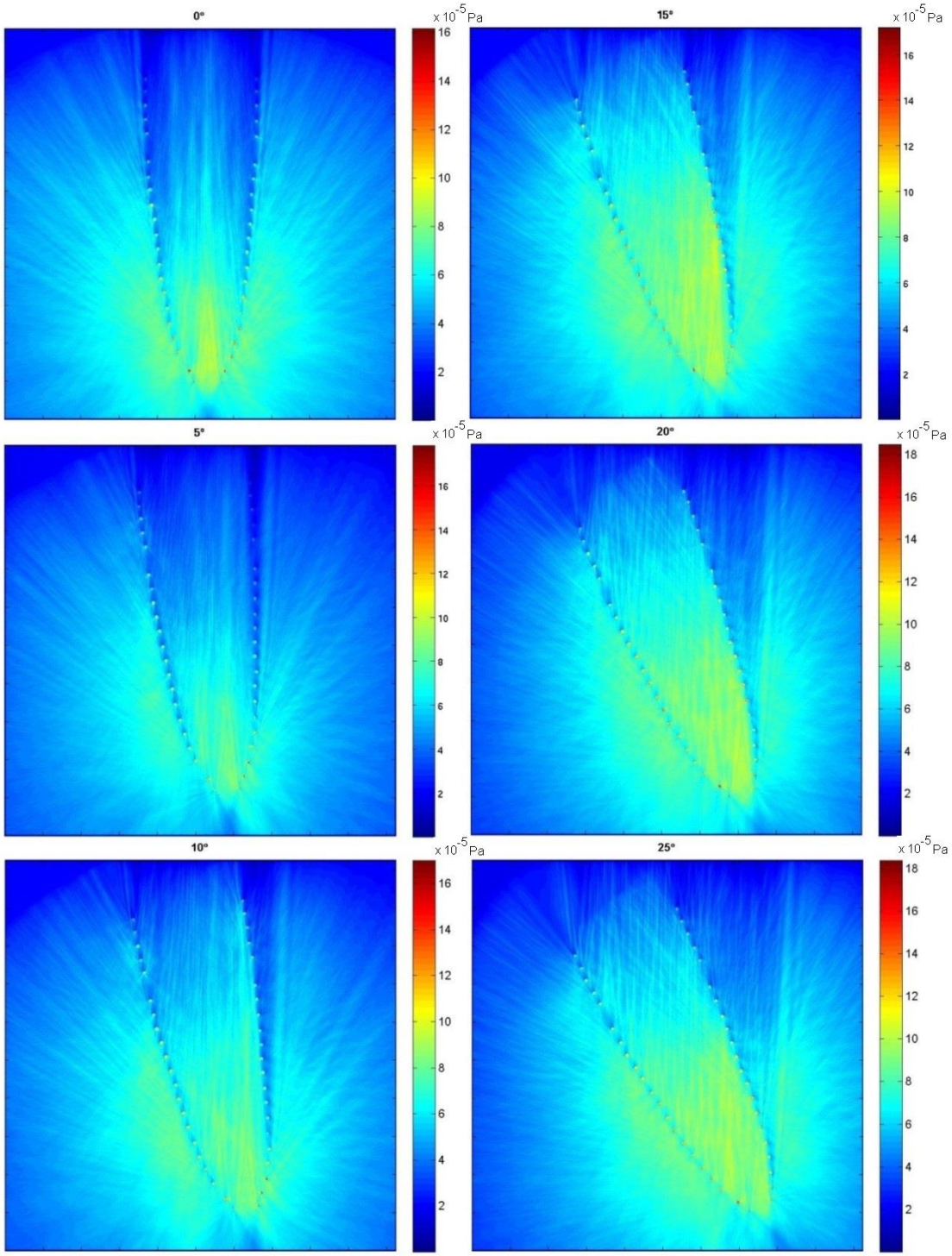

Fig: 5.14: Simulation of sound propagation at the tip of the teeth with opposite teeth (L17 and R17) missing, for jaw angles 0°-25° in 5 degree intervals. The plane wave is coming from the bottom of each graph with a frequency of 100 kHz.

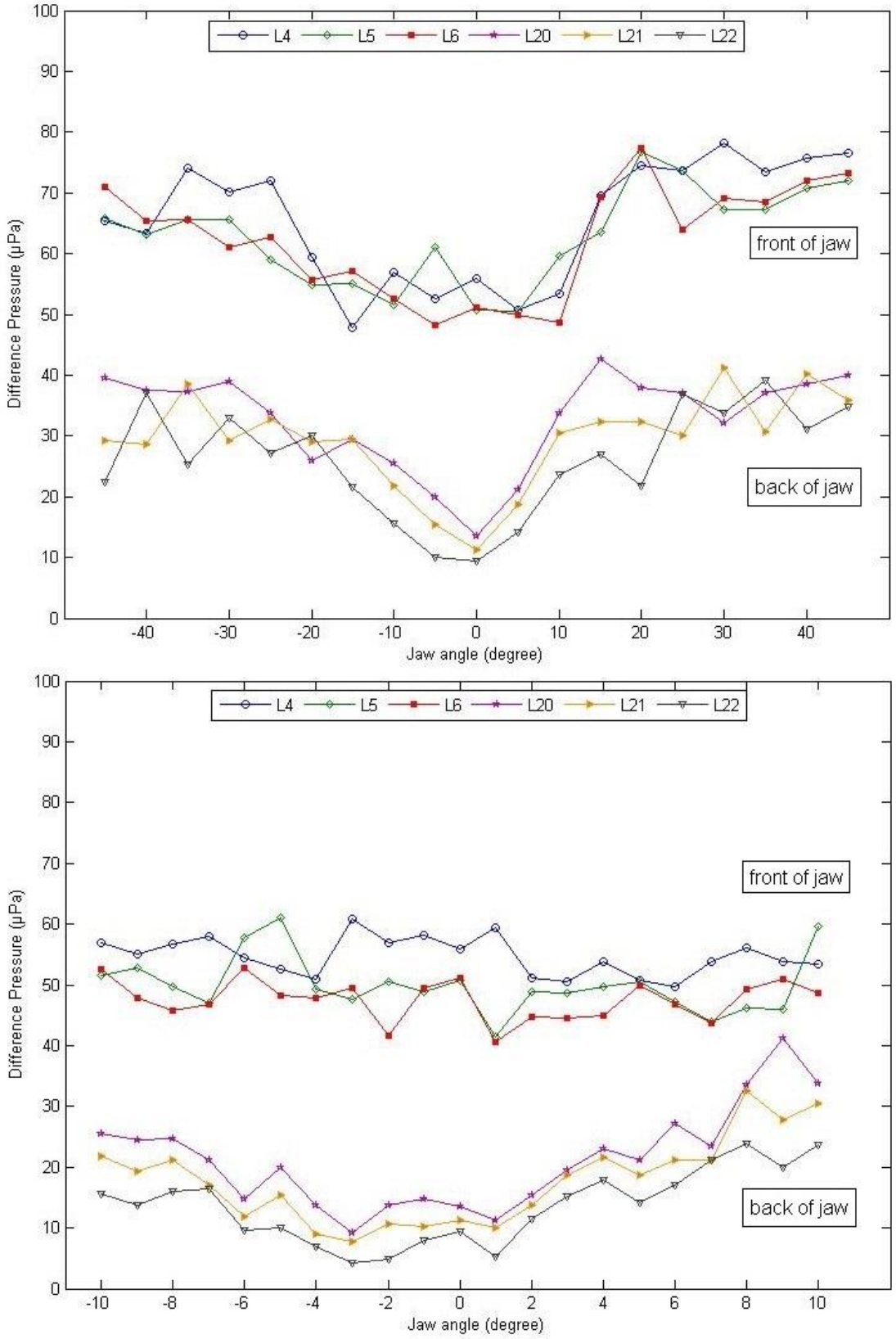

Fig. 5.15: Difference pressure at front and back teeth at the left side of the jaw for a frequency of 100 kHz and for angles -45° to +45° in 5 degree intervals and for angles -10° to +10° in 1 degree intervals. Teeth L17 and R17 are missing.

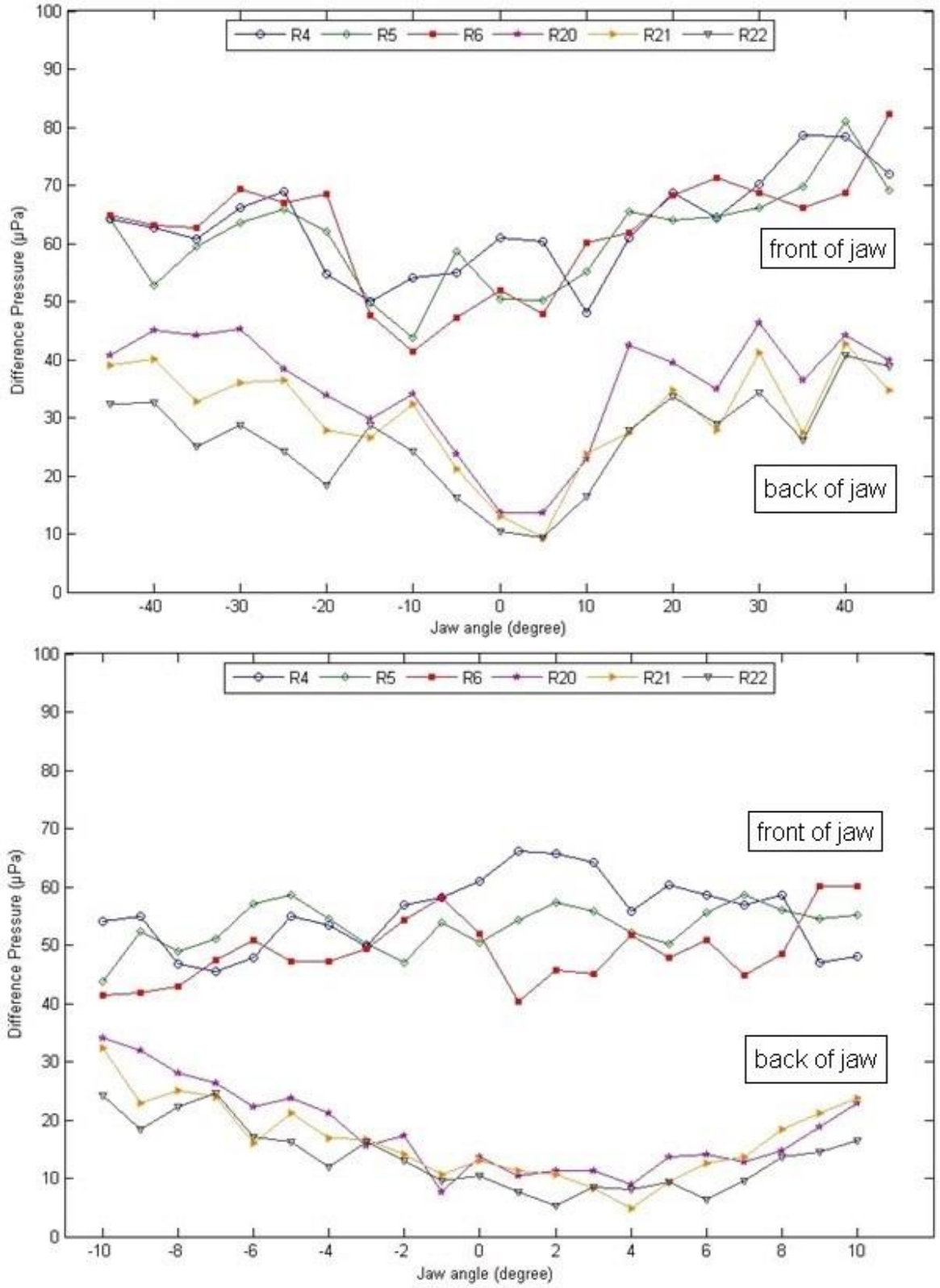

Fig. 5.16: Difference pressure at front and back teeth at right jaw side for 100 kHz and for angles -45° to +45° in 5 degree intervals and -10° to +10° in 1 degree intervals. Teeth L17 and R17 are missing.

5.4.2 Multiple teeth missing

The pressure distribution of a plane wave with a frequency of 100 kHz is displayed in Fig. 5.17 for the tip of the teeth for angles 0° to 25° in 5 degree intervals. Teeth R5, R14, R17 and L9 are missing, counting from the front of the jaw. The highest pressure for an angle of 0° can be seen at the front teeth and decreases towards the back of the jaw. Pressure values are overall lower compared to pressure values at the jaw with all teeth present. At the inside of the jaw, the pressure decreases at the back on the right side when a sound wave arrives from the right due to shadowing of the teeth. The pressure increases on the left side. The pressure distribution on the outside of the jaw at the back teeth is reversed, with an increasing pressure on the right side and a decreasing pressure on the left jaw side. There is less shadowing in the back on the right jaw side due to several teeth missing, leading to a fluctuating pressure distribution.

Figure 5.18 shows the pressure at the left side of the jaw for angles -45° to +45° in 5 degree intervals and -10° to +10° in 1 degree intervals at the tip of the teeth for tooth 4, 5 and 6 in the front of the jaw and tooth 20, 21 and 22 in the back of the jaw. Teeth R5, R14, R17 and L9 are missing. There is a trend in pressure for the rear teeth on the left between ±45°, but no noticeable tendency for -10° to 10°. The pressure at the front teeth fluctuates strongly and shows no trend. The lowest pressure at tooth L4 was measured at an angle of 2° with 47.97 µPa and at -3° with 50.66 µPa. The pressure then increases with fluctuations until it reaches a peak at 20° with 71.78 µPa and at -35° with 74.10 µPa. The pressure at tooth L5 fluctuates also strongly from -10° to 10°. The lowest pressure was measured at an angle of 6° with 40.37 µPa and at -7° with 41.01 µPa. The pressure with fluctuations until it eventually reaches the highest pressure at an angle of 40° with 72.65 µPa and at -45° with 71.63 µPa. The pressure at tooth L6 fluctuates between 0° and 10° and shows no noticeable change from 0° to -10°. The lowest pressure was measured at an angle of 1° with 37.37 µPa and at -8° with 40.94 µPa. The pressure then increases until it reaches its peak at 45° with 69.97 µPa and at -45° with 71.63 µPa. There is a trend for the pressure at the back teeth from -45° to 45°. The pressure at L20 fluctuates from -10° to 10° with a lowest pressure at 1° with 11.27 µPa and at -3° with 8.34 µPa. The pressure then increases with fluctuations until it reaches its peak at 15° with 44.62 µPa and at -30° with 38.98 µPa. The lowest pressure at tooth L21 was measured at 1° with 11.10 µPa and at -3° with 4.11 µPa. The pressure then increases with a few fluctuations until it reaches a peak at 20° with 36.91 µPa and -15° with 29.51 µPa. It then increases again until it reaches the highest pressure at 40° with 41.43 µPa and at -35° with 38.63 µPa. The pressure at tooth L22

is lowest at an angle of 1° with a pressure of 6.00 µPa and at an angle of -3° with 2.98 µPa. The pressure then increases with a few fluctuations until it reaches its first peak at 15° with 27.82 µPa and at -20° with 29.06 µPa. It then increases again until it reaches the highest pressure at 45° with 35.68 µPa and at -40° with 37.07 µPa.

Figure 5.19 shows the same parameters as Fig. 5.18, but for the teeth on the right jaw side. Teeth R5, R14, R17 and L9 are missing. The pressure at tooth R4 shows strong fluctuations. The lowest pressure was measured at an angle of 4° with 40.94 µPa and at -8° with 43.44 µPa. The pressure then increases and reaches its peak at an angle of 35° with a pressure of 72.15 µPa and at -25° with 68.84 µPa. The pressure at tooth R5 changes only slightly for angles -10° to 10°. The lowest pressure was measured at an angle of 9° with 43.34 µPa and at -3° with 41.12 µPa. The pressure then increases with fluctuations until it reaches its peak at 40° with 74.21 µPa and at -25° with 65.82 µPa. For R6, the pressure is lowest at an angle of 3° with 42.06 µPa and at -9° with 39.56 µPa. It fluctuates strongly between -10° and 10°. The pressure then increases until it reaches its peak at 45° with 76.60 µPa and at -30° with 69.26 µPa. Contrary to measurements on the left teeth, pressure values on the right side of the jaw show a trend and fewer fluctuations. The lowest pressure for R20 was measured at an angle of 3° with 11.70 µPa and at -1° with 8.68 µPa. The pressure then increases until it reaches a peak at 20° with 41.68 µPa and at -15° with 34.19 µPa. It then increases with a few fluctuations until it reaches its highest pressure at 40° with 44.03 µPa and at -30° with 45.24 µPa. The pressure at tooth R21 increases gradually from its lowest point at 3° with a pressure of 8.63 µPa and at -1° with 11.86 µPa to a peak pressure at 15° with 33.13 µPa and at -10° with 32.34 µPa. The pressure then increases with a few fluctuations until it reaches the highest point at 40° with 42.34 µPa and at -40° with 40.06 µPa. The lowest pressure at tooth R22 was measured at an angle of 4° with 4.05 µPa and at 0° with 9.41 µPa. The pressure then increases until it reaches its first peak at 20° with 29.95 µPa and at -15° with 28.80 µPa. The pressure then increases on both sides until it reaches its highest pressure at an angle of 40° with 39.96 µPa and at -40° with 32.51 µPa.

In summary, the results show strong pressure fluctuations at the front teeth inside the jaw for all angles and on both jaw sides. There are also pressure fluctuations at the back teeth, but not as strongly as at the front. A trend is still noticeable. The lowest pressure at the rear teeth on the left was measured at -3° (Fig. 5.18). The lowest pressure at the rearmost tooth on the

right was measured at around 4° (Fig. 5.19). Even though there is an isolation between the right and left rearmost tooth, there is only a slight trend in pressure when multiple teeth are missing. These measurements indicate that sound localization possibly still occurs, but with decreased performance.

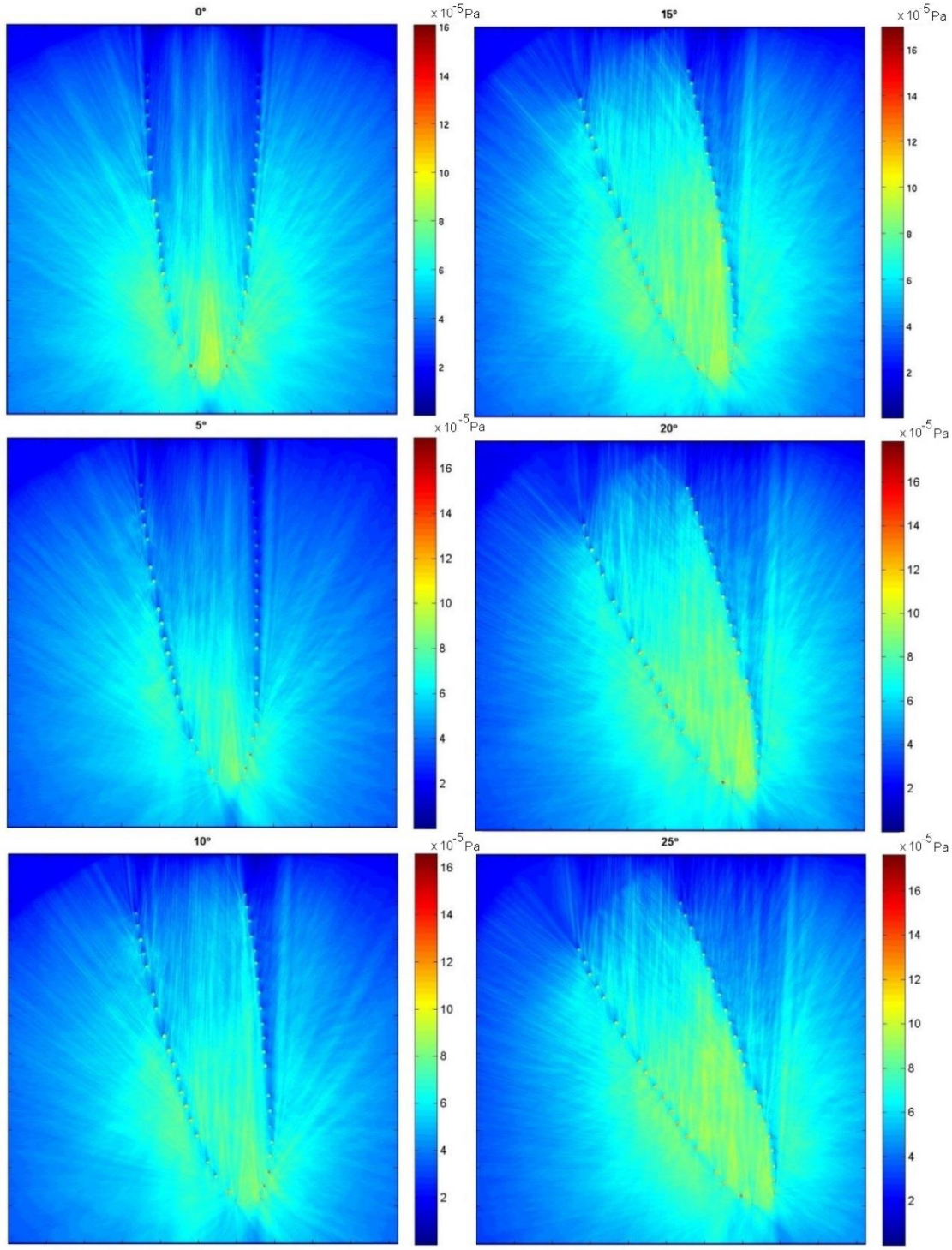

Fig. 5.17: Simulation of sound propagation at the tip of the teeth for a frequency of 100 kHz and for jaw angles 0° to 25° in 5 degree intervals. Teeth R5, R14, R17 and L9 are missing. The plane wave is coming from the bottom of each graph.

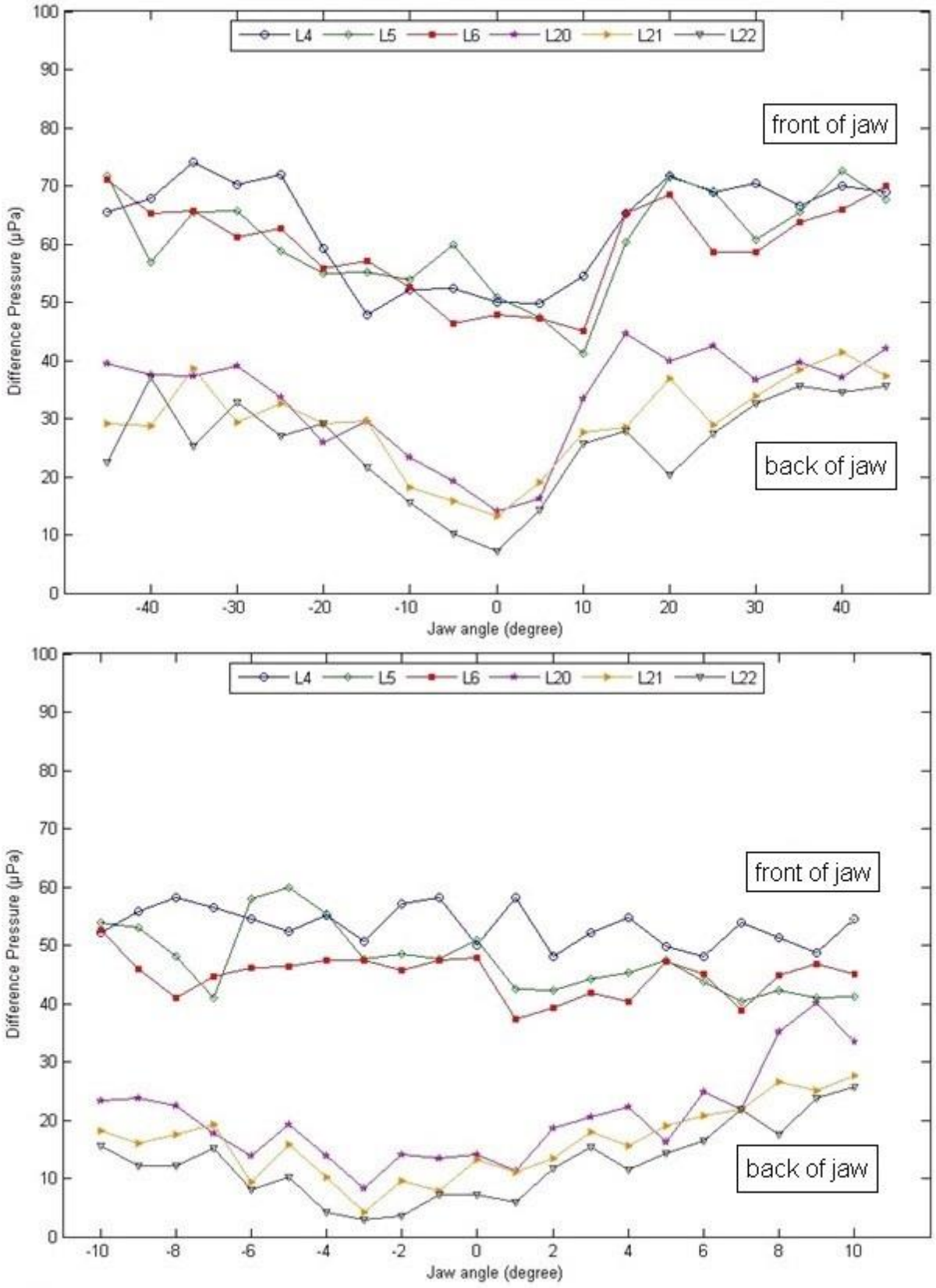

Fig. 5.18: Difference pressure at front and back teeth at left jaw side for 100 kHz and for angles -45° to +45° in 5 degree intervals and -10° to +10° in 1 degree intervals. Teeth R5, R14, R17 and L9 are missing.

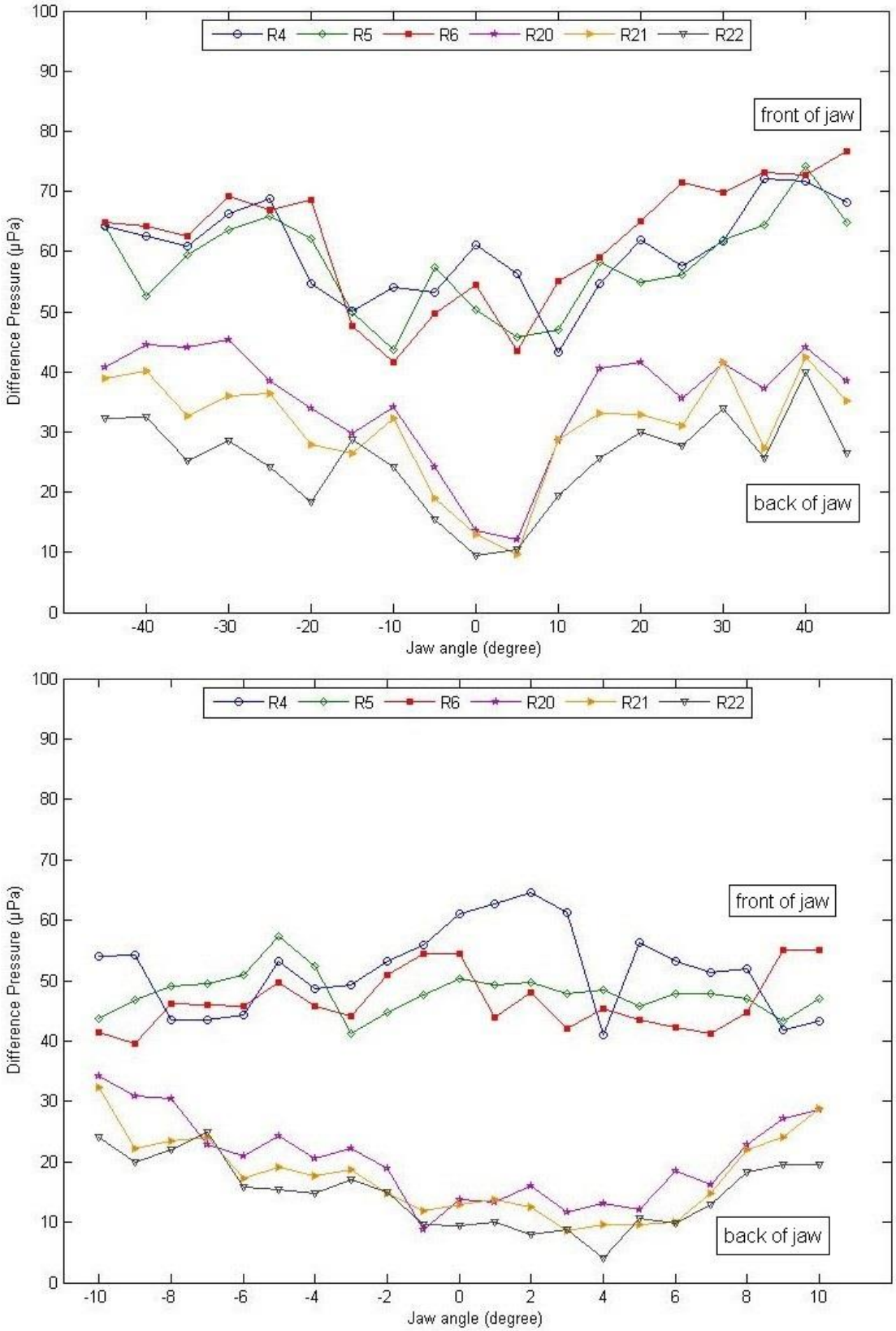

Fig. 5.19: Difference pressure at front and back teeth at the right side of the jaw for a frequency of 100 kHz and for angles -45° to +45° in 5 degree intervals and for angles -10° to +10° in 1 degree intervals. Teeth R5, R14, R17 and L9 are missing, counting from the front of the jaw.

5.5 Pressure distribution at all teeth for a 100 kHz sound wave

Fig. 5.20 shows the difference pressure at each tooth on both left and right jaw side for an angle of 0° and 5° at a frequency of 100 kHz. It shows the pressure distribution at the teeth after the wave propagated through the jaw. The pressure decreases continuously from the front teeth L1 and R1 until it reaches the lowest pressure at the rear tooth L22 and R22 for both angles. There are a few pressure fluctuations for the teeth in the first half of the jaw, particularly at tooth R4 and R6 for 0° and at R1, R3, R5, R7 and R9 for 5°. This is possibly due to the gap at the front teeth between R2 and R3.

Comparing the pressure distribution for each tooth on the left jaw side for an angle of 0° and 5°, a gradual decrease can be seen with fluctuations for both angles from tooth L1 to tooth L10 (Fig. 5.21). After this point, the pressure at both angles decreases almost parallel to each other, with lower values for an angle of 0°, until L20. After L20, the pressure continues to decrease noticeably for 0°. However, the pressure at an angle of 5° decreases only slightly for the rearmost three teeth.

The pressure at the bottom of the teeth is overall higher than at the tip of the teeth with fewer fluctuations. Fig. 5.22 shows that the pressure values on the left and right side of the jaw are very similar. The pressure difference decreases gradually from 86.40 µPa for R1 and from 83.50 µPa for L1 to a pressure of 9.24 µPa for R22 and 8.79 µPa for L22 respectively.

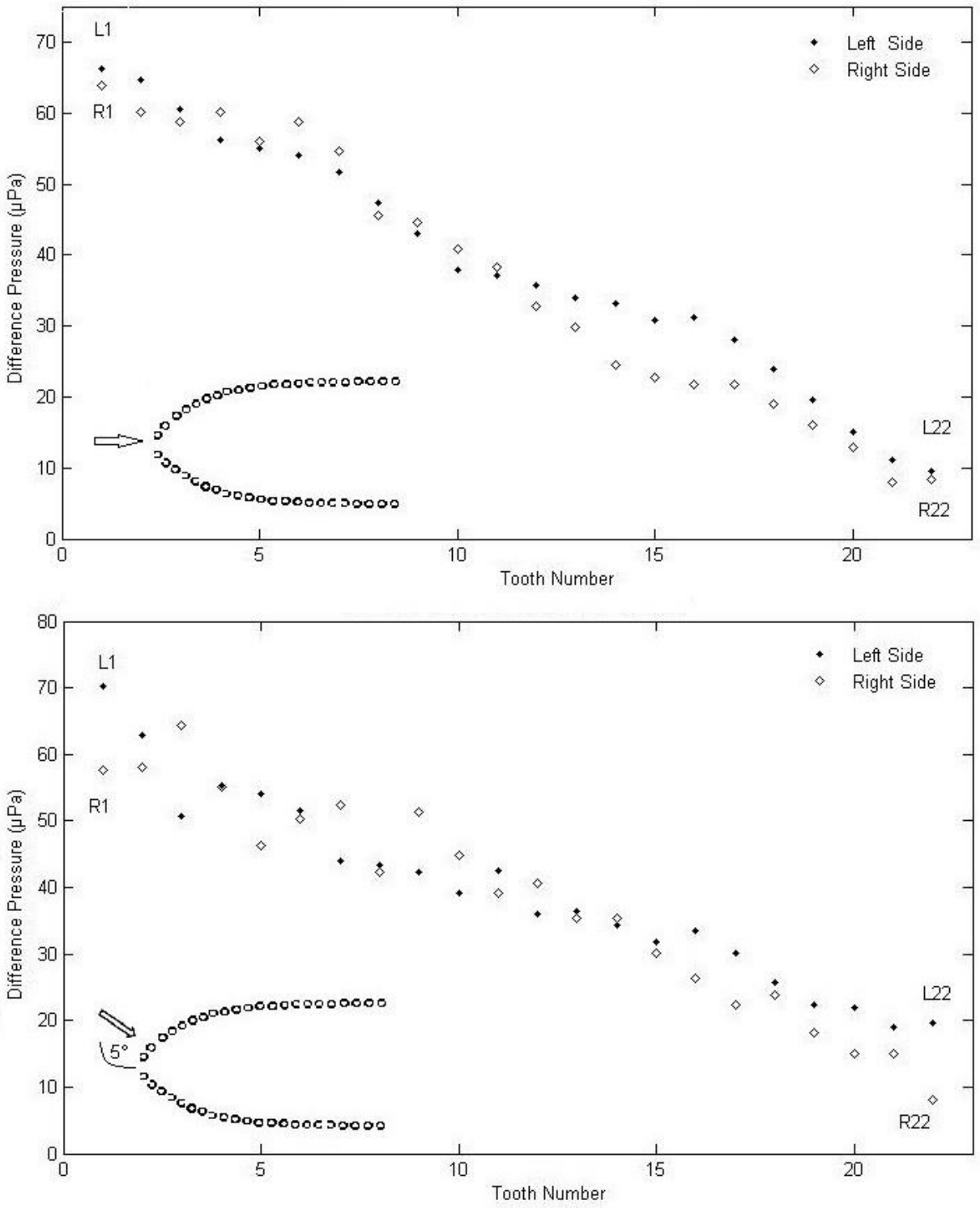

Fig. 5.20: Difference pressure at the tip of the teeth for an angle of 0° (above) and 5° (below) at a frequency of 100 kHz.

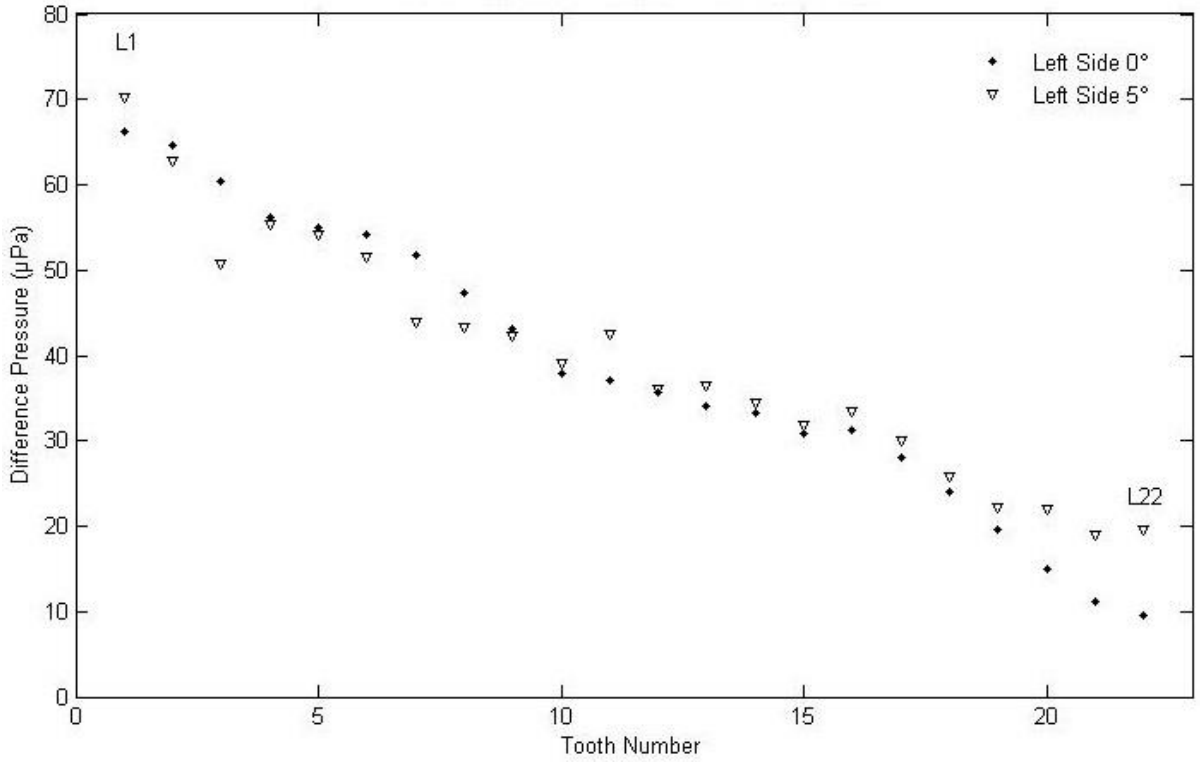

Fig. 5.21: Difference pressure at the tip of the teeth on the left jaw side for an angle of 0° and 5° at a frequency of 100 kHz.

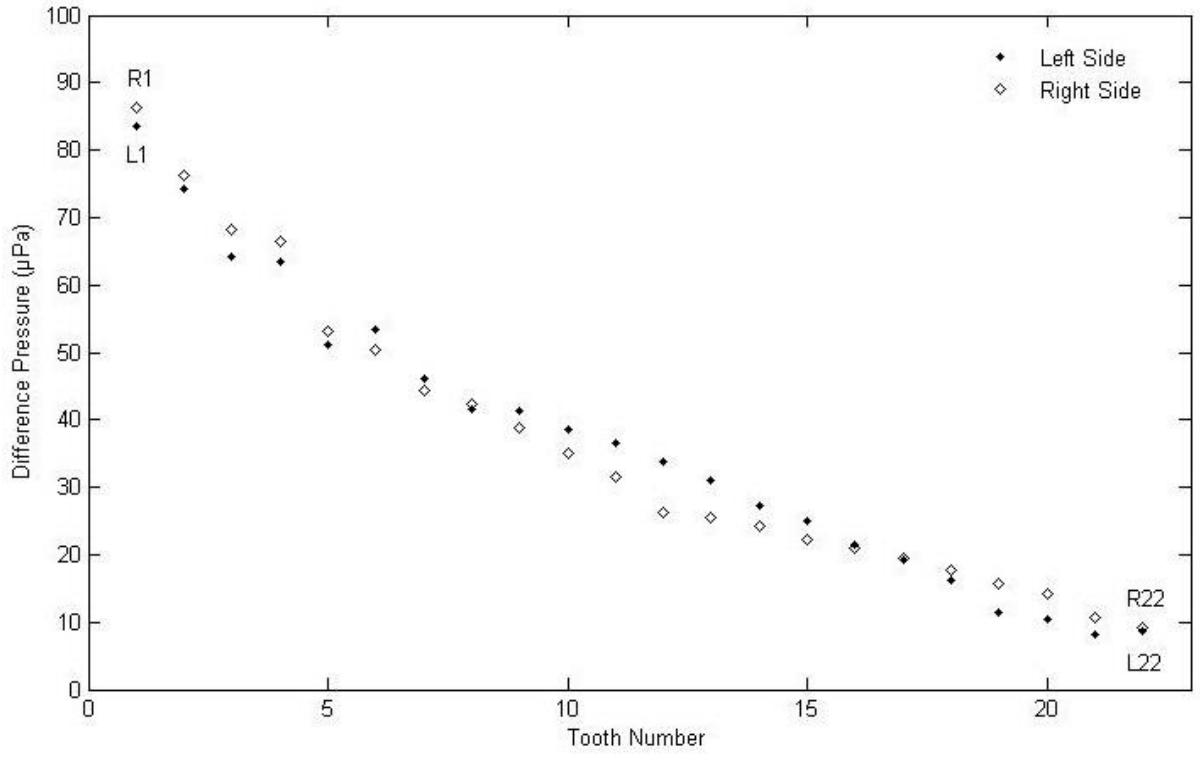

Fig. 5.22: Difference pressure at the bottom of the teeth for both jaw sides for 0° at a frequency of 100 kHz.

5.6 General Conclusion

Sound propagation was modelled for a plane wave going through the tip and the base of the teeth at different angles. The pressure change for different frequencies as well as missing teeth was also investigated.

The simulations were run for 1° intervals for an incoming signal at angles from 0° to ±10° and for 5° intervals from ±10° to ±90°. High variations are shown with relative angles between the jaw and incoming acoustic waves, with most of the directional hearing between approximately ±15°. This result supports the angular resolutions observed for dolphins (e.g. Au 1993). Pressure values after 15° fluctuate strongly, which suggests that the sound wave interference after this angle leads to a highly disordered pressure distribution, resulting in insignificant data. The complete simulations show the relation between neighbouring teeth and the attenuation or amplification of the signals at other teeth. The pressure at the back teeth shows a noticeable gradual change, particularly between 0° and ±15°.

The results show that the propagation of sound varies with the size and position of the teeth. A plane wave coming from the front and propagating towards the back of the jaw shows a first peak in the acoustic signal directly after hitting the tooth in the front. There is only a slight difference between the pressure at a frequency of 20 kHz and 100 kHz, with smaller values for 20 kHz. For an angle of 0°, the signal shows a symmetric distribution with the highest pressure at the front of the teeth. The pressure at the rear of the jaw is lower with almost no sound in the middle of the jaw between the teeth. The course of the pressure distribution throughout the jaw at each tooth was examined on the example of two different angles, 0° and 5°. There is a gradual pressure decrease from the front tooth toward the rear for both jaw sides and both angles.

Particularly the colour-coded images show the noticeable pressure change on each jaw side for changing angles. The images present a positive angle change, meaning that the sound wave is impinging on the right of the jaw. In this case, the pressure at the inside of the jaw in the back increases at the left teeth and decreases on the right teeth. This occurs due to the shadowing of the teeth. The pressure on the outside of the teeth is reversed with increasing pressure on the right jaw side, which is the wave facing side, since there are no obstacles between the impinging wave and the teeth. The pressure on the left side is however reduced due the shadowing of the teeth. These results of the pressure distribution around the teeth on

the inside as well as outside occur for the two different frequencies as well as for missing teeth and different tooth diameter with only minor differences between the parameters.

Pressures at the teeth with larger tooth diameter show a more distinct difference between the left and right jaw side. Shadowing of the teeth is more noticeable than for a smaller tooth diameter. The isolation between the right and left teeth for larger tooth diameter is increased, which indicates that sound localization is enhanced. Multiple missing teeth in the back lead to larger gaps between teeth and therefore a more fluctuating pressure inside the jaw. The teeth are mainly missing on the right jaw side, which means that for positive angle changes, the sound wave can propagate unhindered through the gap. Less shadowing of the teeth occurs.

In conclusion, the simulations show the important role the teeth play in sound reception, as they attenuate, mask or enhance sound in specific configurations similar to those observed in live dolphins.

6 Discussion

6.1 Interaction between Teeth, Gular pathway and Pan bone

There are several hypotheses on the sound reception pathway in toothed whales, with the three most likely ones discussed here. Norris (1964, 1968) was the first to assume that the fatty tissue in the melon and lower jaw is a pathway for sound emission and reception and that sound enters first a thin wall in the lower jaw bone, then travelling through the fat tissue to the inner ear. Other researchers supported this hypothesis (e.g. Bullock et al. 1968, Brill et al. 1988, Møhl et al. 1999, Houser et al. 1999). A different theory came up in 1990. Goodson and Klinowska investigated the idea that the teeth of odontocetes may play a role in sound reception, pointing out the distinctive feature of the tooth arrangement in toothed whales in comparison with other mammals. Odontocetes have evenly spaced homodont teeth. Dobbins et al. (2001, 2007) suggested that the teeth act as endfire array. Nelson (2005) found that a sperm whale's teeth resonated at the animal's echolocation frequency. The hypothesis of teeth as sound reception pathway was investigated further in this thesis. Since the beginning of this thesis, a new hypothesis for a sound reception pathway in odontocetes has appeared. Cranford et al. (2008a, 2008b, 2009, 2014) discovered via finite element analysis that sound, coming from the front of a Cuvier's beaked whale's (*Ziphius cavirostris*) jaw, enters the head below the tongue region, propagates through the throat and an opening in the posterior part of the lower jaw. Sound then travels, as already suggested by Norris (1964), through the fatty tissue in the hollow lower jaw to the inner ear. Cranford found that for this hypothesis to work, the bony wall on the medial inner side of the lower jaw has to be absent, which is the case in all toothed whales.

This thesis investigated the possible relation between the teeth and sound reception. That the mandibular lipid in toothed whales is connected to sound propagation was already proven by various researchers (e.g. Varanasi and Malins 1972, Ketten 2000). However, the exact way of sound until it reaches the animal's ear is still not entirely clear. Brill et al. (1988) investigated the connection between a dolphin's jaw and sound reception and conducted experiments with the animal's jaw, but also the teeth, acoustically shielded. The animal was not able to find its target, which shows that either the jaw or the teeth or possibly both have an influence on echolocation. McCormick et al. (1970) investigated the sound conduction to a dolphin's ear by

holding a vibrator against the front tooth of the animal's lower jaw and at the end of the mandible itself. They measured large potentials in the organ of the Corti in the cochlea, suggesting that sound must reach the ear through bone conduction. These findings could again also imply a connection between the teeth and sound reception.

The theory of the teeth acting as passive resonators has been investigated further by Dible (2008) and Dible et al. (2009). They investigated the possibility of the teeth acting as end-fire array as well as the hypothesis of band-gap hearing. Resonant modes within the teeth of a bottlenose dolphin showed measurements in the band of 115 to 135 kHz using Laser Doppler Vibrometry (LDV). These frequencies lie within the animal's echolocation signal.

Dible et al. (2009) measured the receive directivity patterns for various frequencies for the left and right ear of the dolphin. These measurement points were located further in the back of the animal's jaw. The authors modelled the jaw bone as reflecting nodes and included an absorbing condition at the jaw channel ends. These parameters were not considered in this thesis. Experiments conducted in this thesis focussed on the sound wave interference pattern between the teeth. Jaw bone or surrounding tissues were not taken into account and the pressure distribution outside the jaw was not investigated. A direct comparison is therefore not possible. However, as presented in this thesis, the colour-coded simulation images show the pressure distribution inside as well as outside the area of the tooth structure. Fig. 5.8 and Fig. 5.11 for example show the interference for all the teeth for different angles at a frequency of 100 kHz, for the tip and bottom of the teeth respectively. The area outside the jaw at the rear tooth is closest to the animal's ears. These findings can therefore to some extent be compared with Dible et al.'s (2009). Particularly the pressure distribution at the teeth with larger tooth diameter show a similarity to Dible et al.'s results.

While the pressure at the rearmost teeth at an angle of 0° is similar for both sides outside the jaw, it changes noticeably with changing jaw angle. The pressure on the left side decreases continuously with increasing angle, whereas it increases at the tooth on the right side. The teeth in the front are shadowing the back teeth on the wave averted side, while the teeth on the jaw side facing the wave are impinged on unhindered. These findings can also be seen in Dible et al.'s (2009) graph, which shows a distinct difference between measurements at the left and right ear for changing angles (Fig. 6.1).

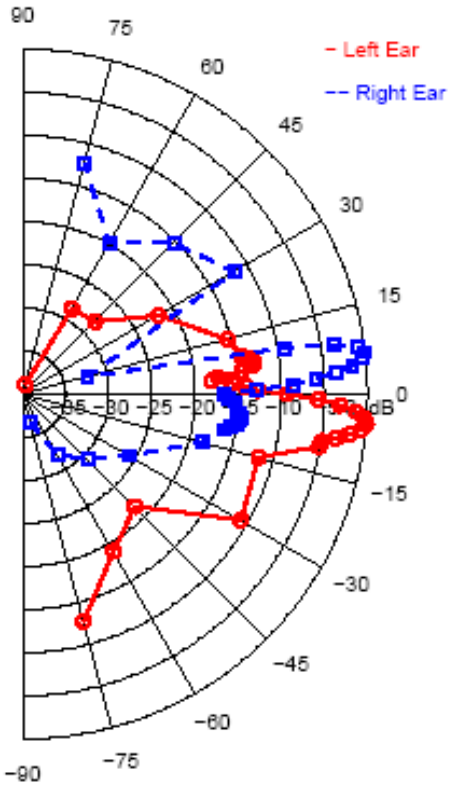

Fig. 6.1: Receive directivity pattern for a bottlenose dolphin's left and right ear at a frequency of 100 kHz (adapted from Dible et al. 2009).

An isolation between the left and right ear can be seen with intensities at the left ear decreasing for positive angles and increasing for negative angles; the opposite outcome is the case for intensities at the right ear. Although, as already mentioned, the values cannot be entirely compared due to the differences between the two models, the colour-coded simulations in Fig. 5.11 show the same trend in pressure as Dible et al.'s (2009) findings do.

When looking at the interference inside the jaw at the rearmost teeth on both sides, it is noticeable that the pressure distribution is converse compared to pressure distributions outside the jaw. Although an isolation between left and right side still exists, the pressure at the left side increases for positive angles and decreases for negative angles. The opposite occurs for the pressure at the right side: a pressure decrease can be seen for positive angles and an increase for negative angles (Fig. 6.2). These results are consistent with the colour-coded images in chapter 5 (e.g. Fig. 5.11). A plane wave coming for example from an angle of 10° and impinging on the right side of the jaw shows high pressure distribution on the outside of the jaw and low pressure on the inside of the jaw near the rearmost tooth. While the area on the

outside is hit unhindered by the acoustic wave, the area on the inside is shadowed by the teeth. This situation is converse for the left jaw side.

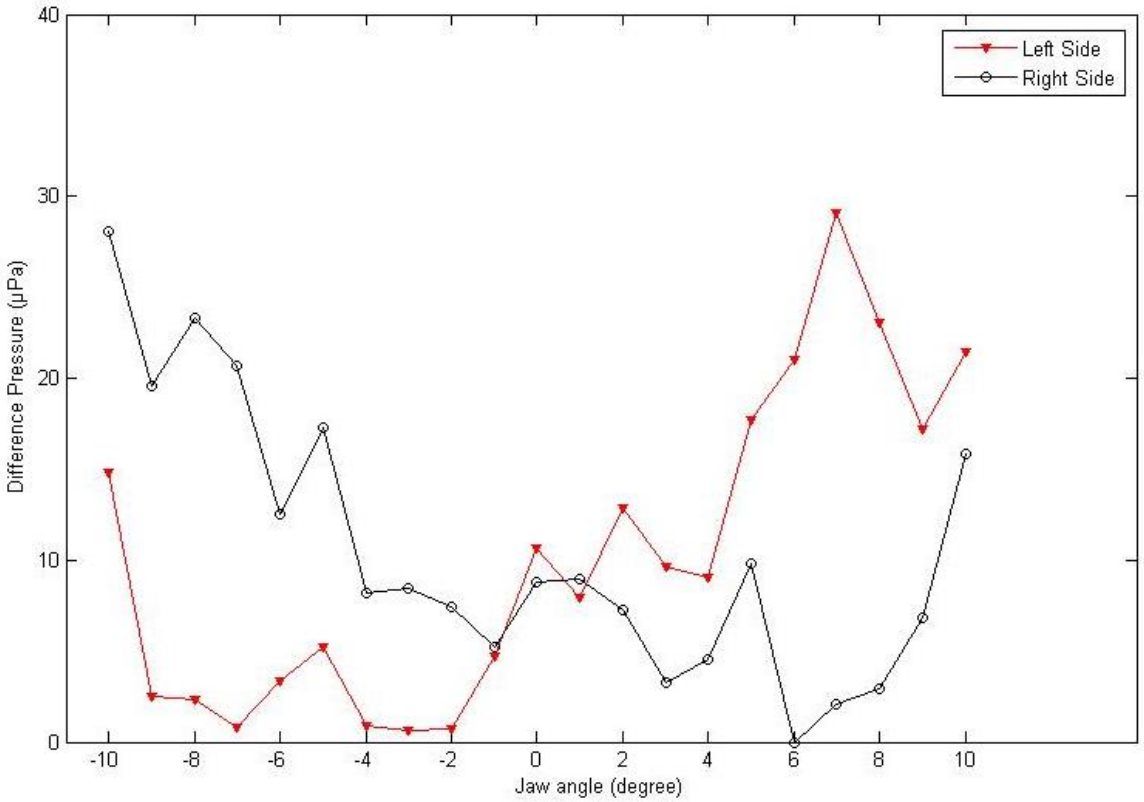

Fig. 6.2: Difference pressure measured at tooth L22 and R22 inside the lower jaw for angles -10° to +10° at 100 kHz.

The effect of multiple missing teeth on the pressure distribution was compared to a model with all teeth present. This was also investigated by Dible et al. (2009). Results seen in this thesis show that there is still a trend in pressure distribution when teeth are missing, but with overall lower pressure values lower for simulations with multiple teeth missing than when all teeth are present (Fig. 6.3). This can also be seen in Dible et al.'s results. However, the findings in this thesis can only partly be compared with Dible et al.'s. The authors investigated the effect of missing teeth on their band-gap model, comparing the sound pressure for missing teeth and all teeth present, but looking at different frequencies and not different angles. Their band-gap model consisted of 22 layers of scattering elements, representing the dolphin's teeth, whereas the simulations in this thesis display the 44 elements in the form of a dolphin's lower jaw structure. The only possible comparison was therefore the one between pressures for 100 kHz, which as already mentioned showed a similar outcome for both cases. These results lead to the conclusion that directional hearing is still possible, even if teeth are missing.

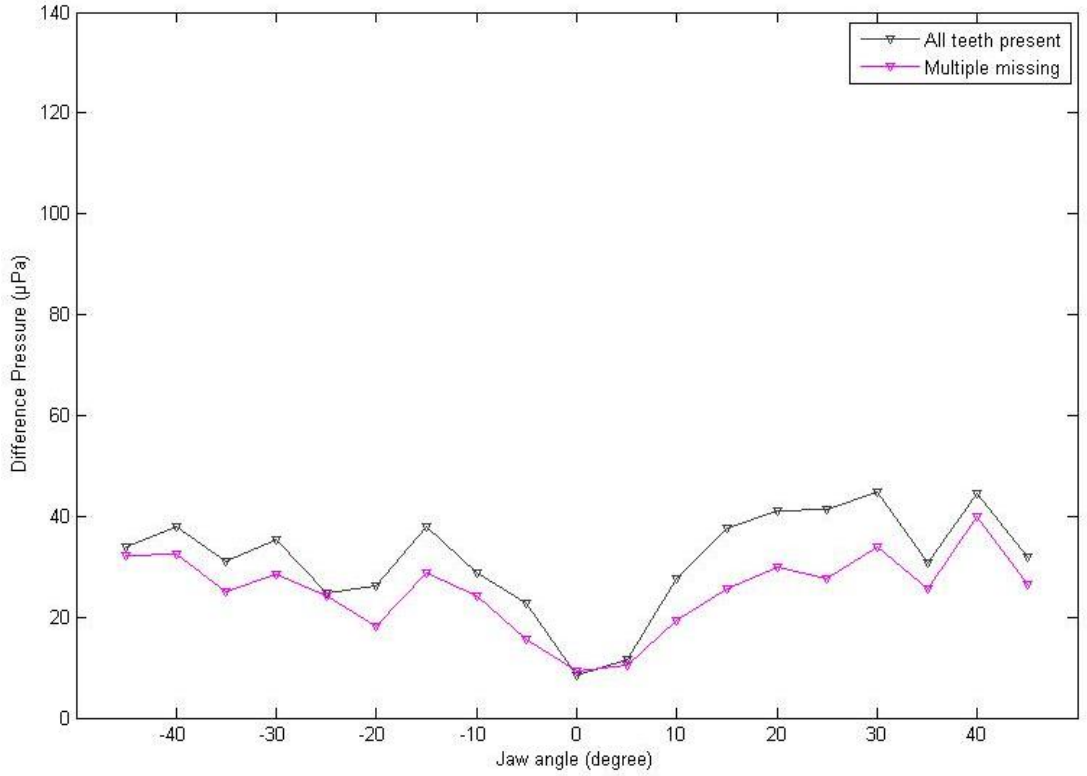

Fig. 6.3: Difference pressure at tooth R22 for angles -45° to +45° for multiple teeth missing and all teeth present at 100 kHz.

Simulations conducted by Cranford et al. (2008a, 2008b) showed that sound entering the mandible from below the horizontal plane at an angle of -18° reached the ear with a lower amplitude than a sound wave arriving from the horizontal plane. This was also observed in psychoacoustic experiments conducted by Au and Moore (1984). These findings show a logical discrepancy to the idea of the gular pathway in which sound entering from below the mandible should theoretically have a direct access to the gular region.

A comparison of Cranford et al.'s (2008a, 2008b) findings and the results of this thesis is not entirely possible, since the authors used 3-D simulations in order to examine the propagation of a sound wave through the head of *Ziphius cavirostris* in both the horizontal and vertical plane, whereas simulations in this thesis were limited to 2-D. They also considered jaw bone and tissues, whereas in this thesis only the teeth were considered. However, as can be seen in the 2-D simulations, there is some shadowing of the gular region by the teeth, when the sound wave is coming from in front of the jaw at 0° in the horizontal plane (Fig. 5.8). This contradicts Cranford et al.'s (2008a) results who reported high pressure amplitudes received at the ears for a sound wave arriving at 0°.

Another difficulty for an accurate comparison was that the authors' regarded only an angle of 0° and 2°, not taking any other angle of the horizontal plane into account, whereas the simulations in this thesis consider various angles in the horizontal plane. However, Cranford et al.'s (2008a) findings for a sound wave coming from an angle of 2° on the horizontal coincide with the results of this thesis. The authors reported that the signal of the sound wave arriving at the head slightly to the left reached the right ear with some time delay and reduced intensity. This can also be seen in the findings of Chapter 5 for frequencies 20 kHz and 100 kHz.

Even though these pathways are different, it may be possible that all three are part of the hearing process in odontocetes. For each one of the pathways to work, jaw and teeth have to feature a certain structure. Norris (1969, 1980) hypothesized that the pan bone is the region where sound enters first due to the very thin area which he called the acoustic window. Cranford et al. (2008a) pointed out that their gular pathway can only work because the medial bony wall in the mandible of odontocetes is absent. For the tooth pathway to work, the teeth have to be homodont and equally spaced, which is the case in all odontocete species with teeth. These special characteristics in all three cases indicate that all three pathways play a role in sound reception.

Although Cranford et al. (2008a) hypothesized that acoustic waves enter the head through the gular region, the authors pointed out that their gular pathway did not negate jaw hearing. They showed through simulations a possible flexural wave mechanism for jaw hearing, with waves being translated into pressure and shear waves when hitting the area of the pan bone. This combination of the two waves created flexural waves within the pan bone which then propagated through the acoustic lipid and the TPC. According to Cranford et al.'s simulations, this proposed mechanism depends on geometry and elastic properties of the lower jaw and the frequency and angle of incidence of the sound wave. The authors also suggested that the flexural wave mechanism of the mandible may indicate that the jaw functions as a tonotopic frequency filter, letting certain frequencies pass at specific places of the jaw. Frequency filtering was also suggested by Dible et al. (2009), but in relation to the teeth acting as acoustic stop band. They hypothesized that the teeth act as a frequency filter dependant on the angle of the incoming sound wave.

Looking at the gular pathway, a sound wave travels only through the soft tissues in the lower jaw and not the bone. This is the fastest way with the least resistance. Considering the teeth as

primary sound receptor, sound arriving at the teeth leads to tooth vibrations which in turn lead to signal transmission through the mandibular fat to the inner ear. While the gular pathway transmits signals very fast, Cranford et al. (2008a) do not mention a relation to the directional hearing capacity of *Ziphius cavirostris*. A possibility may be that the gular region plays a main part for odontocetes for distant signals, whereas the teeth play a part for nearby signals, when the animal is closing in on its target. The results show that there is already a slight pressure change at the back teeth for a change of the jaw angle from 0° to ±1°. Depending on the sensitivity of odontocetes' hearing, this could indicate that the animals are able to determine the direction of a target already by only slightly turning their head.

Norris' (1969, 1980) findings showed best sensitivities at the mandible at angles between 10° and 30°. For sound waves hitting the mandible at these angles, the animal has to turn its head considerably. The closer the dolphin gets to its target the less time it has for head movement and scanning. This is again an indication that while lower jaw hearing is effective for echolocation at a larger distance, tooth hearing takes place when the animal is close to its target. A possible explanation is the tooth spacing (~11.4 mm) of the bottlenose dolphin, which is equal to a wavelength, leading to amplified sound waves. This wavelength occurs for the animal's higher echolocation frequencies. The closer the dolphin gets to its target the higher is the frequency of its emitted sound (Au 1993). Bottlenose dolphins echolocate in a wider range of frequencies, between 40 and 150 kHz. This indicates that jaw and gular region are possibly used for a different echolocation frequency spectrum than the teeth, for example for frequencies below 100 kHz.

6.2 Sound localization

The localization of sound depends on interaural time (ITD) and intensity difference (IID). As seen in the colour coded images in Chapter 5, there is a difference in the pressure of the plane wave at the teeth on the right and left side. Higher pressure means stronger vibrations of the teeth; the different pressure values at the teeth on the left and right jaw side with changing jaw angles can therefore already be seen as an indication that the teeth play a part in sound localization. Although this thesis focusses mainly on the pressure distribution inside the jaw between the teeth, the pressure distribution can also be seen outside the jaw in the colour coded images. As shown in Fig. 6.2, the pressure at the rear teeth on the left side inside the jaw is higher than on the right side for a sound wave impinging from the right; a reverse effect can be

seen for the acoustic wave coming from the left side of the animal's head. These different pressures or intensities occur as already mentioned before due to the shadowing of the sound wave by the teeth. The work in this thesis investigated the possible effect of tooth resonances on sound conduction. Band gap hearing as suggested by Dible et al. (2009) was not investigated. The results show that the interferences at the rear teeth inside the jaw lead to a tendency of the pressure distribution; this is not the case for the front teeth. It is therefore suggested that sound localization takes mainly place at the back of the jaw, which coincides with the sound reception pathways via acoustic window as well as the gular region. However, the teeth in the front of the jaw are necessary for this to work. Without the shadowing of the front teeth and the backscattering of sound waves between the teeth in the front, the pressure distribution at the back teeth would be different. A decrease in pressure could already be seen for teeth missing in the back of the jaw, although the difference was only minimal and the trend of the pressure distribution stayed almost the same (Fig. 6.3). However, Dible et al.'s (2009) findings show that the isolation at the left and right ear is reduced at lower frequencies when all teeth are absent. There was no isolation between ears at a frequency of 120 kHz when all teeth are missing, showing the loss of localization capability at higher frequencies. This indicates that although an exact number of teeth is not a required parameter affecting the sonar performance, sound localization is noticeably decreased or even non-existent when all teeth are absent.

Dible's (2008) findings showed a high attenuation of sound waves in the lower jaw bone with an attenuation level of 1.8 $dBmm^{-1}$. These findings suggest that sound coupling from the front of the jaw to the acoustic window is not very likely, indicating that if sound propagates through the teeth and lower jaw bone, this conduction path only occurs in the back of the jaw. This means that although sound waves are backscattered at the front teeth inside the jaw, the sound conduction through the bone takes only place at the rear teeth, which are situated near the acoustic lipid. The path through bone from teeth to acoustic lipid is thereby only very short and attenuation minimal. The backscattering between teeth in the front is however still essential for the outcome of the pressure distribution in the back. The isolation between the teeth at the left and right jaw side could also indicate that each tooth row functions as its own array, which is primarily sensitive to the waveform at higher frequencies. This array shows an improved bearing resolution in the near-field, which is beneficial for the dolphin when closing in on its target. The overlayed receiving beam patterns of the teeth on both sides of the jaw enable the

animal to compare the received sounds and track targets very accurately in angle and range (Fig. 6.2).

If teeth were to act as passive resonators, then the findings of this thesis show that the teeth are more sensitive to pressure changes at a frequency of 100 kHz, which is a frequency within the echolocation range of a bottlenose dolphin. These pressures on the teeth lead to tooth vibrations, which in turn lead probably to conduction through bone at the back teeth to the acoustic lipid and inner ear. Strong tooth resonances at a bottlenose dolphin's echolocation frequency (115 – 135 kHz) were also measured through Laser Doppler Vibrometry by Dible et al. (2009), indicating that the teeth play a role in sound conduction. The results show higher pressure on the left and lower pressure on the right teeth in the back of the jaw for a sound wave arriving at the right side of the dolphin's jaw. The reverse can be seen when the wave is coming from the left side. These different pressures are suggested to tell the animal the direction of the target or obstacle underwater. Additional to the discrimination between different intensities or pressures, it is also suggested that the animal can localize targets by measuring the different arrival time of the acoustic wave. A sound wave arriving for example first at the right jaw side reaches the right teeth first and then the left teeth. The animal can thereby identify the location of the target.

That sound localization is particularly enhanced in dolphins is possibly due to the animals' jaw structure as well as the regular spacing of their teeth. The lower jaw of a bottlenose dolphin is diverging at an angle of 12°. Graf et al. (2009) measured the pressure distribution for a separation between half jaws by 20% to compare different jaw angles. The findings showed a decreased difference between pressures at the teeth on both jaw sides, meaning the localization capability of the dolphin is reduced. It is therefore suggest that the 12° angle of the bottlenose dolphin is possibly the most desirable for the directional hearing. The regular tooth spacing is, as mentioned before, possibly also a factor in the enhanced sound localization. The 1 cm spacing between teeth is approximately one wavelength at the echolocation frequency of bottlenose dolphins, which leads to constructive interference along the row of the teeth on each side. It is suggested that the given trend in pressure at the rear teeth can only exist due these two features.

Teeth are known to be great conductors for vibrations. Land mammals can receive sound through air and bone conduction (Nummela 2009). SoundBite hearing aids for example, used

by humans with single-sided deafness or conductive hearing loss, transmit sound via the teeth from the functional ear through bone to the non-functional ear where the signals are then processed (Miller 2010). Ozer et al. (2002) found that vibrations of the teeth of a human's lower jaw stimulated bone conduction, leading to the transmission of auditory sensations. Sensitivities were measured at the forehead and at the teeth of a human, showing that the teeth were more sensitive than the forehead. Bone conduction hearing in humans using the teeth has been suggested by various researchers (Dahlin et al. 1973, Stenfelt and Håkansson 1999, Muramatsu et al. 2013). Since teeth are, unlike the jaw, bones that are not covered by skin, they can transfer sound excitation more easily. Muramatsu et al. (2013) conducted experiments with a hearing aid attached to a tooth. This actuator converted tooth vibrations to sound signals. The author's results show that sound was received through the teeth.

These findings show that, at least in humans or land mammals in general, teeth can be the primary receptor for sound, transmitting the signals through the bone of the skull to the inner ear. In each of these experiments, the hearing aid was implemented on a single tooth and one ear was still functional, receiving sound via air conduction and the outer and middle ear. The external auditory meatus (outer and middle ear) of odontocetes is very thin and partly occluded; sound can therefore not be received through this region. The auditory bulla is acoustically isolated from the skull by the mandibular fat, which also shows why sound can not be received through the external auditory meatus (Nummela 2009).

Contrary to the experiments of sound conduction via a single human tooth, research on the role of dolphin teeth in sound reception was believed to be an interaction between every tooth of the lower jaw, mainly in relation to the accuracy of directional hearing (Goodson and Klinowska 1990; Dobbins 2001, 2007). This thesis investigated the effect of sound at a single tooth and also at the teeth as a whole, while changing the angle of the jaw. The results show that there is a pressure change for each tooth with changing angle. For the tip of the back teeth and a frequency of 100 kHz for example, there is a sharp rise in pressure for a jaw angle from 0° to ±15° (Fig. 5.9, Fig. 5.10). These measurements show that sound pressure is high when the wave is hitting the animal's jaw on the right side at -15°. The pressure decreases with the animal's head turning towards 0° and increases again until the jaw reaches an angle of 15°. That the pressure at the back teeth is lower for a sound wave coming from directly in front of the animal is consistent with the observation that the rear teeth are shadowed by the teeth in the front of the jaw. These pressure changes tell the animal possibly when sound has passed,

making the teeth a kind of detector for the direction of the incoming sound wave. The pressure values after these degrees fluctuate strongly, which suggests that they might be simply random interference patterns and not significant. The above mentioned pressure increase from 0° to ±15° at the rear teeth shows a trend of the sound pressure, which could be an indication of directional hearing.

6.3 Time-domain Modelling

The pressure difference was measured for the tip and bottom of the teeth in order to compare measurements for different diameters, and for 20 and 100 kHz. Other simulations included measurements for opposite and multiple teeth missing. The plane wave has the most impact when hitting the jaw first. There are high pressure variations at the front of the jaw, where the teeth are closer to each other and the jaw is narrower. The wider the jaw, the lower is the pressure. This could also be due to the scattering of the wave and the shadowing of the area in the back of the jaw by the front teeth. For a sound wave coming from an angle of 0°, there is little scattering compared to the other angles.

The results show that there is no apparent tendency for the pressure at the front teeth for any parameter change. The pressure fluctuates strongly, particularly between angles ±15°. Contrary to this, there is a trend in pressure at the back teeth with a gradual increase from 0° to ±15°. Amplitudes at the bottom of the teeth are higher at the front teeth compared to measurements at the tip of the teeth. The pressure at the back teeth on the left side is on the other hand lower for the bottom of the teeth, whereas the pressure on the right side is similar to values measured at the tip of the teeth. For most of the data, the pressure at the back teeth shows a trend from an angle of 0° to ±15° for frequencies 20 kHz and 100 kHz as well as for opposite and missing teeth at the tip of the teeth. After this point, the pressure fluctuates strongly. This suggests that the first 10° to 15° for both positive and negative degrees are most important for directional hearing.

These degrees for sound reception are also the area of the receiving beamwidth measured by Au and Moore (1984). They measured a beamwidth of 13.7° for a horizontal plane and a frequency of 120 kHz. A beamwidth of 30.4° was measured for 30 kHz. It was therefore suggested that the capability of directional hearing depended on the frequency. In 2004, Au measured a transmission beamwidth of 10° for the horizontal and vertical plane and a slightly

broader receiving beamwidth. Zaytseva et al. (1975) measured a beamwidth of 8.2° for a frequency of 80 kHz for a horizontal plane. However, their experiment was not as accurate as Au and Moore's (1984) and the dolphin used in the experiment was able to move its head, while swimming towards the signal hydrophone. The results of this thesis show that there is already a pressure change for a jaw angle change from 0° to ±1° at the back teeth (Fig. 5.9 – 5.19). Since pressure values at the front teeth fluctuate strongly and show no trend, only the back teeth were taken into account. If pressure on the teeth leads in fact to vibrations which lead to the transmission of sound signals through the acoustic window and finally the inner ear, this indicates that the dolphin's directivity is much more accurate than initially assumed. This could suggest that the animal is able to determine a target's location after moving its head by only one degree.

The pressure trend at the back teeth relates to the findings by various researchers (Varanasi and Malins 1972, Møhl et al. 1999, Koopman et al. 2006, Rommel et al. 2009). They found that the mandibular fat in toothed whales is located in a cavity at the posterior part of the mandible, reaching directly to the tympanoperiotic complex. The fat is known to be linked to sound transmission to the inner ear, having a low sound absorption. Møhl et al. (1999) also found that the region with the highest sensitivity for a sound wave arriving at the head was slightly forward of the acoustic window.

The amount of teeth in odontocetes varies widely with species. Species like narwhals (*Monodon monoceros*) and beaked whales (*Ziphiidae*) have only a few teeth or even no teeth at all. Male narwhals have usually one spiralled tusk, reaching a length up to 3 m, whereas the teeth of the females generally remain inside the skull. There are also occasional irregularities with females sometimes developing one tusk, male narwhals no tusk or even the development of two tusks (Heide-Jørgensen 2009). Beaked whales have in general also only a few teeth. The teeth in the upper jaw are usually entirely absent, whereas the lower jaw contains one or two pairs (Mead 2009). Au (1993) observed an aged toothless bottlenose dolphin (*Tursiops truncatus*), which was still capable of detecting targets. All of these toothed whales are still able to echolocate. Au (1993) therefore suggested that sound cannot be transmitted via the teeth. The suggestion of this thesis is that sound is transmitted via the teeth through the mandibular bone and fat to the inner ear where the signals are then processed. The teeth are believed to enhance the animals' directional hearing. Narwhals and beaked whales may not have enough teeth to form an array, but it is still possible that the vibration of sound on their

teeth leads to sound transmission through the lower jaw, fat and finally the inner ear. That a toothless dolphin was still able to locate targets underwater can also be explained by this proposition. Teeth are mainly suggested to be connected to the accuracy of odontocetes' directional hearing. The simulations show that there is still a trend in pressure when the dolphin misses several teeth, even though the pressure fluctuates slightly for an angle from 0° to ±10° (Fig. 5.10). This suggests that even without all the teeth, sound can still be received, but directivity may be less precise.

6.4 Acoustic Modelling of Dolphin Reception

The results of this thesis are limited to 2-D simulations, displaying the pressure for one plane of the tooth. Tip and bottom of the teeth were chosen for the measurements. The 2-D simulations do not include the jawbone or surrounding tissues, only the teeth. The results show therefore not a 100 % accuracy in comparison with the reality, but can be seen as an approximation of it. 3-D simulations would come closer to reality, taking the whole tooth into account.

Results show that multiple scattering changes with diameter change. These effects are exacerbated as teeth increase in diameter, for example looking at the bottom of the teeth. They significantly modify the signals received by each tooth, showing that the teeth cannot be considered as isolated, point-like receivers. These effects are again only modelled in the horizontal plane. 3-D propagation is likely to enhance these effects, especially as the model is refined and other acoustic scatterers, such as blubber, skin and pan bone are considered.

6.5 Biosonar Applications

According to various researchers, the alignment of bottlenose dolphins' teeth in the lower jaw, the specific jaw angle as well as the fact that the animals' teeth are similar, are all components indicating a certain purpose for this anatomy (Goodson and Klinowska 1990, Dobbins 2007, Dible et al. 2009). This observation led to the assumption that the teeth must play a role in sound reception and possibly improve the directional hearing. If this hypothesis is true, it could be used to improve current biosonar designs. Theoretical studies by Dobbins (2001, 2007) and Dible et al. (2009) for example showed that dolphins' teeth are aligned in the lower jaw in a pattern consistent with that of hydrophones in an efficient end-fire array. These results are important for the assessment of systems inspired by dolphin jaws but using real

hydrophones. The receiving area of each hydrophone needs to be carefully considered, and by adequately varying the respective sizes, it should be possible to amplify or attenuate incoming signals to favour specific angles. The relative positions of the hydrophones can also be shifted to create different receiving directivity patterns. By varying the spacing between half-arrays for example, one can increase the amount of sound reaching the back of the jaw and focus it on narrow areas, or reduce it nearly completely, favouring sound reception by the teeth. The use of genetic algorithms or similar approaches is a potentially promising way to match the full array configuration to the expected beam pattern, creating more versatile biosonar designs.

Bio-inspired sonar designs can benefit from the insights that acoustic modelling offers in the possible mechanisms of sound reception, in this case by bottlenose dolphins. Even if the biological mechanisms are not exactly shown to be possible with the simulations, the sensor geometries proposed for natural systems can be of use for the design of man-made systems. The results from the 2-D simulations show the limits of considering dolphin teeth as point-like receivers. Both theoretical studies and experimental demonstrations should take into account the possibility of multiple scattering between the individual hydrophones and their mounting. The results show how the signal amplitude on each tooth is affected by the ten closest teeth. This has implications for the processing of electrical signals from each receiver.

6.6 Marine Mammals and Sound Reception

The bottlenose dolphin (*Tursiops truncatus*) has been a highly investigated species among odontocetes. The animal is known for its high evolved sonar system, detecting even very small targets under water. The U.S. Navy Marine Mammal Program (MMP), which is based in San Diego, uses bottlenose dolphins as well as California sea lions (*Zalophus californianus*) to detect underwater mines and recover objects from sea (Houser et al. 2010). This is a very delicate task requiring exact precision. After using several other animals for these tasks, the MMP settled on bottlenose dolphins. One of the reasons could be that the directional hearing capability of these animals outperformed the directional hearing of other toothed whales. If the geometrical structure of the dolphin jaw and teeth is the reason for this precise directivity, it could suggest that the 12° jaw angle is an ideal angle for sonar.

The results show that the sound pressure at the teeth changes with changing tooth size. Pressure at the bottom of the teeth with a bigger diameter showed a wider reception beamwidth

than at the tip of the teeth with a smaller diameter, but only for the left jaw side at the back. The pressure at the bottom of the teeth was overall lower than at the tip of the teeth. However, the difference between pressure values at the bottom and tip of teeth was only minor and a change of tooth diameter might not make a big difference for the directional hearing.

The jaw geometry of bottlenose dolphins is similar to the geometry of other toothed whales. In almost all odontocetes, the teeth in the mandible are divided into two straight rows at an angle of 10° - 20° (Dobbins 2007). Killer whales (*Orcinus orca*) for example have 10 - 14 teeth on each side of the jaw with an average diameter of 2.5 cm and a length of 13 cm (Heyning and Dahlheim 1988). The sperm whale (*Physeter macrocephalus*) has a very narrow mandible with 20 to 26 teeth on each side with a diameter of about 10 cm and a tooth length between 7.62 cm - 20.32 cm (Whitehead 2009). The male of the Cuvier's beaked whale (*Ziphius cavirostris*) has two large front teeth in the lower jaw with a length of approximately 8 cm. The other teeth are vestigial and do not evolve. The teeth of the females, which are between 15 - 40 on each side of the mandible, never erupt and remain in the gum tissues (Heyning and Mead 2009). Even though the teeth of Cuvier's beaked whales remain in their gums, it is possible that the pressure of a sound wave reaches the teeth after propagating through the gum tissue. The fact that the jaw angle of toothed whales is always between 10° – 20° leads to the suggestion that the structure of the jaw is mostly important for the animals' directional hearing. Depending on jaw angle, tooth spacing and probably also the amount of teeth in the mandible, sound pressure is distributed differently in the mandible, therefore presumably changing the preciseness of the directivity.

6.7 Investigated Objectives

The specific questions investigated in this thesis will be addressed in short in this section:

1. Is there a difference in sound pressure for an incident sound wave with the frequency in which a bottlenose dolphin whistles and echolocates?

   Contrary to findings by Zaytseva et al. (1975) and Au and Moore (1984), the results of this thesis show only a slight pressure difference between a frequency of 20 kHz and 100 kHz (Fig. 5.6 - Fig. 5.10). The pressure at 20 kHz was overall lower than at 100 kHz, which is supported by results of the researchers. However, the difference is only minimal and not as distinctive as in the measurements observed by for example Au and Moore (1984), which

was already discussed earlier. There is no change in the receiving beamwidth. Frequency filtering was also not obvious in Cranford et al.'s (2008a) findings regarding the gular pathway. This could imply that for the frequency to have an effect on the pressure distribution, the program has to include soft tissues and the other parameters of the mandibular structure.

2. Does a change of the size of the area the sound wave impinges on have an effect on the sound pressure and to what extent? Tip and bottom of the teeth are in this case chosen as an example.

   The results show that the pressure distribution changes depending on the size of the area the sound wave strikes. The pressure at the front teeth is higher for a larger area, in this case the bottom of the teeth, than for the tip of the teeth. At the back teeth, the pressure is lower on both jaw sides at the bottom of the teeth. There are stronger fluctuations for the pressure at the front of the jaw for the bottom of the teeth in comparison to the tip of the teeth. Results at the back teeth show that the pressure changes only slowly for the first ±10°. On the right side of the jaw, the peak pressure is reached at 30° for R20 and R22, and at 35° for R21 for positive angles.

3. Is there a difference in sound pressure at the teeth after the sound wave impinges on different angles of the dolphin jaw?

   The pressure was measured at the front and back teeth for an angle of -90° to +90°, in 1 degree steps from -10° to +10° and 5 degree steps from -10° to -90° and +10° to +90°. There is a trend in pressure at the back teeth between ±15°. Pressure after these angles fluctuates slightly, which suggests that it is only noise and not significant for the results. The pressure at the front teeth shows also fluctuations between ±15°, which indicates that the front teeth might not be linked to the directional hearing of the animals. However, without the front teeth there would be no shadowing of the back which is necessary to obtain these results.

4. Are there characteristic features in the sound pressure around the area of the gular pathway?

   The pressure around the gular region is shadowed by the front teeth, particularly for a sound wave coming from the front of the jaw at 0°. This contradicts Cranford et al.'s (2008)

findings who measured high sensitivities at this region. However, since the authors used 3-D modelling for their simulations and took only the soft tissues such as acoustic fat and skin into account, these findings cannot entirely be compared with the results of this thesis.

7 Conclusion and Future Work

Field observations show that dolphin teeth are aligned in the lower jaw in a pattern similar to hydrophones in an efficient end-fire array (Goodson and Klinowska 1990, Dobbins 2001, Dobbins 2007, Dible et al. 2009). The jaw of a bottlenose dolphin (*Tursiops truncatus*) for example is diverged at an angle of 12°. These investigations have been used both to explain sound reception by dolphins and to design new biosonars. This thesis used 2-D modelling to investigate the propagation and sound distribution of a returning plane sound wave impinging on the teeth of a bottlenose dolphin. For the measurements, the base and tip diameters of teeth were used from the cast of the dolphin jaw. The pressure at each tooth was measured for a jaw with all teeth present, opposite teeth missing and multiple teeth missing. A difference in pressure was also investigated for the echolocation and whistle frequency of the animal. However, the latter showed no significant change in pressure, leading to the suggestion that further parameters like surrounding tissue or bone velocity are needed. It is also possible that the 2-D model is not sufficient enough to show a significant pressure change for different frequencies.

Results of the simulations show multiple scattering between the teeth with a trend in pressure at the back teeth. This was the case for all teeth present as well as teeth missing. The pressure at the rear increases gradually with a change of angle from the signal coming from an angle of 0° to ±15°. Pressure values after this point fluctuate strongly, which indicates that the sound wave interference after these angles leads to an erratic pressure distribution, possibly resulting in insignificant data. The pressure at the front teeth shows erratic fluctuations for all angles, indicating that the front teeth are not linked to the animal's hearing. The results show that there is a relation between the pressure distribution and the teeth, particularly for the tip of the teeth. Even though the pressure at the front fluctuates strongly with changing angle, the presence of the front teeth is necessary in order to get the pressure at the back. Without the masking of the front teeth, the pressure at the rear would fluctuate as well and show no trend. One could say that the front teeth "tidy up" the sound distribution in the jaw to receive the sound pressure at the back. The sound pressure in the back shows a trend, which suggests a possible connection to the directional hearing.

Looking at all the teeth in the mandible, a gradual pressure decrease can be seen from the front of the jaw to the rear. According to various researchers, the signal propagation at each tooth is possibly delayed to arrive at the inner ear simultaneously (Goodson and Klinowska 1990, Dobbins 2001, 2007, Dible et al. 2009). Even though this thesis did not investigate their findings further, the results show that a propagation delay of the signals would be one possible conclusion.

Since toothed whales are known to move their head when approaching a target and the results show that there is already a trend in pressure at each back tooth, this could suggest that the animals are able to use the pressure difference at one tooth to determine the direction of a target. Findings of a pressure change for an angle change of 1° support this suggestion. The pressure difference between the rearmost teeth on the left and right jaw side with changing jaw angle shows an isolation between the two teeth, which could indicate the potential for providing sound localization. Another indication for the role of the teeth in sound reception is that teeth are great conductors for vibrations. Higher pressure means stronger tooth vibrations. Sound waves impinging on the two lines of teeth at for example the echolocation frequency of odontocetes lead possibly to vibrations of the animals' teeth and the subsequent transmission of the sound waves through the jaw bone and lipid to the inner ear.

Overall it can be said that the teeth are likely to play a part in sound reception. The 2-D simulations in this thesis are limited to the teeth and do not consider jaw bone or surrounding tissue for the measurements. The next step would be to look into 3-D modelling, which is more realistic. This should again take the teeth as well as the surrounding tissues and pan bone into account. A look at other odontocetes might also be advantageous to examine the difference between species.

References

Ainslie M. A. and J. G. McColm (1998): A simplified formula for viscous and chemical absorption in sea water. J. Acoust. Soc. Am. **103**(3), 1671-1672.

Amundin, M. and S.H. Andersen (1983): Bony nares air pressure and nasal plug muscle activity during click production in the harbour porpoise, *Phocoena*, and the bottlenose dolphin, *Tursiops truncatus*. J. Exp. Biol. **105**, 275-282.

Andersen, S. (1970): Directional Hearing in the Harbor Porpoise (*Phocoena phocoena*). Invest. Cetacea **2**, 260-263.

Anderson, J. D., Hannam, A. G. and B. Mathews (1970): Sensory Mechanisms in Mammalian Teeth and Their Supporting Structures. Phys. Rev. **50**(2), 171-195.

Anderson, M. E. (2000): A 2-D non-linear wave propagation solver written in open-source Matlab code. IEEE Ultrasonics Symposium **2**, 1351-1354.

Aroyan, J. L., Cranford, T. W., Kent, J. and K. S. Norris (1992): Computer modeling of acoustic beam formation in *Delphinus delphis*. J. Acoust. Soc. Am. **92**, 2539-254.

Aroyan, J. L. (2001): Three-dimensional modeling of hearing in *Delphinus delphis*. J. Acoust. Soc. Am. **110**(6), 3305-3318.

Au, W. W. L., Floyd, R. W. and J. E. Haun (1978): Propagation of Atlantic bottlenose dolphin echolocation signals. J. Acoust. Soc. Am. **64**(2), 411-422.

Au, W. W. L. and R. H. Penner (1981): Target detection in noise by echolocating Atlantic bottlenose dolphins. J. Acoust. Soc. Am. **70**(3), 687-693.

Au, W. W. L., Penner, R. H. and J. Kadane (1982): Acoustic behavior of echolocating Atlantic Bottlenose Dolphins. J. Acoust. Soc. Am. 71(5), 1269-1275.

Au, W. W. L. and P. W. B. Moore (1984): Receiving Beam Patterns and Directivity Indices of the Atlantic Bottlenose Dolphin (*Tursiops truncatus*). J. Acoust. Soc. Am. **75**, 255-262.

Au, W. W. L., Moore, P. W. B. and D. Pawloski (1986**)**: Echolocation transmitting beam of the Atlantic bottlenose dolphin. J. Acoust. Soc. Am. **80**, 688-694.

Au, W. W. L., Penner, R. H. and C. W. Turl (1987): Propagation of Beluga Echolocation Signal. J. Acoust. Soc. Am. **82**, 807-813.

Au, W. W. L. and D. Martin (1989): Insights into Dolphin Sonar Discrimination Capabilities from Human Listening Experiments. J. Acoust. Soc. Am. **86**, 1662-1670.

Au, W. W. L. and D. Pawloski (1992): Cylinder Wall Thickness Difference Discrimination by an Echolocating Atlantic Bottlenose Dolphin. J. Comp. Physiol. A **172**, 41-47.

Au, W. W. L. (1993): The Sonar of Dolphins. Springer Verlag, New York.

Au, W. W. L., Kastelein, R. A., Rippe, T. and N. M. Schooneman (1999): Transmission Beam Pattern and Echolocation Signals of a Harbor Porpoise (*Phocoena phocoena*). J. Acoust. Soc. Am. **106**, 3699-3705.

Au, W. W. L. (2004): Dolphin sonar detection and discrimination capabilities. J. Acoust. Soc. Am. **115**, 2614.

Au, W. W. L. and M. C. Hastings (2008): Principles of marine Bioacoustics. Springer, New York, 679 pp.

Au, W. W. L., Houser, D. S., Finneran, J. J., Lee, W.-J., Talmadge, L. A. and P. W. Moore (2010): The acoustic field on the forehead of echolocating Atlantic bottlenose dolphins (*Tursiops truncatus*). J. Acoust. Soc. Am. **128**(30), 1426-1434.

Bel'kovich, V. M., Borisov, I. V., Gurevich, V. S. and N. L. Krushinskaya (1969): Echolocating Capabilities of the Common Dolphin (*Delphinus delphis*), Zool. Zhurn. **48**, 876-883.

Berenger, J.-P. (1994): A perfectly matched layer for the absorption of electromagnetic waves. J. Comput. Phys.Vol. **114**(1), 185-200.

Blevins, C. E. and B. J. Parkins (1973): Functional anatomy of the porpoise larynx. Am. J. Anat. **138**, 151-164.

Blomberg, J. (1974): Unusual lipids.II. Head oil of the north Atlantic pilot whales, *Globicephala melaena*. Lipids **9**, 461-470.

Blomberg, J. and B. N. Jensen (1976): Ultrasonic studies on the head oil of the North Atlantic pilot whale (*Globicephala melaena*). J. Acoust. Soc. Am. **60**, 755-758.

Blomberg, J. and L. E. Lindholm (1976): Variations in lipid composition and sound velocity in melon from the North Atlantic pilot whale, *Globicephala melaena*. Lipids **11**, 153-156.

Blomqvist, C. and M. Amundin (2004): High-frequency burst-pulse sounds in agonistic/aggressive interactions in bottlenose dolphins, *Tursiops truncatus*. In: Echolocation in bats and dolphins. J. A. Thomas, Moss, C. F. and M. Vater (eds.), University of Chicago Press, 425-431.

Branstetter, B. K., Moore, P. W., Finneran, J. J., Tormey, M. N. and H. Aihara (2012): Directional properties of bottlenose dolphin (*Tursiops truncatus*) clicks, burst-pulse, and whistle sounds. J. Acoust. Soc. Am. **131**(2), 1613-1621.

Brekhovskikh, L. M. and Yu. P. Lysanov (2003): Fundamentals of Ocean Acoustics. 3rd edition, Springer Verlag, New York, 270 pp.

Brill, R. L. (1988): The Jaw-hearing dolphin: Preliminary behavioral and acoustical evidence. In: Animal Sonar: Processes and Performance. P.E. Nachtigall & P.W.B. Moore (eds.), NATO ASI Series, Plenum Press, New York, 281-287.

Brill, R. L., Moore, P. W. B., Helweg, D. A. and L. A. Dankiewicz (2001): Investigating the dolphin's peripheral hearing system: Acoustic sensitivity about the head and lower jaw. Technical Report–1865, 1-14.

Bullock, T. H., Grinnell, A. D., Ikezono, E., Kameda, K., Katsuki, Y., Nomoto, M., Sato, O., Suga, N. and K. Yanagisawa (1968): Electrophysiological Studies of Central Auditory Mechanisms in Cetaceans. Z. Vergleich. Physiol. **59**, 117-156.

Busnel, R. G. and A. Dziedzic (1966): Acoustic signals of the pilot whale, *Globicephala melaena*, and of the porpoises, *Delphinus delphis* and *Phocoena phocoena*. In: Whales, dolphins and porpoises. K. S. Norris, Würsig, B., Wells, R. S. and M. Würsig (eds.), University of California Press, Berkeley, 607-646.

Busnel, R. G. and A. Dziedzic (1967): Resultats metrologiques experimentaux de l'echolocation chez le *Phocaena phocaena* et leur comparison avec ceux de certaines chauves-souris. In: Animal Sonar Systems: Biology and Bionics. R. G. Busnel (ed.), Laboratoire de physique acoustique, Jouy-en-Josas, France, 307-335.

Chellapilla, K. (1998): Combining Mutation operators in evolutionary programming. IEEE Transactions on Evolutionary Computation Vol. **2**(3), September 1998, 91-96.

Costidis, R. and S. R. Rommel (2012): Vascularization of air sinuses and fat bodies in the head of the Bottlenose dolphin (*Tursiops truncatus*): morphological implications on physiology. Aquatic Physiology **3**, 102-124.

Cranford, T. W. (1992): Functional morphology of the odontocete forehead: implications for sound generation. Dept of Biology, University of Calilfornia, 276.

Cranford, T. W., Amundin, M. and K. S. Norris (1996): Functional morphology and homology in the odontece nasal complex: implications for sound generation. J. Morphol. **228**, 223-285.

Cranford, T. W., van Conn, W. G., Chaplin, M. S., Carr, J. S., Kamolnick, T. A., Carder, D. A. and S. H. Ridgway (1997): Visualizing dolphin sonar signal generation using high-speed video endoscopy. J. Acoust. Soc. Am. **102**, 3123.

Cranford, T. W. (2000): In Search of Impulse Sound Sources in Odontocetes. In: Hearing by Whales and Dolphins. W. W. L. Au, Popper A. N. and R. R. Fay (eds.), Springer Verlag, New York, 109-156.

Cranford, T. W., Krysl, P. and J. A. Hildebrand (2008a): Acoustic pathways revealed: simulated sound transmission and reception in Cuvier's beaked whale (*Ziphius cavirostris*), Bioinsp. & Biomim. **3**, 1-10.

Cranford, T. W., McKenna, M. F., Soldevilla, M. S., Wiggins, S. M.,Goldbogen, J. A., Shadwick, R. E., Krysl P., St Leger, J. A. and J. A. Hildebrand (2008b): Anatomic geometry

of sound transmission and reception in Cuvier's beaked whale (*Ziphius cavirostris*), Anat. Record **291**.

Cranford, T. W., Krysl, P. and J. A. Hildebrand (2009): "Rivers" of sound in Cuvier's beaked whale (*Ziphius cavirostris*): Implications for the evolution of sound reception in odontocetes. J. Acoust. Soc. Am. **125**(4), 2677.

Cranford, T. W., Krysl, P. and M. Amundin (2010): A new acoustic portal into the odontocete ear and vibrational analysis of the tympanoperiotic complex. PLoS One. 2010 Aug 4;5(8):e11927. doi: 10.1371/journal.pone.0011927.

Cranford, T. W., Trijoulet, V., Smith, C. R. and P. Krysl (2014): Validation of a vibroacoustic finite element model using bottlenose dolphin simulations: the dolphin biosonar beam is focused in stages. Bioacoustics **23**(2), 161-194.

Dahlin, G.C., Allen, F. G. and E. W. Collard (1973): Bone-conduction thresholds of human teeth. J. Acoust. Soc. Am. **53**(5), 1434-1437.

Dawson, S. M. (1991): Clicks and Communication: The Behavioural and Social Contexts of Hector's Dolphin Vocalizations. Ethology **88**, 265-276.

Dible, S.A., Flint, J.A. and P.A. Lepper (2006): Laser Doppler Vibrometry Measurement of the Lower Jaw and Teeth of the Atlantic Bottlenose Dolphin (*Tursiops truncatus*). Proc. 8th ECUA, Portugal, 365-370.

Dible, S. (2008): Sonar Properties of the Lower Jaw of the Atlantic Bottlenose Dolphin (*Tursiops truncatus*). Doctoral Thesis.

Dible, S. A., Flint, J. A. and P. A. Lepper (2009): On the role of periodic structures in the lower jaw of the Atlantic bottlenose dolphin (*Tursiops truncatus*). Bioinsp. & Biomim. **4**(1), 1-9.

Diercks, K. J., Trochta, R. T. Greenlaw, R. C. F. and W. E. Evans (1971): Recording and Analysis of Dolphin Echolocation Signals. J. Acoust. Soc. Am. **49**, 1729-1732.

Dobbins, P.F. (2001): Modelling Dolphin Echolocation Reception. Proc. I.O.A. 23(4), 123-132.

Dobbins, P.F. (2007): Dolphin Sonar – Modelling a new receiver concept. Bioinsp.& Biomim. **2**, 19-29.

Dormer, K. J. (1979): Mechanism of sound production and air recycling in delphinids: cineradiographic evidence. J. Acoust. Soc. Am. **65**, 229.

Dudzinski, K. M., Thomas, J. A. and J. D. Gregg (2009): Communication in Marine Mammals. In: Encyclopedia of Marine Mammals 2nd Edition. Perrin, W. F., Würsig, B. and J. G. M. Thewissen (eds.), Academic Press, San Diego, 260-269.

Evans, W. E. and J. H. Prescott (1962): Observations of the sound production capabilities of a bottlenose porpoise: a study of whistles and clicks. Zoologica 47, 121-128.

Evans, W. E., Southerland, W. W. and R. G. Biel (1964): The directional characteristics of delphinid sounds. In: Marine Bio-acoustics. W. N. Tavolga (ed.), Pergamon Press, Oxford, 353-370.

Evans, W. E. and B. A. Powell (1966): Discrimination of different metallic plates by an echolocating delphinid. In: Animal Sonar Systems – Biology and Bionics. R. G. Busnel (ed.), Laboratoire de Physiologie Acoustique, Jouy-en-Josas, France, 363-383.

Evans, W. E. (1967): Vocalization among marine animals. In: Marine Bio-Acoustics Vol. **2**, W. N. Tavolga (ed.), Pergamon Press, New York, 159-186.

Fisher, F. H. and V. P. Simmons (1977): Sound absorption in sea water. J. Acoust. Soc. Am. **62**(3), 558-564.

Fitzgerald, J. W. (1999): The Larynx-Melon-Vestibular Lips (LMVL). Model of the dolphin sonar. II. The melon beam former.J. Acoust. Soc. Am. **105**(2), 1262.

Foote, K. G. (1980): Importance of the swimbladder in acoustic scattering by fish: A comparison of gadoid and mackerel target strengths. J. Acoust. Soc. Am. **67**(6), 2084-2089.

Fogel, D. B. (1997): The Advantages of Evolutionary Computation. In Lundth, D., Olsson, B. & A. Naraganan (eds.): Biocomputing and Emergent Computation 1997, World Scientific press, 1-11.

Francois, R. W. and G. R. Garrison (1982): Sound absorption based on ocean measurements: Part I: Pure water and magnesium sulphate contributions. J. Acoust. Soc. Am. **72**(3), 896-907.

Fraser, F. C. (1947): Sound emitted by dolphins. Nature **160**, 759.

Fraser, F. C. and P. E. Purves (1954): Hearing in Cetaceams. Bulletin of the British Museum **2**, 103-116.

Glaeser, G. (1999): Reflections on Spheres and Cylinders of Revolution. J. Geometry and Graphics **3**(2), 121-139.

Goodson, A.D. & M.A. Klinowska (1990): A proposed echolocation receptor for the bottlenose dolphin (*Tursiops truncatus*): Modelling the receive directivity from tooth and lower jaw geometry. In: Sensory Abilities of Cetaceans. J. Thomas and R. Kastelein (ed.), NATO ASI Series A: Plenum Press, New York, 255-267.

Graf, S., Blondel, P., Megill, W. M. and S. E. Clift (2009): Acoustic modelling of dolphin sound reception and implications for biosonar design. Oceans 2009 – Europe. New York: IEEE, 1519-1524.

Gurevich, V. S. and W. E. Evans (1976): Echolocation discrimination of complex planar targets by the beluga whale (*Delphinapterus leucas*). J. Acoust. Soc. Am. **60**(1), S5-S6.

Hall, J. D. and C. S. Johnson (1971): Auditory thresholds of a killer whale *Orcinus orcus* Linnaeus. J. Acoust. Soc. Am. **51**, 515-517.

Hammer, C. E. Jr. and W. W. L. Au (1980): Porpoise echo-recognition. An analysis of controlling target characteristics. J. Acoust. Soc. Am. **68**(5), 1285-1293.

Hatakeyama, Y. and H. Soeda (1990): Studies on echolocation of porpoises taken in salmon gillnet fisheries. In: Sensory Abilities of Cetaceans: Laboratory and field evidence. J. A. Thomas and R. A. Kastelein (eds.), Plenum Press, New York, 269-281.

Heide-Jørgensen, M. P. (2009): Narwhal, *Monodon monoceros*. In: Encyclopedia of Marine Mammals 2nd Edition. Perrin, W. F., Würsig, B. and J. G. M. Thewissen (eds.), Academic Press, San Diego, 754-758.

Herman, L. M. and W. N. Tavolga (1980): The communication systems of cetaceans. In: Cetacean behaviour: Mechanisms and functions. L. M. Herman (ed.), Wiley-Interscience, New York, 149-209.

Heyning, J. E. and M. E. Dahlheim (1988): *Orcinus orca*. Mammalian Species **304**, 1-9.

Heyning, J. E. and J. G. Mead (2009): Cuvier's beaked whale (*Ziphius cavirostris*). In: Encyclopedia of Marine Mammals 2nd Edition. Perrin, W. F., Würsig, B. and J. G. M. Thewissen (eds.), Academic Press, San Diego, 294-295.

Houser, D.S., Helweg, D.A. & P.W. Moore (1999): Classification of dolphin echolocation clicks by energy and frequency distributions. J. Acoust. Soc. Am. **106**(3), 1579-1585.

Houser, D.S., Helweg, D.A., Chellapilla, K. & P.W. Moore (2000): Creation of a biomimetic model of dolphin hearing through the use of evolultionary computation. IEEE Washington, Congress on Evolutionary Computation **1**, 496-502.

Houser, D.S., Martin, S., Phillips, M. Bauer, E., Herrin, T. & P.W. Moore (2003): Signal processing applied to the Dolphin-Based Sonar System. Oceans 2003 Proc. Vol. **1**, San Diego, 297-303.

Houser, D.S., Finneran, J., Carder, D., Van Bonn, W. Smith, C., Hoh, C., Mattrey, R. & S. Ridgway (2004): Structural and functional imaging of bottlenose dolphin (*Tursiops truncatus*) cranial anatomy. J. Exp. Biol. **207**, 3657-3665.

Houser, D.S., Finneran, J. J. & S. H. Ridgway (2010): Research with Navy Marine Mammals Benefits Animal Care, Conservation and Biology. International Journal of Comparative Psychology **23**, 249-268.

Johnson, C.S. (1966): Sound detection thresholds in marine mammals. In: Marine Bio-acoustics Vol. 2. W.N. Tavolga (ed.), Pergamon Press, New York, 247-260.

Johnson, C.S. (1967) Sound detection thresholds in marine mammals. In: W. N. Tavolga (ed.), Marine Bio-Acoustics II, Pergamon Press, Oxford, 247-260.

Kellogg, W. N. and R. Kohler (1952): Responses of the porpoise to ultrasonic frequencies. Science **117**, 239-243.

Kellogg, W. N., Kohler, R. and H. N. Morris (1953): Porpoise sounds as sonar signals. Science **117**, 239-243.

Kellogg, W. N. (1958): Echo Ranging in the Porpoise. Science **128**, 982-988.

Kellogg, W. N. (1959): Auditory perception of submerged objects by porpoises. J. Acoust. Soc. Am **31**, 1-6.

Kellogg, W. N. (1960): Auditory scanning in the dolphin. Psychological Record **10**, 25-27.

Ketten, D. R. (2000): Cetacean Ear. In: Hearing by Whales and Dolphins. W. W. L. Au, Popper, A. N. and R. R. Fay (eds), Springer Verlag, New York, 43-108.

Kinsler, L. E., Frey, A. R., Coppens, A. B. and J. V. Sanders (2000): Fundamentals of acoustics. John Wiley & Sons, NY, 547 pp.

Koopman, H. N., Budge, S. M., Ketten, D. R. and S. J. Iverson (2006): The topographical distribution of lipids in the mandibular fat bodies of odontocetes: Remarkable complexity and consistency. J. Oceanographic Engineering, Special Issue on the Effects of Sound in the Marine Environment **31**, 95-106.

Koopman, H. N. (2007): Phylogenetic, ecological and ontogenetic factors influencing the biochemical structure if the blubber of odontocetes. Marine Biology **151**, 277-291.

Krysl, P., Cranford, T. W., Wiggins, S. M. and J. A. Hildebrand (2006): Simulating the effect of high-intensity sound on cetaceans: Modeling approach and a case study for Cuvier's Beaked whale (*Ziphius cavirostris*). J. Acoust. Soc. Am. **120**, 2328-2339.

Krysl, P., Cranford, T. W. and J. A. Hildebrand (2007): Lagrangian finite element treatment of transien vibration/acoustics of biosolids immersed in fluids. Int. J. Numer. Methods Eng. **74**(5), 754-775.

Kuc, R. (1996): Biologically motivated adaptive sonar system. J. Acoust. Soc. Am. **100**(3), 1849-1854.

Kuc, R. (1997): Biomimetic sonar locates and recognizes objects. J. Ocean. Eng. **22**(4), 616-624.

Kuperman, W. and P. Roux (2007): Underwater Acoustics. In: Handbook of Acoustics. T. D. Rossing (ed.), Springer Verlag, Heidelberg, 149-204.

Lammers, M. O., Au, W. W. L., Aubauer, R. and P. E. Nachtigall (2004): A comparative analysis of echolocation and burst-pulse click trains in *Stenella longirostris*. In: Echolocation in Bats and Dolphins. J. A. Thomas, Moss, C. F. and M. Vater (eds.), University of Chicago Press, Chicago, 414-419.

Lammers, M. O., Schotten, M. and W. W. L. Au (2006): The spatial context of free-ranging Hawaiian spinner dolphins (*Stenella longirostris*) producing acoustic signals. J. Acoust. Soc. Am. **119**(20), 1244-1250.

Leighton, Y. T. G., Finfer, D.C., Finfer, P., White, P. R. and G.-H. Chua (2010): Clutter suppression and classification using twin inverted pulse sonar (TWIPS) B and J. K. DIX, Proc. R. Soc. A **466**, 3453–3478.

Lilly, J. C. and A. M. Miller (1961): Sounds Emitted by the Bottlenose Dolphin. Science **133**, 1689-1693.

Liu, Q. H. (1998): The Pseudospectral Time-Domain (PSTD) Algorithm for Acoustic Waves in Absorptive Media. IEEE T, Ultrason Ferr. **45**, 1044-1055.

Liu, Y. W. (2012): Hilbert Transform and Applications. Intech, Rijeka, 291-300.

Lurton, X. (2002): And Introduction to Underwater Acoustics: Principles and Applications. 1st edition, Springer Verlag, New York. 347 pp.

Lurton, X. (2010): And Introduction to Underwater Acoustics: Principles and Applications. 2nd edition, Springer Verlag, New York. 724 pp.

MacKay, R. S. (1966): Telemetering physiological information from within cetaceans, and the applicability of ultrasound to understanding in vivo structure and performance. In: Whales, Dolphins and Porpoises. K. S. Norris (ed.), University of California Press, Berkeley, 445-470.

MacKay, R. S. and H. M. Liaw (1981): Dolphin vocalization mechanisms. Science **212** (4495), 676-678.

Madsen, P. T., Jensen, F. H., Carder, D. and S. Ridgway (2011): Dolphin whistles: a functional misnomer revealed by heliox breathing. Biol. Lett. (2012) **8**, 211-213.

Matthews, B. (1977): Responses of intradental nerves to electrical and thermal stimulation of teeth in dogs. J. Physiol. 264, 641-664.

McBride, A. F. (1956): Evidence for echolocation in cetaceans. Deep-Sea Research **3**, 153-154.

McCormick, J. G., Wever, E. G., Palin J. and S. H. Ridgway (1970): Sound conduction in the dolphin ear. J. Acoust. Soc. Am. **48**, 1418-1428.

McCormick, J. M., Wever, E. G., Ridgway, S. H. and J. Palin (1980): Sound reception in the porpoise as it relates to echolocation. In: Animal Sonar Systems. R. G. Busnel and J. F. Fish (eds.), Plenum Press, New York, 449-467.

McKenna, M. F., Goldbogen, J. A., Leger, J. St., Hildebrand, J. A. and T. W. Cranford (2007): Evaluation of Postmortem Changes in Tissue Structure in the Bottlenose Dolphin (*Tursiops truncatus*). The Anatomical Record **290**, 1023-1032.

Mead, J. G. (2009): Beaked Whales, Overview, *Ziphiidae*. In: Encyclopedia of Marine Mammals 2nd Edition. Perrin, W. F., Würsig, B. and J. G. M. Thewissen (eds.), Academic Press, San Diego, 94-97.

Medwin, H. and C. S. Clay (1998): Fundamentals of Acoustical Oceanography. Academic Press, Boston. 712 pp.

Miller, R. J. (2010): It's time we listened to our teeth: The SoundBite hearing system. Am. J. Orthod. Dentofacial Orthop. **138**(5), 666-669.

Møhl, B., Au, W. W. L., Pawloski, J. and P.E. Nachtigall (1999): Dolphin hearing: relative sensitivity as a function of point of application of a contact sound source in the jaw and head region. J. Acoust. Soc. Am. **105**(6), 3421-3424.

Moore, P. W. B. and D. A. Pawloski (1990): Investigations on the control of echolocation pulses in the dolphin (*Tursiops truncatus*). In: Sensory abilities of cetaceans: Laboratory and field evidence. J. A. Thomas and R. A. Kastelein (eds.), Plenum Press, New York, 305-316.

Moore, P. W. B. and D. A. Pawloski (1993): Interaural time discrimination in the bottlenose dolphin. J. Acoust. Soc. Am. **94**(3), 1829-1830.

Moore, P. W. B., Pawloski, D. A. and L. A. Dankiewicz (1995): Interaural Time and Intensity Difference Thresholds in the Bottlenose Dolphin (*Tursiops truncatus*). In: Sensory Systems of Aquatic Mammals. K. A. Kastelein, Thomas, J. A. and P. E. Nachtigall (eds.), De Spil Publishers, Woerden, 11-23.

Morente, J. A., Gimenez, G., Porti, J. A. & M. Khalladi (1995): Dispersion Analysis of a TLM Mesh of Symmetrical condensed nodes with Stubs. IEEE Transactions on Microwave Theory and Techniques **43**(2), 452-456.

Muramatsu, M., Kurosawa, J., Oikawa, Y. and Y. Yamasaki (2013): Communication aid utilizing bone-conducted sound via teeth by means of mouthpiece form actuator. Proc. Meetings Acoust. **19**, Psychol. Physiol. Acoust., Montreal, 1-8.

Nelson, M. (2005): The possible role of teeth in sperm whale (*Physeter macrocephalus*) echolocation. MSc Thesis School of Biological Sciences, University of Wales, Bangor.

Norris, K. S. and J. H. Prescott (1961): Observations on Pacific cetaceans of Californian and Mexican waters. Univ. Calif. Publ. Zool. **63**(4), 291-402.

Norris, K. S., Prescott, J. H., Asa-Dorian, P. V. and P. Perkins (1961): An experimental demonstration of echolocation behaviour in the porpoise *Tursiops Truncatus* (Montagu). Biol. Bull. **120**, 163-176.

Norris, K. S. (1964). Some problems of echolocation in cetaceans. In: Marine Bio-Acoustics. W.N. Tavolga (ed.), Pergamon Press, New York, 316-336.

Norris, K. S. and W. E. Evans (1966): Directionality of echolocation clicks in the rough-tooth porpoise, *Steno bredanensis*. In: Marine Bio-Acoustics. W. N. Tavolga (ed.), Pergamon Press, New York, 305-316.

Norris, K.S. (1968): The echolocation of marine mammals. In: The Biology of Marine Mammals. H. T. Andersen (ed.), Academic Press, New York, 391-423.

Norris, K. S. (1969): The echolocation of marine mammals. In: The Biology of Marine Mammals. H. T. Anderson (ed.), Academic Press, New York, 215-234.

Norris, K. S. and G. W. Harvey (1974): Sound transmission in the porpoise head. J. Acoust. Soc. Am. **56**(2), 659-664.

Norris, K. S. (1980): Peripheral sound processing in odontocetes. In: Animal Sonar Systems. R. G. Busnel and J. F. Fish (eds.), Plenum Press, New York, 495-509.

Nummela, S. (2009): Hearing. In: Encyclopedia of Marine Mammals 2nd Edition. Perrin, W. F., Würsig, B. and J. G. M. Thewissen (eds.), Academic Press, San Diego, 553-562.

Overstrom, N. A. (1983): Association between burst-pulse sounds and aggressive behavior in captive Atlantic bottlenose dolphins (*Tursiops truncatus*). Zoo Biology **2**, 93-103.

Ozer, E., Adelman, C., Freeman, S. and H. Sohmer (2002): Bone conduction hearing on the teeth of the lower jaw. J. Basic Clin. Physiol. Pharmacol. **13**(2), 89-96.

Penner, R. H. and A. E. Murchison (1970): Experimentally demonstrated echolocation in the amazon river porpoise, Inia geoffrensis (Blainville). Proc. Ann. Conf. Biol. Sonar and Diving Mammals, 17-37.

Potter, J. R. and E. A. Taylor (2001): On novel reception models for bottlenose dolphin echolocation. Proc. I. O. A. **24**, 103-112.

Purves, P. E. (1967): Anatomical and experimental observations on the cetacean sonar system. In Animal Sonar Systems, Biology and Bionics. R. G. Busnel (ed.), Laboratoire de Physiologie Acoustique, Jouy-en-Jouy, 197-270.

Purves, P. E. and G. Pilleri (1986): Echolocation in Whales and Dolphins. Academic Press, London. 261 pp.

Renaud, D. L. and A. N. Popper (1978): Sound Localization by the Bottlenose Porpoise (*Tursiops truncatus*). J. Exp. Biol. **63**, 569-585.

Rhodes, D. R. (1959): Introduction to Monopulse. New York: McGraw-Hill, 92-96.

Ridgway, S. H., McCormick, J. G. and E. G. Wever (1974): Surgical approach to the dolphin's ear. J. Exp. Zool. **177**, 265-276.

Ridgway, S. H., Carder, D. A., Green, R. F., Gaunt, A. S., Gaunt, S. L. L. and W. E. Evans (1980): Electromyographic and pressure events in the nasolaryngeal system of dolphins during sound production. In: Animal Sonar Systems. R. G. Busnel and J. F. Fish (eds.), Plenum Press, New York, 239-250.

Ridgway, S. H. (1980): Electrophysiological experiments on hearing in odontocetes. In Animal Sonar. P. E. Nachtigall and P.W. B. Moore, (eds.), Plenum Press, New York, 483-493.

Ridgway, S. H. and D. A. Carder (1988): Nasal Pressure and sound production in an echolocating white whale, *Delphinapterus leucas*. In Animal Sonar. P. E. Nachtigall and P.W. B. Moore, (eds.), Plenum Press, New York, 54-60.

Ridgway, S. H. and D. A. Carder (1989): Tactile sensitivity, somatosensory responses, skin vibrations, and the skin surface ridges of the bottlenose dolphin, *Tursiops truncatus*. In: Sensory Abilities of Cetaceans: Laboratory and Field Evidence. J. A. Thomas and R. Kastelein (eds.), Plenum Press New York, 163-179.

Robertson, W. M. and J. F. Rudy II (1998): Measurements of acoustic stop bands in two-dimensional periodic scattering arrays. J. Acoustic. Soc. Am. **104** (2) Pt.1, 694-699.

Rommel, S. A., Pabst, D. A. and W. A. McLellan (2009): Skull Anatomy. In: Encyclopedia of Marine Mammals 2nd Edition. Perrin, W. F., Würsig, B. and J. G. M. Thewissen (eds.), Academic Press, San Diego, 1033-1047.

Schenkkan, E. J. (1973): On the comparative anatomy and function of the nasal tract in odontocetes (Mammalia, Cetacea). Bijdragen Dierkunde **43**, 127-159.

Schevill, W. E. and B. Lawrence (1953): Auditory response of a bottlenosed dolphin, *Tursiops truncatus*, to frequencies above 100 kc. J. Exp. Zool. **124**, 147-165.

Schevill, W. E. and B. Lawrence (1956): Food finding by a captive porpoise (*Tursiops truncatus*). Breviora, Museum of Comparative Zoology **53**, 1-15.

Simard, P., Lace, N., Gowans, S., Quintana- Rizzo, E. Kuczai, II, S. A. Wells, R. S. & D. A. Mann (2011): Low frequency narrow-band calls in bottlenose dolphins (*Tursiops truncatus*): Signal properties, function, and conservation implications. J. Acoust. Soc. Am. **130** (5), 3068-3076.

Simmonds, J, E. and D. N. MacLennan (2005): Fisheries Acoustics: Theory and Practice. Wiley-Blackwell 2nd edition, Oxford. 437 pp.

Soldevilla, M. S., M. F. McKenna, S. M. Wiggins, R. E. Shadwick, T. W. Cranford and J. A. Hildebrand (2005): Cuvier's beaked whale (*Ziphius cavirostris*) head tissues: physical properties and CT imaging. J. Exp. Biol. **208**, 2319-2332.

Stenfelt, S. P. Y. and Bo E. V. Håkansson (1999): Sensitivity to bone conducted sound: excitation of the mastoid vs. the teeth. Scandinavian Audiology **28**(3), 190-198.

Stryer, L. (1995): Biochemistry, 4th edition. W. H. Freeman and Company, New York. 843 pp.

Supin, A. Y. and V. V. Popov (1993): Direction-dependent spectral sensitivity and interaural spectral difference in a dolphin: Evoked potential study. J. Acoust. Soc. Am. **93**, 3490-3495.

Thomas, J., Stoermer, M., Bowers, C., Anderson, L. and A. Garver (1988): Detection abilities and signal characteristics of echolocating false killer whales (*Pseudorca crassidens*). In: Animal Sonar Processing and Performance. Nachtigall, P. E. and P. W. B. Moore, Plenum Press, New York, 323-329.

Turner, R. N. and K. S. Norris (1966): Discriminating echolocation in a porpoise. J. Exp. Anal. Behav. **9**, 534-544.

Uhen, M. D. (2002): Dental morphology (cetacean), Evolution of. In: Encyclopedia of Marine Mammals. W. F. Perrin, Würsig, B. and J. G. M. Thewissen (eds.), Academic Press, San Diego, 316-319.

Varanasi, U. and D. C. Malins (1971): Unique lipids of the porpoise (*Tursiops gilli*): Differences in triacyclglycerols and wax esters of acoustic (mandibular and melon) and blubber tissues. Biochimica et Biophysica Acta, 231, 415-418.

Varanasi, U. and D. C. Malins (1972): Triacylglycerols Characteristic of Porpoise Acoustic Tissues: Molecular Structures of Diisovaleroglycerides. Science **176**, 926-928.

Varanasi, U. Feldman, H. R. and D. C. Malins (1975): Molecular basis for formation of lipid sound lens in echolocation cetaceans. Nature **255**, 340-343.

Varanasi, U., Markey, D. and D. C. Malins (1982): Role of Isovaleroyl lipids in channeling of sound in the porpoise melon. Chemistry and Physics of Lipids **31**, 237-244.

Viceconti, M., Bellingeri, L., Cristofolini, L. and A. Toni (1998): A comparative study on different methods of automatic mesh generation of human femurs. Med Eng Phys. 20(**1**):1-10.

Wever, E. G., McCormick, J. G., Palin, J. and S. H. Ridgway (1971a): The Cochlea of the dolphin, *Tursiops truncatus*: General Morphology. Proc. Nat. Acad. Sci. USA 68(**10**), 2381-2385.

Wever, E. G., McCormick, J. G., Palin, J. and S. H. Ridgway (1971b): The Cochlea of the dolphin, *Tursiops truncatus*: The basilar membrane. Proc. Nat. Acad. Sci. UAS 68(**11**), 2708-2711.

Wever, E. G., McCormick, J. G., Palin, J. and S. H. Ridgway (1972): Cochlear structure in the dolphin *Lagenorhynchus obliquidens*. Proc. Nat. Acad. Sci. USA **69**, 657-661.

White, Jr., M., Norris, J. C., Ljungblad, D. K., Barton, K. and G. N. di Sciara (1978): Auditory thresholds of two beluga whales (*Delphinapterus leucas*). In: Hubbs/Sea World Research Inst. Tech. Rep., 78-109.

Whitehead, H.: Sperm Whale (*Physeter macrocephalus*). In: Encyclopedia of Marine Mammals 2nd Edition. Perrin, W. F., Würsig, B. and J. G. M. Thewissen (eds.), Academic Press, San Diego, 1091-1097.

Wojcik, G. L., Fornberg, B., Waag, R. Carcione, L., Mould, J., Nikodym, L. and T. Driscoll (1997): Pseudospectral methods for large-scale bioacoustics models. Proc. 1997 Ultrasonics Symposium, 1501-1506.

Wood, F. G. and W. E. Evans (1980): Adaptiveness and ecology of echolocation in toothed whales. In: Animal Sonar Systems. R. G. Busnel and J. F. Fish (eds.), Plenum Press, New York, 381-425.

Yuan, X., Borup, D., Wiskin, J. W., Berggren, M., Eidens, R. and S. Johnson (1997): Formulation and validation of Berenger's PML absorbing boundary for the FDTD simulation of acoustic scattering. IEEE Transactions on Ultrasonics, Ferroelectronics and Frequency Control 44, 816-822.

Zahorodny, Z. P., Koopman, H. N., S. M. Budge (2009): Distribution and development of the highly specialized lipids in the sound reception systems of dolphins. J. Compar. Physiol. B: Biochem. Syst. Environ. Physiol. **179**, 783-798.

Zaytseva, K. A., Akopian, A. I. and V. P. Morozov (1975): Noise Resistance of the Dolphin Auditory Analyzer as a Function of Noise Direction. BioFizika **20**, 519-521.

Zook, J. M. and R. A. DiCaprio (1990): A potential system of delay-lines in the dolphin auditory brainstem. In: Sensory Abilities of Cetaceans: Laboratory and Field Evidence. Thomas, J. A. and R. A. Kastelein eds., NATO ASI Series **196**, Plenum Press, New York, 181-193.

Zuckerwar, A. J. (1997): Speed of sound in fluids. In: Encyclopedia of Acoustics Vol. 1. Crocker, M. J. (ed.), John Wiley, New York, 69-79.

A1. Matlab program

Matlab function to implement 2-D solution of the nonlinear wave equation using a pseudospectral/staggered A-B method, including attenuation modelled with two relaxation mechanisms. This version accepts an arbitrary excitation function at arbitrary points on the 2-D grid.

```
function solve_sps2d(med,iters,excit,attn,record)
nonlin_flag = (sum(med.ba(:)) > 0);
dt = med.stabf*min([med.dx med.dz])/max(med.c(:));
dt2 = dt/2;
K = med.rho.*med.c.^2.*ones(med.num_axpts,med.num_latpts);
xax = [-med.num_latpts/2+0.5:med.num_latpts/2-0.5]*med.dx;
zax = [-med.num_pml:med.num_axpts-med.num_pml-1]*med.dz;
alpha_max = -log(med.pml_ampred).*med.c ./ (K.*med.dx);
quadratic = ([med.num_pml:-1:1].'/med.num_pml).^2;

left_alpha = -K(:,1:med.num_pml) .*...
   alpha_max(:,1:med.num_pml) .*...
   repmat(quadratic.',med.num_axpts,1);
right_alpha = -K(:,med.num_latpts-med.num_pml+1:med.num_latpts) .*...
   alpha_max(:,med.num_latpts-med.num_pml+1:med.num_latpts) .*...
   repmat(fliplr(quadratic.'),med.num_axpts,1);
top_alpha = -K(1:med.num_pml,:) .*...
   alpha_max(1:med.num_pml,:) .*...
   repmat(quadratic,1,med.num_latpts);
bottom_alpha = -K(med.num_axpts-med.num_pml+1:med.num_axpts,:) .*...
   alpha_max(med.num_axpts-med.num_pml+1:med.num_axpts,:).*...
   repmat(flipud(quadratic),1,med.num_latpts);

ps_axshifts = [[0:1:med.num_axpts/2-1] [-med.num_axpts/2:1:-1]].'*i*pi;
ps_axshifts = repmat(ps_axshifts,1,med.num_latpts);
ps_latshifts = [[0:1:med.num_latpts/2-1] [-med.num_latpts/2:1:-1]].'*i*pi;
ps_latshifts = repmat(ps_latshifts,1,med.num_axpts);
fft_axscale = 1/(med.num_axpts*med.dz/2);
fft_latscale = 1/(med.num_latpts*med.dx/2);

ab1 = (dt/24) * 26; ab2 = (dt/24) * -5;
ab3 = (dt/24) * 4 ; ab4 = (dt/24) * -1;

p = zeros(med.num_axpts,med.num_latpts);
px = zeros(med.num_axpts,med.num_latpts);
pz = zeros(med.num_axpts,med.num_latpts);
vx = zeros(med.num_axpts,med.num_latpts);
vz = zeros(med.num_axpts,med.num_latpts);
dpx = zeros(med.num_axpts,med.num_latpts);
dpz = zeros(med.num_axpts,med.num_latpts);
dvx = zeros(med.num_axpts,med.num_latpts);
dvz = zeros(med.num_axpts,med.num_latpts);
div_u = zeros(med.num_axpts,med.num_latpts);

if attn.flag ~= 0
  S = zeros(med.num_axpts,med.num_latpts,4,5);
  dS = zeros(med.num_axpts,med.num_latpts,4,5);
```

```
  kt1 = attn.kappas1./attn.taus1;
  kt2 = attn.kappas2./attn.taus2;
  tk_term = kt1 + kt2;
end

if nonlin_flag ~= 0
  w = zeros(med.num_axpts,med.num_latpts,6,5);
  dw = zeros(med.num_axpts,med.num_latpts,6,5);
else
  w = zeros(med.num_axpts,med.num_latpts,4,5);
  dw = zeros(med.num_axpts,med.num_latpts,4,5);
end

psf = zeros(iters,med.num_latpts);
tic
t0 = clock;
start_time = cputime;
forc_time = 0; fft_time = 0;    relax_time = 0;
pml_time = 0;  adbash_time = 0; update_time = 0;
output_time = 0;
tsp = [1:5];

clf
rec_count = 0;
for cr = 1:iters
  t_stage = cputime;
  if cr<=size(excit.p,1)/2
     for cpt = 1:length(excit.ax)
      p(excit.ax(cpt),excit.lat(cpt)) = excit.p(cr*2-1,cpt);
    end
  end
  forc_time = forc_time + (cputime-t_stage);

  t_stage = cputime;
  dpx = real(ifft(fft(p.').*ps_latshifts)).' *fft_latscale;
  dpz = real(ifft(fft(p).*ps_axshifts)) *fft_axscale;
  fft_time = fft_time + (cputime-t_stage);

  t_stage = cputime;
  if attn.flag ~= 0
    sum1x = S(:,:,1,tsp(4))./attn.taus1 + S(:,:,2,tsp(4))./attn.taus2;
    sum2x = px*tk_term;
    dS(:,:,1,tsp(4)) = -S(:,:,1,tsp(4))./attn.taus1 + px.*kt1;
    dS(:,:,2,tsp(4)) = -S(:,:,2,tsp(4))./attn.taus2 + px.*kt2;

    sum1z = S(:,:,3,tsp(4))./attn.taus1 + S(:,:,4,tsp(4))./attn.taus2;
    sum2z = pz*tk_term;
    dS(:,:,3,tsp(4)) = -S(:,:,3,tsp(4))./attn.taus1 + pz.*kt1;
    dS(:,:,4,tsp(4)) = -S(:,:,4,tsp(4))./attn.taus2 + pz.*kt2;
  end
  relax_time = relax_time + (cputime-t_stage);

   t_stage = cputime;
  pml_vxleft = left_alpha .* vx(:,1:med.num_pml);
  pml_vxright = right_alpha .* ...
    vx(:,med.num_latpts-med.num_pml+1:med.num_latpts);
   pml_vztop = top_alpha .* vz(1:med.num_pml,:);
```

```
pml_vzbottom = bottom_alpha .* ...
    vz(med.num_axpts-med.num_pml+1:med.num_axpts,:);

dw(:,:,1,tsp(4)) = (-1./med.rho) .* dpx;
dw(:,1:med.num_pml,1,tsp(4)) =  dw(:,1:med.num_pml,1,tsp(4)) + pml_vxleft;
dw(:,med.num_latpts-med.num_pml+1:med.num_latpts,1,tsp(4)) = ...
    dw(:,med.num_latpts-med.num_pml+1:med.num_latpts,1,tsp(4)) + pml_vxright;

dw(:,:,2,tsp(4)) = (-1./med.rho) .* dpz;
dw(1:med.num_pml,:,2,tsp(4)) = dw(1:med.num_pml,:,2,tsp(4)) + pml_vztop;
dw(med.num_axpts-med.num_pml+1:med.num_axpts,:,2,tsp(4)) = ...
    dw(med.num_axpts-med.num_pml+1:med.num_axpts,:,2,tsp(4)) + pml_vzbottom;

pml_time = pml_time + (cputime-t_stage);

 % Integrate one timestep forward by 4th order Adams-Bashforth:
t_stage = cputime;
w(:,:,1:2,tsp(5)) = w(:,:,1:2,tsp(4)) + ...
    (ab1*dw(:,:,1:2,tsp(4)) + ab2*dw(:,:,1:2,tsp(3)) + ...
     ab3*dw(:,:,1:2,tsp(2)) + ab4*dw(:,:,1:2,tsp(1)));

if attn.flag ~= 0
  S(:,:,:,tsp(5)) = S(:,:,:,tsp(4)) + ...
  (ab1*dS(:,:,:,tsp(4))+ab2*dS(:,:,:,tsp(3))+ ...
   ab3*dS(:,:,:,tsp(2))+ab4*dS(:,:,:,tsp(1)));
end
adbash_time = adbash_time + (cputime-t_stage);

% Update velocity vectors:
t_stage = cputime;
vx = w(:,:,1,tsp(5));
vz = w(:,:,2,tsp(5));
update_time = update_time + (cputime-t_stage);

 % Half-integer time step: calculation of pressure
psf(cr,:) = p(record.psf_index+med.num_pml+1,:);

t_stage = cputime;
if cr<=size(excit.p,1)/2
     for cpt = 1:length(excit.ax)
    vz(excit.ax(cpt),excit.lat(cpt)) = excit.vz(cr*2,cpt);
    vx(excit.ax(cpt),excit.lat(cpt)) = excit.vx(cr*2,cpt);
  end
end
forc_time = forc_time + (cputime-t_stage);

 t_stage = cputime;
dvx = real(ifft(fft(vx.').*ps_latshifts)).' *fft_latscale;
dvz = real(ifft(fft(vz).*ps_axshifts)) *fft_axscale;
fft_time = fft_time + (cputime-t_stage);

% Calculate PML boundary region masks:
t_stage = cputime;
pml_pleft = left_alpha .* px(:,1:med.num_pml);
pml_pright = right_alpha .* ...
    px(:,med.num_latpts-med.num_pml+1:med.num_latpts);
```

```
pml_ptop = top_alpha .* pz(1:med.num_pml,:);
pml_pbottom = bottom_alpha .* ...
    pz(med.num_axpts-med.num_pml+1:med.num_axpts,:);

t_stage = cputime;
if attn.flag ~= 0
  dw(:,:,3,tsp(4)) = -K .* (dvx - sum1x + sum2x);
else
  dw(:,:,3,tsp(4)) = -K .* dvx;
end
dw(:,1:med.num_pml,3,tsp(4)) =  dw(:,1:med.num_pml,3,tsp(4)) + pml_pleft;
dw(:,med.num_latpts-med.num_pml+1:med.num_latpts,3,tsp(4)) = ...
    dw(:,med.num_latpts-med.num_pml+1:med.num_latpts,3,tsp(4)) + pml_pright;

if attn.flag ~= 0
  dw(:,:,4,tsp(4)) = -K .* (dvz - sum1z + sum2z);
else
  dw(:,:,4,tsp(4)) = -K .* dvz;
end
dw(1:med.num_pml,:,4,tsp(4)) = dw(1:med.num_pml,:,4,tsp(4)) + pml_ptop;
dw(med.num_axpts-med.num_pml+1:med.num_axpts,:,4,tsp(4)) = ...
    dw(med.num_axpts-med.num_pml+1:med.num_axpts,:,4,tsp(4)) + pml_pbottom;

  if nonlin_flag ~= 0
  if attn.flag ~= 0
    dw(:,:,5,tsp(4)) = dvx - sum1x + sum2x;
  else
    dw(:,:,5,tsp(4)) = dvx;
  end
  dw(:,1:med.num_pml,5,tsp(4)) =  dw(:,1:med.num_pml,5,tsp(4)) + ...
  pml_pleft./-K(:,1:med.num_pml);
  dw(:,med.num_latpts-med.num_pml+1:med.num_latpts,5,tsp(4)) = ...
  dw(:,med.num_latpts-med.num_pml+1:med.num_latpts,5,tsp(4)) + ...
  pml_pright./-K(:,med.num_latpts-med.num_pml+1:med.num_latpts);
  if attn.flag ~= 0
    dw(:,:,6,tsp(4)) = dvz - sum1z + sum2z;
  else
    dw(:,:,6,tsp(4)) = dvz;
  end
  dw(1:med.num_pml,:,6,tsp(4)) = dw(1:med.num_pml,:,6,tsp(4)) + ...
  pml_ptop./-K(1:med.num_pml,:);
  dw(med.num_axpts-med.num_pml+1:med.num_axpts,:,6,tsp(4)) = ...
  dw(med.num_axpts-med.num_pml+1:med.num_axpts,:,6,tsp(4)) + ...
  pml_pbottom./-K(med.num_axpts-med.num_pml+1:med.num_axpts,:);
end
pml_time = pml_time + (cputime-t_stage);

% Integrate one timestep forward by 4th order Adams-Bashforth:
t_stage = cputime;
if nonlin_flag ~= 0
w(:,:,3:6,tsp(5)) = w(:,:,3:6,tsp(4)) + ...
    (ab1*dw(:,:,3:6,tsp(4)) + ab2*dw(:,:,3:6,tsp(3)) + ...
     ab3*dw(:,:,3:6,tsp(2)) + ab4*dw(:,:,3:6,tsp(1)));
else
w(:,:,3:4,tsp(5)) = w(:,:,3:4,tsp(4)) + ...
    (ab1*dw(:,:,3:4,tsp(4)) + ab2*dw(:,:,3:4,tsp(3)) + ...
```

```
      ab3*dw(:,:,3:4,tsp(2)) + ab4*dw(:,:,3:4,tsp(1)));
  end
  adbash_time = adbash_time + (cputime-t_stage);

  % Update displacement and pressure matrices:
  t_stage = cputime;
    px = w(:,:,3,tsp(5));
  pz = w(:,:,4,tsp(5));
    if nonlin_flag ~= 0
    div_u = w(:,:,5,tsp(5)) + w(:,:,6,tsp(5));
    p = -K.*(div_u+0.5*med.ba.*(div_u).^2);
  else
    p = px + pz;
  end

    tsp = [tsp(2:5) tsp(1)];
  update_time = update_time + (cputime-t_stage);

    t_stage = cputime;
    if record.flag == 1
    if round(cr/record.int) == cr/record.int
      [frame_string,err] = sprintf('%0.6d',rec_count);
      eval(['save ' record.fname frame_string ' ' record.list]);
      rec_count = rec_count + 1;

      figure(1)
      image_scale = 2*sum(max(excit.p0));
      image(xax*1e3,zax*1e3,(p/image_scale)*32+32)
      colormap(gray)
      hold on
      plot([min(xax*1e3) max(xax*1e3)], ...
          record.psf_index*med.dz*1e3*[1 1],'w:');
      hold off
      title_string = ['"Propagation after ' ...
            num2str(round(cr*dt*1e7)/10) ' microseconds."'];
      eval(['title(' title_string ');']);
      axis image
      axis xy
      drawnow
    end
  end
  output_time = output_time + (cputime-t_stage);

    percent = round(cr/iters*1000)/10;
  disp(' ')
  disp([num2str(percent) '% done.'])
  rem_time = num2str(round((100-percent)/percent*etime(clock,t0)/60));
  disp([num2str(round(etime(clock,t0)/60)) ' minute(s) elapsed, ~ ' ...
    rem_time ' minute(s) remaining.'])
end

total_time = cputime-start_time;
real_time = toc;

figure(2)
imagesc([1:iters]*dt*1e6,xax*1e3,psf)
colormap(gray)
```

```
disp(' ')
disp(['Peak positive pressure = ' ...
     num2str(max(max(psf/1e6))) ' MPa.']);
title('Time record at range sample indicated')
xlabel('Lateral dimension [mm]')
ylabel('Time [\mus]')

save solve_sps2d psf

disp(' ')
disp('CPU time and percentage by algorithm stage:')
disp(' ')
fprintf('Forcing function:\t %d s\t = %d %%\n',round(forc_time), ...
      round(100*forc_time/total_time))
fprintf('FFTs:\t\t\t %d s\t = %d %%\n',round(fft_time), ...
     round(100*fft_time/total_time))
fprintf('Relaxation:\t\t %d s\t = %d %%\n',round(relax_time), ...
     round(100*relax_time/total_time))
fprintf('PML application:\t %d s\t = %d %%\n',round(pml_time), ...
     round(100*pml_time/total_time))
fprintf('Adams-Bashforth:\t %d s\t = %d %%\n',round(adbash_time), ...
     round(100*adbash_time/total_time))
fprintf('Update:\t\t\t %d s\t = %d %%\n',round(update_time), ...
     round(100*update_time/total_time))
fprintf('Output:\t\t\t %d s\t = %d %%\n',round(output_time), ...
     round(100*output_time/total_time))
fprintf('Total:\t\t\t %d s\n\n',round(total_time))

disp(['Used ' num2str(round(total_time/60)) ' minutes of CPU time.'])
disp(['Ran  ' num2str(round(real_time/60)) ' minutes in real time.'])
disp(['CPU utilization = ' num2str(total_time/real_time) ' %.'])
```

MATLAB function to initialize and call the previous function, which implements a 2-D solution of the nonlinear wave equation using a pseudospectral/staggered A-B method, including attenuation modelled with two relaxation mechanisms. This function solves for a plane wave impinging on circular region:

```
% Parameters defining the excitation:
function solve_dolphin(input_file)
fc = 100e3;
p0 = 1e-6;
rbw = 0.6;
num_cycles = 3;
num_axpts = 2^11;
num_latpts = 2^11;
c0 = 2200;
rho0 = 2035.4;
num_pml = 8;
pml_ampred = 0.1;
nodes_lam = 8;
stabf = 0.2;
lambda = c0/fc;
dx = lambda/nodes_lam;
```

```
dz = lambda/nodes_lam;
ba = 0;
c = c0;
rho = rho0;

load(input_file);

imagesc(c);axis('square');axis('xy');title('\bfSound velocity image');colorbar;pause(1)
dim=size(c);
for i=1:dim(1),
   for j=1:dim(2),
      if c(i,j)==1490,
         rho(i,j)=1000;
      else
         rho(i,j)=2035.4;
      end
   end
end
imagesc(rho);axis('square');axis('xy');title('\bfDensity image');colorbar;pause(1)
dt = stabf*min([dx dz])/max(c(:));

psf_index = fix(num_axpts*0.42);
rec_flag = 1;
rec_fname = 'phan';
rec_int = round(1/fc/dt/20);
rec_list = 'cr p';

ts = (-num_cycles/fc:dt/2:num_cycles/fc).';

excit_p = repmat(imag(hilbert(gauspuls(ts,fc,rbw))),...
          1,num_latpts);
excit_p = p0*excit_p/max(abs(hilbert(excit_p(:))));
rho_c = ones(num_axpts,num_latpts)./(rho.*c);
excit_lat = (1:num_latpts);
excit_ax = ones(size(excit_lat))*(num_pml+1);

excit_vz = excit_p*diag(rho_c(num_pml+1,excit_lat));
excit_vx = zeros(size(excit_p));
excit_vz = zeros(size(excit_p));

% Parameters defining the attenuation:
att_flag = 0;
proc_flag = 0;
kappas1 = [];
kappas2 = [];
taus1 = [];
taus2 = [];

% Load up the structures to be passed to the calculation function:

med = struct('c',c,'rho',rho,'ba',ba,'num_pml',num_pml,...
       'pml_ampred',pml_ampred,'stabf',stabf,...
       'num_latpts',num_latpts,'num_axpts',num_axpts,...
       'dx',dx,'dz',dz);

excit = struct('p0',p0,'p',excit_p,...
         'vx',excit_vx,'vz',excit_vz,...
```

```
        'lat',excit_lat,'ax',excit_ax);

attn =  struct('flag',att_flag,...
        'kappas1',kappas1,'kappas2',kappas2,...
        'taus1',taus1,'taus2',taus2);

record = struct('psf_index',psf_index,'flag',rec_flag,...
         'fname',rec_fname,'int',rec_int,'list',rec_list);

% Call the calculation function:
iters = round((num_axpts*dx/c0)/dt + length(ts)/2);
iters = 15300;
solve_sps2d(med,iters,excit,attn,record)
save solve_phan
```

A2. Papers and Conference Proceedings

Graf, S., Megill, W. M., Blondel, P. and S. E. Clift (2008): Investigation into the possible role of dolphins' teeth in sound reception. J. Acoust. Soc. Am. **123**(5) Pt. 2, 3360.

Graf, S., Blondel, P., Megill, W. M. and S. E. Clift (2009): Acoustic modelling of dolphin sound reception and implications for biosonar design. Oceans 2009 – Europe. New York: IEEE, 1519-1524.

Graf, S., Blondel, P., Megill, W. M. and S. E. Clift (2009): Sound reception in bottlenose dolphins (*Tursiops truncatus*). Results from 2-D and 3-D modelling. UAM 2009, Nafplion, Greece, 8 pp.